CARDIFF UNIVERSITY

Acetylene hydrochlorination using Au supported on activated carbon catalysts.

Anna Lazaridou

Thesis submitted in accordance with the requirement of Cardiff University for the degree of Doctor of Philosophy

2019 – 2022

Abstract

Acetylene hydrochlorination is a major industrial method to produce vinyl chloride monomer (VCM). Traditionally, the manufacture of VCM relied on the use of a $HgCl_2$/C catalyst, posing serious environmental concerns due to the loss of toxic Hg species from the surface of the support to the environment. Consequently, there has been an urgent need for the development of novel, environmentally friendly replacement catalysts.

Chapter 3: In the first part of the thesis, a general approach to identify the best catalyst for the acetylene hydrochlorination reaction using a data set of key performance indicators has been introduced. The proposed universal method allows a direct comparison among metal and metal-free catalysts and demonstrates that Au-based catalysts are the best-in-class materials for this particular reaction.

Chapter 4: This part of the study is focused on identifying the structure-activity relationship of the carbon support, and therefore a sequence of characterizations studies was performed. The physical and chemical properties of the carbonaceous materials, such as the texture, porosity, surface graphitization, surface functional groups, and surface acidic sites distribution were analysed. The results illustrated that the higher activity is associated with high porosity, high graphitization degree and low surface acidic groups. This work aims to illustrate a rationalized set of criteria for support evaluation and development.

Chapter 5: In this study the effect that N-methyl-2-pyrrolidone (NMP) has on improving the activity and the stability of Au-based catalysts has been thoroughly investigated. Using a simple wet impregnation method, a 1 wt.% Au- NMP catalyst has been prepared. The study showed that the Au-NMP catalyst displays higher activity when tested at different temperatures in comparison to the standard catalyst, while it also exhibits a greater performance when compared to the commercial catalyst as validated at Johnson Matthey. Characterisation of the Au-NMP complex, including single crystal diffraction, Raman, IR spectroscopy and NMR, confirmed the coordination of the NMP to the Au centre via the N moiety, while it was identified that the structure of Au-NMP is a salt complex with a 1:2 ratio respectively. Finally, a series of NMP derivatives were used for the preparation of 1 wt.% Au-$NMP_{(derivatives)}$ illustrating that the co-existence of O and N is of a great importance for the high activity of the catalyst, as seen from the comparison of NMP with analogous structures.

Acknowledgments

I would like to thank Graham Hutchings for allowing me to join his team in the Cardiff Catalysis Institute and carrying out my research as part of his group; it has been an honour. Special thanks to Peter Johnston from Johnson Matthey for funding my project and for the valuable advice and guidance throughout my research. I am also grateful to Joost Smit from Johnson Matthey who has also been guiding me during my PhD. The feedback and comments received from all of you have been precious. All of you have been fantastic mentors and I wouldn't be here if it wasn't for your help and support. Thank you!

I would also like to acknowledge the amazing team of mentors in Cardiff. Sam Pattisson, thank you for everything. For the supervision, for the support, the advice and for the guidance you provided when I addressed to you with some personal affairs. You are a superstar. Sam also thank you for proofreading my thesis. Special thanks to Nick and Louise, who have been guiding me during my research, and Angeles who has also joined the VCM team and has helped me to dust off and improve my XAFS analysis skills during our weekly classes.

I would like to thank Dave Morgan for his help with XPS analysis at Cardiff University as well as Benson Kariuki for his help with Single Crystal Diffraction. I wish to recognise the help of Martin Wilding who has been providing XAFS acquisition at the Diamond Light Source. Steve Morris I wouldn't have a rig to work with if it wasn't for you. Thank you for being a hero when in need. Also, thanks to Chris and Greg for the technical support in the Maxent labs.

I am grateful to my research team at the CCI. So many great people and friends that I made through the years, made my PhD time less frustrating. Special thanks to Simon D. for training me on the VCM rigs and passing down his knowledge, and many thanks to Tanja P. for training me on characterisation techniques. I would like to thank Alba for being a great company in the lab and for being a great friend. Also, I wish to thank Yanlin, Alex, Naomi and Isla who have been fantastic. In addition, special thanks to my closest friend Chara P.

The final thank you is dedicated to my beloved parents. I wouldn't be here if it wasn't for them.

Μαμά, Μπαμπά σας αγαπώ και σας ευχαριστώ για όλα!

Table of Contents

Chapter 1

Introduction

1.1 Overview

In this chapter, the fundamentals of heterogeneous catalysis will be discussed. In addition, the recent advantages, and challenges in the development of environmentally friendly catalysts for acetylene hydrochlorination will be outlined. Emphasis will be given on the progression of Au-based catalysts for the replacement of the toxic Hg catalyst for the acetylene hydrochlorination reaction, and their further expansion to industry.

1.2 A brief introduction to catalysis

The term catalysis refers to the phenomenon in which a compound denoted as the catalyst is used to change the rate of a chemical reaction, without being consumed.[1] Catalysis has been known to humanity from ancient times. The earliest example of a catalytic reaction is referred to be the production of alcohol from sugar using yeast. Fermentation has been well-known for over 8000 years, with beer first being produced in ancient Egypt and Mesopotamia.[2] The earliest recorded application of inorganic catalysts is from 1552 by Valerius Cordus when sulfuric acid was employed for the transformation of alcohol to ether.[3] While, the first application of heterogeneous systems is chronicled in the 1800 when Joseph Priestley and Martinus van Marum independently studied the dehydrogenation of alcohol on the surface of metal catalysts.[4] However, neither of them managed to recognise the role of the metals as catalysts, seemingly thinking that the metals only supplied heat for the reaction to process.

The term catalysis was introduced by the Swedish chemist Jöns Jakob Berzelius in 1835, based on the Greek words kata (κατά) meaning under/down and lyein (λύση) translated as loosen, which were combined to form the word kataluein (dissolve) and then katalusis.[5] Both the term and the phenomenon were a subject of dispute during the 19th century until Wilhelm Ostwald proposed a now generally acknowledged description according to which "A catalyst is a substance that accelerates the rate of a chemical reaction without being part of its final products".[6] Catalysis and catalysts nowadays are terms widely used and understood, whereas the International Union of Pure and Applied Chemistry (IUPAC) sets the following definition for catalyst: "A substance that increases the rate of a reaction, without modifying the overall standard Gibbs energy change in the reaction; the process is called catalysis. The catalyst is both a reactant and product of the reaction. The term

catalysis is also often used when the substance is consumed in the reaction (for example: base-catalysed hydrolysis of esters). Strictly, such a substance should be called an activator".[7]

A chemical reaction includes the breaking of the bonds between the reactants, and the formation of new bonds for the creation of new species. Traditionally, catalysts can be divided into three categories 1) Homogeneous catalysts, 2) Heterogeneous catalysts and 3) biocatalysts. Homogeneous catalysts are present in the same phase as the reactants and the products. On the other hand, heterogeneous catalysts are in a different phase from the reactants and products. For instance, heterogeneous systems may include the coexistence of more than one phase, with the most usual case, the involvement of a solid catalyst, while the reactants and products are in the liquid or gaseous phase. Biocatalysts are predominantly proteins. The different classification of catalysts is related to the nature of the systems.[8] In our case, the acetylene hydrochlorination reaction is a heterogeneous system as it involves reactants and products that are in the gas phase while the catalyst is a solid.

1.3 Heterogeneous systems

In industry, approximately 85-90% of the reactions are catalysed, and approx. 80 % of those reaction include heterogeneous systems (Figure 1.1). Heterogeneous catalytic systems display many advantages as they are easy to handle and separate from the reactants whilst, they can also be reused. Furthermore, they can endure under the intense industrial operating conditions and, therefore, heterogeneous catalysts are widely desired in industry for large scale.[9]

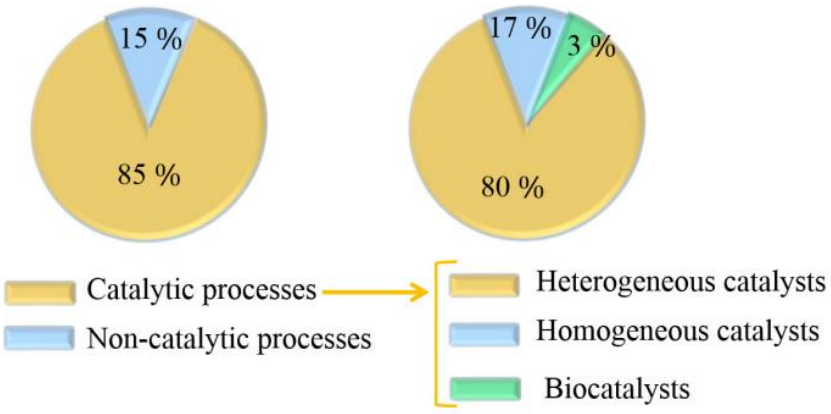

Figure 1.1 Diagram displaying the impact of catalytic processes to the industry and the contribution of heterogeneous catalysis in contrast to other catalytic processes.[7]

For any catalytic reaction, the effect of the catalyst on the reaction rate can be easily described by the potential energy diagram of a catalysed and non-catalysed reaction diagram (Figure 1.2).[10] The difference in the potential energy of the reactants A, B and the product P refers to the change in Gibbs free energy (ΔG) of the reaction. In the absence of the catalyst, the reaction rate is slower due to the high activation energy E^+ that is required. In contrast, upon the presence of a catalyst the rate of the reaction increases as the catalyst provides an alternative pathway for the reaction to proceed that has a lower energy barrier E^+_{cat} than the uncatalyzed reaction. The catalyst eventually does not have any impact on the thermodynamic balance of the chemical reaction.

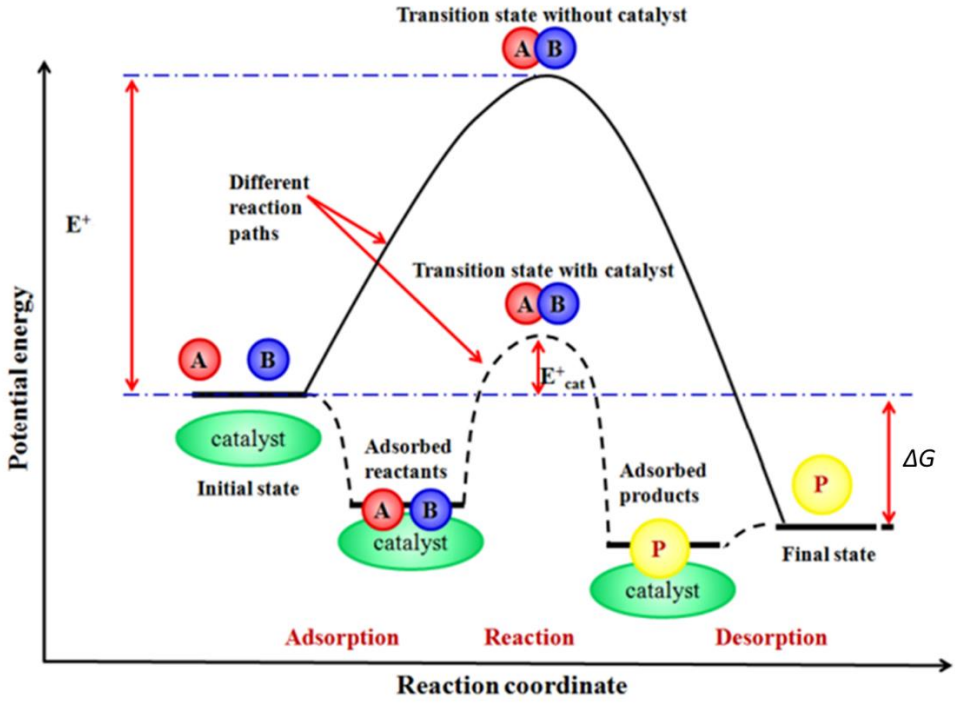

Figure 1.2: Schematic representation of an energy diagram of a chemical reaction in the presence or absence of a catalyst.[11]

For any reaction that follows the scheme: A+ B → P, where A, B are the reactants and P is the product formed, the kinetic rate of the reaction (r) can be expressed as:

$$\mathrm{r} = \mathrm{k}[\mathrm{A}]^{\alpha}[\mathrm{B}]^{\beta} \quad eq.1.1$$

In the equation 1.1 [A] and [B] denote the concentrations of reactants A and B, while α and β represent the exponential factors indicating the orders of reaction. The rate constant k of the reaction can be expressed by Arrhenius equation as followed:

$$\mathrm{k} = \mathrm{A}e^{-\mathrm{Ea/RT}} \quad eq.1.2$$

In the equation 1.2, A is the pre-exponential factor related to frequency of collisions, T is the absolute temperature (K), E_a is the activation energy for the reaction (J mol^{-1}) and R is the universal gas constant (J mol^{-1} K^{-1}). E_a and T affect the rate of a reaction exponentially with E_a representing the energy that is required to start any chemical reaction and it is depending on the nature of the chemical reaction. Decreasing the E_a of a reaction, with the use of a catalyst, the kinetic constant k will enhance, therefore the reaction rate will subsequently increase. Overall, the rate of the catalytic reaction equals to the rate of the slowest step. A typical heterogeneous catalytic process involves a sequence of elementary steps (Figure 1.3).[12] Initially, the reactants are diffused (mass transferred) from the bulk fluid to the external surface of the catalysts, wherefrom the reactants will be further diffused from external surface of the catalyst to its pores. Accordingly, the reactants will be chemisorbed, react on the surface of the catalyst and the produced product will be desorbed from the surface of the catalyst. Following, the product will diffuse from the pore to the external surface of the catalyst until it is finally diffused from external surface of the catalyst to the bulk fluid.[13]

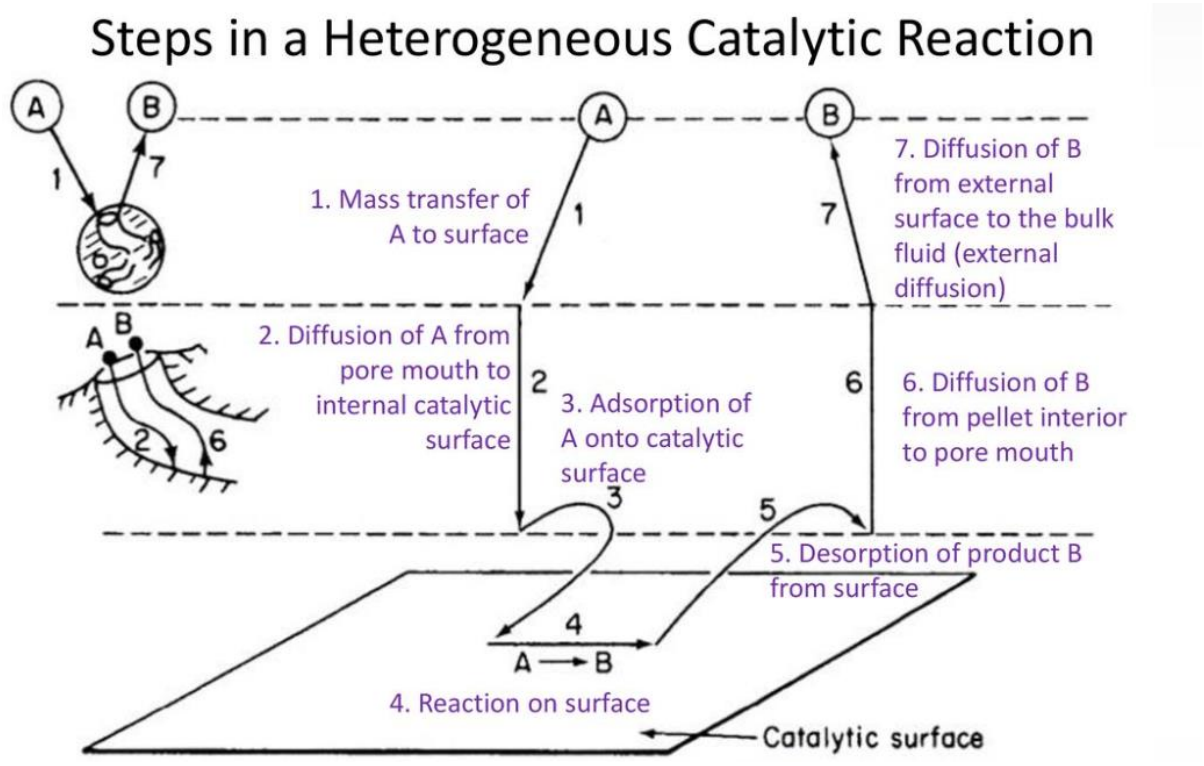

Figure 1.3: Representation of steps in heterogeneous catalytic processes.[13]

1.4 Vinyl Chloride Monomer (VCM) Production

VCM (CH_2=CHCl) is a colourless, flammable gas, with a boiling point of −13.4 °C. VCM has a pleasant odour which can be detected at concentrations of 500 to 2000 ppm. VCM is

denser than air and explosive at concentration of 3.6-25 vol% with air, while only 12 vol% O_2 can be required for ignition. Upon burning, VCM decomposes, generating toxic and corrosive fumes such as hydrogen chloride and phosgene.[14] VCM has an intoxicating effect at concentration of 8-12 vol% causing dizziness, disorientation, and numbness, while it can be lethal at higher concentrations.[15] The first record of VCM being produced can be traced back to 1835 when Justus von Liebig and Henri Victor Regnault treated 1,2-dichloroethane with a solution of potassium hydroxide in ethanol.[16] In 1912 Fritz Klatte patented the synthesis of VCM. The catalytic hydrochlorination of acetylene using a $HgCl_2$ catalyst is protected under the Imperial German Patent DRP 278249 of 11. 10. 1912 and DRP 288584 of 11. 9. 1913.[17]

Worldwide VCM production is expected to grow over the following few years, potentially expanding from 50.67 million tonnes per annum (mtpa) in 2021 to 53.89 mtpa in 2026, showing an overall increase of 6%.[18] VCM is a significant petrochemical intermediate, as it is predominantly used as a precursor material to produce polyvinyl chloride (PVC) *via* suspension polymerization (Figure 1.4).[19] PVC is the third most widely produced polymer, after polyethylene and polypropylene, as it is a desirable material for construction and has found practical applications in other industries. Due to its unique physical properties that depend on the morphology, versatility and structure of the PVC polymer, the flexibility and the rigidity of the material can vary significantly depending on the polymer chain size. Therefore, the high adaptability of PVC leads to a great demand of this polymer, setting subsequently VCM a valuable chemical.[20]

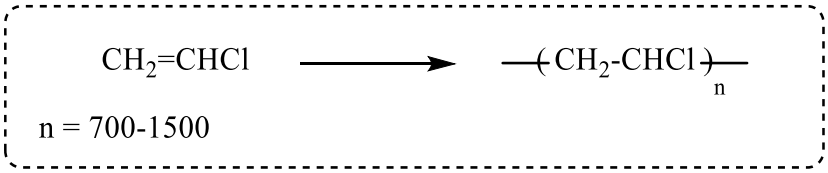

Figure 1.4: Polymerisation of polyvinylchloride (PVC) from Vinyl Chloride Monomer (VCM).[21]

There are several methods to produce VCM depending on the feedstock used. Acetylene and ethylene are C2 hydrocarbon sources that can be utilized for the manufacture of VCM. The major industrial processes to produce VCM are described below.

1.4.1. The balanced process

The balanced process is a significant reaction to produce VCM, representing the manufacture of 95% of the world's supply.[22] Based on oil-derived feedstocks, employing ethylene as a source, it is a multistep reaction that includes the direct chlorination and oxychlorination of ethylene (or ethene, C_2H_4) to produce ethylene dichloride (EDC).[23]

Ethylene dichloride subsequently undergoes thermal cracking to generate the VCM. The direct chlorination step requires lower operating temperatures and yields less by-products in comparison to oxychlorination. During the Oxychlorination process the hydrochloric acid (HCl) that is produced during the direct chlorination step as a major by-product is recycled. This multistep process became the primary process for the VCM production, primarily in Europe and the US, as the increased availability of oil, made ethylene a broadly available feedstock. However, due to rising oil prices, the balanced process is set to become less economically appealing. In addition, the high carbon footprint of oil, related to the intensive process of ethylene extraction requires alternative routes for the production of VCM.[24] Each reaction step for the balanced process can be seen below:

Direct chlorination: $CH_2CH_2 + Cl_2 \rightarrow ClCH_2CH_2Cl$

Oxychlorination: $CH_2CH_2 + 2\ HCl + ½\ O_2 \rightarrow ClCH_2CH_2Cl + H_2O$

EDC pyrolysis: $2\ ClCH_2CH_2Cl \rightarrow 2\ CH_2CHCl + 2\ HCl$

Overall reaction: $2\ CH_2CH_2 + Cl_2 + ½\ O_2 \rightarrow 2\ CH_2CHCl + H_2O$

1.4.2. Direct Acetylene Hydrochlorination reaction to produce VCM

Based on coal for the production of acetylene, the direct acetylene hydrochlorination is a major industrial process to manufacture VCM, in coal-rich countries such as China.[25,26] Today, Asia represents the largest sales market for PVC with a worldwide production expected to increase by ca. 2.3% per year, until the 2024.[27] In this single step reaction process, the acetylene reacts over a catalyst with HCl to produce VCM as seen below:

Direct acetylene hydrochlorination: $CHCH + HCl \rightarrow CH_2CHCl$

This process will be discussed thoroughly in this chapter. Challenges, opportunities, and breakthroughs in the field of catalyst development for the acetylene hydrochlorination reaction will be addressed in detail.

1.5 Hydrochlorination of Acetylene; Hg-based catalysts

Acetylene hydrochlorination reaction is an exothermic process (ΔH = -99 kJ mol^{-1}), typically operated at relatively low pressures of 1-2 bar, and at temperatures varying from 100-200°C.[28] Typically in this process a high metal loaded mercuric chloride (5–12 wt.%) ($HgCl_2$) supported on a high surface area activated carbon is employed as a catalyst.[29] High surface area activated carbons are mainly used as supports due to their chemical resistance in the presence of HCl at high temperatures, advanced acetylene adsorption capacity, relatively low cost and high surface area which ensure high metal adsorption and dispersion.

Therefore, the majority of studies on acetylene hydrochlorination operate employing carbon as the support.[30-33]

Despite the dominance of the $HgCl_2$ catalyst for the production of VCM over the past few decades, this catalyst presents many disadvantages.[34-36] Namely, the $HgCl_2$ catalyst undergoes thermal degradation at elevated reaction (180–220 ^oC) as $HgCl_2$ desorbs from the support surface and is lost to the environment. Additionally, the exothermic nature of the reaction leads to the formation of hot spots in the fixed bed reactor, intensifying the sublimation of $HgCl_2$ from the support.[37] It is estimated that for every 1 ton of VCM produced, approximately 0.6 kg of Hg is leached to the environment.[38] The high volatility of $HgCl_2$ at the reaction temperature results in a high loss of Hg from the catalyst bed, leading to short catalyst lifetimes. Furthermore, the $HgCl_2$ catalyst can catalyse a secondary addition of HCl to VCM decreasing the selectivity of the reaction. The latter of these issues can be dealt using a downstream ethane dichloride cracking unit to attain the VCM product, however this adds to the process complexity.[30]

Different approaches to improve the thermal stability of Hg-based catalysts for the hydrochlorination of acetylene have been developed. Employment of additives, for example potassium halides, in the aqueous solutions of $HgCl_2$ during catalyst preparation increased the activity and the stability of the catalyst by significantly reducing the desorption rates. Furthermore, alkali chlorides, when used as ligands, improved the stability of Hg catalysts. Li *et al*. reported advanced stability over CsCl when co-impregnated with $HgCl_2$ to the support.[39] In addition, Wei *et al*. reported metal oxide supported low-Hg catalysts with improved stability.[40] Despite the different strategies, the thermal stability issues are still unsolved. The loss of $HgCl_2$ does not only lead to the deactivation of the catalysts but also causes serious environmental issues.[29] Despite the attempts to recover the lost Hg, nearly 25% of it is released immediately into the environment. To resolve this problem, the Minamata Convention has agreed on controlling Hg emission by setting a plan of reduction act in 2013, as signed by the United Nations Environment Protection Committee. The agreement came into effect on 16th August 2017. This treaty includes a clause which states that new VCM plants are allowed to use a Hg catalyst after 2017 and all VCM plants must be Hg-free after 2022, if a suitable alternative is found.[41]

1.5.1 Hydrochlorination of Acetylene; Discovery of Au-based catalysts.

In the 1980s two landmarks drew scientific attention towards Au catalysis. Au chemistry had previously been neglected as it was considered a non-active, noble metal. Haruta, and

Hutchings changed the history of Au catalysis.[42] The first one illustrated that Au nanoparticles could oxidise CO at low temperatures,[43] and the latter proving that Au can be used as an active and effective catalyst for the acetylene hydrochlorination reaction.[37] Relying on Shinoba's study, in 1985, Hutchings predicted, and later on confirmed, that Au-based catalysts exhibit great activity for the acetylene hydrochlorination reaction.[37] Originally, Shinoba's work included the methodical investigation of different metal chlorides supported on activated carbons for the acetylene hydrochlorination reaction.[44] His endeavour to associate the catalytic activity with the electron affinity of the central metal cations was unsuccessful and could not be used for the identification of a general trend between activity and chosen parameter. When plotting the activities of metal chlorides versus the affinities of metal cations divided by the corresponding metal valences, Shinoba observed that there are two distinctive groups of metal chlorides (Figure 1.5). The upper section of the plot consists of metals which create stable acetylides including Pd^{2+}, Hg^{2+}, Cu^{2+} and Ag^{+}, whiles the lower part consists of metal cations that make stable complexes with HCl behaving as Friedel-Craft catalysts. Based on the plot, it is visible that some metal cations, despite presenting comparable electron affinities, illustrate completely different activity profiles, as it is for the case of Zn^{2+}, Cd^{2+}, and Hg^{2+}, whose activities drastically differ. Therefore, the data as presented by Shinoba could not offer any direct information between activity and the electron affinities. Moreover, based on Shinoba's methodology the correlation of the activity with the electron affinity considered only a single electron process, while *ex-situ* FTIR studies completed by Smith *et al*.[45] proposed that the hydrochlorination reaction requires the oxidative addition of acetylene to metal centres, which is a 2-electron process.

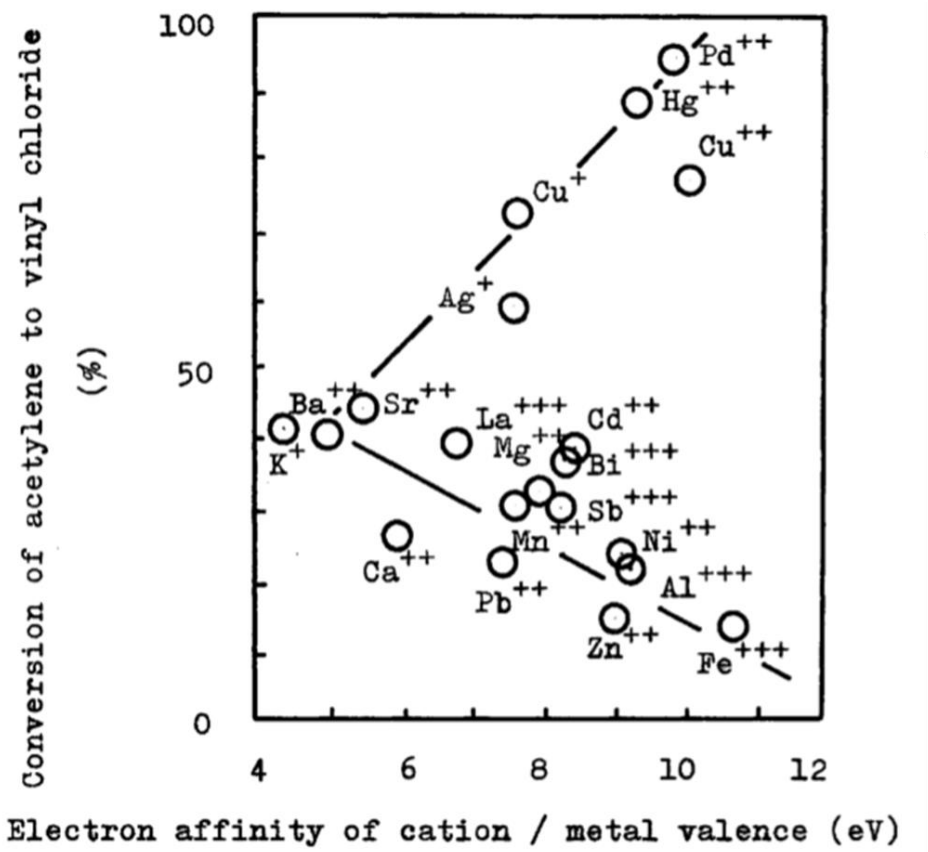

Figure 1.5: Correlation of the hydrochlorination activities of metal chlorides supported on activated carbon and the electron affinities of metal cations divided by the corresponding metal valences.[44]

Re-plotting the data against the standard electron potential, as demonstrated by Hutchings (Figure 1.6), shows that there is a direct correlation between the catalytic activity of the metal chlorides and the standard electrode potential.[37] The increase in the standard electrode potential, leads to enhanced activity of the metal chlorides, suggesting that catalysts with high standard electrode potentials are the most effective for the hydrochlorination reaction. In contrast to Shinoba's graph, it was observed that a single correlation curve was acquired, allowing Hutchings to predict that Au(III) cations, with a higher electrode potential (1.42 V) than Hg(II) (0.7961 V) could potentially have greater catalytic activity in the acetylene hydrochlorination reaction.[46] The redox properties of the metal cations confirmed to be a significant parameter explaining the activity of the catalysts, evidentially suggesting a redox mechanism.

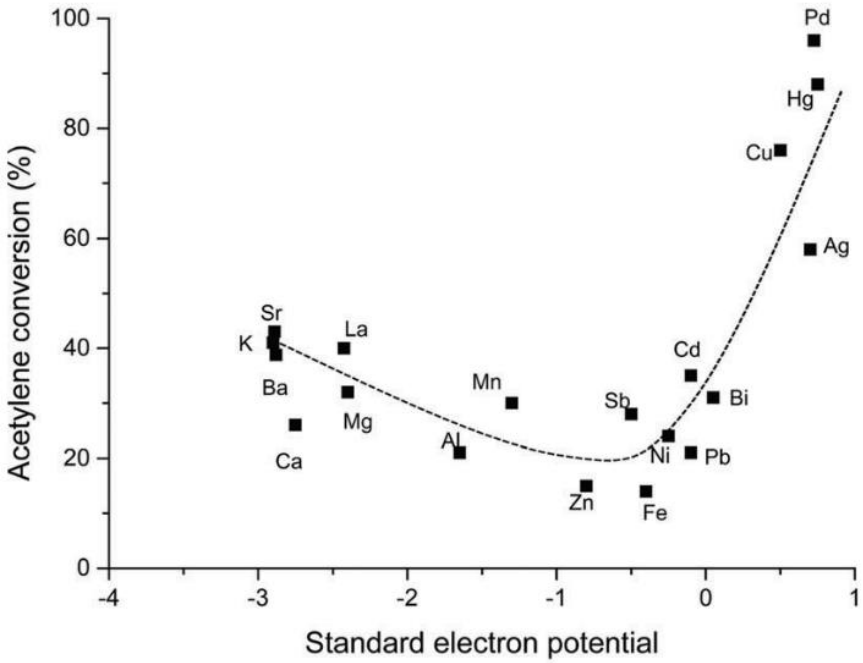

Figure 1.6: Correlation of the hydrochlorination activities of metal chlorides supported on activated carbon and the standard electrode potential.[37]

The correlation between activity and standard electrode potential (E°) has been experimentally confirmed, validating that Au was an effective catalyst for the hydrochlorination of acetylene. The correlation of the standard electrode potential (E°) with the activity has been extensively investigated by Conte *et al*.[47] who confirmed the previous findings. Metal chloride salts have been used for the preparation of catalysts *via* a simple impregnation method where aqua regia was used as a solvent. The precursor salts used in the study were namely the $HAuCl_4$, $PdCl_2$, H_2PtCl_6, $RhCl_3{\cdot}3H_2O$, $IrCl_3{\cdot}3H_2O$ and $RuCl_3{\cdot}3H_2O$. The higher the standard electrode potential, the higher is the activity of the catalyst, with catalytic activity generally decreasing in the following order Au>Ru≈Ir>Pd>Pt≈Rh (Figure 1.7).[48] Recently, this trend had been once again confirmed by Sun *et al*.[48] who used the precursor salts of $H[AuCl_4]{\cdot}3H_2O$, $Ru(C_5H_7O_2)_3$, $Pd(C_5H_7O_2)_2$ and $Pt(C_5H_7O_2)_2$ for the preparation of highly dispersed single site catalysts, synthesised *via* a simple wet impregnation process using acetone as a solvent.[49]

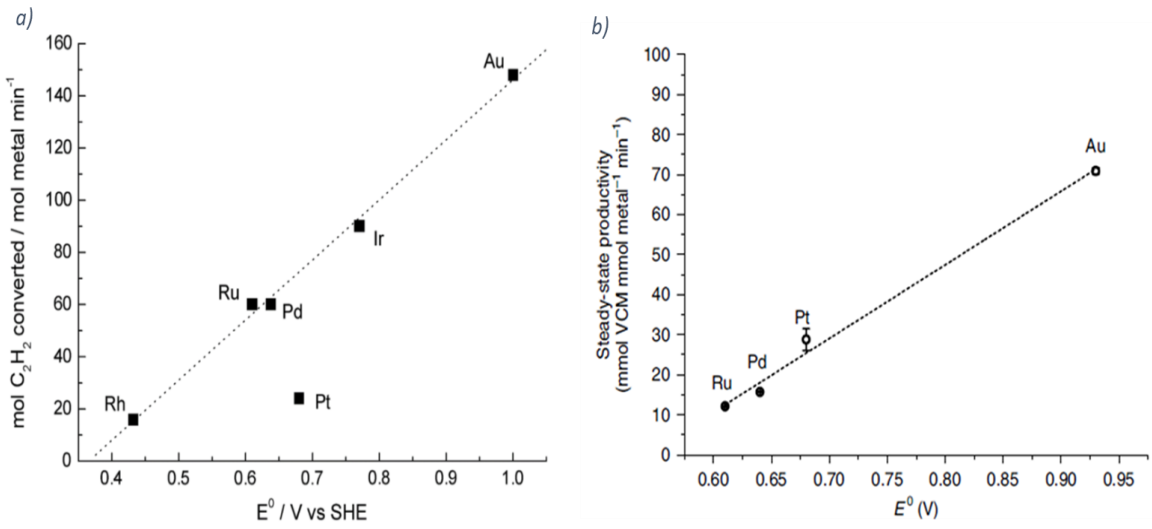

Figure 1.7: a) Correlation between initial acetylene conversion versus the standard electrode potential of the various metals used in this study. Potentials obtained from the reduction potentials of the following chloride salts $(RhCl_6)^{3-}$, $(RuCl_5)^{2-}$, $PdCl_2$, $(PtCl_6)^{2-}$, $(IrCl_6)^{3-}$, and $(AuCl_4)^-$ to the corresponding metals.[48] b) Correlation between the steady-state productivity of acetylene hydrochlorination at 100 min of reaction and the standard electrode potential of the constituent catalyst metals.[49]

1.5.2 Identification of active species on Au -based catalysts.

Initial spectroscopic studies to recognise the nature of active Au species on Au/C catalysts were ineffective to answer the question as to which species were responsible for the activity, as mixtures of Au cations and nanoparticles were observed *via* Au Mössbauer spectroscopy and X-ray photoelectron spectroscopy (XPS) analysis.[50,51] In 2017, Hutchings *et al*.[52] unravelled the mystery behind the nature of the active form for the Au catalyst by performing an *in-situ* X-ray absorption fine structure (XAFS) spectroscopy analysis on 1 wt.% Au supported on carbon prepared by wet impregnation of Au tetrachloride in aqua regia. Unlike XPS, which can cause beam photoreduction of Au (III) salts leading to an overestimation of metallic Au content in the surface of Au/C catalysts,[53] XAFS analysis does not cause any photoreduction due to higher photon incident energy and a lower absorption cross section. This provides a more accurate representation of the Au speciation on the surface of the catalyst.[43] In addition to XAFs studies, scanning transmission electron microscopy (STEM), in compliance with high-angle annular dark-field (HAADF) imagining, on fresh and used catalysts allowed the study of the materials at an angstrom level.[54-56] The high imaging resolution allows the screening of nanometre scale clusters and atoms.

Employing XAFS and STEM-HAADF, it was reported that active catalysts Au/C catalysts consist of single-site cationic Au entities whose activity is associated with the ratio of Au(I) : Au (III). In addition, the *in-situ* monitoring of the catalyst during the reaction allowed the determination of

the dynamic nature of Au cation species, as it was reported that oxidised Au readily shifts from Au(I) to Au(III) and back throughout the reaction, reaching an optimum ratio between Au(I)/Au(III) of 1.5. Furthermore, it was demonstrated that there is a direct correlation between the catalytic activity and Au L_3-edge white-line intensity as determined by the Au(I) : Au(III) ratio (Figure 1.8).[43]

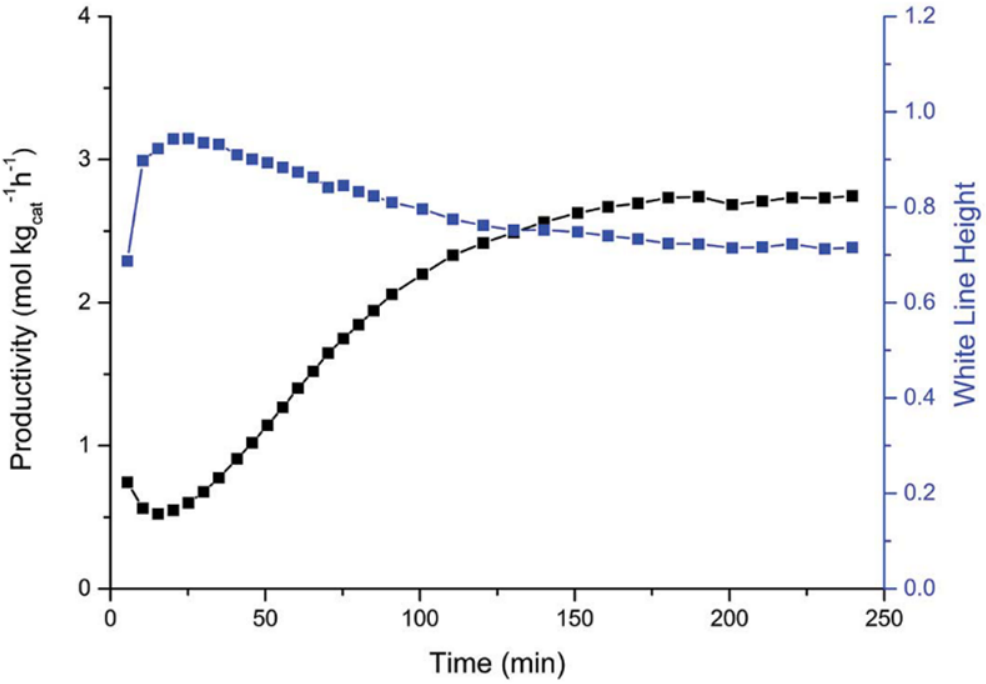

Figure 1.8: Catalytic performance as a function of time-on-line (black) and the change in normalized white-line intensity (blue) as a function of reaction time.[52]

Density functional theory (DFT) calculations have shown that activity of Au catalysts depends on the acetylene adsorption capacity and their consequent activation which are significant elements in the VCM reaction mechanism, as it will be discussed later. However, the adsorption of acetylene over single Au atoms is susceptible to the presence of Cl, with less coordinated centres binding acetylene more strongly and more chlorinated species presenting a lower acetylene affinity.[57] The coexistence of Au(I) and Au(III) species is nevertheless important as this reaction proceeds through a redox mechanism. Single atom species are the active moieties for the hydrochlorination process, not only for Au-based catalysts but other metals as well as other metals, such as Ru,[58] Pt,[59-61] and Cu.[62,63] It has been postulated that the oxidation state of the Pt, as well as the coordination chemistry, of the active single Pt atoms determine the activity profile of the catalysts. In particular, the catalytic activity of single atom (SA) Pt decreases accordingly: Pt(II)−Cl (SA)≫Pt(II)−N(SA) ≈Pt(IV)–Cl(SA)>Pt(0) nanoparticles. Once again, the advanced catalytic performance of

Pt(II)−Cl single atoms is attributed to the increased acetylene adsorption capacity in comparison to other single atom Pt site.[59]

1.5.3 Deactivation and regeneration of Au-based catalysts

As discussed in the previous section, single-site Au species supported on carbon are identified as the active sites for acetylene hydrochlorination, however, despite their great activity, the Au-based catalysts suffer from deactivation. There are two main pathways leading to catalysts' deactivation, namely the reduction of the active Au cationic species [Au (III) and Au(I)] to metallic Au, and the polymerisation of carbonaceous materials on the surface of the catalyst, leading to coke deposition.[64,65] The reaction conditions, such as the gas hourly space velocity, the temperature of the reaction, and the feed ratio of HCl:C_2H_2, the loading of Au metal and the nature of the catalyst support, are decisive factors regulating the deactivation mechanism.[66]

The deactivation of Au on carbon catalyst was investigated by Nkosi *et al*.[66] who studied the impact of temperature on the deactivation rate. Based on this work, two main deactivation mechanisms were identified and associated with the reaction temperature. It was observed that at high temperatures of 120 to 180 °C, Au/C catalyst deactivation was ascribed to the reduction of Au (III) or Au (I) to Au (0), while at low temperatures of 60 to 100 °C, the deactivation was associated with the formation of a polymeric carbonaceous materials on the surface of the catalyst (Figure 1.9).

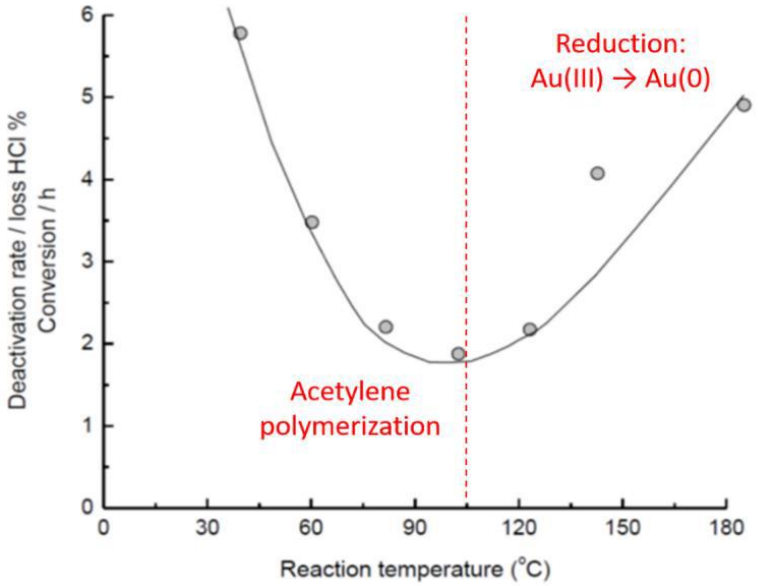

Figure 1.9: Effect of temperature on rate of deactivation of Au/C catalysts for the acetylene hydrochlorination.[66]

Using transmission electron microscopy (TEM) analysis, Johnston *et al*.[28] reported the formation of carbonaceous polymer and carbon-containing nanotubes on the catalyst surface of 1 wt.% Au/C catalyst prepared using aqua regia as a solvent. Both at low and the high magnification there is a clear formation of a significant amount of carbonaceous polymer and carbon-containing nanotubes on the catalyst surface (Figure 1.10). Analysis of the nanotubes indicated that these resulted from acid-catalysed acetylene polymerisation over strong acid sites introduced from the aqua regia solvent during preparation.[67]

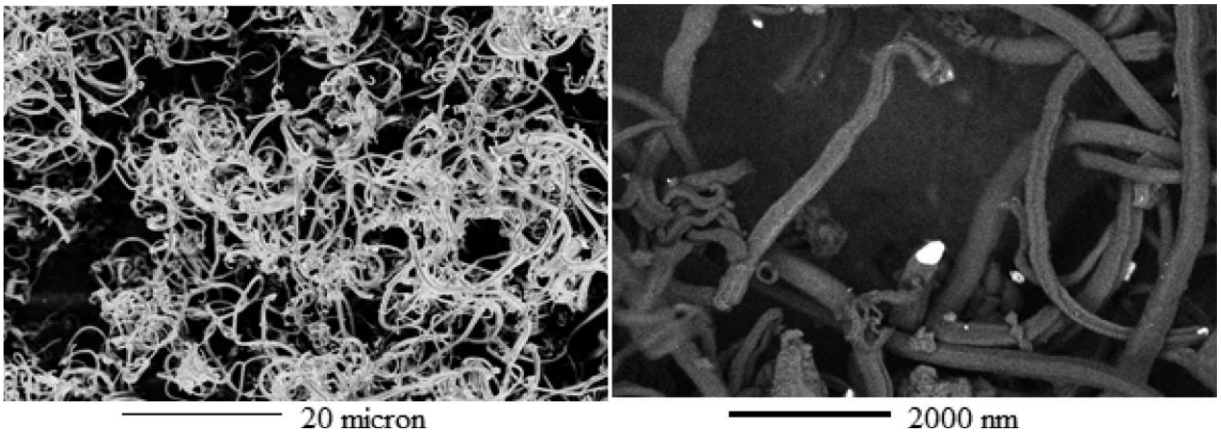

Figure 1.10: TEM analysis of spent aqua regia 1 wt.% Au/C catalyst after use for 24 days at low magnification showing the extent of carbon nanofibers formed on the catalyst (right) and high magnification showing the Au nanoparticle at the tip of the carbon nanofiber (left).[30]

The sublimation, and loss, of Hg from the surface of the catalyst does not allow in principle for the catalyst to be reactivated, as the active component of the catalyst is cleaved from the surface. However, in the case of Au-based catalysts, regeneration is achievable. The deactivation of the Au/C catalysts can be reversed, and the catalysts can be easily re-generated through a range of different methods. Au-based catalysts can be reactivated online and off-line. Online regeneration of Au/C catalysts can be achieved by introducing in the feed line, at the reaction temperature, oxidizing agents such as HCl, Cl_2, NO and NO_2 which eventually reoxidise the metallic Au to the active Au cationic species. It was also noticed that the reactivated catalysts *via* this treatment presented a full recovery of their catalytic activity and exhibited a slower decay afterwards.[51]

Furthermore, it has been demonstrated that it is possible to regenerate Au/C catalysts by an off-line process that includes the treatment of the Au catalysts with boiling aqua for 20 mins, a method that does not alter the overall metal loading. In addition, it has also been

described that Au catalysts can be reactivated using a simple iodohydrocarbon treatment. Based on this method, the inactive agglomerated Au nanoparticles can be redispersed to smaller particles, while it has also been observed that metallic Au has also been reoxidised.[68,69] Finally, it has also been reported coke residuals can be removed by an air oxidation process. This method showed to recover the area of the fresh catalyst, without however, oxidizing the Au(0) to Au(I) and Au(III).[51]

1.5.4 Reaction Mechanism of Acetylene Hydrochlorination

The reactant feed and ratio play a crucial role in the catalytic activity of the Au-based catalyst. Of the two reactants, acetylene shows a poisoning effect on Au catalysts, acting as a reducing agent, causing the reduction of active Au^{n+} species to metallic Au.[70] In order to understand the role of each reactant, Conte *et al*.[71] conducted a series of studies where the importance of each individual reactant has been demonstrated. The effect of C_2H_2 and HCl was investigated as a set of experiments were run, using a 1:1 molar reactant ratio at 180 °C, as followed:

- Experiment A: C_2H_2/HCl (2 h) → He/HCl (2 h) → C_2H_2/HCl (2 h)
- Experiment B: He/HCl (2 h) →C_2H_2/HCl (2 h) →He/ HCl (2 h)
- Experiment C: C_2H_2/HCl (2 h) → C_2H_2/He (2 h) → C_2H_2/HCl (2 h)
- Experiment D: C_2H_2/He (2 h) → C_2H_2/HCl (2 h) → C_2H_2/He (2 h)

The outcomes of the experiments are illustrated in figure 1.11. As it can be noted C_2H_2 and HCl can alter the final performance of the catalyst in opposite ways. From experiments A and B it can be seen that HCl has a positive effect on the activity of the catalyst. In process A, where the middle step involves the introduction of, He/HCl, it is noticed that the catalytic activity remains intact when the reactant gases are reintroduced in the final part of the experiment. In test B, where the primary step involves treatment with, He/HCl, upon the introduction of the acetylene, the activity is enhanced. This behaviour can be attributed to the fact that the initial HCl treatment oxidizes some metallic Au, as observed during in catalyst reactivation studies.[72]

On the other hand, the detrimental role of C_2H_2 can be observed in the next set of experiments. In process C, where the intermediate step involves the introduction of C_2H_2/He, it is noticed that the catalytic activity decreases significantly after the reactant gases are reintroduced in the last phase of the study. In process D, where the preliminary step involves the introduction of C_2H_2/He, it is noticed that when reactant gases are brought online, the activity of the catalyst is noticeably lower in comparison to a standard reaction

without interruption of the reactants. Based on the experiments that were conducted it was clear that C_2H_2 and HCl play a critical a role in activation/deactivation of the catalyst.

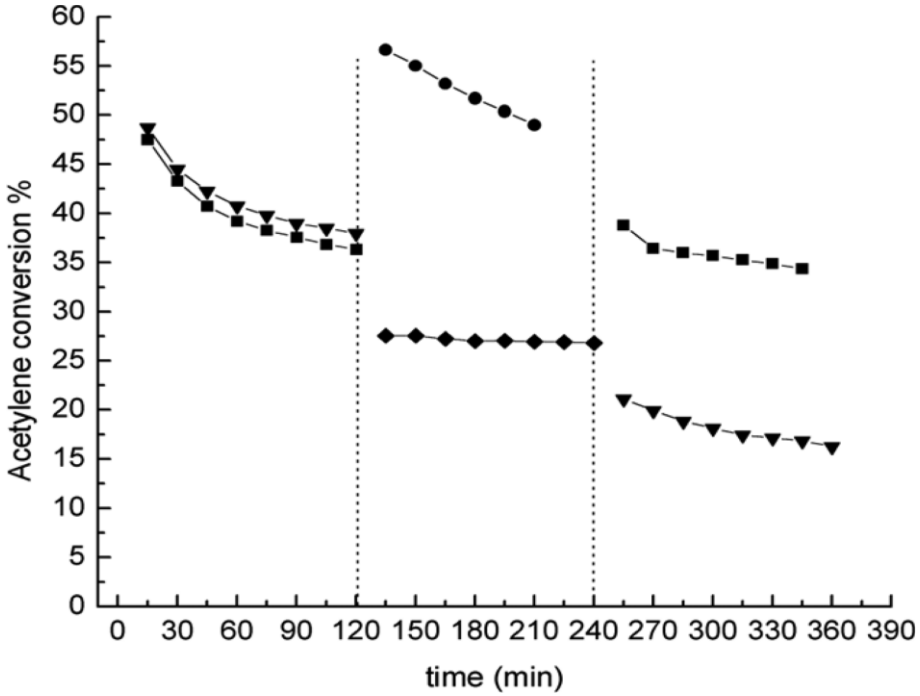

Figure 1.11: Sequential flow experiments to evaluate the effect of each reactant for the hydrochlorination reaction of acetylene over Au/C catalyst. (Experiment A ■) C_2H_2/HCl (2 h)→ He/HCl (2 h) → C_2H_2/HCl (2 h), (experiment B ●) He/HCl (2 h) → C_2H_2/HCl (2 h) → He/HCl (2 h), (experiment C ▼) C_2H_2/HCl (2 h) → C_2H_2/He (2 h) → C_2H_2/HCl (2 h); and (experiment D ◆) C_2H_2/He (2 h) → C_2H_2/HCl (2 h) → C_2H_2/He (2 h).[71]

Kinetic studies on Au/C catalysts illustrate that the reaction is first order with respect to C_2H_2 and HCl, therefore the overall reaction kinetics is second order.[72] In addition, it has also been suggested that an activated speciation of C_2H_2-Au-HCl complex is formed as a reaction intermediate.[73] In contrast to the $HgCl_2$/C catalysts the kinetics studies showed that the rate-determining step of the reaction involves addition of HCl to a C_2H_2-Hg complex in an Eley-Rideal fashion instead of a Langmuir-Hinshelwood mechanism.[73,74] When examining processes that include unsaturated bonds, there are two ways that substituents can be added: syn-addition (substituent molecules added to an alkene ($R_2C=CR_2$) or alkyne (RC≡CR) on same side) and anti-addition (substituent molecules added to an alkene ($R_2C=CR_2$) or alkyne (RC≡CR) on opposite sides). Moreover, for unsymmetrical molecules, addition of hydrogen halides to unsaturated bonds, can lead to Markovnikov or anti-Markovnikov products. With C_2H_2 being a symmetrical molecule, the reaction of C_2H_2 and HCl does not provide mechanistic information as only one product is possible to be

generated. For this reason, the mechanism of hydrochlorination of longer chain acetylenes have been investigated by Conte *et al*.,[71] using the substrates (Figure 1.12).

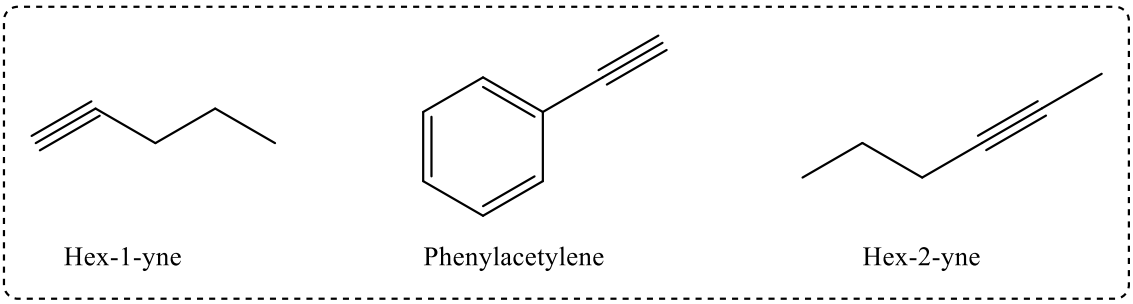

Figure 1.12: Substituted alkyne substrates used to investigate the mechanism of HCl addition across the alkyne bond.[63]

Based on the study it was shown that hydrochlorination of hex-1-yne leads to the formation four different products (Figure 1.13). ^{1}H NMR spectroscopy showed that there is high selectivity towards the Markovnikov products **1** and **2** while only traces of by the anti-Markovnikov product **4** were observed and product **3** not formed. Hex-2-yne showed to be inactive, as no products were formed, demonstrating the significance of steric hindrance in this reaction. ^{1}H NMR spectroscopy on the deuterated reagents was employed to understand whether the Markovnikov products are formed by syn or anti addition of HCl. For hex-1-yne/DCl, only one deuterated Markovnikov product with anti-stereochemistry was detected, leading to the conclusion that that this product is formed *via* anti addition of DCl to hex-1-yne.

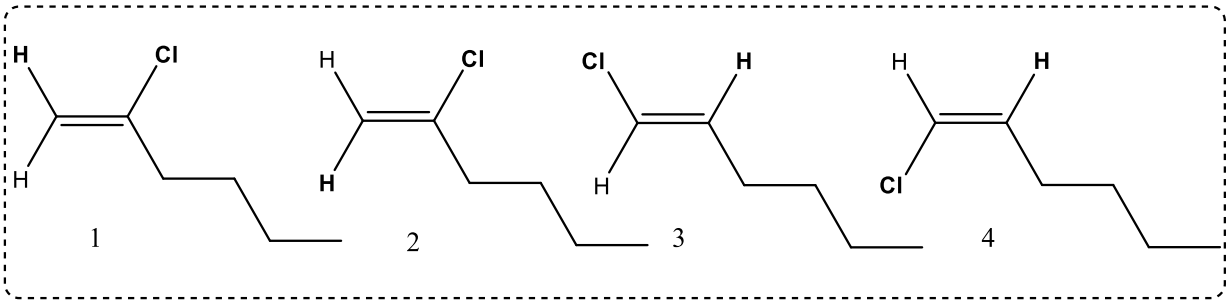

Figure 1.13: Possible Regioselectivity and Stereochemistry of the Addition of HCl to hex-1-yne: 1 Markovnikov with syn HCl Addition, 2 Markovnikov with anti HCl Addition, 3 anti- Markovnikov with syn HCl Addition, and 4 anti-Markovnikov with anti HCl Addition.[71]

Phenylacetylene was less active than hex-1-yne, as a result of the conjugation of the triple bond with the aromatic ring. Of the possible four products (Figure 1.14) the main ones were determined to be the Markovnikov products **5** and **6** while only traces of the for the anti-

addition of HCl **8** product were detected. Once again, the product **7** has not been recorded.71

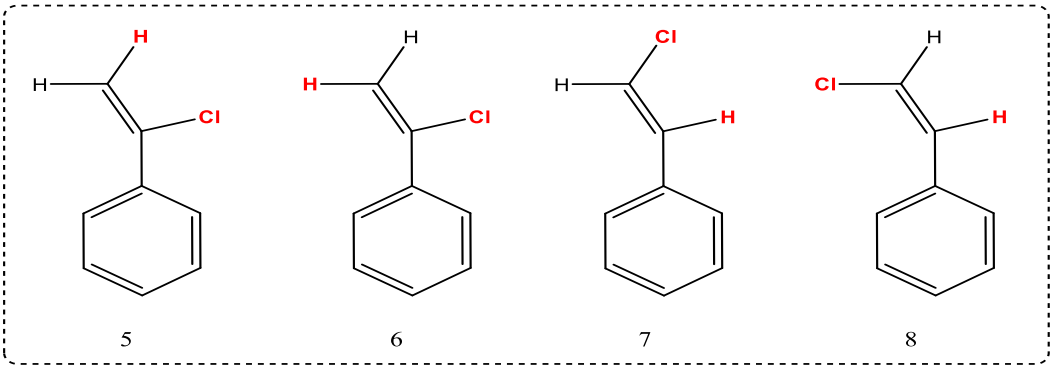

Figure 1.14: Possible Regioselectivity and Stereochemistry of the Addition of HCl to hex-1-yne: 1 Markovnikov with syn HCl Addition, 2 Markovnikov with anti HCl Addition, 3 anti- Markovnikov with syn HCl Addition, and 4 anti-Markovnikov with anti HCl addition.[71]

According to the experimental evidence, it is possible to suggest that the reaction mechanism by which alkyne hydrochlorination occurs using the Au catalyst that the addition of HCl is complying with the Markovnikov rule and in an anti-configuration to the alkyne. In addition, it has also been postulated that the hydrochlorination of acetylene over Au/C catalyst, involves a C_2H_2-Au-HCl complex (Figure 1.15). This complex can be illustrated as a distorted six membered ring between Au (III) centre, Cl and CH≡CH with chloride as the counter ion.[75] According to the mechanism, there is a dynamic alteration between Au(I) and Au (III) species as observed by *in-situ* extended X-ray absorption fine structure spectroscopy (EXAFS). Initially, the oxidative addition of HCl to Au(I)-Cl leads to the creation of a Au(III) complex, accompanied by the addition of C_2H_2 and finally the reductive elimination of C_2H_3Cl.[44,76] The mechanism proposed above associates the theoretical studies with the experimental results based on a redox couple of Au(I)/Au(III) species.

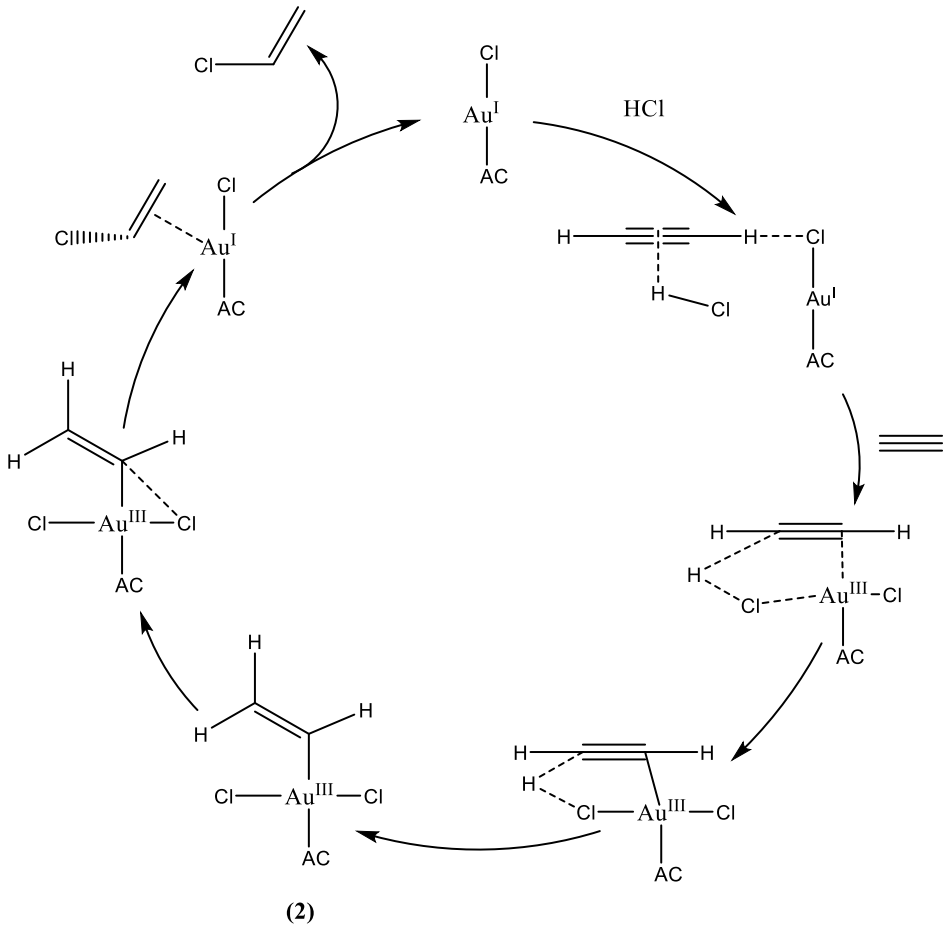

Figure 1.15: Proposed model for the hydrochlorination of acetylene over Au/C catalyst.[75]

1.5.5 Approaches and novelties on catalyst preparation

The method of catalyst preparation is crucial for its catalytic activity. Aqua regia has been widely used in research for catalyst preparation.[30,77] However, from an industrial point of view, it is a non-desirable solvent to use. The corrosive, hazardous, environmentally unfriendly profile of this solvent raises many concerns regarding its practice. Moreover, Au catalysts prepared using aqua regia, suffer from rapid deactivation due reduction of the active species a fact that is associated with the introduction of acid sites during the catalyst preparation.[30] Preparation of Au/C catalysts as using aqua regia demands approximately 500 kg aqua regia per tonne of catalyst produced. Therefore, the usage of aqua regia in the catalyst preparation creates worries both from an economic and a technical perspective, regarding the processing, recovering, and discarding of this toxic and corrosive solvent. In 2010 Zhao *et al*. reported the less hazardous, and safer in comparison to conventional aqua regia, organic aqua regia (OAR) which is a mixture of thionyl chloride ($SOCl_2$) and N,N-dimethylformamide (DMF).[78] The Au supported on activated carbon catalysts prepared

using OAR exhibited a high catalytic activity while prepared from aqueous $HAuCl_4$. However, the corrosive nature of OAR does not offer a sustainable alternative to more commonly used aqua regia. Last of all, the rising cost of Au over the past years requires the use a low Au metal loading (<0.25 wt%). Unfortunately, Au loadings of Au/C catalysts prepared from aqua regia below ca. 0.3% present difficulties in the catalyst activation, completely prohibiting the usage of this solvent for catalyst preparation.[30,79]

In 2017 Johnson Matthey focused on the development a Au/C catalyst in the need of substituting the toxic $HgCl_2$/C catalyst that were used in tubular fixed bed reactors in China.[30] Seeking to discover a catalyst that would secure the stability of the active Au cationic species, Au-ligand complexes that contained a wide range soft and hard donor atoms were investigated. It was observed that ligands with soft donor atoms such as cyanides, thiourea, thiosulfate, thiocyanate demonstrated greater stability in comparison to ligands with hard donor ligands such as halides, nitrogen, and oxygen atoms. Table 1.1 summarizes the results of the screening studies, in which the catalytic activity of the cationic Au complexes has been assessed for acetylene hydrochlorination reaction.

Au precursor complex	***Au %***	***conversion %***
$Au(CS(NH_2)_2)_2$	0.1	95
$Na_3Au(S_2O_3)_2$	0.1	86
$KAu(CN)_2$	0.1	85
$(NH_4)_3Au(S_2O_3)_2$	0.1	75
$KAu(SCN)_4$	0.1	74
$Ca_3[Au(S_2O_3)_2]_2$	0.1	74
$KAu(CN)_4$	0.1	69
$Au(NCNH_2)_2$	1.0	55
$HAuCl_4$ + Aqua regia	1.0	52
$HAu(C_3Cl_3N_3O_3)_3Cl$	1.0	52
$[Au(P(NCH_2CH_2OCH_2CH_2)_3)_2]NO$	1.0	33
$[(AuCl)_2dppe]$	1.0	14
$[Au(en)_2]Cl_3$	1.0	14
$HAuCl_4 + H_2O$	1.0	11
Blank Carbon extrudate (no Au)	0	7

Table 1.1: Catalyst screening of Au/C catalysts prepared using different precursor complexes. Test conditions: catalyst 5g, HCl flow 60 mL/min, C_2H_2 flow: 50 mL/min. Reactor temperature = 130 °C, total Gas Hourly Space Velocity (GHSV) = 500 h^{-1}. Conversion measured after 24 h reaction time online.[30]

The catalytic activity of Au complexes that include sulphur-containing ligands such as the Au-thiosulfate, Au-thiourea, Au-thiocyanate, exhibited greater activity than the catalysts resulting from $AuCl_3$. The advanced activity of the immobilised Au-ligand complexes permits the Au loading to be reduced to the range of 0.15−0.6% metal loading, offering economic advantage while attaining acceptable conversion values. Furthermore, low Au metal ensures minimisation of the reaction exotherm within the reactor and the avoidance of hot-spots formation within the reactor. In addition, all the catalysts have been produced in this study included the immobilisation of cationic Au complex on carbon extrudates from aqueous solutions, eventually averting the application of aqua regia. The Au-S containing catalyst developed during this project is currently commercialised as part of the Johnson Matthey's PRICAT catalyst finding application in the only Hg-free process currently offered for license (DAVY VCM process).[80]

It has also been reported that atomically dispersed cationic Au species catalysts can be prepared using low polarity, low boiling point solvents. Utilizing a simple wet impregnation method, where acetone was employed as a solvent, highly dispersed cationic species of Au/C, Ru/C, Pd/C and Pt/C catalysts with relatively high metal loadings were reported.(49) Wei *et al*.[81] and co-workers reported a low Au loading of 0.25 wt% by coordinating Au cations with thiocyanate (–SCN). It is postulated that thiocyanate species can decrease decreases the electrode potential of Au (III) cations from 0.926 V to 0.662 V, therefore preventing the Au catalyst deactivation by the reduction caused from acetylene.

1.5.6 Effect of the ligand environment

The nature of ligand choice in Au acetylene hydrochlorination has been partially studied, with catalyst preparations using Schiff-base Au complexes,[81] thiourea complexes,[82] and a range of other Au(III) and Au(I) sulphur containing complexes.[83-85] While the metal nuclearity and oxidation state have been thoroughly studied in catalysts prepared from aqua regia, inadequate information exists around the ligand environment surrounding the metal centres. In 2020 Malta *et al*.[86] reported a Cl K-edge XANES study on Au/AC catalyst where it was illustrated that 3 distinctive Cl species are present, namely the unreactive inorganic Cl, the covalently bound C–Cl and the Au–Cl species. In addition, it was suggested that Au–Cl species have a dynamic relationship upon heating and during reaction conditions, as variations in Au–Cl bond hybridisation and bond length surface are observed. Furthermore, Cl is withdrawn from the carbon surface throughout the reaction, indicating the significance of surface groups in influencing Au–Cl speciation.

Also, the role of the O on the surface support has also been investigated by Pattisson *et al*.[87] who modified the surface of the support using a Hummers chemical oxidation method before depositing Au. It was reported that highly oxidized carbon supported catalysts exhibited an advanced activity when compared to standard Au/C material, with an optimum level of 18 O at %, as further oxidation leads to surface area and microporosity decrease leading to less active materials. Despite the great activity the catalysts showed, they suffered from rapid deactivation however, a correlation between low temperature activity and O at % was observed. O functionalities, in the form of phenol, carboxylate, and ether, are considered to be descriptors of low temperature activity with the relative concentration of O directly correlating with light-off temperatures. In addition, Pérez-Ramírez *et al*.[81] reported that oxygenated surface functional groups influence the catalyst's stability. Study of a range of carbons with variable O amounts illustrated that high level of acidic functionalities on the carbon host leads greater amount of coking in Pt and Ru catalysts, significantly increasing the deactivation rate. Similarly, Au catalysts exhibited a higher activity, yet poor stability on supports that bore higher amounts of O.

Dawson *et al*.[88] recently prepared Au/C carbon catalysts doped with S, using a range of S-containing compounds, illustrating that S is a promising promoter for the Au catalysed hydrochlorination of acetylene. It has been reported that catalyst activity was found to be sensitive to the identity of the cation in the sulphate precursor and, also the order of preparation. In particular, pre-washing the carbon support with sulfuric acid resulted in catalysts with a high activity, whilst post-washing, results in catalysts with a poorer performance than the pre-washed, which however were still more active than Au/C-AR. EXAFS indicated the presence of another interaction other than Au-Cl, most likely to be that of Au-S species. Furthermore, Qi and collaborators,[89] demonstrated that trimethylsulfonium iodide, in the preparation of Au/C catalysts, leads to catalysts with higher activity due to increased adsorption capacity of C_2H_2 and HCl on the surface of the S-doped catalyst. In addition, Duan *et al*.[90] reported that high valency S groups such as $-SO_3H$ and $-SO_2H$ can increase the stability of Au centres while smaller valence type moieties such as -SH do not present the same effect, with the Au catalysts suffering from rapid deactivation.

1.6 Thesis overview

The aims of this thesis are outlined below:

1. Although there is a wide availability of literature publications and patents applied every year discussing novel catalysts developed for the acetylene hydrochlorination

reaction, the identification of the best catalytic system for this reaction is a subject of dispute. For the acetylene hydrochlorination reaction, there are many catalytic systems that claim to be alternatives for the environmentally toxic Hg catalyst. The broad range of catalytic systems, including monometallic catalysts, bi/tri-metallic catalysts and metal-free catalysts, have been widely investigated by a variety of research groups. A better understanding of the available literature could give the answer as to what is the best catalyst for the hydrochlorination process. For this reason, a new methodology to actively compare catalysts that present intrinsic differences and have been tested at different conditions will be provided. The suggested methodology relies on identifying the crucial parameters that will allow assessment of the catalysts' activity. Using acetylene hydrochlorination reaction as a model reaction, a process that has been widely studied by many independent researchers for decades, we will aim to identify the best catalyst for this reaction, by evaluating data provided by literature.

2. Activated carbon is a common support used for the preparation of catalysts for the acetylene hydrochlorination reaction. This host offers a wide range of advantages as it allows the preparation of highly active catalysts while ensuring high dispersion of Au active species on the surface of the support. The effect that activated carbon support poses on the stability and activity of the catalysts will be investigated. Using commercially available activated carbons, the surface chemistry and the structural properties of the materials will be extensively studied employing a wide range of characterisations techniques in the effort of identify the structural-activity relationships between active centres and hosts.

3. Ligands play a major role in the activity, stability, and selectivity for this class of catalysts. Unfortunately, the effect that ligands have is still subject of dispute as there is no consensus around their exact role. In this study a range of different ligands will be screened with the aim of discovering the best in class. The recognition of the role that N-methylpyrrolidone (NMP), in improving the activity and the stability of single-site Au catalysts, set the focus on the effect that this ligand has on stabilising Au centres. Range of different techniques to characterise Au-NMP interactions both before and after the catalyst preparation will be discussed thoroughly.

1.7 References

1. Chorkendorff I., Niemantsverdriet J. W., Introduction to catalysis, concepts of modern catalysis and kinetics. Willey-VCH, 3rd edn., 2003.
2. Speight J. G., Rules of thumb for petroleum engineers. Willey-VCH, 3rd edn., 2017.
3. Wisniak J., The History of catalysis, from the beginning to Nobel prizes. Educac. Quimica, 2010, **21**, 60–69.
4. Lindström B., Pettersson L., A brief history of catalysis. CatTech., 2003, **7**, 130–138.
5. Steinborn D., Fundamentals of Organometallic Catalysis. Willey-VCH, 1st edn., 2012.
6. Ostwald W., Catalysis. Zeitschrift für Elektrotechnik und Elektrochemie, 2008, **7**, 995–1003.
7. Dybkaer R., Unit "katal" for catalytic activity (IUPAC Technical Report). Appl. Chem., 2001, **73**, 927–931.
8. Qiao X., Zhao C., Zhou Z., Guan Q., Li W., Constructing pyridinic N-rich aromatic ladder structure catalysts from industrially available polyacrylonitrile resin for acetylene hydrochlorination. ACS Sustain Chem Eng. 2019, **7**, 17979–17989.
9. Wacławek S., Padil V. V. T., Černík M., Major advances and challenges in heterogeneous catalysis for environmental applications: a review. Ecol. Chem. Eng. S., 2018, **25**, 9–34.
10. Olson A. R., The study of chemical reactions from potential energy diagrams. Trans. Faraday Soc., 1931, **27**, 69-76.
11. Saini S., Designing clusters for efficient catalytic activity at a realistic condition from first-principles simulation. Doctoral dissertation, Indian Institute of Technology Delhi (IITD), New Delhi, 2020.
12. Roduner E., Understanding catalysis. Chem. Soc. Rev., 2014, **43**, 8226–8239.
13. Klaewkla R., Arend M., Hoelderich F. W., A Review of mass transfer controlling the reaction rate in heterogeneous catalytic systems. Mass Transfer-Advanced Aspects, 2nd edn., 2011.
14. Arnold G., Tan S. R., Construction Materials. Routledge, 2nd edn., 2014.

15. Fralish M. S., Downs J. W., Vinyl Chloride Toxicity. StatPearls Publishing LLC, 1st edn., 2022.

16. Fire F. L., Vinyl Chloride. Fire Eng., 1986, **139**, 39–40.

17. Weber M., Deußing G., A man who was 20 years ahead of his time'': the polymer pioneer Fritz Klatte. Date published: January 2018, date cited: February 15 2023, available from: https://www.konline.com/en/Media_News/News/129_birthday_of_polymer_pioneer_Fritz_Klatte.

18. Eggar C., Vinyl Chloride Monomer (VCM) Industry Installed Capacity. Date published: September 2022, date cited: February 15 2023, available from: https://reportlinker.com/p06485687/Vinyl-Chloride-Monomer-VCM-Industry-Installed-Capacity-and-Capital-Expenditure.

19. Trotuş I. T., Zimmermann T., Schü F., Catalytic reactions of acetylene: A feedstock for the chemical industry. Chem. Rev., 2014, **114**, 1761–1782.

20. Titow W., PVC Technology. Springer Dordrech, 1st edn., 1984.

21. Terselius B., Rånby B., Phase structure of polyvinyl chloride (PVC) and PVC/polymer blends. Pure & Appl. Chem., 1981, **53**, 421–448.

22. Benyahia F., The VCM process economics: Global and raw material impacts. Proceedings of the 1st Annual Gas Processing Symposium, 2009, **1**, 415–422.

23. Carroll W. F., Johnson R. W., Moore S. S., Paradis R. A., Applied Plastics Engineering Handbook: Processing, materials, and applications. Elsevier, 2nd edn., 2017.

24. Zichittella G., Ceruti A., Guillén-Gosálbez G., Pérez-Ramírez J., Catalyst: A step forward for PVC manufacture from natural gas. Chem. 2022, **14**, 883–885.

25. Lin Y., Wang S., Wu Q., Larssen T., Material flow for the intentional use of mercury in China. Environ Sci Technol., 2016, **50**, 2337–2344.

26. Schobert H., Production of acetylene and acetylene-based chemicals from coal. Chem. Rev., 2014, **12**, 1743–1760.

27. Zhong J., Xu Y., Liu Z., Heterogeneous non-mercury catalysts for acetylene hydrochlorination: progress, challenges, and opportunities. Green Chem., 2018, **20**, 2412-2427.

28. Stephen A., Hashmi K., Dean F. T., Modern gold catalyzed synthesis. Wiley-VHC, 1st edn., 2012.

29. Malta G., Freakley S. J., Kondrat S. A., Hutchings G. J., Acetylene hydrochlorination using Au/carbon: a journey towards single site catalysis. Chem. Comm., 2017, **53**, 11733-11746

30. Johnston P., Carthey N., Hutchings G. J., Discovery, development, and commercialization of gold catalysts for acetylene hydrochlorination. J. Am. Chem. Soc. 2015, **137**, 14548–14557.

31. Zhang H., Dai B., Wang X., Xu L., Zhu M., Hydrochlorination of acetylene to vinyl chloride monomer over bimetallic Au-La/SAC catalysts. Ind. Eng. Chem., 2012, **25**, 49–54.

32. Hou L., Zhang J., Pu Y., Li W., Effects of nitrogen-dopants on Ru-supported catalysts for acetylene hydrochlorination. RSC Adv., 2016, **22**, 18026–18032.

33. Pu Y., Zhang J., Yu L. Jin Y., Li W., Active ruthenium species in acetylene hydrochlorination. Appl. Catal. A. Gen., 2014, **488**, 28–36.

34. Agnewr J. B., Shankar H. S., Catalyst deactivation in acetylene hydrochlorination. Ind. Eng. Chem., Prod. Res. Dev. 1986, **25**, 19–22.

35. Liu C., Peng J., Ma A., Zhang L., Li J., Study on non-isothermal kinetics of the thermal desorption of mercury from spent mercuric chloride catalyst. J. Haz. Mater., 2017,**15,** 325–333.

36. Hutchings G. J., Grady D. T., Hydrochlorination of acetylene: The effect of mercuric chloride concentration on catalyst life. Appl. Catal., 1985, **17**, 155–60.

37. Hutchings G. J., Vapor phase hydrochlorination of acetylene: Correlation of catalytic activity of supported metal chloride catalysts. J. Catal., 1985, **96**, 292–295.

38. Ren W., Duan L., Zhu Z., Du W., An Z., Xu L., Zhang C., Zhuo Y., Chen C., Mercury transformation and distribution across a polyvinyl chloride (PVC) production line in China. Environ. Sci. Technol., 2014, **48**, 2321–2327.

39. Xu X. L., Zhao J., Lu C. S., Zhang T. T., Di X. X., Gu S. C., Li X. N., Improvement of the stability of Hg/AC catalysts by CsCl for the high temperature hydrochlorination of acetylene. Chin. Chem. Let., 2016, **27**, 822–826.

40. Wei X., Shi H., Qian W., Luo G., Jin Y., Wei F., Gas-phase catalytic hydrochlorination of acetylene in a two-stage fluidized-bed reactor. Ind. Eng. Chem. Res., 2009, **48**, 128–133.

41. Ankrah R., Homepage | Minamata Convention on Mercury. Date published: December 2022, date cited: February 16 2023, available from https://www.mercuryconvention.org/en

42. Hutchings G. J., Haruta M., A golden age of catalysis: A perspective. Appl. Catal. A: Gen., 2005, **291**, 2–5.

43. Okumura M., Fujitani T., Huang J., Ishida T., A career in catalysis: Masatake Haruta. ACS Catal., 2015, **5**, 4699–4707.

44. Shinoda K., The vapor-phase hydrochlorination of acetylene over metal chlorides supported on activated carbon. Chem Lett., 1975, **5**, 219–220.

45. Smith D. M., Walsh P. M., Slager T. L., Studies of silica-supported metal chloride catalysts for the vapor-phase hydrochlorination of acetylene, J. Catal., 1968, **11**, 113–130.

46. Zhong J., Xu Y., Liu Z., Heterogeneous non-mercury catalysts for acetylene hydrochlorination: Progress, challenges, and opportunities. Green Chem., 2018, **20**, 2412–2427.

47. Conte M., Carley A. F., Hutchings J. G., Reactivation of a carbon-supported gold catalyst for the hydrochlorination of acetylene. Catal. Lett., 2008, **124**, 165–167.

48. Conte M., Carley A. F., Attard G., Herzing A. A, Kiely C. J., Hutchings G. J., Hydrochlorination of acetylene using supported bimetallic Au-based catalysts. J Catal., 2008, **257**, 190–198.

49. Sun X., Dawson S. R., Parmentier T. E., Malta G., Davies T. E.., He Q., Li L., Morgan M. D., Carthey N., Johnston P., Kondrat A. S., Freakley J. S., Kiely C. J., Hutchings G. J., Facile synthesis of precious-metal single-site catalysts using organic solvents. Nat Chem., 2020, **12**, 560–567.

50. Malta G., Freakley S. J., Kondrat S. A., Hutchings G. J., Acetylene hydrochlorination using Au/carbon: A journey towards single site catalysis. Chem. Comm., 2017, **53**, 11733–11746.

51. Nkosi B., Adams M. D., Coville N. J., Hutchings G. J., Hydrochlorination of acetylene using carbon-supported gold catalysts: A study of catalyst reactivation. J. Catal. 1991, **128**, 378–386.

52. Malta G., Kondrat S. A., Freakley S. J., Davies C. J., Lu L., Dawson R. S., Thetford A., Gibson K. E., Morgan D. J., Jones W., Wells P. P., Johnston P., Catlow R. A., Christopher J., Kiely C. J., Hutchings G. J., Identification of single-site gold catalysis in acetylene hydrochlorination. Science, 2017, **355**, 1399–1403.

53. Fong Y. Y., Visser B. R., Gascooke J. R., Cowie B. C.C., Thomsen L., Metha G F., Buntine A. M., Harris H. H., Photoreduction kinetics of sodium tetrachloroaurate under synchrotron soft X-ray exposure. Langmuir, 2011, **27**, 8099–8104.

54. Lu J., Aydin C., Browning N. D., Gates D., C., Imaging isolated gold atom catalytic sites in zeolite NaY. Angew. Chem., 2012, **124**, 5944 –5948.

55. Allard L. F., Borisevich A., Deng W., Si R., Flytzani-Stephanopoulos M., Overbury S.H., evolution of gold structure during thermal treatment of Au/FeOx catalysts revealed by aberration-corrected electron microscopy. J Electron Microsc., 2009, **58**, 199–212.

56. Yang M., Allard L. F., Flytzani-Stephanopoulos M., Atomically dispersed Au-(OH)x species bound on titania catalyze the low-temperature water-gas shift reaction. J. Am. Chem. Soc., 2013, **135**, 3768–3771.

57. Kaiser S. K., Fako E., Surin I., Krumeich F., Kondratenko V. A., Kondratenko E. V., Clark A. H., López N., Pérez-Ramírez J., Performance descriptors of nanostructured metal catalysts for acetylene hydrochlorination. Nat. Nanotechn., 2022, **17**, 606–612.

58. Zhang M., Zhang H., Li F., Peng W., Yao L., Dong Y., Peng W., Yao L., Dong Y., Xie D., Liu Z., Li C., Zhang J., Construction of Ru-N single sites for effective acetylene hydrochlorination: Effect of polyethyleneimine modifiers. ACS Sustain. Chem. Eng., 2022, **10**, 13991–4000.

59. Kaiser S. K., Fako E., Manzocchi G., Krumeich F., Hauert R., Clark A. H., Safonova O. V., López N., Pérez-Ramírez J., Nanostructuring unlocks high performance of platinum single-atom catalysts for stable vinyl chloride production. Nat Catal., 2020, **3**, 376–385.

60. Kaiser S. K., Lin R., Mitchell S., Fako E., Surin I., Krumeich F., Hauert R., Safonova O. V., Kondratenko V. A., Kondratenko E. V., Collins S. M., Midgley M., López N.,

Pérez-Ramírez J., Controlling the speciation and reactivity of carbon supported gold nanostructures for catalysed acetylene hydrochlorination. Chem. Sci., 2019, **10**, 359-369.

61. Jones J., Xiong H., DeLaRiva A. T., Peterson E.J., Pham H., Challa S. R., Qi G., Oh S., Wiebenga M. H., Hernández H. I. P., Wang Y., Datyel A. K., Thermally stable single-atom platinum on ceria catalysts via atom trapping. Science, 2016, **353**, 150–154.

62. Jia Y., Zhang T., Liu M., Zhang J., Han Y., Effect of different heteroatoms anchoring a Cu single-atom catalyst on acetylene hydrochlorination. J. Phys. Chem., 2022, **48**, 20401–20410.

63. Wang T., Jiang Z., Tang Q., Wang B., Wang S., Yu M., Chang R., Yue Y., Zhao J., Interactions between atomically dispersed copper and phosphorous species are key for the hydrochlorination of acetylene. Commun. Chem., 2022, **5**, 1–10.

64. Davies C. J., Miedziak P. J., Brett G. L., Hutchings G. J., Vinyl chloride monomer production catalysed by gold: A review. Chin. J. Cat., 2016, **37**, 1600–1607.

65. Zhu M., Wang Q., Chen K., Wang Y., Huang C., Dai H., Yu F., Kang L., Dai B., Development of a heterogeneous non-mercury catalyst for acetylene hydrochlorination. ACS Catal., 2015, **5** 5306–5316.

66. Nkosi B., Coville N. J., Hutchings G J., Adams M. D., Friedl J., Wagner F. E., Hydrochlorination of acetylene using gold catalysts: A study of catalyst deactivation. J. Catal., 1991, **128**, 366–377.

67. Carthey N. A., Johnston P., Smidt M. L., Improvements in catalytic processes. Patent application WO2010/055341A3, August 12, 2010.

68. Duan X., Tian X., Ke .J, Yin Y., Zheng J., Chen J., Cao Z., Xie Z., Yuan Y., Size controllable redispersion of sintered Au nanoparticles by using iodohydrocarbon and its implications. Chem. Sci., 2016, **7**, 3181–3187.

69. Duan X., Yin Y., Tian X., Ke J., Wen Z., Zheng J., Hu M., Ye L., Yuan Y., C–X (X = Cl, Br, I) bond dissociation energy as a descriptor for the redispersion of sintered Au/AC catalysts. Chin. J. Cat., 2016, **37**, 1794–1803.

70. Malta G., Kondrat S. A., Freakley S. J., Davies C. J., Dawson S., Liu X., Lu L., Dymkowski K., Fernandez-Alonso F., Mukhopadhyay S., Gibson E. K., Wells P. P., Parker S. F., Kiely C. J., Hutchings G. J., Deactivation of a single-site gold on carbon

acetylene hydrochlorination catalyst: An X-ray absorption and inelastic neutron scattering study. ACS Catal., 2018, **8**, 8493–8505.

71. Conte M., Carley A. F., Heirene C., Willock D. J, Johnston P., Herzing A. A, Kiely C. J., Hutchings, G. J., Hydrochlorination of acetylene using a supported gold catalyst: A study of the reaction mechanism. J. Catal., 2007, **250**, 231–239.
72. Conte M., Carley A. F., Hutchings G.J., Reactivation of a carbon-supported gold catalyst for the hydrochlorination of acetylene. Catal. Lett., 2008, **124**, 165–167.
73. Hutchings G. J., Catalysis: A golden future. Gold Bull., 1996, **29**, 123–130.
74. Hutchings G. J., Grady D.T., Effect of drying conditions on carbon supported mercuric chloride catalysts. Appl. Catal., 1985, **16**, 411–415.
75. Malta G., In situ study of Au/C catalysts for the hydrochlorination of acetylene. Doctoral dissertation, Cardiff University, Cardiff, 2018.
76. Wan F., Chao S., Guan Q., Wang G., Li W., Reaction mechanisms of acetylene hydrochlorination catalyzed by $AuCl_3$/C catalysts: A density functional study. Catal, Commun., 2017, **101**, 120–124.
77. Friedl J., Wagner F. E., Nkosi B., Towert M., Coville N. J., Adams M. D., Hutchings G. J., ^{197}Au Mössbauer study of the deactivation and reactivation of a carbon-supported $AuCl_4^-$ hydrochlorination catalyst. Hyperfine Interact., 1992, **69**, 767–770.
78. He H., Zhao J., Wang B., Yue Y., Sheng G., Wang Q., Yu L., Hu Z. T., Li X., Highly active AuCu-based catalysts for acetylene hydrochlorination prepared using organic aqua regia. Materials, 2019, **12**, 1310-1315.
79. Bishop P.T., Carthey N. A., Johnston P., Catalyst and method for its preparation. Patent application WO2013008004A2, July 10, 2016.
80. Decarbonising chemicals production. Johnson Matthey, date cited: February 16 2023, available from: https://matthey.com/en/products-and-markets/chemicals.
81. Zhou K., Jia J., Li C., Xu H., Zhou J., Luo G., Wei F., A low content Au-based catalyst for hydrochlorination of C_2H_2 and its industrial scale-up for future PVC processes. Green Chem., 2015, **17**, 356–364.
82. Huang C., Zhu M., Kang L., Dai B., A novel high-stability Au(III)/Schiff-based catalyst for acetylene hydrochlorination reaction. Catal. Commun., 2014, **5**, 61–65.

83. Yin X., Huang C., Kang L., Zhu M., Dai B., Novel $AuCl_3$ –thiourea catalyst with a low Au content and an excellent catalytic performance for acetylene hydrochlorination. Catal. Sci. Technol., 2016, **6**, 4254–4259.

84. Hong G., Tian X., Jiang B. B., Liao Z., Wang J., Yang Y., Zheng J., Improvement of performance of a Au–Cu/AC catalyst using thiol for acetylene hydrochlorination reaction. RSC Adv., 2016, **6**, 3806–3814.

85. Qi X., Li W., Gu J., Guo C., Zhang J., Gold–glutathione complex catalysts with carbon support for non-mercury catalytic acetylene hydrochlorination. RSC Adv., 2016, **107**, 105110–105118.

86. Malta G., Kondrat S. A., Freakley S. J., Morgan D. J., Gibson E. K., Wells P. P., Aramini M., Gianolio D., Thompson P. B. J., Johnston P., Hutchings G. J., In situ K-edge X-ray absorption spectroscopy of the ligand environment of single-site Au/C catalysts during acetylene hydrochlorination. Chem. Sci., 2020, **11**, 7040-7052.

87. Pattisson S., Malta G., Dawson S., Dummer N. F., Smith L. R., Lazaridou A., Morgan D. J., Freakley S. J., Kondrat S. A., Smit J. J., Johnston P., Hutchings G. J., Lowering the operating temperature of gold acetylene hydrochlorination catalysts using oxidized carbon supports. ACS Catal. 2022, **22**, 14086–14095.

88. Dawson S., Pattisson S., Malta G., Dummer N. F., Smith L. R., Lazaridou A., Allen C. S., Davies T. E., Freakley S. J., Kondrat S. A., Kiely C. J., Johnston P., Hutchings G. J., Sulfur promotion in Au/C catalyzed acetylene hydrochlorination. Small, 2021, **17**, 1-10.

89. Qi X., Chen W., Zhang J., Highly effective carbon-supported gold-ionic liquid catalyst for acetylene hydrochlorination. RSC Adv., 2019, **9**, 21931–21938.

90. Duan X., Ning L., Yin Y., Huang Y., Gao J., Lin H., Tan K., Fang H., Ye L., Lu X., Yuan Y., Sulfur moiety as a double-edged sword for realizing ultrafine supported metal nanoclusters with a cationic nature. ACS Appl. Mater. Interf., 2019, **11**, 11317-11326.

Chapter 2

Experimental

2.1 Introduction

This chapter presents the details regarding the preparation methods used for catalysts synthesis, the testing conditions and the characterization techniques employed for the analysis of the catalysts.

2.2 Catalyst Preparation

2.2.1. Preparation of supported Au catalysts *via* wet impregnation on activated carbon.

The Au precursor, $HAuCl_4 \cdot 3H_2O$ (Alfa Aesar, 20 mg, assay 49%) was dissolved in dry acetone (2.7 ml, 99.8%) and allowed to stir for 10 mins. Accordingly, the solution was added dropwise, with stirring, to, activated dry carbon (0.99 g). A range of different commercially available activated carbon materials were used as support. The solution was left to stir for 1 h and finally dried under N_2 at 45 °C for 16 h. Unless specified otherwise, all catalysts were prepared with a 1 wt.% Au loading, denoted 1% Au/AC and the carbon support was used without any additional treatment.

2.2.2. Preparation of supported Au-organic compound catalysts *via* wet impregnation on activated carbon.

All carbon-supported Au catalysts with organic compound additives were prepared *via* a wet impregnation method. Activated carbon (NORIT ROX 0.8) was initially ground to obtain a powder (150 mesh). The various organic compounds (OC) and the Au precursor, $HAuCl_4 \cdot 3H_2O$ (Alfa Aesar, 20 mg, assay 49%) were dissolved in dry acetone (2.7 ml). The Au -OC solution was stirred overnight. Accordingly, the solution was added dropwise, with stirring, to activated carbon support (0.99 g) in order to obtain a catalyst with a final metal loading of 1 wt.%. The resulting powder was dried at 45 °C for 16 h under a flow of N_2. The catalysts prepared using different OCs were denoted as Au-OCs/AC.

2.3 Catalyst Testing

2.3.1 Reactor design

Acetylene hydrochlorination reactions were tested in an automated purposed built reactor (Figure 2.1). The reactor is comprised of stainless-steel components, inert perfluoroalkoxy (PFA) tube and Swagelok connection fittings. The components of the system were

connected *via* a Process Interface unit (PI).[1] The PI unit was equipped with a 16-bit analogue to a digital convertor to acquire signal from the pressure transducer (to act as an over-pressure interlock for the gas flows) and an 8-channel electromechanical relay module to operate each individual 2- and 3-way solenoid valve. In addition, the PI unit supplied power and communication to the Mass Flow Controllers (MFCs). All the reaction parameters were set and controlled by the LAB Interface software (IGI Systems Ltd) which acted as a monitor and data logger.[2] The reactor also contained sensors for the reactant gases. High pressure and gas alarm interlocks were triggered when pressure exceeded 2 bar causing the system to shut down leaving only a flow of inert gas in the system.

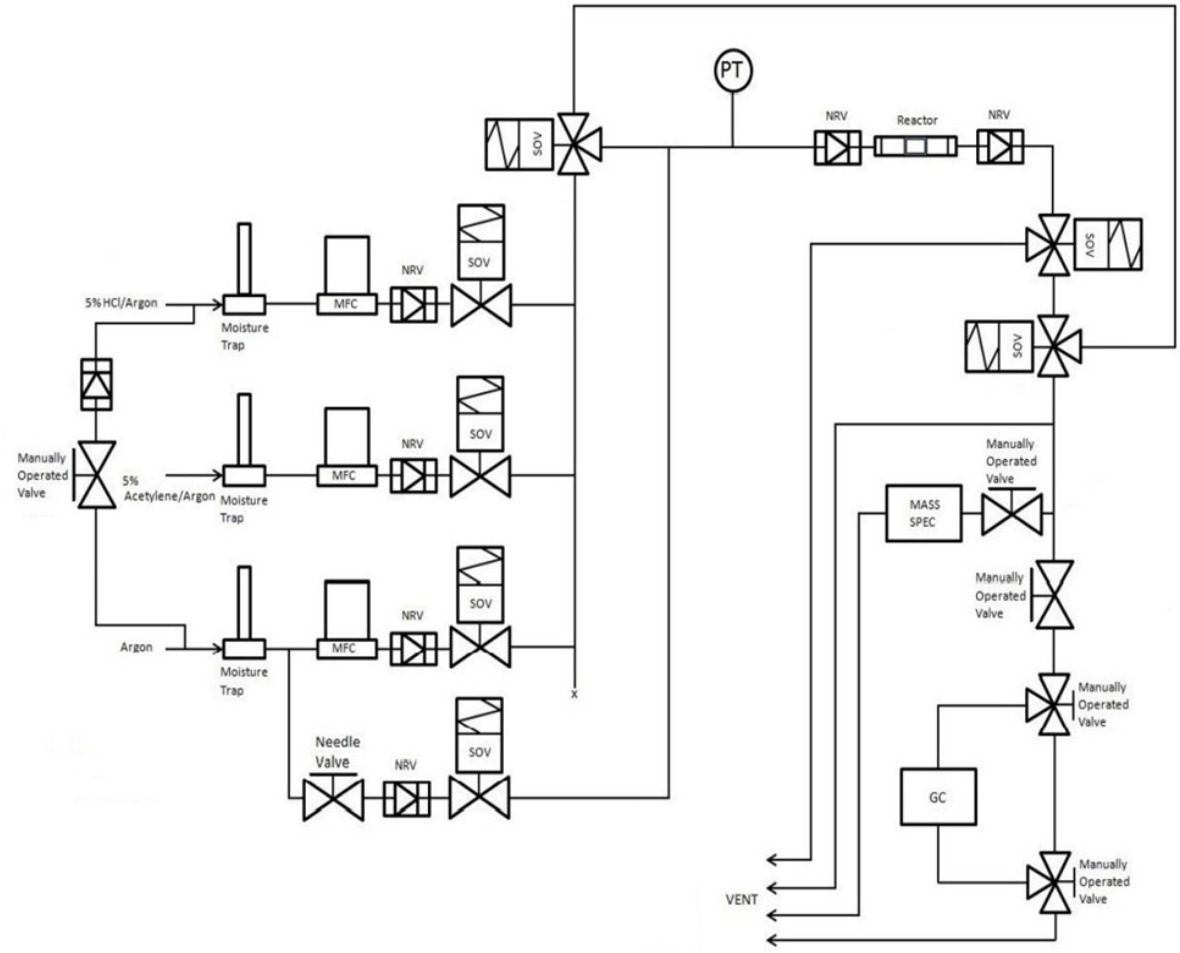

Figure 2.1: Diagram of the acetylene hydrochlorination reactor. The acronyms are the following: NRV - non-return valve, MFC - mass flow controller, SOV - solenoid valve, PT -pressure transducer, mass spec - mass spectrometer and GC – gas chromatograph.

Diluted gases of acetylene and hydrogen chloride balanced in argon were used. Typical concentrations of 5% acetylene/argon, 5% hydrogen chloride/argon and 99.9999% Argon were employed. All gases passed through a moisture trap (Agilent, CP17971) to exclude the presence of water and moisture entering the reactor. The gas flows were regulated

using electronic MFCs (Brooks instruments, thermal MFCs, GF series, Ar 0 – 100 ml/min, acetylene and HCl 0 – 50 ml/min). Reaction mixture gases were passed through the reactor when the desired set temperature had been reached or by-passed during ramp heating. The by-passed reactant gas mixture during the heating period was analysed by gas chromatography and used as a blank for reference. Simultaneously, during the heating, the reactor and catalyst were purged with argon to ensure the minimization of moisture on the surface of the catalyst. When reaching the set reaction temperature, the reactant gases would flow through the reactor tube and accordingly the gases mixtures and products would then flow to the gas chromatograph for periodic sampling (5 min).

For a typical reaction, the catalyst was contained in a quartz tube (230 x 6 mm). Stainless steel reactor tubes are avoided as they can promote side reactions such as oligomerization and polymerization of acetylene at high temperatures. The catalyst was packed in the reactor at the centre of the quartz tube supported on 1 cm of glass wool. The reactor tube would be clamped on a vertical tube furnace (Carbolite, MTF 10/15/130) and sealed with 2 cylindrical Ultra-torr Swagelok fittings. The temperature of the reactor was monitored *via* a K-type thermocouple.

2.3.2 Testing conditions

The reactant gases used in this study are highly flammable, toxic, and corrosive.[3-5] For safety precautions, diluted gases of acetylene and hydrogen chloride balanced in argon were employed. All the gases passed through moisture traps to eliminate the introduction of moisture in the reactor. Prior to starting the reaction, the catalyst would be heated to the reaction temperature at 5 ^{o}C min^{-1} while exposed to argon. For a typical reaction, the reaction mixture gas of acetylene (23.56 ml min^{-1}), hydrogen chloride (23.76 ml min^{-1}) and additional argon (2.70 ml min^{-1}) was introduced (total gas flow of 50 ml min^{-1}) into the heated reactor chamber containing 90 mg of sample at a total gas hourly space velocity (GHSV) of ~17,000 h^{-1}, keeping the C_2H_2: HCl ratio at a constant value of 1: 1.02. Typical time on stream experiments were conducted for 240 min (4 h). These are the conditions used for all data reported, unless otherwise stated. Analysis of the gas mixture and products was achieved by time-on-line gas chromatography, using a Varian CP-3800 GC fitted with a Poropak-N packed column and a flame ionization detector (FID).[6]

All time-on-line data was reported with a ±1% acetylene conversion, determined by repeat analysis with the same catalyst under the same reaction conditions. After the reaction, the catalyst was left to cool down to room temperature under argon flow, while the reactor was also purged with argon to remove any remaining reaction gases in the lines.

The catalytic activity of the catalysts is described in terms of acetylene conversion (Equation 2.1). To obtain the value of the blank acetylene counts, several GC runs were recorded while the reactant gases were by-passing the reactor. The average value of the acetylene peak areas of the blanks was used as the blank acetylene area.

Overall, the acetylene conversion % is expressed as:

$$\frac{Blank\ acetylene\ area - Reaction\ acetylene\ area}{Blank\ acetylene\ area}\ x\ 100\ eq.\ 2.1$$

Vinyl Chloride Monomer (VCM) is a highly flammable, carcinogenic, and toxic compound. For this reason, the calibration of the VCM is not conducted.[5] For Au-based catalysts, it is confirmed to *via* online mass spectrometry that VCM is the main product detected.(52) . Selectivity is greater than 99%. Selectivity was calculated by associating the VCM area peak counts to the conversion of acetylene. No other peaks-products were observed during the reaction testing of the catalysts.

2.3.3 Gas chromatography

Chromatography is a physical separation method in which the components can be distinguished and distributed between two phases, one stationary phase and one mobile phase. The term gas chromatography refers to the chromatographic techniques employing a gas mobile phase and solid or liquid stationary phases. Gas chromatography is the predominant technique used to separate and analyze volatile compounds. The major limitations relating the type of compounds applicable for GC analysis are concerning the stability of the molecules as they need to be stable and easily vaporized without decomposing or reacting with the components of the stationary phase and mobile phase. GC analysis allows the study of gases, liquids and solids, with the latter typically solubilized in volatile solvents. Both organic and inorganic compounds can be analysed.[7]

Typically, a gas chromatograph (GC) consists of a carrier gas system, injector, gas chromatographic column, detector, and data processing unit. The mobile phase includes a carrier gas, preferably an inert gas with negligible adsorption capacity such as N_2. A GC analysis starts with the introduction of the sample mixture into the mobile phase, the carrier gas, which continuously flows through the system delivers the sample mixture to the injector. The sample is injected using a 6-port valve, i.e., Valco 6 port valve that has been calibrated (10-100 μL).[8] The sample mixture with the carrier gas is carried to the GC column and the separation of the mixture components is determined by the interaction of the of the components with the stationary phase. Compounds with stronger interactions with the stationary phase elute later than the ones with weaker interactions. This mechanism allows

components to leave the column and enter the detector at different times. The time at which a compound is detected is termed the retention time (RT).[9]

The columns for gas chromatography can be divided into packed and capillary columns. A packed column is typically a rigid metal tube filled with small particles, often coated with a thin film of a high molecular weight polymer layer. Capillary columns are made of a glass or a fused silica tube with a small internal diameter. Most capillary column stationary phases are cross-linked and covalently bonded to the fused-silica surface. The amount of stationary phase in a capillary column is denoted by its film thickness. It is of high importance that the stationary phase of the GC columns has high chemical, physical and thermal stability, low vapour pressure, and good selectivity for the sample components. The column temperature is one of the most decisive parameters in GC analysis and its exact regulation is of paramount importance. To achieve effective and reliable separation the GC column has to be set at a constant temperature (isothermal separation mode) or be modified according to a predetermined temperature programme (temperature gradient).[10] As the components are separated, they gradually exit the column and enter the detector.

Detectors interact with the analyte molecules. The interactions are converted into an electrical signal that is then sent to a recording or data storage device. There is a range of detectors that may be used with GC, two of the most commonly used are; thermal conductivity detectors (TCDs) and flame ionization detectors (FIDs). For analysis of the acetylene hydrochlorination reaction, a flame ionization detector (FID) is used. FID uses hydrogen flow mixed with the carrier gas. The mixture is ignited, and the analytes are burnt. The ions formed during the combustion process are collected in a cylindrical electrode at a high voltage applied between the jet of the flame and the electrode. The resulting current is magnified and detected. The converted signal is translated as a chromatogram, a plot of intensity of signal (μV) versus elapsed time.[11]

2.4 Characterization

2.4.1 X-ray Diffraction

Powder X-ray diffraction (XRD) is a non-destructive analytical technique employing X-rays for the characterization of crystalline materials. X-rays are a form of high energy electromagnetic radiation with low wavelength. Since the wavelength of an X-ray is similar to the distance between atoms in a crystal, a special interference effect called diffraction can occur, resulting in a pattern of higher and lower intensities. If the X-ray waves are in alignment, the signal is amplified, a phenomenon called constructive interference. If the signals are out of alignment the signal is destroyed, a phenomenon called destructive

interference (Figure 2.2).[12] Bragg's Law determines the conditions needed for constructive interference to occur (Equation 2.2). Constructive interference appears only when the difference in wavelengths of the scattered X-rays is equal to an integral multiple of the wavelength. Bragg's law associates the wavelength of electromagnetic radiation (λ), to the diffraction angle (theta, θ) and the lattice spacing in a crystalline sample (d).[13]

$$n\lambda = 2d_{(hkl)}sin\theta \quad eq.2.2$$

Where n = an integer, λ = wavelength of X-rays, d(hkl)= Miller inter-planar distance index and θ= angle between the incident beam and the reflecting plane.

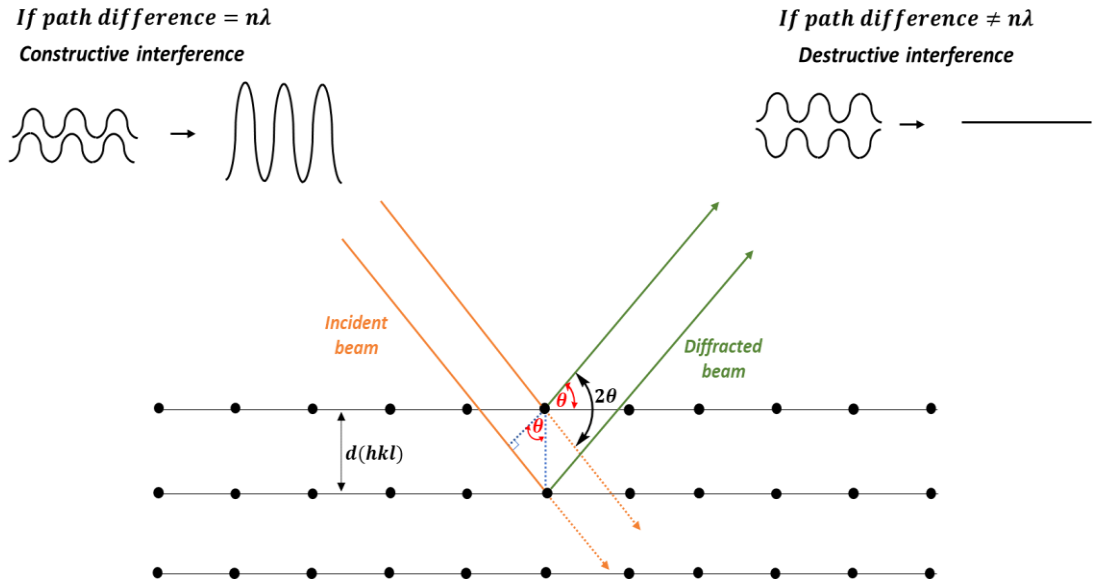

Figure 2.2: Schematic representation of diffracted beams in crystal lattice.[14]

Powders and crystals can be characterized by XRD. The setup of an X-ray diffractometer consists of three basic elements: an X-ray tube, a sample holder, and an X-ray detector. During an X-ray diffraction experiment a sample is cantered in the middle of the instrument and illuminated with a beam of X-rays. X-rays are generated in a cathode ray tube upon heating a tungsten filament to produce electrons. The accelerating electrons bombard a metal target material, typically a Cu, Co, Mo or Fe foil. On impact, electrons obtain efficient energy to dislodge the inner shell electrons of the target material producing characteristic X-ray spectra. These X-rays pass through a monochromator to form a parallel, uniform, and collimated beam. Once, the beam of X-rays is directed towards a sample, the sample absorbs these x-rays and re-emits them in the form of new x-rays. The re-emitted radiation is recorded by the detector and presented in the form of a graph. The X-ray tube and the detector rotate simultaneously, to scan through a programmed 2θ range. The type of the

pattern and its position can give information about the crystal structure and lattice parameters and other information such as residual stress, phase composition, crystal size and oriented growth of the crystals. A schematic presentation of the XRD set up is shown in figure 2.3.[14] Each different crystalline solid has an exclusive diffraction pattern (diffractogram). For metallic Au, reflections appear at 2θ angles of 38°, 44°, 64° and 78°, relating to the Au set of planes (111), (200), (220) and (311) respectively.[15]

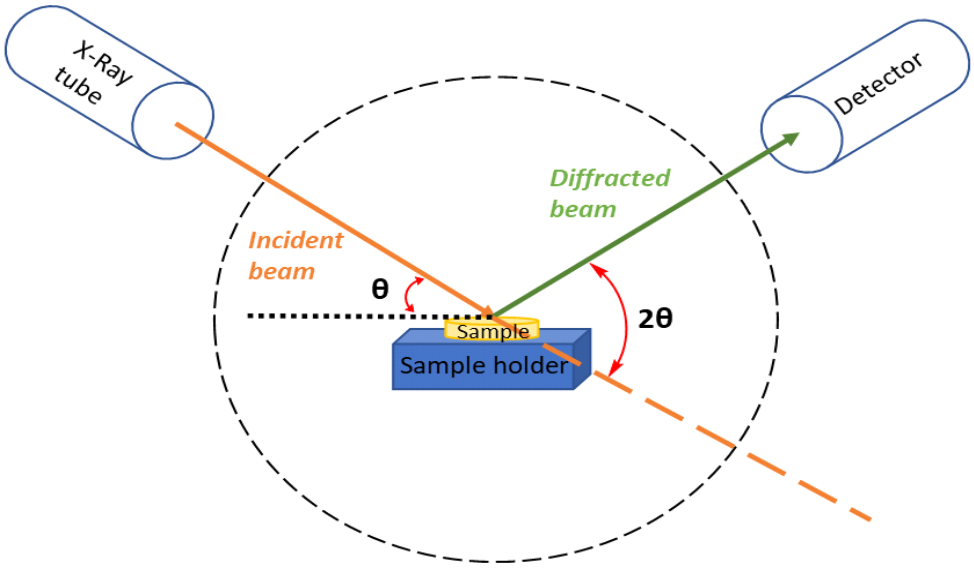

Figure 2.3: Schematic diagram of x-ray diffractometer.[16]

The diffracted X-rays are detected and counted. Each crystalline solid will have a different structure, set of d-spacings, and intensities creating a unique "fingerprint". In addition to the identification of the material, XRD allows to measure the size and the shape of the crystallites. Using the Scherrer equation (Equation 2.3) the particle size can be estimated.

$$L = \frac{\kappa\lambda}{\beta cos\theta} \quad eq.2.3$$

Where: L is crystallite size, λ is the X-ray wavelength of the X-ray radiation, β is the line broadening at half of the maximum intensity (FWHM), θ diffraction angle and κ is a dimensionless shape factor (normally between 0.9-1) which is related to the shape of the crystallite. The Scherrer equation is highly important when performing *in-situ* XRD measurements, to acquire a quantitative evaluation of particle size growth whilst the catalyst is subject to heat or exposure to reaction gases. It should be noted that despite the great advantages this technique offers, there are limitations. The exact detection limit depends on the density, atomic number, and crystal structure of the compounds in the sample.[16] Reflections corresponding to metallic Au are present at 2θ angles of 38°, 44°, 64° and 78°, related to the Au set of planes (111), (200), (220) and (311).

Powder X-Ray diffraction: Experimental analysis

Powder X-ray Diffraction (XRD) analysis was performed between 10° and 80° 2θ using an X'Pert Pro PAN Analytical powder diffractometer. A Cu Kα radiation source operating at 40 keV and 40 mA was employed. Analysis of the acquired spectra was performed using X'Pert High Score Plus software. Observed peaks were allocated by direct comparison with the International Centre for Diffraction Data database. The Scherrer equation was used to calculate the mean crystallite size using 0.9 as a value for K and a silicon standard as reference.

Single-crystal crystallography: Experimental analysis

Single-crystal X-ray Diffraction data were recorded at ambient temperature on an Agilent SuperNova Dual Atlas diffractometer, using Cu and Mo mirror monochromators of wavelengths λ = 1.5418 and λ = 0.7107 Å respectively. Crystal structure solution was conducted by SHELXT1 and refined with a SHELXL2. Non-hydrogen atoms were refined with anisotropic displacement parameters.

2.4.2 Thermogravimetric analysis (TGA)

Thermogravimetric analysis, or thermogravimetry, is a technique in which the mass of a sample is recorded as a function of temperature or time, whilst the sample is subjected to a regulated temperature program and atmosphere. The gases used in the analysis can be inert, such as N_2, He, or AR, oxidizing such as air or O_2, or reducing such as forming gas (mixture of H_2 and N_2). Most TGA experiments utilize an inert purge gas, as it allows the sample to only react to temperature during decomposition. Heating samples under inert atmosphere is known as pyrolysis. The mass loss observed during analysis can be attributed to moisture loss, decarboxylation, pyrolysis, loss of solvent, oxidation, decomposition, and other chemical processes depending on the analysis.[17] Thermogravimetric analysis provides a quantitative measurement of the mass lost but does not specify the nature of the mass lost. Numerous techniques are employed to study the gas products from a TGA experiment. This approach is called evolved gas analysis, (EGA). The most common types of Evolved Gas Analysis (EGA) systems are the following ones:

TGA-FT-IR: A Thermogravimetric Analyzer (TGA) linked to a Fourier Transform Infrared Spectrometer (FT-IR). Upon heating the sample during the TGA analysis, volatile materials and/or combustion products are generated. The produced gases are transferred to the IR cell. The most common evolved gases during IR analysis are water, carbon dioxide, carbon monoxide or common solvents which have characteristic absorption frequencies in the IR spectra.

TGA-MS: A Thermogravimetric Analyzer (TGA) connected to a Mass Spectrometer (MS). Mass spectrometry is a highly sensitive technique that allows the identification of compounds by their mass to charge ratio denoted as *m/z*. Detection of low levels of volatile compounds emitted from the surface of the heated sample can be achieved with the combination of a TGA with a MS. The volatile desorbed materials or combustion products are transferred to the MS in real time where the components can be identified. This technique is most valuable when the emitted gases or breakdown products are known in advance.

Experimental analysis

TGA was carried out in a Perkin Elmer TGA-4000. Approximately 20 milligrams of sample were deposited in the auto sampler and heated from 30 - 800 °C at 10 °C/min, under N_2 flow of 20 ml/min.

2.4.3 Fourier Transform Infrared Spectroscopy (FTIR)

Fourier Transform Infrared Spectroscopy is a non-destructive analytical technique used for characterization of samples as it provides qualitative and quantitative information of the molecular structure and chemical bonding of a sample. Since IR radiation can be selectivity absorbed at definite wavelengths when passing through a sample, contingent upon the nature of the material, it can inform about the vibrational bond energies of covalent bonds in a sample. In an FT-IR measurement, a beam of mid- infrared energy is illuminated at a sample and the absorption is recorded over a range of different frequencies resulting to a spectrum of characteristic pattern. Each material generates a unique spectrum. The absorption is related to the concentration of the sample as described by Lambert-Beer's law (Equation 2.4) according to which:

$$A=\varepsilon lc \quad eq.2.4$$

Where A is the absorbance, ε is the is the molar attenuation coefficient or molar absorptivity, l is the optical path length and c is the molar concentration.[18]

Experimental analysis

FTIR has been widely used for the characterization of samples. It has been extensively used for the analysis of oxygenated groups on activated carbon materials see Chapter 4 and for the analysis of Au-Organic Compounds materials see Chapter 5.

For the analysis of O functionalities in activated carbons as described in Chapter 4 the samples were heated at a constant rate under N_2 flow. The adsorbed CO and CO_2 caused by the decomposition of the surface oxygenated species on the carbon were monitored by

the FT-IR. The activated carbons were heated in a fixed-bed flow reactor. The sample (150 mg) was fixed in a quartz tube (7 mm i.d.) between two pieces of quartz wool. The sample was heated from 25 ^{o}C to 600 ^{o}C in 5 ^{o}C steps under a constant N_2 flow (100 ml/min). Analysis of the effluent gases was carried out by a Gasmet FT-IR with a 0.4 L sample cell. For analysis of O functional groups on carbons, samples should be heated the sample up to 1100 ^{o}C, however, due to equipment limitations heating was only feasible to a 600 ^{o}C maximum.

For the analysis of Au-Organic Compounds materials as described in Chapter 5, analysis was performed in Varian Cary 400 FT-IR Spectrometer. Infrared spectra were recorded in reciprocal centimetres (cm^{-1}).

2.4.4 Raman spectroscopy

Raman spectroscopy is a non-destructive analytical technique that provides information related to the chemical structure, phase polymorphy, and crystallinity of materials. It allows qualitative and quantitative analysis offering a range of vital surface information. Upon the exposure of a sample to monochromatic light, an electron can absorb the energy and rise to a virtual energy level. Accordingly, the electron can go back to its initial energy level whilst emitting light of a characteristic wavelength. If the energy of the light is equal to the energy of the incident beam, Rayleigh scattering is observed. If the emitted energy differs from the energy of the incident light, Raman scattering occurs. Subject to the final vibrational level of electron, Raman scattering can be divided to stokes lines and anti-stokes lines. When the frequency of the scattered wavelength is less than that of the incident wavelength, stokes lines are observed in the Raman spectrum. Conversely, when the frequency of the scattered wavelength is higher than that of the incident wavelength, anti-stokes lines are observed.[19]

Experimental analysis

Raman spectra were obtained using a Renishaw invia Raman microscope. The laser is a Modu-Laser Argon ion Stellar-REN, class 3B (serial number NL0336REN311ACR). Average laser power 25 mW, beam diameter 0.65 nm, beam divergence 0.95 mrad, radiation emitted 514 nm, beam stability < 30 μrad and peak power 50 mW.

2.4.5 Brunauer-Emmett-Teller (BET) surface area analysis

Adsorption is the adhesion of atoms ions or molecules to a surface, and it differs from absorption which involves the permeation of a liquid or solid. The application of an inert gas adsorption to study the porosity and the surface properties of materials is known as the

Brunauer-Emmett-Teller (BET) surface area analysis (Figure 2.4). BET is a multi-point measurement of a material's specific surface area through gas adsorption and the formation of a monolayer coverage of the adsorbed gas.[20]

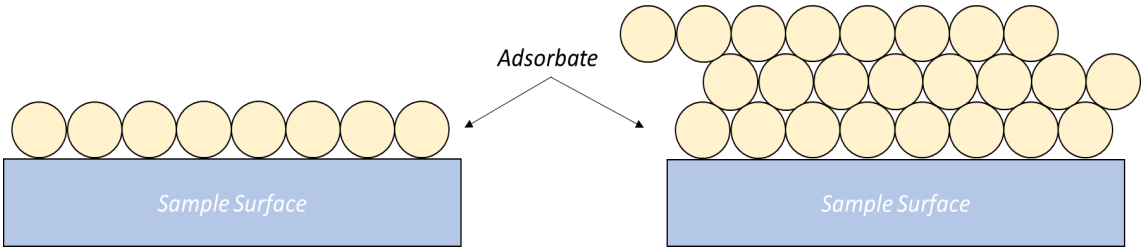

Figure 2.4: Schematic of the adsorption of gas molecules onto the surface of a sample showing (a) the monolayer adsorption model assumed by the Langmuir theory and (b) s the multilayer adsorption model assumed by the BET theory.[20]

Prior to the analysis, the sample is degassed to remove water and any adsorbed species and contaminants. The sample is subsequently exposed to the inert gas for the analysis. Typically, N_2 is used which is adsorbed to the solid sample due to van der Waals forces between the gaseous and solid phase. As the interaction between the gaseous and solid phases is weak, the surface is cooled using liquid N_2 to obtain detectable amounts of adsorption. Accordingly, the sample is being subjected to known amounts of N_2 throughout periodic times. As the size of the N_2 gas molecules are known, the amount of adsorbed gas can be correlated to the total surface area. The monomolecular layer, and the rate of adsorption can be used to calculate the specific surface area of a solid sample and its porous geometry.

The BET equation 2.5 defines the relationship of the amount of the adsorbed gas molecules at a given relative pressure.

$$\frac{1}{X\left(\frac{P_O}{P}-1\right)} = \frac{C-1}{X_m C}\left(\frac{P}{P_O}\right) + \frac{1}{X_m C} \qquad eq.2.5$$

Where X = absorbed gas quantity, X_m = adsorbed monolayer gas quantity, P = equilibrium gas pressure, P_o = saturation pressure and C= BET constant expressed as

$$C = exp\left(\frac{E_1 - E_L}{RT}\right) \quad eq.2.6$$

Where E_1 = heat of adsorption for monolayer formation, E_2= heat of adsorption for second and higher multilayer formation, R= gas constant and T= temperature (K).

When the BET equation can be plotted as a straight line using the mathematical form y=ax+b, where

$$y = \frac{P}{X(P_O - P)} \quad eq.2.7$$

$$x = \frac{P}{P_O} \; eq.2.8$$

$$gradient \; a = \frac{C-1}{X_m C} \quad eq.2.9$$

$$and \; intecept \; b = \frac{1}{X_m C} \quad eq.2.10$$

The value of the slope of the line are used to calculate the monolayer adsorbed gas quantity X_m and the BET constant C.

The total surface area (S_{total}) and the specific surface area (S_{bet}) are given by the following equations:

$$S_{total} = \frac{X_m N_a A_m}{V} \quad eq.2.11$$

Where X_m = adsorbed monolayer gas quantity, N_a = Avogadro's constant, A_m = molar volume of adsorbate equal to 0.162 nm^2 for a N_2 molecule and V= the molar volume of the adsorbate gas equal to 22414 ml.

$$S_{BET} = \frac{S_{total}}{a} \quad eq.2.12$$

Where S_{total} = total surface area and a = the mass of the solid sample

Experimental analysis

Samples were degassed at 130 °C for 16h with a Quantachrome Flovac degasser and then weighed accurately before analysis using a Quantachrome Quadrasorb BET. N_2 porosimetry analysis was performed at -196 °C, over the range P/P_0 = 0.05 – 0.2.

2.4.6 Mass spectrometry.

Mass spectrometry was used for the analysis of the Au-Organic compound materials. This technique is used for measuring the mass and therefore the molecular weight of a molecule. Furthermore, structural information can be obtained by measuring the masses of the produced fragments when molecules break apart upon ionization. A typical mass spectrometer consists of an ionization source in which sample molecules are charged, a mass analyser in which ions are separated by their mass to charge ratio and a detector in

which separated ions are recorded. The neutral particles (molecules or radicals) cannot be detected, while the charged fragments are recorded as peaks at different m/z ratios. The m/z value is a dimensionless number.

In a classical analysis a small amount of analyte is vaporized into the ionization source where it is bombarded by a high energy electron stream. This electron bombardment leads to the formation of cationic radical fragments, that flow through a strong magnetic field that deflects them into different paths according to the m/z ratio. A variety of mass analyzers such as magnetic ion traps, time-of-flight or quadrupoles can be employed. The quadrupole mass analyzer is a very common type that consists of four equidistant, parallel solid rods. An oscillating magnetic field is developed in the space between the space of the rods. For a granted field, only one m/z value will go through the quadrupole region and reach the detector. Fragments that are not of the selected m/z ratio are discharged on the rods or removed by the vacuum.

The mass spectrum is recorded as a bar graph with mass values on the x axis and intensity or relative abundance values on y axis. The highest peak is called the base peak and is assigned an intensity of 100%, while the peak that corresponds to the original cation radical is called the molecular ion or parent peak.[21]

Experimental analysis

High Resolution Mass Spectrometry (HRMS) was performed on a Waters LCT Premier (ESI-(+) and APCI-(+)) or a Waters GCT Premier (EI) system.

2.4.7 X-ray photoelectron spectroscopy

XPS is a qualitative and approximate surface sensitive analysis technique that provides information about the surface composition, elemental oxidation state, and molecular structure. It relies on the photoelectric effect according to which when a beam of X-rays of specific energy irradiates a sample, the electrons of the atom can be excited and emitted. The kinetic energy of the emitted electrons is dependent of the incident photon energy and their binding energy as described in equation 2.13.

$$E_k = hv - EB - \varphi_{\mathrm{sp}} \quad eq.2.13$$

Where E_k = the kinetic energy of photoelectron, hv = the incident photon energy, EB = the binding energy at the Fermi level and φ_{sp}: work function of XPS spectrometer (a constant with an average value between 3 and 5 eV). The X-Ray spectrometer can measure the kinetic energy of the emitted photoelectron and record a spectrum of intensity versus its binding energy. XPS allows the detection of all the elements apart from H and He as the

lack of inner electrons and paired outer electrons (He) make them resistant to ionization. The detection limit of this technique is 0.1 atomic %. Detection depth (d) is subject to the escape depth of photoelectrons (X-ray wavelength and sample composition) with general values of 0.5-3 nm (metal), 2-4 nm (inorganic) and 4-10 nm (organic).

Every element has a characteristic spectrum which is the basis for elemental analysis. Based on the peak position on the spectrum, information such as the nature of the chemical environment and the oxidation state of the element can be obtained, whilst the peak intensity can provide information about the relative content. The peak area depends on a variety of factors; path of photoelectron, presence of impurities, X-ray intensity and spectrometer condition, thus XPS can provide relative contents and not total values. The main parts of an XPS system include an X-ray source, a vacuum chamber, an electron analyzer, and a detector. XPS usually employs a Al Kα or Mg Kα X-ray as the excitation source with a fixed energy (hv) of respectively 1253.6 eV and 1486.3 eV. An XPS system is operated under ultra-high vacuum range of 10^{-6} to 10^{-8} pascals, to prevent adsorption and scattering of ejected electrons by the atmosphere gas molecules.

Experimental analysis

XPS analysis was performed on a Thermo Fisher K-alpha XPS spectrometer equipped with a monochromatic Al X-ray source. For survey scans data was obtained at pass energies of 150 eV and 40 eV for high resolution scans by a 1 eV and 0.1 eV step extent accordingly. For data analysis CasaXPS software was used employing Scofield sensitivity factors and an energy dependence of -0.6, after removal of a Shirley background. Spectra were calibrated to C1s peak at 284.8 eV.

Greatly appreciated is the help of David Morgan who is the Surface Analysis Manager at Cardiff University, as he performed the analysis and assisted with data elaboration.

2.4.8 Nuclear Magnetic Resonance (NMR)

Nuclear Magnetic Resonance (NMR) spectroscopy is a non-destructive analytical technique that provides information related to the local magnetic field around atomic nuclei. Therefore, NMR can give information related to features of the molecular structure such as configuration, conformation, and intermolecular interactions of compounds. NMR is based on the interaction of the nuclei of atoms with a magnetic field. Protons and neutrons are spinning nucleons defined by a nuclear spin quantum number (m), which can be described with the value of -1/2 or + 1/2. Protons and neutrons combined framework the atomic nuclei, whose magnetic characteristic is described by the nuclear spin (I). The I indicates the total

number of spin states that a nucleus can assume (equivalent to 2I+1), each of which has its own spin quantum number m in the range −I, −I+1, …, I−1, I. When I = 0 all the opposite m are paired, suggesting that the number of protons and/or neutrons are odd and the molecules are called paramagnetic. Nuclei with I = 0 have only one spin state therefore, they are said to be magnetically inactive and cannot be directly detected by NMR experiments. The NMR method is applied exclusively for nuclei that present I ≠ 0 and are called diamagnetic. For magnetically active compounds the magnetic field facilitates possible spin-states of the nucleus to differentiate in energy. NMR technique can create observable transitions between the spin states.[22,23]

The scale of the spectrum is usually marked in parts per million (ppm) of the applied field or frequency or in frequency units (Hz).

Experimental analysis

^{1}H and ^{13}C NMR spectra were recorded in acetone-d6 on Bruker Fourier 300, Ultrashield 400, or Ascend 500 instruments. Chemical shifts are reported in parts per million (ppm) and are referenced to the residual solvent resonance as the internal standard acetone-d6: δ = 2.05 ppm for ^{1}H NMR. Data are reported as follows: chemical shift, multiplicity (br s = broad singlet, s = singlet, d = doublet, t = triplet, q = quartet, p = pentet, sept = septet, br m = broad multiplet, m = multiplet, mc = centrosymmetric multiplet), coupling constants (Hz) and integration.

2.4.9 X-ray Absorption Fine-Structure

X-ray Absorption Fine-Structure (XAFS) is an element-specific spectroscopic technique that provides information about the chemical state and environment of a probe atom. XAFs is sensitive to the oxidation state, distances, coordination number and species of the atoms surrounding the selected element. XAFS allows bulk sample analysis, including crystals, glasses, liquids, heterogeneous mixtures and permits low-concentration elemental analysis (typically down to a few ppm). It is a short-range technique, implying that it is not necessary for the element examined to be part of an ordered crystalline phase.[24]

XAFS studies the X-ray absorption as a function of the incident radiation energy, at energies near and above the core-level binding energies of a specific element. When the incident X-ray energy is equal to or greater than the Binding Energy of a core electron, it can be excited from its quantum level to an unoccupied level or the continuum. This phenomenon is known as the photo-electron effect, and it occurs at energies which are specific to the absorbing atom. The absorption edge is the energy at which a sharp rise in the absorption is observed due to the excitation of an electron from the core level to the continuum. The rise covers a

range of energy of 10-20 eV. In an XAFS spectrum, the energies involved are in a range from a few hundred eVs (soft X-rays) to several thousands of eVs (hard X-rays). The name of the edge is given by the origin of the quantum level of the core electron. An edge generated by excitation of an electron from the 1s orbital is called the K-edge. Accordingly, an edge produced by the excitation from the 2s, 2p1/2 and 2p3/2 orbitals are named the L_1, L_2 and L_3 edge, correspondingly.

The excitation of an electron from its quantum level to unoccupied orbitals or the continuum leaves a core hole that has a lifespan of femtoseconds and is filled by an electron from a higher energy orbital state. There are 2 main mechanisms that can occur which are accompanied by an energy release. The first of these is X-ray fluorescence which happens when a higher energy electron core-level electron fills the deeper core hole, ejecting an X-ray of well-defined energy equal to the difference in the energies of the two orbitals. The second process known as Auger effect occurs when an electron from a higher-energy orbital fills a core hole, and a second electron is emitted into the continuum. X-ray fluorescence is more prone to arise than Auger emission in the hard X-ray regime, but for lower energy X-ray absorption, Auger emission dominates.

XAFS measures the X-ray absorption coefficient μ, a function of energy at energies near and above these absorption edges. Overall, an XAFS measurement is typically performed in transmission mode and records the energy dependence of X-ray absorption coefficient μ just and above the binding energy of a selected core level of a known atomic species.[25] The Lambert-Beer equation 2.14 explains the relationship between the incident and the transmitted beam through a sample:

$$Io = Ite^{\mu(E)t} \quad eq.2.14$$

Where I_o= the incident Intensity, I = intensity, t = length of cuvette μ= absorption coefficient depending strongly on X-ray energy E and atomic number Z, and on the density ρ and atomic mass A as seen in eq 2.15:

$$\mu \approx \frac{\rho Z^4}{AE^3} \quad eq.2.15$$

Comparing I to I_o at increasing energy over the absorption edge, it is possible to determine the energy dependence of μ(E) and generate an X-ray absorption spectrum. An X-ray absorption spectrum is recorded from around 200 eV below an absorption edge of interest to about 1000 eV over the edge. A typical XAFS spectrum consists of two distinct regions. One of the regions is denoted as X-ray absorption near edge structure (XANES), where the energy of the photon is enough to excite a core electron to unfilled orbitals. This region is

set within ~50 eV of the absorption edge. The second region is known as Extended X-ray absorption fine structure (EXAFS) where the oscillatory structure after the electron has been ejected and it can be >1000 eV past the edge (Figure 2.5). The separation in regions is made to ease the data analysis. The details of each region and its characteristics will be discussed below.

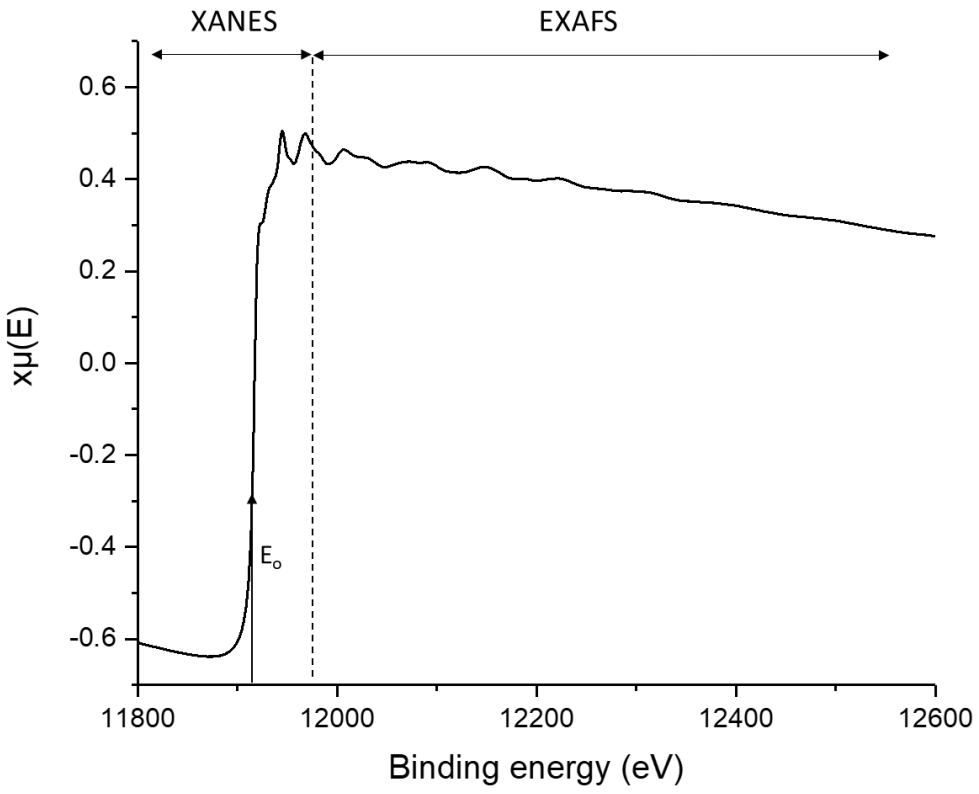

Figure 2.5: Schematic diagram of an X-ray absorption spectroscopy spectrum of the Au-L_3 edge showing the absorption edge, the XANES and EXAFS regions.

2.4.9.1 X-ray Absorption Fine-Structure; X-ray Absorption Near Edge (XANES)

The area on the XAS spectra starting approximately 50 eV below the absorption edge is known as X-ray Absorption Near Edge (XANES) region. It is associated with the electronic transition from core to higher levels of the probe element, based on the dipole selection rules according to which Δl= +/- 1, Δj = +/- 1, Δs=0. For XANES, the interpretation of the wavefunction by a physical equation is not possible, as in the EXAFS region, however, it is still feasible to obtain important information such as the oxidation state and discriminate the different phases of a material. A significant and typical application of XANES is the utilization

of the edge position shift to determine the oxidation state. In addition, XANES analysis based on linear combinations of known spectra from standard compounds is sufficient to determine the ratios of different oxidation states and the presence of different phases.

The XANES region can contain the following characteristics, an absorption edge Eo, a pre-edge and a post-edge.

- The absorption Edge, E_o: The absorption edge is related to the excitation of a core electron to the continuum and is the most prominent feature in the XANES. An increase in valence states leads to shifting of the edge position due to the stronger electrostatic attraction from the nucleus which results in the need of higher energy to cause excitation. The energy of the edge for Au is 11919 eV and each element has its own characteristic. E_o depends on the oxidation state, and it can rise by a few eV per oxidation state, and coordination geometry. In the XANES region the L_2 and L_3 edges of transition metals contain an intense preliminary peak at the top of the absorption edge that is known as white line. Historically, the term white line is derived from the fact that, initially, X-ray spectra were collected on film and while strong absorption at a certain energy left the photographic negative unexposed, this resulted in the formation of a white line on the film. For the Au-L_3 edge, the white line arises from the excitation of a 2p3/2 core electron to unoccupied 5d orbital states. It must be raised that the E_o can also refer to other quantities as well. It can be defined operationally, based on the shape of the spectrum for instance by choosing the first inflection point or by the steepest inflection point or a point halfway up the edge. It can also be taken from a table, or it can be chosen as to make the EXAFS equation for a model structure to match the data as well as possible. These ways of setting the E_o values result in values that diverge among them by some eV values.

The pre-edge is used in 2 distinctive ways; to identify the featureless part of the spectrum before the sharp rise associated with the edge or to identify small features below the midpoint of the rising portion of the spectrum, such as small sharp peaks. The pre-edge features occur below the energy of the rising edge due to transitions of core electrons to empty states close to the Fermi level. These transitions are not allowed according to the dipole selection rules yet can occur due to orbital hybridisation. Pre-edges contain information related to symmetry, local geometry, and electronic state around the absorbing atom.

- Post-edge: The post edge is contingent to multiple scattering features. The analysis of the post-edge provides information regarding the local atomic structure and geometry.[26]

Normalized XANES spectra of three Au references with the following oxidation states, Au^0, Au^+ and Au^{3+} are presented in Figure 2.6. Linear Combination Fitting (LFC) was performed to determine the Au oxidation states of Au catalysts, using known standards such as Au foil, $[AuCl_2]^-$ and $[AuCl_4]^-$, with an oxidation state of Au^0, Au^+ and Au^{3+}. The spectrum of the Au^0 reference does not contain a normalized white line-height, whistle the spectra of Au^+ and Au^{3+} display a normalized white line-height of 0.6 and 1.1, correspondingly.[27]

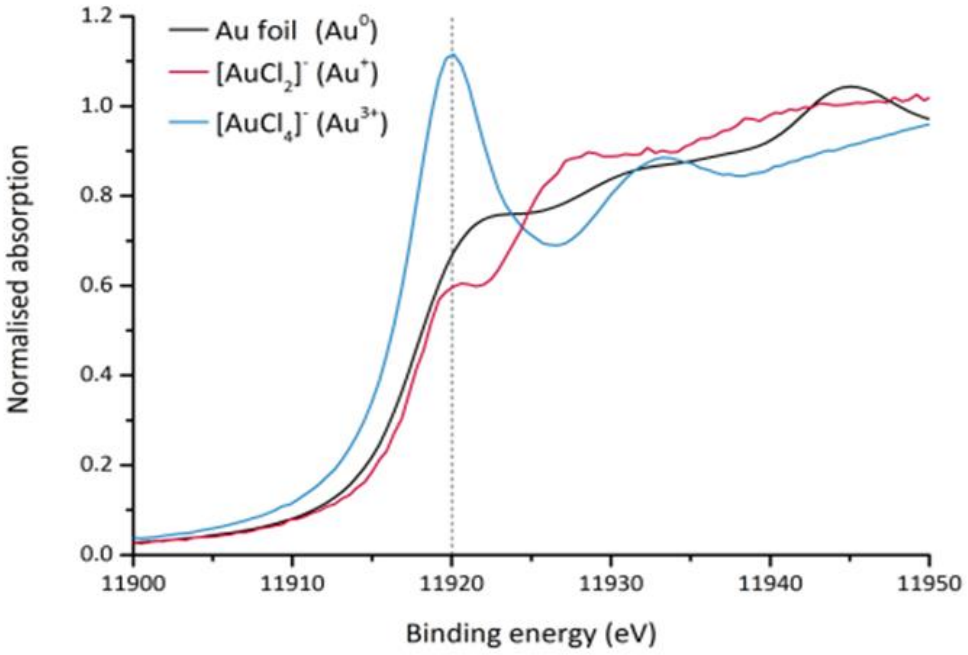

Figure 2.6: Au-L_3 edge XANES region of Au foil, $[AuCl_2]^-$ and $[AuCl_4]^-$, Au standards with an oxidation state of Au^0 Au^+ and Au^{3+}, respectively.[22]

2.4.9.2 X-ray Absorption Fine-Structure; The extended X-ray absorption fine structure region (EXAFS)

EXAFS focuses on the oscillations that are observed in the XAS spectrum derived from the interactions of the outgoing photoelectron with the surrounding environment of the selected element. This section of the spectrum can provide information related to the local geometrical structure, the identity, and the coordination chemistry of the closest neighbours of the targeted atoms.[28] The observed oscillations can be explained in the following way. The discharge of a photoelectron in an isolated atom leads to photoelectron propagation as an unperturbed isotropic wave. In the case of molecules, the absorber atom is surrounded

by neighbours, which can cause the photoelectron to back scatter. This results in the scattered photoelectron returning to the absorbing atom. The backscattering can interfere with the emitted electron constructively or destructively depending upon the waves being in phase or out of phase. When the backscattered and the outgoing wave are in phase, constructive interference will enhance the amplitude of the final wave. At different excitation energies, the outgoing wave will have a different wavelength and phase, and destructive interference with the backscattered wave is probable. These interactions result in the energy-dependent oscillations in the EXAFS region of the spectrum (Figure 2.7).

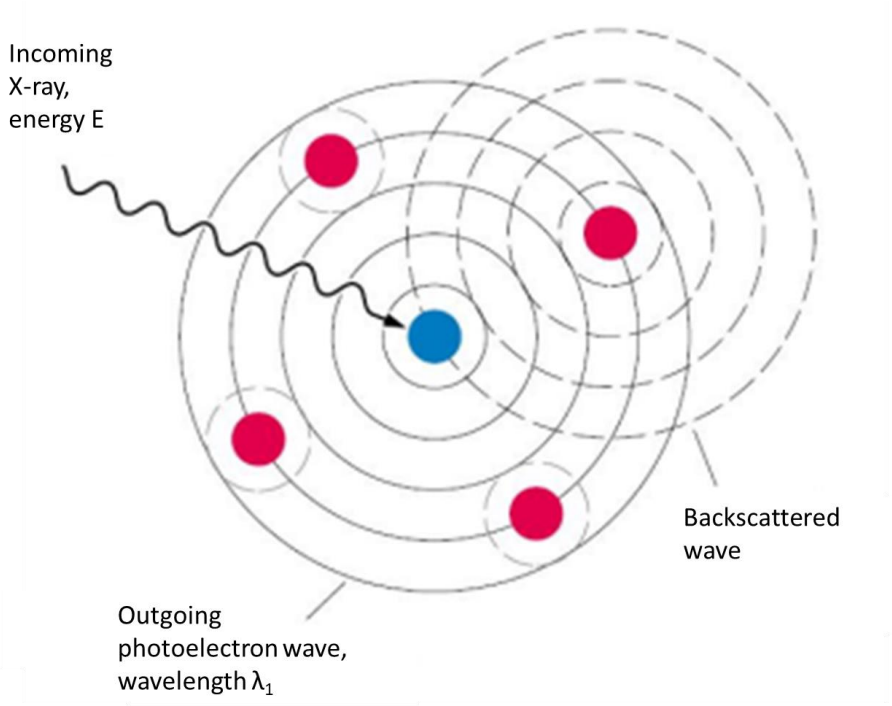

Figure 2.7: Schematic image of backscattering of the spherical photoelectron wave, originating from the blue absorber, by its red nearest neighbours.[24]

The photoelectron produced by the absorption process can be expressed in terms of the wave behaviour of a wavelength value (Equation 2.16) defined as

$$\lambda = \frac{2\pi}{k} \quad eq\ 2.16,$$

$$with\ wave\ vector\ k = \sqrt{\frac{2m_e(E - E_0)}{\hbar^2}}\ eq.2.17$$

where E_o is the absorption edge energy m_e and is the electron mass and ħ is Planck's constant. The electron scattering process depends on range of factors such as:

- The atomic number of the scatterer: heavier atoms will scatter more than lighter ones.
- The distance of the absorber and the scatterer.
- The Debye Waller factor according to which decay of the EXAFS signal will become greater with increasing thermal disorder.
- The energy of the scattered electron.

The EXAFS equation associates the EXAFS signal to structural parameters as modelled by Stern.[29] This model considers only a single scattering process in which the excited photoelectron is backscattered to the same atom. Nevertheless, it is established that several scatterings take place in one system alone so, the EXAFS equation takes into account the summation of the waves produced by the outgoing photoelectron wave function and the backscattered wave function from each coordination shell (Equation 2.18) in which the photon-electron interacts with at least two or more atoms before returning to the targeted atom.[30]

$$\chi(k) = \sum_j \frac{So^2 N_j f_j(k) e^{-2k^2\sigma_j^2}}{kR_j^2} \sin\left[2kR_j + \delta_j(k)\right] \quad eq.\,2.18$$

- j = coordination shell
- $S_o^2 N_j$ = terms that adjust the amplitude of the EXAFS signal and are independent from the wave vector. For a single scattering, Nj is the atoms coordinated to number to a certain shell (coordination number) and S_o^2 is the amplitude reduction factor, related to the presence of an empty core level and multi-electron excitations (typical values are 0.7 -1.1).[28] Each element has a unique S_o^2 value.
- $f_j(k)$ = factor that describes the elemental sensitivity of EXAFS. In general, atoms with more electrons scatter photoelectrons more strongly at higher wavenumbers. Since this factor depends on the number of electrons, it is similar between elements with a similar number of electrons. Thus, Cl and S cannot be distinguished solely by their scattering amplitude.
- $e^{-2k^2\sigma_j^2}$ = is known as the Debye–Waller or EXAFS isotropic factor and describes the decrease of the signal with rising thermal or static disorder. The locations of the atoms from their equilibrium atomic levels can be disturbed by thermal or static disorders and this effect becomes more significant the further from the absorber, resulting in the reduction of the EXAFS signal.
- R_j factor that describes the average interatomic distance of the absorber-scatter.
- sin $(2kR_j + \delta_j(k))$ = factor that describes for the oscillations in the EXAFS signal with a phase given by $2kR_j + \delta_j(k)$. $2R_j$ relates to the photoelectron path multiplied by its

wavenumber (k) to determine the phase. The interaction of the photoelectron with the nuclei of the absorbing atom and with the nuclei of the neighbouring atoms of the photoelectron path is ascribed to the $\delta_j(k)$ term.

Experimental analysis

X-ray Absorption Fine Structure (XAFS) analysis was conducted at the Diamond Light Source in Harwell using the B18 beamline. Measurements were completed *via* a QEXAFS setup with a fast-scanning Si (111) double crystal monochromator or a 36 element Ge fluorescence detector. Data analysis for X-ray absorption spectroscopy was performed using IFEFFIT. IFEFFIT is a library and set of interactive programs for the analysis of X-ray absorption fine-structure (XAFS) data and includes the Athena and Artemis software. Athena was used as part of the XANES analysis while Artemis is used for EXAFS analysis.

Ex-situ sample analysis at the Au L_3 absorption edge in transmission mode was performed. All analysis was completed with reference to an Au foil standard, $KAuCl_4$ and $AuCl_2^-$ standard compounds. A minimum of 5 runs were conducted on each sample for XANES analysis and the data averaged, resulting in an error value of ± 5%. The assistance of Martin Wilding in performing the XAFS experiments at the Diamond Light Source, is appreciatively recognized.

2.4.10 Boehm Titration

Boehm titration is a technique used to verify the acidic oxygen surface functional group content on carbon. The technique uses bases of various strengths such as $NaHCO_3$, Na_2CO_3, and NaOH to neutralize different acidic oxygen surface functionalities. The weakest base, $NaHCO_3$, neutralizes the strongest acidic carbon surface functionalities (CSFs) such as carboxylic groups. Na_2CO_3 neutralizes carboxylic and lactonic groups while, the strongest base NaOH, neutralizes carboxylic, lactonic and phenolic groups. The volume of CSFs can be identified by the difference in the uptake of each base.[31] The activated carbons used in this study are described in Chapter 4.

Experimental analysis

Activated carbon (1.5g) was added in 50 ml of 0.05 M of one of the three reaction bases ($NaHCO_3$, Na_2CO_3, and NaOH). The mixture was left to stir at room temperature for 16h. The mixture was filtered, and a 10 mL aliquot was collected. The collected aliquot was acidified with the addition of 20 mL of 0.05 M HCl solution. Accordingly, the acidified solution was purged with N_2 to remove any dissolved CO_2 from the solution over the period of 1h. Subsequently, the sample was titrated using 0.05 M NaOH and the endpoint was determined with phenolphthalein. All titrations were carried out at room temperature.[31]

2.5 List of chemicals and suppliers

List of all the chemicals that have been used for the synthesis and experiments that are described in this thesis.

Chemical	Formula	Supplier	Purity
5 % Acetylene/argon	C_2H_2/Ar	BOC	95
5 % Hydrogen chloride/argon	HCl/Ar	BOC	95
Argon	Ar	BIP	99.9999
Chloroauric acid	$HAuCl_4 \cdot 3H_2O$	Alfa Aesar	99.99
Activated carbon, Norit ROX 0.8	A.C.	Johnson Matthey	-
Acetone extra dry ACRO seal	$(CH_3)_2CO$	Acros Organics	99.8
Activated carbon, NORIT KB-B	A.C.	Cabot Corporation	-
Activated carbon, CECAL2S	A.C.	Johnson Matthey	-
Activated carbon, CECAL4S	A.C.	Johnson Matthey	-
Activated carbon, GSX	A.C.	Cabot Corporation	-
Phenanthroline	$C_{12}H_8N_2$	Alfa Aesar	99.0
3.4.7.8-Tetramethyl-1.10-phenanthroline	$C_{16}H_{16}N_2$	Sigma Aldrich	98.0
Bathophenanthroline	$C_{24}H_{16}N_2$	Sigma Aldrich	97.0
1.10-phenanthroline-5-amine	$C_{12}H_9N_3$	Sigma Aldrich	97.0
5,6-Epoxy-5,6-dihydro-[1,10]phenanthroline	$C_{12}H_8N_2O$	Sigma Aldrich	98.0
N,N,N,N-Tetramethyl-thiourea	$C_5H_{12}N_2S$	Thermo Fisher Scientific	98.0
N-Methyl-2-pyrrolidone	C_5H_9NO	Sigma Aldrich	99.5
2-Mercaptobenzimidazole	$C_7H_6N_2S$	Sigma Aldrich	98.0

2-mercaptobenzoxazole	C_7H_5NOS	Sigma Aldrich	95.0
2-Methylcyclopentanone	$C_6H_{10}O$	Sigma Aldrich	98.0
2-Pyrrolidone	C_4H_7NO	Sigma Aldrich	99.0
Cyclopentanone	C_5H_8O	Sigma Aldrich	≥99
1-Vinyl-2-pyrrolidinone	C_6H_9NO	Sigma Aldrich	99.0
1-Methylpyrrolidine-2-thione	C_5H_9NS	Fluorochem	99.0
N-Methyl-2-piperidone	$C_6H_{11}NO$	Sigma Aldrich	99.0
1-Methylpyrrolidine	$C_5H_{11}N$	Sigma Aldrich	98.0
Platinum (II) acetyleacetonate	$Pt(C_5H_7O_2)_2$	Sigma Aldrich	97.0
Copper(II) chloride dihydrate	$CuCl_2 \cdot 2H_2O$	Sigma Aldrich	99.999

2.6 References

1. IGI Systems Process Interface. Date cited: January 2 2023, available from: http://www.igisystems.co.uk/process-interface.html.
2. LAB Interface Software Application and Process Interface Hardware. Date cited: January 2 2023, available from: http://www.igisystems.co.uk/LAB-Interface.html.
3. Safety data sheet of acetylene. Date cited: January 6 2023, available from: https://www.gasandsupply.com/docs/SDS/Acetylene%20SDS.pdf.
4. Safety data sheet of hydrogen chloride. Date cited: January 6 2023, available from: https://www.sigmaaldrich.com/GR/en/sds/aldrich/295426.
5. Safety data sheet of vinyl chloride monomer. Date cited: January 8 2023, available from:https://www.shintech.com/UserFiles/files/Safety-Data-Vinyl-Chloride-Monomer.pdf.
6. Absorbents products: Porapak series. Date cited: January 8 2023, available from: https://www.glsciences.com/product/gc_packings/column_packing/01412.html.
7. Kitson F. G., Larsen B. S., McEwen C. N., Gas chromatography and mass spectrometry, Academic Press, 2nd edn., 1996.
8. Sample Injection – Valco 6 port valve. Date cited: January 10 2023, available from: https://www.vici.com/support/app/app11j.php
9. Skoog D. A., West D. M., Holler F. J., Crouch S. R., Fundamentals of analytical chemistry. Thomson Learning, 8th edn., 2004.

10. Tolley H. D., Tolley S. E., Wang A., Lee M. L., Moving thermal gradients in gas chromatography, J. Chromatography A, 2014, **1374**, 189-198.

11. Szepesy L., Gas chromatography, Iliffe Books Ltd., 1st edn., 1970.

12. Warren B. E., X-Ray Diffraction Methods. J. Applied Phys., 1941, **12**, 375-384

13. Drenth J., X-ray Diffraction: Principles. John Wiley & Sons Ltd Ed., 1st edn., 2003

14. Bragg W. L., The structure of some crystals as indicated by their diffraction of X-rays. Proc. R. Soc. Lond., 1913, 89, 248–277.

15. Rozhdestvina V. I., Mudrovskii E. A., Levitskii T., Contact mass transfer and phase formation in the Au-Pb system. Inorg. Mat., 2007, **43**, 816–821.

16. Niemantsverdriet J. V., Spectroscopy in catalysis. Willey-VCH, 3rd Edition, 2007.

17. Basu P., Biomass gasification, pyrolysis and torrefaction. Academic Press, 3rd edn., 2018.

18. Hasegawa T., Fundamentals of FT-IR: Infrared Spectroscopy for Understanding of a Condensed Matter. Springer, 1st edn., 2001

19. Petry R., Schmitt M., Popp J., Raman spectroscopy-a prospective tool in the life sciences. Chemphyschem., 2003, **4**, 14–30.

20. Brunauer S., Emmett P. H., Teller E., Adsorption of gases in multimolecular layers. J. Am. Chem. Soc.,1938, **60**, 309–319.

21. Ionin B. I., Ershov B. A., The Fundamentals of NMR Spectroscopy. NMR Spectrosc. Org. Chem., 1970, **54**, 1–59.

22. Tampieri A., Szabó M., Medina F., Gulyás H. A brief introduction to the basics of NMR spectroscopy and selected examples of its applications to materials characterization. Phys. Sci. Rev., 2021, **6**, 1–41.

23. Zaikin V., Varlamov A., Mikaia A., Prostakov N., Fundamentals of Mass Spectrometry. Russ. Acad. Sciences, 2013, **19**, 399-445.

24. Conradson S. D., A technique to probe local structure. Los Alamos Science, 2000, **26**, 423–435.

25. Newville M., Fundamentals of XAFS. Rev. Mineral. Geochem., 2014, **78**, 33–74.

26. Bunker G., Introduction to XAFS a practical guide to X-ray Absorption fine structure spectroscopy. Cambridge University Press, 1st edn., 2010.

27. Malta G., Kondrat S. A., Freakley S. J., Davies C. J., Lu L., Dawson R. S., Thetford A., Gibson K. E., Morgan D. J., Jones W., Wells P. P., Johnston P., Catlow R. A., Christopher J., Kiely C. J., Hutchings G. J., Identification of single-site gold catalysis in acetylene hydrochlorination. Science, 2017, **355**, 1399–1403.

28. Ravel B., Newville, M., Athena, Artemis, Hephaestus: data analysis for X-ray absorption spectroscopy using IFEFFIT. J. Synchrotron Rad., 2005, **12**, 537–541.

29. Stern E. A., Structure determination by X-ray absorption .Contemp. Phys., 1978, **19**, 239–310.

30. Calvin S., XAFS for Everyone. CRC Press,1st edn., 2003.

31. Boehm H. P., Some aspects of the surface chemistry of carbon blacks and other carbons. Carbon N. Y., 1994, **32**, 759–769.

Chapter 3

Systematic review and data comparison of best-in-class catalysts for the acetylene hydrochlorination.

3.1 Introduction

In this chapter a general methodology that allows rapid screening of different catalytic systems for any reaction for the identification of the best-in-class system will be described. Using literature data published on the acetylene hydrochlorination reaction as a case study, a simple method to compare catalysts that have been tested over a range of conditions will be explained. There are many reports claiming that, for the acetylene hydrochlorination reaction, Au is the best catalytic system as it exhibits better activity in comparison to other precious metals, non-precious metals as well as metal free materials.[1] However, in addition to Au, there are many other claims which suggest other catalysts may rival Au, with claims of being higher activity or stability, and represent a viable alternative to the toxic mercuric chloride catalysts. In this chapter, the above claims will be discussed thoroughly with normalisation of literature data being used to attempt a fair comparison.

The motivation behind this work arose during the challenging times presented by COVID-19. As access to the laboratory was restricted, it was the published literature that facilitated a better understanding of the best catalytic system for the acetylene hydrochlorination reaction upon normalising of crucial performance parameters. The introduced method can be widely used for a rapid screening and identification of the best catalytic system for any reaction of interest. Indeed, in our published work, this approach was also used for comparison of data relating to the selective oxidation of methane, however in this chapter only acetylene hydrochlorination will be discussed.[2]

3.2 Overview

In industry, approximately 85-90% of the reactions utilise a catalyst, and approximately 80% of those reactions rely on heterogeneous catalytic systems.[3] Therefore, catalysis is profoundly significant for world prosperity and is a fundamental area of ongoing scientific investigation. The design criteria for the development of novel catalytic systems for any reaction is a constant endeavour that relies on years of research. In the acetylene hydrochlorination reaction, there are many catalytic systems that have been suggested to be alternatives for the environmentally toxic Hg catalyst. Different catalytic systems such as

monometallic catalysts and bi/tri-metallic catalysts, as well as metal free catalysts, have been widely investigated by a variety of research groups.[4] The wide scope of catalyst design leads to discovery of new catalysts every year with each research group claiming that their novel catalyst is the best.

Direct comparison of catalytic systems that present intrinsic differences, and that have been studied under varying conditions, cannot lead to reliable conclusions. Identifying the best catalytic system, for a particular reaction, is therefore challenging. Ideally, for a given reaction, all catalysts should be tested at the same experimental conditions, in order to conduct a straight comparison between the catalysts. Unfortunately, this is not a feasible task, as different research groups test their catalysts at various conditions, therefore a direct comparison might provide perplexing evidence as to which is the best catalytic system for a particular reaction.

The question that is inevitably raised is whether it is possible to find the best catalyst for a reaction based on the available literature data. The answer to this broad question will be attempted to be given using the published data of a very specific reaction; acetylene hydrochlorination. However, it must be noted that any reaction could be used as a model to answer this question on the condition that data is accessible. Using the acetylene hydrochlorination reaction as a model, collecting information from the present literature it will be endeavoured to answer the above question. Acetylene hydrochlorination to produce vinyl chloride monomer (VCM) is a well investigated reaction with an increasing number of research papers being published and patents claimed annually, hence the data provided should be efficient for this study.

3.3 An introduction to the methodology

Assessing the activity of a catalyst is a complicated process as there are many parameters and variables to be taken into consideration. For the industrial acetylene hydrochlorination reaction, tubular fixed bed reactors are commonly employed.[1,4,5] The simple design of fixed bed reactors have made them widely popular for the manufacture of large-scale chemicals and intermediates. These reactors are mainly used for heterogeneously catalysed gas phase reactions that involve solid catalyst pellets. For exothermic reactions, a cooling medium is also attached to the reactor tubes.[6] For these types of reactors, the catalytic performance depends significantly on the catalyst mass, metal loading, contact time, gas hourly space velocity (GHSV), reaction temperature, pressure, and reactants concentration.[7] Evidently, the catalytic activity can be subjected to a variety of different parameters.

Theoretically It would be ideal if all catalyst for any reaction would be studied at the same operating conditions, as this would allow a direct comparison of the data. Nevertheless, in the field of heterogeneous catalysis it is most common that catalysts are assessed at a wide range of different experimental conditions. Assessing catalysts that have studied at different reaction conditions can lead to misleading conclusions. Available literature data reports the performance of catalysts at various reaction conditions, and in most cases the catalytic performance of a system is presented at the optimal reaction conditions. Hence, it is possible for catalysts with vastly different intrinsic activities to exhibit similar activity profiles when factors such as mass transfer effects are not taken into consideration.

To address this issue, a general approach that will allow a fair comparison of catalysts will be described. This method relies on basic engineering concepts, the selection and identification of the most important parameters of the operational figures and the further normalisation of the key variables. It should be noted that there is a wide range of factors that can be considered, yet it is important to recognize the mains ones to be the productivity, selectivity, lifetime, stability, deactivation, and environmental footprint of the catalyst. The following steps includes normalising the key reaction rates. For instance, if there are variations in the range of temperatures under which the catalysts have been assessed, then an estimate of the activation energy to normalise the rates can be applied. The final step is the comparison of the normalised data in a constructive way to reach a conclusion. This approach will be demonstrated using the acetylene hydrochlorination reaction. There are many reviews that summarise much of the available literature data, however in most of them the catalysts are compared by the acetylene conversion, despite being evaluated at different operating conditions. On that basis, it is not possible to determine which catalyst is the best. So, there is a need to develop a general, rapid, and effective approach to compare the catalyst performance for any reaction.

3.4 Study of the acetylene hydrochlorination

The development of novel non-Hg catalysts to produce vinyl chloride monomer (VCM) became imperative after the Minamata convention in 2013.[8] VCM is a key intermediate for the production of polyvinyl chloride (PVC), which is the third major commodity chemical, with an annual global production that exceeds 40 million tons and a predicted annual increase of 2.3% by 2024.[4,5] PVC can be used in numerous practical applications, and is traditionally produced *via* polymerisation of VCM.[4] A major industrial process to produce VCM relies on the direct acetylene hydrochlorination, thus this reaction has a major industrial interest.[6]

Over the past few decades, the interest for the acetylene hydrochlorination reaction both in academia and industry has increased sharply. For the acetylene hydrochlorination reaction, the number of patents exceeds the number of research papers that are published each year (Figure 3.1). From the high number of patents on the acetylene hydrochlorination reaction over the academic publications it is apparent that there is an active commercial interest for the development of a novel catalyst for this particular reaction.[22] Acetylene hydrochlorination is a good example to study the proposed methodology as there is a great number of data available, there is a wide range of different catalytic systems to study with the catalysts illustrating an excellent selectivity to VCM regardless of the metal nature. In addition, this reaction is carried out at near ambient pressure and the ratios of the reactants are limited to a slight excess of HCl. Therefore, the number of key reaction parameters are reduced for this test case.

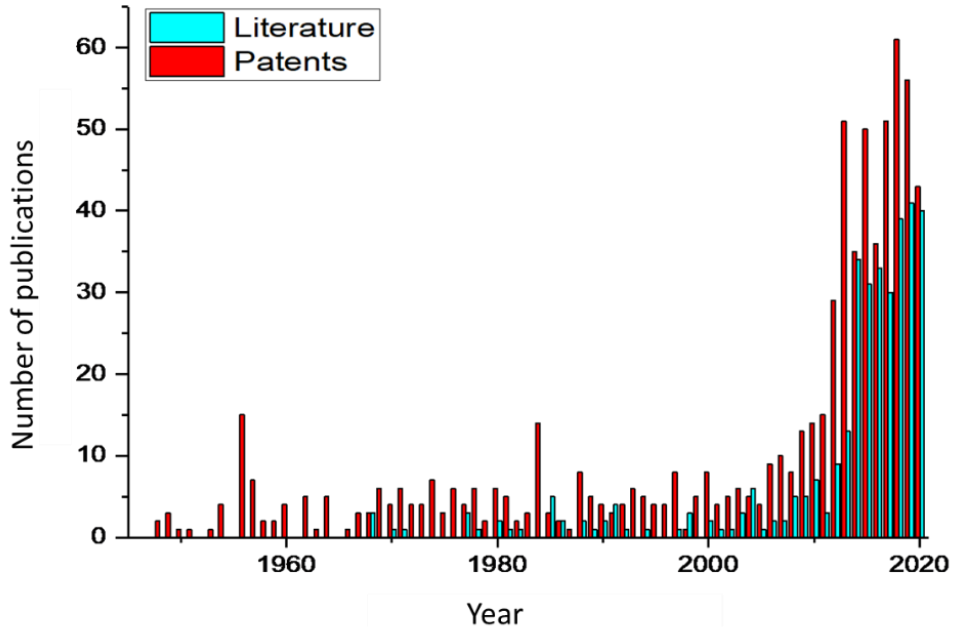

Figure 3.1: A search of papers and patents relating to “acetylene hydrochlorination” between 1945 and 2020, Key: red = patent applications, blue = research publications (Source: data derived from Scopus & Google Patents). Figure adapted from reference 2.

The field of catalysts that have been developed for the acetylene hydrochlorination reaction involves a broad range of systems, which will be discussed in the following sections.

3.4.1 Au based catalysts.

Au supported on activated carbon catalyst has for long been investigated as potential substitute for the toxic $HgCl_2$ for the acetylene hydrochlorination reaction. The developments of Au-based catalysts for acetylene hydrochlorination have been thoroughly

reviewed by Hutchings and collaborators.[4,9,10] At the early stages of Au-based catalyst preparation, aqua regia was used as a solvent to ensure the solubilisation of Au precursors.[11] From an industrial point of view, it is a non-desirable solvent to use. The corrosive, hazardous, environmentally unfriendly profile of this solvent raises many concerns regarding its practice. In addition, the aqua regia synthesised Au-based catalyst are less stable and suffer from deactivation due to polymerisation of acetylene on the surface of the catalyst, which is induced by the presence of acid sites that were introduced by the solvent.[10,12]

To avoid the use of aqua regia during the preparation and to enhance the stability of the active sites under reaction conditions, different approaches have been developed. It is possible to prepare effective Au supported on activated carbon catalysts using low polarity, low boiling point solvents such as acetone.[13] Efforts to prepare Au catalysts using water as a solvent and $HAuCl_4$ as a gold precursor resulted in catalysts with poor activity.[14] However, it was demonstrated that the coordination of Au centre with an organic ligand, can lead to the formation of highly active Au based catalysts when using water as a solvent. The novel Au-thiosulfate, -thiocyanate, -thiourea complexes exhibit greater activity and stability when compared to Au-halides, -nitrogen, or -oxygen complexes. The above-mentioned catalysts have been prepared by immobilisation of the cationic Au complex on activated carbon support employing an aqueous solution, eventually avoiding the use of aqua regia (Table 3.1).[10,15]

Au precursor complex	Au %	[a]Conversion %
$Au(CS(NH_2)_2)_2$	0.1	95
$Na_3Au(S_2O_3)_2$	0.1	86
$KAu(CN)_2$	0.1	85
$(NH_4)_3Au(S_2O_3)_2$	0.1	75
$KAu(SCN)_4$	0.1	74
$Ca_3[Au(S_2O_3)_2]_2$	0.1	74
$KAu(CN)_4$	0.1	69
$Au(NCNH_2)_2$	0.1	55
$HAuCl_4$ + Aqua regia	1.0	52
$HAu(C_3Cl_3N_3O_3)_3Cl$	1.0	52
$[Au(P(NCH_2CH_2OCH_2CH_2)_3)_2]NO_3$	1.0	33
$[(AuCl)_2dppe]$	1.0	14
$[Au(en)_2]Cl_3$	1.0	14
$HAuCl_4 + H_2O$	1.0	11

Blank Carbon extrudate	-	7

Table 3.1: Catalyst screening of Au/C catalysts containing a range of soft and hard ligands. Reaction conditions involve 5g of catalysts tested at 130 °C at a total GHSV=500 h^{-1}. [a]Activity expressed as the conversion recorded after 24 h time on-line.

The Au-S containing ligand catalysts stabilise the Au cationic active centres and inhibit the reduction of Au cationic species to metallic Au (0), increasing the stability of the catalyst. The conversion of the best-in-class Au thiosulfate catalyst is recorded to be higher than 90% with the selectivity being greater than 99%. This improved activity was observed at low 0.1.% Au loading. In contrast, aqua regia Au/C catalysts require a higher metal loading of ≥ 0.3 % due to challenges in catalyst activation, when loading is lower.[10] Au thiosulfate catalyst is commercially validated as Johnson Matthey's PRICAT catalysts for the development of Hg-free process (DAVY VCM process). Additional Au-S containing complexes have also been investigated by other groups. Zhang *et al.* demonstrated that Au glutathione (GSH) supported on activated carbon display great activity in contrast to monometallic Au systems due to increase in the chemisorption of HCl.[16] Furthermore, Zhu *et al.*[17] reported an active $AuCl_3$-thiourea supported on carbon catalyst, while in 2016 Luo *et al.*[18] observed that the addition of trichloroisocyanuric acid (TCCA) improved the stability of the Au based catalyst. Wei *et al.* reported a low content Au based catalyst that includes a complex of Au with thiocyanate (SCN) of great stability due to the decrease of the electrode potential of Au^{3+} from 0.926 V to 0.662 V.

In addition, some research groups focus on the N-containing ligands. In 2014 Dai *et al.*[20] described a highly active and stable Au(III)/Schiff-base catalyst $[AuCl_2(phen)]Cl$. The enhanced activity of the novel catalyst was ascribed to the coordination of 1,10-phenanthroline, which prevents the reduction of Au^{3+} to metallic Au (0) by stabilising the Au centre. Moreover, a chlorotriphenylphosphine Au ($AuPPh_3Cl$), prepared by incipient wetness impregnation of chloroauric acid and triphenylphosphine (TPP) was reported by Zhang and his co-workers.[21] The advanced activity of the catalyst was attributed to the presence of TPP that stabilises the Au^{n+} active centres, preventing their reduction to metallic Au (0).

Another alternative to the use of aqua regia has been the discovery in 2010 by Li *et al.,* who introduced the the ''organicus liquor regius'' also called Organic Aqua Regia (OAR) which is a which is a mixture of thionyl chloride (SOCl2) and N,N-dimethylformamide (DMF).[22] The Au supported on activated carbon catalysts prepared using OAR exhibited a high catalytic activity. In addition, the used catalyst could be regenerated when treated with the

OAR solution. It is postulated that the active site of the catalysts includes Au-S complexes, whereas residual N atoms may increase the electron density of the Au centre through electron transfer, which accordingly inhibits the reduction of the Au^{3+} species, therefore stabilizing the cationic Au species. Additionally, it is suggested that the electron-rich catalyst, as the one produced with OAR, increases the adsorption of HCl while weakening C_2H_2 chemisorption, precluding the reduction of the active Au cationic species caused by C_2H_2.[23]

3.4.2 Additional monometallic catalysts

Considering the high value of Au, there has been an increasing attention on developing more cost-effective catalysts based on other noble metal or non-precious metals. Interestingly, Pt is approximately 40% less expensive than Au which from an economics perspective seems to be appealing. In 2020, Ramirez *et al*.[24] reported single atom Pt catalysts to demonstrate an advanced activity in comparison to their nanoparticle analogues. It was indicated that the oxidation state and coordination environment of the single Pt atoms (SA) determined the activity profile of the catalysts, as it was shown that the activity decreases in the following order: Pt(II)−Cl (SA)≫Pt(II)−N (SA)≈Pt(IV)–Cl (SA)>Pt(0) nanoparticles. The advanced catalytic performance of Pt(II)−Cl single atoms is attributed to the increased acetylene adsorption capacity in comparison to another single atom Pt site. In addition, it was reported that the choice of the support did not affect the activity of the Pt catalysts, while it affected the stability of the catalysts. In the field of Pt-based single atom catalysts, Hutchings *et al*. demonstrated that the activity of single atom Pt catalysts prepared using acetone as a solvent exhibited a lower activity in comparison to the equivalent single atom Au catalyst.[25] To the date the number of studies on Pt catalysts is limited, as the relatively poor performance of these materials in comparison to Au-based systems discourages further studies. However, the recent advances in nano structuring of Pt the active site expands the scope for further optimisation Pt catalysts to improve their activity.

DFT studies performed by Dai *et al*. illustrated that the activation energy for $HgCl_2$, $AuCl_3$ and $RuCl_3$ is 16.3, 11.9 and 9.1 kcal/mol respectively, suggesting that Ru-based catalysts may be a good candidate as catalyst for the hydrochlorination of acetylene.[26] Unlike Au and Pt catalysts that consist of active single atoms, Ru catalysts display an opposite particle size dependency. The active site for Ru-based catalysts has been an issue of dispute as it has not been explicitly identified whether RuO_2, RuO_x, $RuCl_3$ or Ru_xCl_y are responsible for the activity. For instance, it has been reported by Li *et al*.[27] that RuO_2 is the active site for the acetylene hydrochlorination reaction, while on the other hand, Zhang conducted a series

of studies that on Ru_xCl_y and illustrated that the optimum catalytic performance was achieved over the Ru_5Cl_7/AC.[28] More recently, Ramirez and collaborators identified active RuO_xCl_y nanoparticles of approximately 1.5 nm size supported on polyaniline-derived N-doped carbon as the most efficient catalyst.[29]

In addition, further attention has been drawn to the development of Cu catalysts. Despite the higher metal loading of Cu-based catalysts (5-15 wt.%), the relatively low price and abundance of this metal, sets it as the most promising non-noble metal catalysts alternative. Unfortunately, Cu-based catalysts are less active and suffer from rapid deactivation which is attributed to the agglomeration of active species and coke deposition.[30] Different approaches for the improvement of the Cu-based catalysts include support modification, ionic liquids coordination and ligand addition.[30-33] Zhou *et al.*[34] described a highly active Cu supported on N-doped carbon nanotubes catalyst, while the active species were suggested to be Cu^+ and Cu^{2+}. Similarly, Zhao and his co-workers reported a $CuCl_2$ deposited on graphitic carbon nitride catalyst that exhibited great activity.[35] Accordingly, Li *et al*.[36] studied highly active Cu supported on phosphorus doped spherical activated carbon catalysts confirming the active species to be Cu^+ and Cu^{2+}. More recently, Zhao *et al*. reported a Cu-N-methyl-pyrrolidone supported on spherical activated carbon (Cu-NMP/SAC) catalyst that exhibited improved activity and stability in comparison to Cu/ SAC catalyst. It is postulated that the addition of NMP ligand enables the high dispersion of Cu species, while stabilising the active Cu^+ and Cu^{2+}, and restrain the coke deposition.[37] DFT studies propose that high reactivity is attributed to the favourable catalyst–ligand interactions which reduce the adsorption of C_2H_2 and VCM, while enhance the adsorption of HCl, and prevent the carbon deposition caused by acetylene agglomeration.[38]

In the quest of discovering environmentally friendly catalysts that are cost-effective, Pd catalysts have been widely investigated. Despite their great initial activity, Pd catalysts suffer from rapid deactivation, due to the volatility of Pd active species under the reaction conditions.[39] Over the past few years numerous Pd-based catalysts were studied such as Pd/AC, Pd/HY,[40] Pd–K/NFY,[41] Pd/NC,[42] $(NH_4)_2PdCl_4$/AC,[43] Pd/g-C_3N_4,[44] Pd-IL/AC,[45] however, all the above systems require further development as issues including metal nuclearity changes, sintering, leaching and coke deposition are observed. The active site of Pd catalysts is a controversial matter of dispute without a general consensus. Recently, Li and collaborators, reported a Pd single-atom catalyst to exhibit a better catalytic activity in comparison to Pd nanoparticles or Pd clusters analogues. Specifically, it was identified that N-doped supports act as strong anchoring sites for cationic Pd^{2+}, while the advanced activity is attributed to the enhanced basicity of N-doped carbon material which activates

the acidic acetylene and HCl molecules around Pd active sites.[46] In contrast Ramirez *et al.* reported that, for Pd-based catalysts, metallic nanoparticles exhibit higher performance than single atoms.[47]

In addition, attention has been paid to other metal systems that include Bi,[48,49] Sn,[50,51] mechanically activated Ag,[52] Ir,[53] which have been found to be active for the acetylene hydrochlorination reaction but show stability issues due to loss of active species and the formation of carbonaceous deposits. The majority of monometallic catalysts exhibit a significantly lower activity and stability compared to monometallic Au, whereas some catalytic systems present reduced selectivity to VCM due to polymerization reactions.[54]

3.4.3 Bimetallic and trimetallic catalysts

In 2008 Hutchings *et al*. reported bimetallic Au-based catalysts. As stated, the presence of an additional noble metal such as Pd, Pt, Ir, Rh and Ru, did not have any constructive influence on the activity and stability or even selectivity of bimetallic catalysts. In particular a Au/Pd catalyst exhibited high initial activity but poor selectivity towards VCM. Moreover, the bimetallic Au/Pd catalysts suffered from rapid deactivation due to polymerisation of acetylene on the surface of the catalyst causing coke deposition. The bimetallic Au/Pt catalysts displayed a similar like activity and stability profile. On the other hand, the Au/Ir and Au/Rh catalysts showed improved activity with slight variation in the selectivity, while addition of Ru catalyst did not show any significant contribution. In conclusion monometallic Au systems were suggested to be best catalysts for this reaction, as the addition of a metal additive reduced the standard electrode potential of the system, leading to lower activities.[55]

Further representative studies in the field of bimetallic Au-based catalysts for the acetylene hydrochlorination reaction include Zhang *et al*. who reported that doping Au catalysts with Co stabilizes the catalytically active Au^{+} species and inhibit the reduction of Au^{3+} into metallic Au (0). The increased activity was attributed to the higher standard electrode electric potential of the novel bimetallic Au–Co(III) catalyst.[56] In addition, Wei *et al*. demonstrated that Bi additives stabilise the active Au^{3+} sites, due to electron transfer from Bi^{3+} to Au^{3+} preventing the reduction to Au(0).[57] In addition, Cu has also been studied as an additive for Au-based catalysts. Li *et al.* reported a bimetallic Au/Cu catalyst supported on ionic liquid modified activated carbon that exhibited a great catalytic activity and stability, as it was suggested that the addition of $CuCl_2$ prevented reduction of Au^{3+} species, while in situ re-oxidizes the reduced Au(0) species to the active Au cationic species.[58]

Similarly, trimetallic catalytic systems have drawn attention and have been widely investigated by a plethora of research groups. For instance, Zhang *et al*. studied a Au–

Co(III)–Cu(II) catalyst which was reported to have great activity and long-term stability as a result of the synergistic effects of Co(III) and Cu(II).The advanced activity of the trimetallic Au-based system is attributed to the ability of Co^{3+} and Cu^{2+} to stabilise the Au cationic active species.[59] Moreover, an equal system of Ru–Co(III)–Cu(II) was also reported to have a higher activity in comparison to the equivalent monometallic Ru catalyst. Likewise, it was suggested that the Co^{3+} additives stabilise the Ru species enabling the formation of high valent ruthenium oxides, while the Cu^{2+} species inhibit the reduction of $RuCl_3$ precursor.[60] Accordingly, the synergistic influence on Au-based catalyst of In^{3+} and Cs^{+} were reported by Li *et al.* who reported that enhance the activity and the stability over the Au-based catalyst. In particular, the incorporation of In^{3+} as third metallic component to AC supported AuCs catalyst stabilises the Au^{3+} centre and increases the adsorption HCl, while preventing the agglomeration of Au^{3+} to metallic Au (0).[61]

3.4.4 Metal-free catalytic systems

Metal-free systems are a growing research field. The advantages of designing metal-free catalysts are associated with low cost due to removal of the precious metal. Heteroatom doped catalysts exhibit an advanced activity, as the incorporation of heteroatoms such as N, B, and S into the sp^2 hybridized network of the material can enhance the electron density of the catalyst. Therefore, heteroatom doped metal-free catalysts exhibit an improved adsorption of HCl over the electron-rich catalyst or augmented adsorption of C_2H_2. Furthermore, heteroatom doping can impede the formation of coke deposition.[62]

N-doped metal-free catalysts have been widely investigated by many researchers. It has been recorded that SiC supported on N-doped carbon (SiC/C–N) illustrates high acetylene conversion and selectivity over 150 hours, while it is postulated that carbon atoms connected to pyrrolic N species are the active sites.[63] Covering the SiC layer of Polydopamine (PDA) also results in generation of active material which endures its stability for 350 h on stream, slowly losing its activity eventually due to coke deposition, which block the active site.[64] The existence of various N species such as pyrrolic N, pyridinic N, and quaternary N complicates the respective of catalytic speciation. To the date there is not an agreement on the nature of the active site for the N-doped carbon materials. There is a range of different doping precursors that can be used to prepare N-doped carbon materials. Polyaniline,[65] urea,[66] melamine,[66] ammonia,[67] have been widely used in this area.

Other researchers are turning to multiple heteroatom doping, as an approach to further improve activity and stability of metal-free systems. Zhu *et al.*[68] reported B and N-doped graphene oxide (B,N–G), while Li *et al*. developed S and N co-doped carbon materials due

to the synergistic effect between S and N atoms. Zeolites have also been shown to demonstrate high activity and selectivity, as Liu *et al*. reported that zeolite 13X is active when tested at 300 °C, which is associated with the structural properties of the material.[69]

Despite the multiple claims that metal-free systems are cost effective due to the absence of metal centre, this claim should be carefully re-evaluated. Provided that the most active catalysts comprise low metal loadings, with the metal being recycled at the end of catalysts lifetime, it is often the modified carbon support that is the most expensive part of the catalyst. Furthermore, the preparation of metal-free catalysts often depends on multistep complicated synthetic routes, which are not desirable from an industrial and economic point of view. Additionally, non-metal catalysts exhibit a lower rate of deactivation, as the deactivation pathway is associated with the reduction of the metal cation to metal and subsequent sintering which is not a possibility in metal-free catalysts.[2] On the other hand, deactivation in non-metal catalysts is attributed to coke formation. Even though the preparation and strategic design of novel heteroatom doping metal free catalysts can improve the electronic properties of the catalyst by constraining coke formation, it can also increase the electron density of the material, strengthening the chemisorption of reactant gases and decreasing the re-adsorption of the product.

The presence of different N species on the surface of N-doped materials, such as pyrrolic N, pyridinic N, and quaternary N obscures identification of the active sites. Up to the present there is not an agreement on the speciation of the active sites for the N-doped carbon materials. The available data that has been reported for metal-free catalysts is presented in table 2. The majority of the published data has been reported for temperatures from 180-220 °C.

3.5 Identification of the major performance parameters

The urge to find a substitute for the industrial Hg catalyst, demands to take into account the engineering aspect as well. Currently, the acetylene hydrochlorination reaction employs a fixed bed multi tubular reactor, with a fixed catalyst volume.[23] Therefore, the catalyst productivity expressed in $mol_{VCM} \cdot kg_{catalyst}^{-1} h^{-1}$ is one of the most important parameters that should be considered, as this value has to be equal or greater than in the current catalyst operating in the reactor. In addition, space time yield (STY) is an important feature that is also widely used to describe amount of product that can be produced in a reactor per unit time per amount of catalyst. Another vital parameter, highly important for commercial use, is the catalyst lifetime. Currently, the Hg catalyst has a lifetime in commercial operation of several months, so, a sustainable option for a drop-in catalyst replacement should include

a stable catalyst with an expanded lifetime. Ideally recording data on catalyst lifetime demands the reaction be studied over several months, nevertheless, the rate of catalyst deactivation during the initial period of time-on-stream can be readily obtained from published data and it is proposed to use this as being indicative of the overall deactivation profile.

As mentioned earlier, the selectivity to the desired product is typically a highly important parameter in heterogenous catalysis. In the case of the acetylene hydrochlorination this is not an issue of concern. Supported metal catalysts that are active typically have selectivity to vinyl chloride greater than 99% with a selectivity of 99.9% predominantly observed in most of the examples. It should be noted that, as a result of the high cost of acetylene, the variation in selectivity between 99.0% and 100% can affect the financial aspect for the utilisation of a catalyst for commercial use. Therefore, selectivity for the acetylene hydrochlorination reaction is a significant constraint that is taken under consideration, when evaluating the different catalytic systems. For reactions where a mixture of product is observed, selectivity should be a more essential factor than productivity, especially if product purification and separation is arduous.

It could be noted that turnover frequency could be also used as an alternative parameter for the comparison of different catalytic systems. Turnover frequency (TOF) associates the amount of reactant particles converted per unit of time to the total active sites. However, the identification of the active sites in heterogeneous catalytic systems is in most of the cases a challenging task. For instance, for the Au-based catalyst, in-situ XAS studies revealed that active sites are consisted of Au^{n+} species, whist, previous XPS analysis portrayed an overvaluation of metallic Au (0) species in the expense of Au^{n+} due to photoreduction of Au^{3+}.[70] For the majority of catalytic systems, the TOF value is not stated as a result of insufficient evidence of total catalytically active species present.

Overall, the two key parameters for the comparison of catalysts for acetylene hydrochlorination are identified to be catalyst productivity and deactivation rate. Hence, it is these two parameters that should be plotted against each other to determine the best catalyst for the reaction. It must be clarified that the key parameters, depend on the catalysed reaction in question and for many reactions other key parameters will be important, with different plots required to effectively assess catalyst performance.

3.6 Data acquisition and normalisation

The acetylene hydrochlorination reaction has been widely studied over the past few decades, by many research groups worldwide, therefore there is a plentiful source of data.

Information regarding catalytic performance has been recorded based on all available patents and research publications. There is not a clear tendency on the catalyst testing conditions, as each research group, follows different experimental procedures for catalyst testing. Data acquired from the publications included a variety of experimental conditions that include different reactant ratios, reactant flow rates, catalyst mass/volume, metal loading, and temperature. When comparing catalysts that are intrinsically different among them, it is essential to take into account all the divergent conditions and study the data recorded under kinetic control rather than those that are diffusion limited.[71] However, in the available literature such data is rarely reported. However, as many of the reported studies were performed at high acetylene conversions; it was not possible to solely use data at low conversions (< 30%). Data recorded under mass transfer limitations were disregarded.

As the data is obtained at various operational conditions, normalisation is necessary. Initially, the productivity ($mol_{VCM}kgcatalyst^{-1}\ h^{-1}$) is calculated based on the data available in terms of reactant ratios, reactant flow, catalyst mass, vinyl chloride selectivity and acetylene conversion. Unfortunately, not in all the reports the above parameters are included. Due to insufficient information in numerous reports, it has not been possible to evaluate the productivity and assess the catalytic performance of some systems. Furthermore, some reports allegedly state advanced catalytic activity, without providing adequate information, thus those reports are excluded from this study. As the data covers a wide range of reaction temperatures, it is required for the productivity values be normalised. The majority of the publications report catalytic studies to be performed at 180 °C, with the activation energy for those different catalytic systems being approximated at 30 kJ mol^{-1},[15] as seen from Table 3.2. The overall data has been reported including the temperature range from 100 to 320 °C, however, only data between 160-200 °C is analysed and normalised.

Catalyst	Activation Energy (kJ mol^{-1})	Reference
Au/NC-473	30.4	72
$RuCl_3$/AC	31.8	73
K_2PdCl_4	30	74
Au/CeO_2&AC	28.2	75
Cu/AC	34	76
Au-$N(CN)_2$/AC	32.8	77

Table 3.2: Reported activation energies of acetylene hydrochlorination for a variety of catalytic systems.

Therefore, it is proposed that the productivity between 160-200 °C can be normalised using equation 3.1.

$$mol_{VCM}kg_{cat}^{-1}h^{-1}\ at\ 180^{o}C = mol_{VCM}kg_{cat}^{-1}h^{-1}\ at\ T_R \cdot exp\left[\left(\frac{Ea}{R}\right)x\left(\left(\frac{1}{T_{180^{o}C}}\right)-\frac{1}{T_R}\right)\right]\ eq.3.1$$

Where E_a is the activation energy for the process (kJ mol^{-1}), R is the molar gas constant ($J{\cdot}K^{-1}{\cdot}mol^{-1}$), T_R is the reaction temperature in Kelvin at which the data was obtained and $T_{180°C}$ is 453.15 K.

As mentioned earlier in this chapter, a secondar parameter for catalytic evaluation is, the rate of catalyst deactivation. Deactivation rate is defined as the function of decreasing acetylene conversion and time (% h^{-1}), given by equation 3.2.

$$Deactivation\ rate\ (\%\ h^{-1}) = \frac{X_{residual}(\%) - X_{max}(\%)}{\Delta t(h)}\ eq.3.2$$

Where $X_{residual}$ is the acetylene conversion at steady, X_{MAX} is the maximum acetylene conversion and Δt = time required for conversion to decrease from maximum to residual point.

Based on the above equations the normalised productivities and deactivation rates have been calculated. Tables 3.3 and 3.4 illustrate the normalised productivities of metal based catalytic systems that have been used in this study. Table 3.5 demonstrates the normalised productivities of metal-free based systems.

Catalyst	*Catalyst mass (g)*	*Max. C_2H_2 conv. (%)*	*Residual C_2H_2 conv. (%)*	*T (°C)*	*Normalised productivity (mol_{VCM} kg_{cat}^{-1} h^{-1})*	*Deactivation rate (% h^{-1})*	*Ref.*
1.27%$AuCl_3$/5PPy-CNT	0.8	95	85	180	7.3	0.11	23
1.0%Au/Cs/NAC	0.2	99	99	180	120	0	78
1.0%Au-dichlorophenyl-phosphine	0.8	97	96	180	116	0.09	79
1.0%Au-tetramethylam-monium chloride	0.8	97	94	180	111	0.27	79
1.0%Au-ATMP/AC	0.8	97	94	180	111	0.15	80
1.0%Au-HEDP/AC	0.8	94	90	180	103	0.38	80
1.0%Au/In(III)/Cs(II)/AC	0.2	93	89	180	98	0.15	75
1.0%Au/ACF- H_2O	0.2	79	79	180	97	0	81
1.0%Au1/Sn1/AC	1.3	99	95	170	75	0.09	82
1.0%Au/CeO_2/AC	0.4	95	89	180	70	0.38	56
1.0%Au/NAC	0.1	78	73	180	66	1	82
1.0%Au1/Cs4/AC	0.2	100	100	180	62	0	83
1.0%$AuCl_3$/TiO_2/AC	0.8	92	81	180	59	1.38	84
1.0%Au1/Cs4/AC	0.2	94	89	180	49	0.13	83
1.0%Au/20%P-SAC	2.0	100	97	170	42	0.13	87
1.0%Au/In(III)/Cs(II)/AC	1.0	96	60	180	36	0.14	75
1.0%Au/Ba(II)1/AC	2.0	97	95	200	24	0.09	92
1.0%Au/5SiO_2/AC	1.0	70	65	180	13	0.46	98
1.0%Au/MCN	0.8	93	76	180	13	2.44	99
1.0%Au-5SiO_2/AC	1.0	53	40	180	10	1.44	98
1.0%Au/AC	0.25	94	20	200	8.0	1.06	24
1.0%Au/AC-0.76M H_2SO_4 pre-wash	0.09	70	52	200	6.5	4.90	102
1.0%Au/A.C. (acetone)	0.09	23	23	200	5.6	0	13
1.0%Au:Ir(99:1)/AC	0.2	37	25	180	3.9	2.93	55
1.0%Au/AC	0.2	25	21	180	2.8	0.88	55
1.0%Au:Ir(95:5)/AC	0.2	37	21	180	2.8	3.88	55
1.0%Au:Pd(99:1)/AC	0.2	35	16	180	1.6	4.75	55
1.0%Au:Ir(80:20)/AC	0.2	38	13	180	0.99	6.38	55
1.0%Au/C-AR	0.09	19	19	200	0.86	0	102
1.0%Au/NC	0.25	95	79	200	4.5	1.33	29
0.5%$AuPPh_3Cl$/AC	1.3	96	95	170	38	0.02	21
0.5%$AuPPh_3Cl$/AC	1.3	96	85	170	30	0.06	21
0.5% Au1-GSH3 (pH=8.3)/AC	1.2	82	76	170	26	0.46	16
0.5%Au on AC-413K	2.5	74	66	200	19	0.67	72
0.49%[$AuCl_2$(phen)]Cl	2.0	95	93	180	25	0.07	20
0.41%Au1/g-C_3N_4	0.35	70	70	180	1.7	0	104
0.4%Au($CS(NH_2)_2$)/ AC	2.0	79	70	170	46	0.58	17
0.4%$HAuCl_4$/g-C_3N_4	0.35	72	15	180	0.074	7.68	104
0.25%Au/Cu/Cs/AC	2.0	84	81	180	41	0.19	88
0.25%Au/Cu/Cs/AC	1.0	89	65	180	26	0.09	88
0.25%Au-SCN-Cu	0.15	72	63	180	14	0.01	19
0.25%Au-SCN-Cu	0.15	96	93	180	10	0.38	19
0.1%Au-5%[Prmim]/AC	0.4	77	71	180	16	3.05	58
0.1%Au/Cu-IL/AC	0.2	77	77	180	36	0	58

Table 3.3:Normalised productivities for the acetylene hydrochlorination reaction of Au based systems.

Catalyst	*Catalyst mass (g)*	*Max. C_2H_2 conv. (%)*	*Residual C_2H_2 conv. (%)*	*T (°C)*	*Normalised productivity (mol_{VCM} kg_{cat}^{-1} h^{-1})*	*Deactivation rate (% h^{-1})*	*Ref.*
1.0%Pd/AC	0.2	13	3	180	0.057	2.38	55
1.0%Pd/NFY	0.4	99	47	160	2.0	9.45	41
0.9%Pd/K/NFY	4.0	99	99	160	8.9	0	41
0.8%Pd/4PANI-HY	4.0	97	95	160	8.2	6.70 x 10-3	101
0.5%Pd-10IL/AC	0.2	98	95	160	100	0.68	43
1.0%Pt/AC	0.2	5	5	180	0.16	0	55
1.0%Pt/AC	0.25	91	91	200	49	0	24
1.0%Pt/AC	0.25	60	46	200	12	0.19	24
1.0%Pt/NC	0.25	59	13	200	3.4	1.54	24
1.0%Ru/AC-NHN	0.8	93	92	180	32	0.03	91
1.0%Ru with 1-isopropyl imidazole ligand on A.C.	2.4	98	82	180	42	0.67	86
1.0%Ru-15%TPPB/AC	2.0	100	100	170	39	0	89
1.0%Ru-10%TPPB/AC	2.0	100	96	170	36	0.14	89
1.0%Ru/AC-NHN	0.8	93	92	180	32	0.03	91
1.0%Ru with thiourea on A.C.	0.45	85	82	170	30	0.12	73
1.0%Ru-5%TPPB/AC	2.0	96	83	170	28	0.08	28
1.0%Ru/SAC-N700	2.0	100	100	170	22	0	93
1.0%Ru/Co(III)/Cu(II)/SAC	2.0	99	99	170	22	0	60
1.0%Ru/Co/SAC	4.0	95	95	170	20	0	83
1.0%Ru/K/SAC	2.0	93	87	170	17	0.14	94
1.0%Ru/AC–NH_2	0.8	73	66	180	16	0.17	91
1.0%Ru–O/AC–O	0.8	100	93	180	16	0.28	95
1.0%Ru-1-isopropyl imidazole/AC	2.4	100	100	180	16	0	90
1.0%Ru-in-MCNT	0.8	91	80	170	7.3	1.15	100
1.0%Ru/AC	0.8	80	62	180	7.1	0.75	95
1.0%Ru/AC	0.8	48	35	180	4.5	0.29	91
1.0%Ru-tetrazolium/AC	2.4	53	53	180	4.3	0	86
1.0%Ru on N.C. with graphene layer	0.25	90	75	200	4.0	1.25	29
1.0%Ru/AC	2.0	76	36	170	5.1	0.83	89
1.0%Ru/Cu/SAC	4.0	72	69	170	11	0.06	83
1.0%Ru-in-CNT	0.8	99	95	170	10	0.55	100
1.0%Ru/AC-NO_2	0.8	75	53	180	10	0.47	91
1.0%Ru-pyrazole/AC	2.4	83	80	180	10	0.34	86
1.0%Ru-out-CNT	0.8	45	37	170	1.6	1	100
1.0%Ru/AC	0.2	15	8	180	0.35	1.93	55

1.0%Ru-out-MCNT	0.8	43	25	170	0.70	1.84	100
0.1%Ru/Co(III)/Cu(II)/SAC	2.0	99	96	170	10	7.80 x 10-3	60
15%Cu on IL/C (MOMTPPC)	2.0	92	90	180	15	0.05	96
15%Cu/10%HMPA /SAC	1.2	87	81	180	13	0.57	97
15%Cu/10%HMPA /SAC	1.2	97	87	180	7.9	0.11	97
15%Cu/10%HMPA /SAC	1.2	97	90	180	4.6	0.10	97
4.2%Cu/Ru(400 ppm) - CNTs	0.2	52	52	180	33	0	90
4.24%Cu/CNTs	0.2	8	8	180	0.78	0	90
13.7%Hg/AC	7.0	86	39	180	0.69	9.00	106
0.1%HgCh-SiO_2	20.0	82	73	181	5.4	0.50	103
6.9%Zn/SBMC-600, (Zn=73.7ppm)	1.0	99	97	200	1.7	0.16	105
1.0%Ir/AC	0.2	15	5	180	0.16	2.53	55
1.0%Rh/AC	0.2	5	3	180	0.057	0.55	55

Table 3.4: Normalised productivities for the acetylene hydrochlorination reaction of Pd, Pt, Ru, Cu, Hg, Zn, Ir and Rh systems.

Catalyst	Catalyst mass (g)	Max. C_2H_2 conv. (%)	Residual C_2H_2 conv. (%)	T (°C)	Normalised productivity (mol_{VCM} kg_{cat}^{-1} h^{-1})	Deactivation rate (% h^{-1})	Ref.
S,N–C	1.2	82.3	76	180	2.01	1.1	107
PANI-AC-900	0.72	76.27	73	180	1.90	0.4	66
NS–C–NH_3	0.25	80	80	220	4.36	0.0	68
Activated Carbon marked as CBC	2.82	33	31.04	180	1.28	0.1	109
N-dopped Carbon	0.5	95.4	92	220	2.66	1.7	110
SBMC-600	1	98.6	97	200	1.70	0.2	105
Activated Carbon marked as PBC	2.82	26.4	26.42	180	0.93	0.0	108
NC-II	0.25	63	33.5	250	2.33	2.7	110
NC-III	0.25	35	30.5	250	1.93	0.4	110
Activated Carbon marked as CCN	2.82	20.7	20.7	180	0.57	0.0	108
Activated Carbon marked as WBC	2.82	20.7	10.67	180	0.15	0.0	108
NC-I	0.25	59	1	250	0.01	5.3	107
g-C_3N_4/AC	0.8	67	55	180	2.27	1.6	111
N-doped carbon	0.8	71	67	180	2.36	0.1	112
N-Carbon-Z4M1	2	60	45	180	1.05	0.3	113
N-OMC-Ox	2	33.5	31	180	1.47	0.1	114
g-C3N4: MF-600	0.4	94.5	94.5	220	1.46	0.0	115
1H-imidazole	0.4	60	60	220	0.59	0.0	116
PSAC-N	1.6	80	58	250	1.45	0.1	117
13X zeolite	2.67	98.5	77.6	320	0.57	4.6	69
NC-800-700 Nitrogen-modified carbon	0.75	98.7	97.8	260	1.61	0.0	118
25% HMT/AC	0.4	60	60	220	0.59	0.1	119
3%S/BSAC-800	1.2	47	42	180	1.67	0.0	120
N@CBCFE	1.2	58	57	220	3.22	0.3	121
NC-800	1	97.39	97.39	220	1.25	0.2	122
PAN-400-air	0.5	82	82	220	0.87	0.0	123
NR-CAC	2	97.9	96.2	220	1.51	0.0	124

Table 3.5: Normalised productivities for the acetylene hydrochlorination reaction of metal-free catalytic systems.

Published reports where only the initial activity of a catalyst is described without including any further discussion about the activity and stability catalyst through the reaction time, have also been excluded from this study. It should be stated that even though it is important to observe the activity of a catalyst over a prolonged period of time to allow for deactivation to be estimated, this is not always feasible. Also, it should be clarified that whilst productivity was normalised to 180 °C, the deactivation rate is based on the decrease in activity at the original testing temperature. Whereas productivity is related to temperature, as shown in the equation 1, there is no such connection between deactivation and temperature. For Au catalysts, the deactivation mechanism depends on reaction temperature. At low reaction temperatures, deactivation predominantly occurs by the coke deposition while at higher temperatures deactivation is caused by reduction of Au^{n+} to Au^{0}.(30) For this reason, data recorded outside the range of 160-200 °C has also been excluded from this work due to assumptions about deactivation rates outside of this range.[31]

3.7 Comparison of supported metal catalysts

Over the past few years, a wide variety of different metal catalysts have been suggested to be great alternatives for the Hg catalyst used in VCM production. As noticed in Tables 3.3, 3.4 and 3.5, the high conversion of acetylene that is reported, does not necessarily correspond to high productivity. Also, it can be easily observed that for most studies activated carbon is the main choice of support, as it is a material that has a wide range of physical properties, and it can endure high temperatures and harsh conditions of the acetylene hydrochlorination reaction. Most of the catalysts reported have been prepared typically by impregnation of a metal salt onto carbon support. Using the information from Table 3.2, it is feasible to plot the normalised productivity versus deactivation rate. It can be easily seen from the graph (Figure 3.2) that Au catalysts exhibit higher activity, with smaller deactivation rates followed by Ru, Cu, Pd, Ir, Rh, Co, Pt, Non-metal catalysts. Specifically, for Ru, Cu and Pt catalysts, it is observed that Au is 3 times more active, as the best-in-class Ru, Cu and Pt catalysts have normalised productivities that are a third of that of Au. On the other hand, the best in class of Pd catalyst exhibit a high value of normalised productivity of approximately 100 $mol_{VCM}kg_{cat}^{-1}h^{-1}$, but it shows a deactivation rate that is significantly higher than for several Au catalysts, disqualifying the use of this Pd catalyst for commercial use.

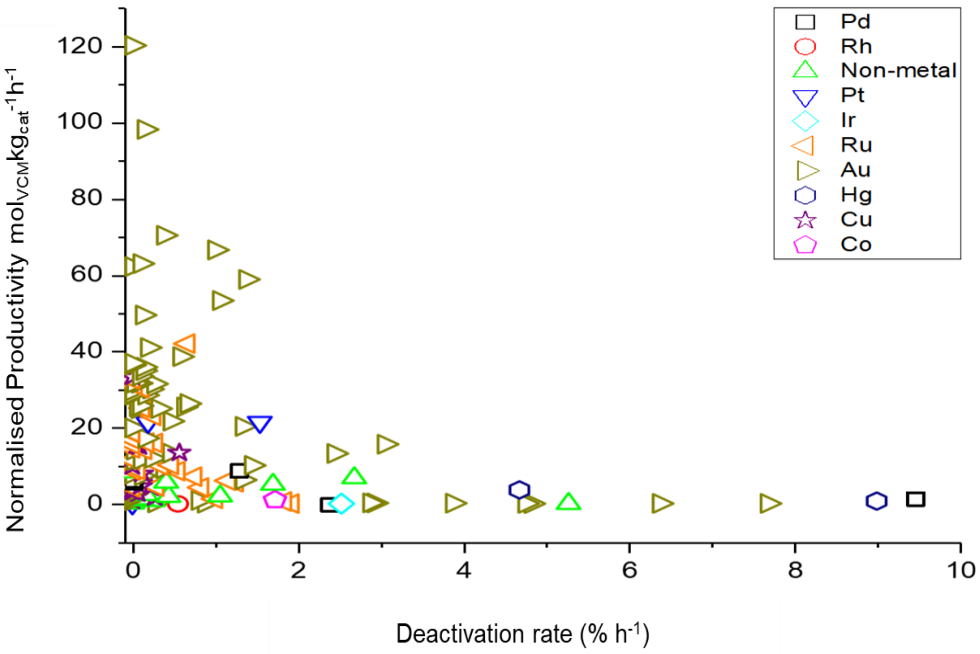

Figure 3.2: Normalised productivity plotted against deactivation rate for different metal containing catalytic systems. The metal centre of the catalysts is in the legend. Normalised productivity and deactivation rate were calculated in accordance with equations (1) and (2), respectively. Figure adapted from reference 2.

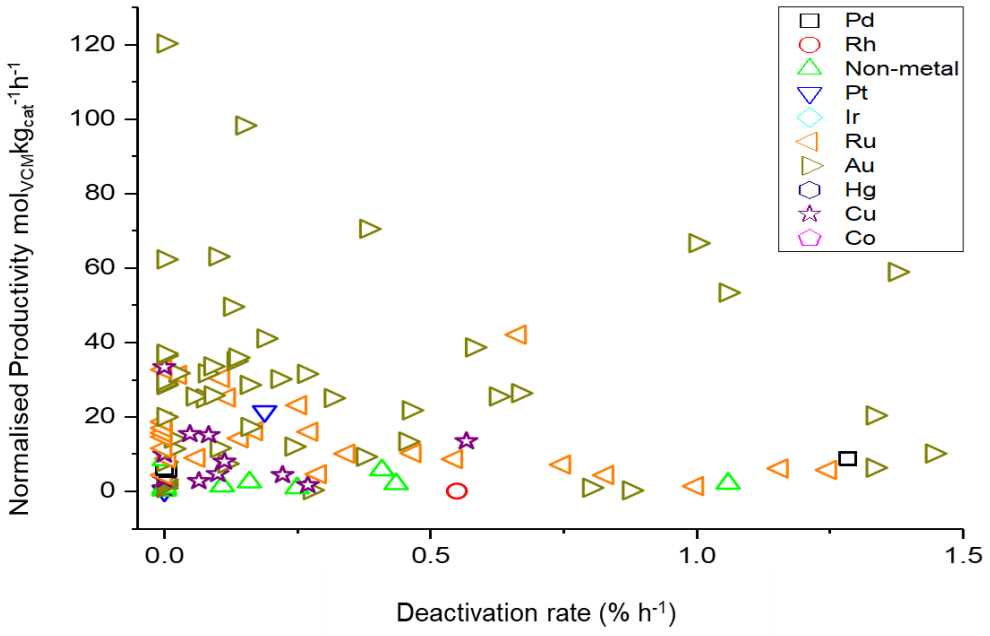

Figure 3.3: Emphasis at low deactivation rates of the normalised productivity against deactivation rate for different catalytic systems. Figure adapted from reference 2.

This analysis confirms the original prediction that Au would be the best catalyst for the acetylene hydrochlorination reaction (Figure 3.4).[9] Relying on published data reported by

different research groups, the same conclusion is achieved (Figure 3.5).[9] As predicted in 1985 by Hutchings, who re-plotted the data for the divalent metal cations described originally by Shinoda, against the standard electrode potential, Au should exhibit a higher activity in comparison to any other metal. It is postulated that the superior activity of Au-based catalyst for the acetylene hydrochlorination reaction, is related to the increased electrode potential, which suggests that the reaction happens *via* a redox mechanism.[52] It has been established that active sites for Au-based catalysts is associated with highly dispersed Au^{n+} cations with catalytic activity being dependent on Au^{+}:Au^{3+} ratio.[125] The initial prediction included data for over 30 metal chloride catalysts, however, no data was available for precious metals Au, Pt, and Ru. Following studies confirmed the correlation between acetylene conversion versus the standard electrode potential as seen from Figure 3.4.

For the majority of most metal systems, as seen from Figure 3.4, the normalised productivity line up with the correlation trend, whilst some examples such as Bi, Ir, Hg and Pt are observed below the correlation line. This behaviour can be attributed to the low volume of research publications of those systems, as there are significantly more literature reports studying Au, Cu, and Ru-based catalysts. The drastically smaller number of publications on Pt-based catalysts, indicates that the best-in-class Pt catalysts need to be optimised to improve their productivity. Therefore, there is space for further improvement for these metals. Despite the potential optimisation of Bi, Ir, Hg and Pt-based catalysts, they still will not be able to compete Au activity.

Furthermore, as seen in Figure 3.3 Au-based catalysts cover a range of normalised productivity values. This observation can be attributed to the lower activities that Au nanoparticles exhibit. For Au catalysts the VCM productivity is associated with the presence of Au(I) species which are essentially vital for this reaction. However, in the Au-based catalysts a high population Au(III) species is also detected, implying, that the activity is related to the Au(I) – Au(III) redox couple. The reaction could be hypothesised to proceed through the oxidative addition of HCl to Au chloride, followed by the addition of acetylene and reductive elimination of VCM through a Au(I) – Au(III) redox couple.[70] Therefore, the broad range of VCM productivities reflected on Au catalysts is due to the coexistence of cationic Au species with Au nanoparticles. As the population of active species on catalyst that consist of Au nanoparticles is smaller in comparison to the highly dispersed Au cation catalysts, it is inevitable that these materials will present a lower activity.

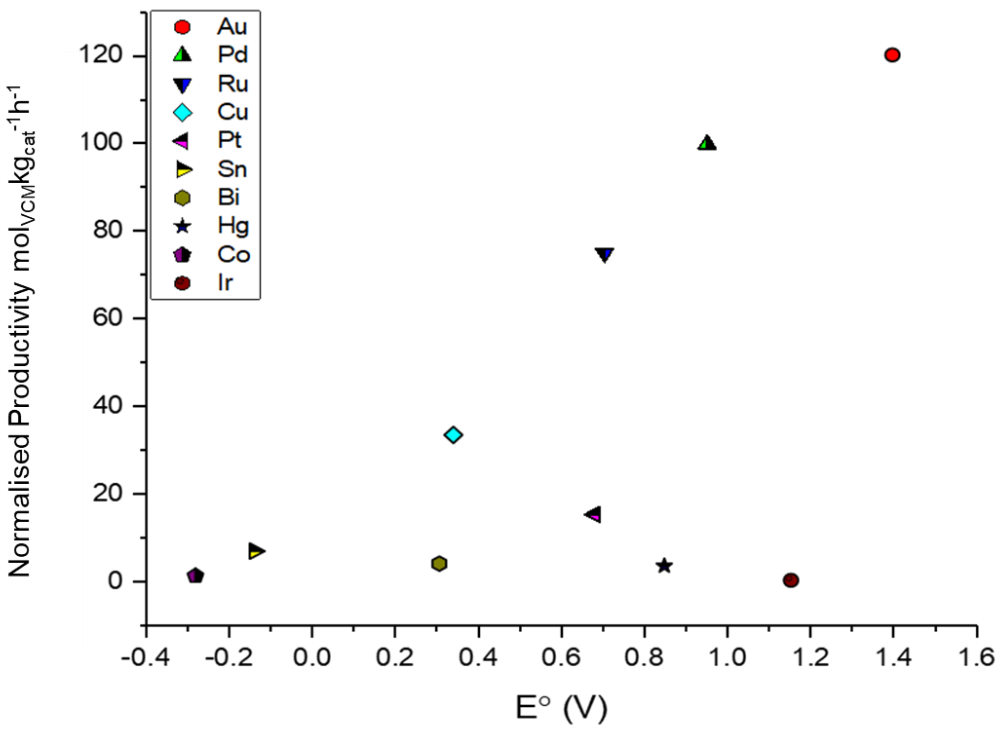

Figure 3.4: Correlation between normalised maximum productivity and standard electrode potential for best-in-class metal cations $M^{2+} + 2e^- \rightarrow M$ or $M^{3+} + 2e^- \rightarrow M^+$.[2]

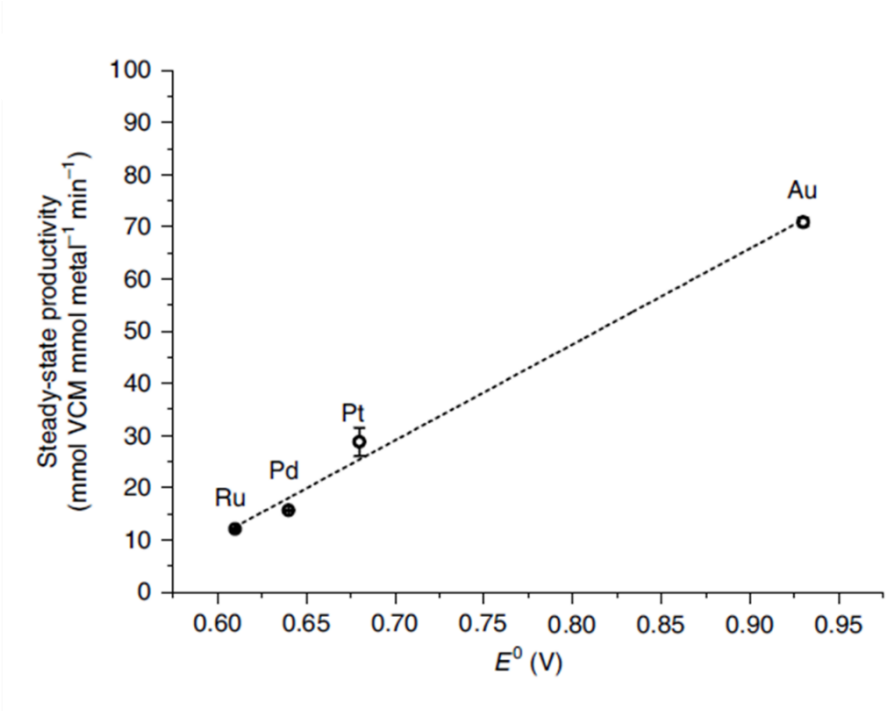

Figure 3.5: Correlation between initial acetylene conversion versus the standard electrode potential of the various metals. Potentials were obtained from the reduction potentials of the following chloride salts, $(RuCl_5)^{2-}$, $PdCl_2$, $(PtCl_6)^{2-}$, and $(AuCl_4)^-$ to the corresponding metals.[13]

3.8 Conclusion

The introduction of a general method, for the comparison of different catalytic systems which have been fundamentally studied at a range of various conditions, is suggested. Relying on the available published literature for the acetylene hydrochlorination, it was feasible to compare catalyst with intrinsic different characteristics, tested at temperatures of 160-200 ^{o}C. The proposed universal method, allowed to conduct a comparison among metal, metal-free and metal-doped catalysts.

As shown, the best catalytic systems for the acetylene hydrochlorination are Au-based catalysts. Au-based catalysts exhibit a higher activity performance, with a lower the deactivation rate in comparison to other metal systems. Most catalysts studied included Au, Pt, Pd, Ru and Cu-based catalysts. Excluding Pd, the catalytic performance of Au exhibited a magnitude of approximately three times that of the next best metals. Despite the great activity of Pd they suffer from a higher deactivation rate than many Au catalysts. Furthermore, metal-free catalysts have a significantly lower activity than metal-based catalysts.

The generalised introduced parameter allows a rapid scanning of reported catalyst for a particular reaction. Apart from productivity and deactivation rate, there are more parameters to be examined such as safety, cost, environmental footprint and the possibility of catalyst regeneration or recycling, the scalability of a proposed preparation method and the overall feasibility of the catalyst synthesis including waste generation. However, a general method of comparing catalyst performance should be undertaken when considering a drop-in replacement for a currently operated commercial catalyst. It should be highlighted that the advantage of this method is to quickly compare published information for a specific reaction, but this should be considered a precursor to experiments based on like-for-like tests and full kinetic studies.

Despite the benefits that the method discussed in the chapter offers, it should be noted that there are challenges that should be taken into consideration for its application. In this case, the deactivation pathways of the catalytic systems significantly depend on the nature of the metal as well as the reactions conditions applied. For instance, when tested at low temperatures Au deactivates due to coke deposition while when tested at high temperatures deactivates due to the agglomeration of reduction of Au^{n+} to Au^{0}.[10] However, it should be noted that a great advantage of this study has been the fact that the majority of the catalysts reported have been tested at 180 ^{o}C, allowing us to use a wide range of data that did not need to be normalised, minimising the potential errors during the analysis. In addition, the

deactivation rates have been calculated based on different time frames. It would be ideal if the catalysts could be tested at longer time frames to ensure that the stability reported is representative of the actual catalytic performance and not merely due to initial changes in oxidation state. In a related point, the catalysts should be tested under kinetic conditions, for the activity and stability to be a reflection of catalytic behaviour. Stability tests that have been acquired at high conversion or obviously mass-transfer limited conditions should not be included in comparisons such as these. Finally, one of the main challenges of this study has been the limited scope of metals that have been investigated for the acetylene hydrochlorination, that do not include Au. Over the past few decades, a great attention has been drawn to Au catalytic systems, therefore, the number of publications on Au catalysts are vastly larger than any other metal system which may explain certain outliers in the comparison of best-in-class catalysts for each metal (Figure 3.4).

As time progresses, the catalyst design criteria for the development of novel catalysts keeps advancing. Future work should focus on comparing the catalysts that are being reported to validate that the suggested generalised methodology facilitates the identification of the best catalysts. Ideally, this study will set the frame for research groups to provide the experimental details that will allow the calculation of the important parameters that are required for the comparison of the catalysts. In addition, this study should be used for the adaptation of the up-to-date standard materials for more useful conclusions. For instance, Au aqua regia prepared catalysts are often presented as the “standard material” to compare the activity of novel catalysts. However, the usage of aqua regia in the catalyst preparation is unattractive and cannot find practical application due to poor activity and stability. If the use of standardise reaction conditions is not feasible, a suitable catalytic standard would greatly facilitate useful comparisons to be made.

3.9 References

1. Zhong J., Xu Y., Liu Z., Heterogeneous non-mercury catalysts for acetylene hydrochlorination: progress, challenges, and opportunities. Green Chem., 2018, **20**, 2412-2427.

2. Lazaridou A, Smith L. R., Pattisson S., Dummer N .F., Smit J. J., Johnston P., Hutchings G. J., Recognizing the best catalyst for a reaction. Nat. Rev. Chem., 2023, **7**, 287–295.

3. Wacławek S., Padil V. V. T., Černík M., Major Advances and Challenges in Heterogeneous Catalysis for Environmental Applications: A Review. Ecol. Chem. Eng. S., 2018, **25**, 9–34.

4. Malta G., Freakley S. J., Kondrat S. A., Hutchings G. J., Acetylene hydrochlorination using Au/carbon: a journey towards single site catalysis. Chem. Comm., 2017, **53**, 11733-11746.

5. Yan Y., Miao J., Yang Z., Xiao F., Yang H., Liu B., Yang Y., Carbon nanotube catalysts: Recent advances in synthesis, characterization and applications. Chem. Soc. Rev., 2015, **44**, 3295–3346.

6. Xu H., Luo G., Green production of PVC from laboratory to industrialization: State-of-the-art review of heterogeneous non-mercury catalysts for acetylene hydrochlorination. J. Ind. Eng. Chem., 2018, **65**, 13–25.

7. Nagata S., Design of fixed bed catalytic reactors. Doctoral dissertation, Iowa State University Of Science and Technology Ames, Iowa, 1963.

8. Zhang M., Wang M., Xu B., Ma D., How to measure the reaction performance of heterogeneous catalytic reactions reliably. Joule, 2019, **3**, 2876–2883.

9. Hutchings G. J., Vapor phase hydrochlorination of acetylene: Correlation of catalytic activity of supported metal chloride catalysts. J. Catal., 1985, **96**, 292–295.

10. Johnston P., Carthey N., Hutchings G. J., Discovery, development, and commercialization of gold catalysts for acetylene hydrochlorination. J. Am. Chem. Soc., 2015, **137**, 14548–14557.

11. Nkosi B., Coville N. J., Hutchings G J., Adams M. D., Friedl J., Wagner F. E., Hydrochlorination of acetylene using gold catalysts: A study of catalyst deactivation. J. Catal., 1991, **128**, 366–377.

12. Carthey N. A., Johnston P., Smidt M. L., Improvements in catalytic processes. Patent application WO2010/055341A3, August 12, 2010.

13. Sun X., Dawson S. R., Parmentier T. E., Malta G., Davies T. E., He Q., Li L., Morgan M. D., Carthey N., Johnston P., Kondrat A. S., Freakley J. S., Kiely C. J., Hutchings G. J., Facile synthesis of precious-metal single-site catalysts using organic solvents. Nat Chem., 2020, **12**, 560–567.

14. Liu X., Conte M., Elias D., Lu L., Morgan D. J., Freakley S. J., Johnston P., Kiely C. J., Hutchings G. J., Investigation of the active species in the carbon-supported gold catalyst for acetylene hydrochlorination. Catal. Sci. Technol., 2016, **6**, 5144–5153.

15. Hashmi A. S. K., Toste F. D., Modern gold catalyzed synthesis. Mod. Willey-VCH, 1st edn., 2008.

16. Qi X., Li W., Gu J., Gu C., Zhang J., Gold-glutathione complex catalysts with carbon support for non-mercury catalytic acetylene hydrochlorination. RSC Adv., 2016, **6**, 105110–105118.

17. Yin X., Huang C., Kang L., Zhu M., Dai B., Novel $AuCl_3$-thiourea catalyst with a low Au content and an excellent catalytic performance for acetylene hydrochlorination. Catal. Sci. Technol., 2016, **6**, 4254–4259.

18. Xu H., Zhou K., Si J., Li C., Luo G., A ligand coordination approach for high reaction stability of an Au-Cu bimetallic carbon-based catalyst in the acetylene hydrochlorination process. Catal. Sci. Technol., 2016, **6**, 1357–1366.

19. Zhou K., Jia J., Li C., Xu H., Zhou J., Luo G., Wei F., A low content Au-based catalyst for hydrochlorination of C_2H_2 and its industrial scale-up for future PVC processes. Green Chem., 2015, **17**, 356–364.

20. Huang C., Zhu M., Kang L., Dai B., A novel high-stability Au(III)/Schiff-based catalyst for acetylene hydrochlorination reaction. Catal. Commun., 2014, **54**, 61–65.

21. Dong Y., Li W., Yan Z., Zhang J., Hydrochlorination of acetylene catalyzed by an activated carbon supported chlorotriphenylphosphine gold complex. Catal. Sci. Technol., 2016, **6**, 7946–7955.

22. Lin W., Zhang R. W., Jang S. S., Wong C. P., Hong J., Organic aqua regia-powerful liquids for dissolving noble metals. Angew. Chemie - Int. Ed., 2010, **49**, 7929–7932.

23. Li X., Zhu M., Dai B., $AuCl_3$ on polypyrrole-modified carbon nanotubes as acetylene hydrochlorination catalysts. Appl. Catal. B Environ., 2013, **142**, 234–240.

24. Kaiser S. K., Fako E., Manzocchi G., Krumeich F., Hauert R., Clark A. H., Safonova O. V., López N., Pérez-Ramírez J., Nanostructuring unlocks high performance of platinum single-atom catalysts for stable vinyl chloride production. Nat Catal., 2020, **3**, 376–385.

25. Duan Z., Jiang Y., Yan M., Wang S., Yuan Z., Zhao Q., Sun P., Xie G., Du X., Ta H., Facile, flexible, cost-saving, and environment-friendly paper-based humidity sensor for multifunctional applications. ACS Appl. Mater. Interfaces, 2019, **11**, 21840–21849.

26. Zhu M., Kang L., Su Y., Zhang S., Dai B., MCl_x (M = Hg, Au, Ru; x = 2, 3) catalyzed hydrochlorination of acetylene – A density functional theory study. Canad. J. Chem., 2013, **91**,120–125.

27. Pu Y., Zhang J., Yu L., Jin Y., Li W., Active ruthenium species in acetylene hydrochlorination. Appl. Catal. A Gen., 2014, **488**, 28–36.

28. Man B., Zhang H., Zhang C., Li X., Dai H., Zhu M., Dai B., Zhang J., Effect of Ru/Cl ratio on the reaction of acetylene hydrochlorination. New J. Chem., 2017, **41**, 14675–14682.

29. Kaiser S. K., Lin R., Krumeich F., Safonova O. V., Pérez-Ramírez J. Preserved in a shell: high performance graphene confined ruthenium nanoparticles in acetylene hydrochlorination. Angew. Chemie - Int. Ed., 2019, **58**, 12297–12304.

30. Wang B., Zhang T., Liu Y., Li W., Zhang H., Zhang J., Phosphine-oxide organic ligand improved Cu-based catalyst for acetylene hydrochlorination. Appl. Catal. A Gen., 2022, **630**, 118461.

31. Yang L., Zhang H., Li L., Peng W., Dong Y., Xie D., Chen S., Zhang Q., Qi J., Guo Z., Huang M., Zhang J., Construction of highly dispersed Cu-P/Cl active sites using

methyldiphenyloxophosphine for efficient acetylene hydrochlorination. ACS Sustain. Chem. Eng., 2023, **11**, 1666–1677.

32. Li F., Wang X., Zhang P., Wang Q., Zhu M., Dai B., Nitrogen and phosphorus co-doped activated carbon induces high density Cu^{+} active center for acetylene hydrochlorination. Chin. J. Chem. Eng., 2023, **59**, 193-199.

33. Wang B., Jin C., Shao S., Yue Y., Zhang Y., Wang S., Chang R., Zhang H., Zhao J., Li X., Electron-deficient Cu site catalyzed acetylene hydrochlorination. Green Energy Environ., 2022, **8**, 1–13.

34. Zhou K., Si J., Jia J.,a Huang J., Zhou J., Luo G., Wei F., Reactivity enhancement of N-CNTs in green catalysis of C_2H_2 hydrochlorination by a Cu catalyst. RSC Adv., 2014, **4**, 7766–7769.

35. Zhao W., Zhu M., Dai B., The preparation of Cu-g-C_3N_4/AC catalyst for acetylene hydrochlorination. Catalysts, 2016, **6**, 1–10.

36. Li H., Wang F., Cai W., Zhang J., Zhang X., Hydrochlorination of acetylene using supported phosphorus-doped Cu-based catalysts. Catal. Sci. Technol., 2015, **5**, 5174–5184.

37. Zhao C., Zhang X., He Z., Guan Q., Li W., Demystifying the mechanism of NMP ligands in promoting Cu-catalyzed acetylene hydrochlorination: Insights from a density functional theory study. Inorg. Chem. Front., 2020, **7**, 3204–3216.

38. Esfahani M. M., Goerlitzer E. S. A., Kunz U., Vogel N., Engstler J., Brunsen A. A., N-methyl-2-pyrrolidone as a reaction medium for gold(III)-ion reduction and star-like gold nanostructure formation. ACS Omega, 2022, **7**, 9484–9495.

39. Zhao J., Yue Y., Sheng G., Wang B., Lai H., Di S., Zhai Y., Guo L., Li X., Supported ionic liquid-palladium catalyst for the highly effective hydrochlorination of acetylene. Chem. Eng. J., 2019, 360, 38–46

40. Wang L., Wang F., Wang J., Tang X., Zhao Y., Yang D., Jia F., Hao T., Hydrochlorination of acetylene to vinyl chloride over Pd supported on zeolite Y. React. Kinet. Mech. Catal., 2013, **110**, 187–194.

41. Wang L., Wang F., Wang J., Effect of K promoter on the stability of Pd/NFY catalysts for acetylene hydrochlorination. Catal. Commun., 2016, **83**, 9–13.

42. Wang B., Yue Y., Jin C., Lu J., Wang S., Yu L, Guo L., Li R., Hu Z. T., Pan Z., Zhao J., Li X., Hydrochlorination of acetylene on single-atom Pd/N-doped carbon catalysts: Importance of pyridinic-N synergism. Appl. Catal. B Environ., 2020, **272**, 1–11.

43. He H., Zhao J., Wang B., Yue Y., Sheng G., Wang Q., Yu L., Hu Z. T., Li X., Design strategies for the development of a Pd-based acetylene hydrochlorination catalyst: Improvement of catalyst stability by nitrogen-containing ligands. RSC Adv., 2019, **9**, 21557–21563.

44. Zhou, X., Zhu, M., Kang, L., Single-Atom X/g-C_3N_4(X = Au_1, Pd_1, and Ru_1) Catalysts for Acetylene Hydrochlorination: A Density Functional Theory Study. Catalysts 2019, **9**, 1–12.

45. He H., Zhao J., Wang B., Yue Y., Sheng G., Wang Q., Yu L., Hu Z. T., Li X., Supported ionic liquid-palladium catalyst for the highly effective hydrochlorination of acetylene. Chem. Eng. J., 2019, **360**, 38–46.

46. Krasnyakova T. V., Nikitenko D. V., Kobets K. D., Krasniakova I.O., Gogilchin A. S., Bugaev A. L., Mitchenko S. A., Stereoselectivity of Acetylene Hydrochlorination over Supported $PdCl_2$/C Catalysts. Kinet Catal., 2023, **64**, 294–302.

47. Kaiser S. K., Fako E., Surin I., Krumeich F., Kondratenko V. A., Kondratenko E. V., Clark A. H., López N., Pérez-Ramírez J., Performance descriptors of nanostructured metal catalysts for acetylene hydrochlorination. Nat. Nanotechn. 2022, **17**, 606–612.

48. Hu D., Wang L., Wang F., Wang, J., Active carbon supported S-promoted Bi catalysts for acetylene hydrochlorination reaction. Chinese Chem. Lett., 2018, **29**, 1413–1416.

49. Hu D., Wang F., Wang J., Bi/AC modified with phosphoric acid as catalyst in the hydrochlorination of acetylene. RSC Adv., 2017, **7**, 7567–7575.

50. Zhou K., Jia J., Li X., Pang X., Li C., Zhou J., Luo G., Wei F.,Continuous vinyl chloride monomer production by acetylene hydrochlorination on Hg-free bismuth catalyst: From lab-scale catalyst characterization, catalytic evaluation to a pilot-scale trial by circulating regeneration in coupled fluidized beds. Fuel Process. Technol., 2013, **108**, 12–18.

51. Wu Y., Li F., Xue J., Lu Z., Sn-imidazolates supported on boron and nitrogendoped activated carbon as novel catalysts for acetylene hydrochlorination. Chem. Eng. Commun., 2020, **207**, 1203–1215.

52. Nkosi B., Coville N. J., Hutchings G. J. Vapour phase hydrochlorination of acetylene with group VIII and IB metal chloride catalysts. Appl. Catal., 1988, **43**, 33–39.

53. Nkosi B., Adams,M. D., Coville N. J., Hutchings, G. J., Hydrochlorination of acetylene using carbon-supported gold catalysts: A study of catalyst reactivation. J. Catal., 1991, **128**, 378–386.

54. Davies C. J., Miedziak P. J., Brett G. L., Hutchings G. J., Vinyl chloride monomer production catalysed by gold: A review. Chin. J. Catal., 2016, **37**, 1600-1607.

55. Conte M., Carley A. F., Attard G., Herzing A. A., Kiely C. J., Hutchings G. J., Hydrochlorination of acetylene using supported bimetallic Au-based catalysts. J Catal., 2008, **257**, 190–198.

56. Zhang H., Dai B., Wang X., Li W., Han Y., Gu J., Zhang J., Non-mercury catalytic acetylene hydrochlorination over bimetallic Au-Co(III)/SAC catalysts for vinyl chloride monomer production. Green Chem., 2013, **15**, 829–836.

57. Zhou K., Wang W., Zhao Z., Luo G., Miller J. T., Wong M. S., Wei F., Synergistic gold-bismuth catalysis for non-mercury hydrochlorination of acetylene to vinyl chloride monomer. ACS Catal., 2014, **4**, 3112–3116.

58. Yu Y., Yue Y., Wang B., He H., Hu Z. T., Zhao J., Li X., Synergy between ionic liiquids and $CuCl_2$ in gas–liquid phase reactions of acetylene hydrochlorination. Catal., 2019. **9**, 1–22.

59. Zhang H., Dai B., Li W., Wang X., Zhang J., Zhu M., Gu J., Non-mercury catalytic acetylene hydrochlorination over spherical activated-carbon-supported Au-Co(III)-Cu(II) catalysts. J. Catal., 2014, **316**, 141–148.

60. Zhang H., Li W., Jin Y., Sheng W., Hu M., Wang X., Zhang J., Ru-Co(III)-Cu(II)/SAC catalyst for acetylene hydrochlorination. Appl. Catal. B Environ., 2016, **189**, 56–64.

61. Wu Y., Li F., Lu Z., Xue J., Activated carbon supported ternary gold-cesium(i)-indium(iii) catalyst for the hydrochlorination of acetylene. Catal. Sci. Technol., 2015, **5**, 4973–4984.

62. Yue Y., Wang B., Wang S., Jin C., Lu J., Fang Z., Shao S., Pan Z., Ni J., Zhao J., Li X., Boron-doped carbon nanodots dispersed on graphitic carbon as high-performance catalysts for acetylene hydrochlorination. Chem. Commun., 2020, **56**, 5174-5177.

63. Li X., Pan X., Yu L., Ren P., Wu X., Sun L., Jiao F., Bao X., Silicon carbide-derived carbon nanocomposite as a substitute for mercury in the catalytic hydrochlorination of acetylene. Nat. Commun., 2014, **5**, 1–7.

64. Li X., Li P., Pan X., Ma H., Bao X. Deactivation mechanism and regeneration of carbon nanocomposite catalyst for acetylene hydrochlorination. Appl. Catal. B Environ., 2017, **210**, 116–120.

65. Zhang C., Kang L., Zh, M., Dai, B. Nitrogen-doped active carbon as a metal-free catalyst for acetylene hydrochlorination. RSC Adv., 2015, **5**, 7461–7468.

66. Zhang T., Zhao J., Xu J., Xu J., Di X., Li X., Oxygen and nitrogen-doped metal-free carbon catalysts for hydrochlorination of acetylene. Chin. J. Chem. Eng., 2016, **24**, 484–490.

67. Dai B., Chen K., Wang Y., Kang L., Zhu M., Boron and nitrogen doping in graphene for the catalysis of acetylene hydrochlorination. ACS Catal., 2015, **5**, 2541–2547.

68. Dong X., Chao S., Wan F., Guan Q., Wang G., Li W., Sulfur and nitrogen co-doped mesoporous carbon with enhanced performance for acetylene hydrochlorination. J. Catal., 2018, **359**, 161–170.

69. Song Z., Liu G., He D., Pang X., Tong Y., Wu Y., Yuan D., Liu Z., Xu Y., Acetylene hydrochlorination over 13X zeolite catalysts at high temperature. Green Chem., 2016, **18,** 5994-5998.

70. Malta G., Kondrat S. A., Freakley S. J., Davies C. J., Lu L., Dawson R. S., Thetford A., Gibson K. E., Morgan D. J., Jones W., Wells P. P., Johnston P., Catlow R. A., Christopher J., Kiely C. J., Hutchings G. J., Identification of single-site gold catalysis in acetylene hydrochlorination. Science, 2017, **355**, 1399–1403.

71. Perego C., Peratello S. Experimental methods in catalytic kinetics. Catal. Today, 1999, **52**, 133–145.

72. Kaiser S. K., Lin R., Mitchell S., Fako E., Surin I., Krumeich F., Hauert R., Safonova O. V., Kondratenko V. A., Kondratenko E. V., Collins S. M., Midgley M., López N., Pérez-Ramírez J., Controlling the speciation and reactivity of carbon supported gold nanostructures for catalysed acetylene hydrochlorination. Chem. Sci., 2019, **10**, 359-369.

73. Wang X., Lan G., Cheng Z., Han W., Tang H., Liu H., Li Y., Carbon-supported ruthenium catalysts prepared by a coordination strategy for acetylene hydrochlorination. Chin. J. Catal., 2020, **41**, 1683–1691.

74. Krasnyakova T. V., Nikitenko D. V., Khomutova E. V., Mitchenko S. A., Catalytic hydrochlorination of acetylene on $PdCl_2$/C supported catalysts: Kinetic isotopic effect of HCl/DCl, stereoselectivity, and mechanism. Kinet. Catal., 2017, **58**, 533–540.

75. Ye L., Duan X., Wu S., Wu T. S., Zhao Y., Robertson A. W., Chou H. L., Zheng J., Ayvali T., Day S., Tang C., Soo Y. L, Yuan Y., Tsang S. C. E., Self- regeneration of Au/CeO_2 based catalysts with enhanced activity and ultra-stability for acetylene hydrochlorination. Nat Commun., 2019, **10**, 914-924.

76. Wang T., Jiang Z., Tang Q., Wang B., Wang S., Yu M., Chang R., Yue Y., Zhao J., Interactions between atomically dispersed copper and phosphorous species are key for the hydrochlorination of acetylene. Commun. Chem., 2022, **5**, 1–10.

77. Zhao J., Wang S., Wang B., Yue Y., Jin C., Lu J., Fang Z., Pang X., Feng F., Guo F., Pan Z., Li X., Acetylene hydrochlorination over supported ionic liquid phase (SILP) gold-based catalyst: Stabilization of cationic Au species via chemical activation of hydrogen chloride and corresponding mechanisms. Chin. J. Catal., 2021, **42**, 334–346.

78. Zhao J., Zhang T., Di X., Xu J., Xu J., Feng F., Ni J., Li X., Nitrogen-modified activated carbon supported bimetallic gold-cesium(I) as highly active and stable catalyst for the hydrochlorination of acetylene. RSC Adv., 2015, **5**, 6925–6931.

79. Li Y., Zhang C., Zhang H., Li L., Zhang J., Oh R., Yao L., Cai M., Li J., Zhang M., Li F., Effects of N-, P-, or O-containing ligands on gold-based complex catalysts for acetylene hydrochlorination. Appl. Catal. A Gen., 2021, **612**, 1–10 .

80. Zhang C., Zhang H., Li Y., Xu L., Li J., Li L., Cai M., Zhang J., al. Hydrochlorination of acetylene over the activated carbon supported Au catalysts modified by N−P−O-containing Ligand. ChemCatChem., 2019, **11**, 3441 –3450.

81. Lai H., Wang B., Yue Y., Sheng G., Wang S., Feng F., Zhang Q., Zhao J., Li X., An alternative carbon carrier in green preparation of efficient gold/carbon catalyst for acetylene hydrochlorination. ChemCatChem., 2019, **11**, 3318–3326.

82. Dong Y., Zhang H., Li W., Sun M., Guo C., Zhang J., Bimetallic Au–Sn/AC catalysts for acetylene hydrochlorination. J. Ind.Eng. Chem., 2016, **35**, 177–184.

83. Zhao, J., Xu, J., Xu, J., Ni, J., Zhang, T., Xu, X., Li, X., Activated-carbon-supported gold-cesium(I) as highly effective catalysts for hydrochlorination of acetylene to vinyl chloride. ChemPlusChem., 2015, **80**, 196–201.

84. Huang C., Zhu M., Kang L., Li X., Dai B., Active carbon supported TiO_2-$AuCl_3$/AC catalyst with excellent stability for acetylene hydrochlorination reaction. Chem. Eng. J., 2014, **242**, 69–75.

85. Kaiser S. K., Surin I., Amorós-Pérez A., Büchele S., Krumeich F., Clark A. H., Román-Martínez M. C., Lillo-Ródenas M. A., Pérez-Ramírez J., Design of carbon supports for metal-catalyzed acetylene. Nat. Commun., 2021, **12**, 4016–4024.

86. Li J., Zhang H., Cai M., Li L., Li Y., Zhao R., Zhang J., Enhanced catalytic performance of activated carbon-supported Ru-based catalysts for acetylene hydrochlorination by azole ligands. Appl. Catal. A Gen., 2020, **592**, 1–10.

87. Wang B., Yu L., Zhang J., Pu Y., Zhang H., Li W., Phosphorus-doped carbon supports enhance gold-based catalysts for acetylene hydrochlorination. RSC Adv., 2014, **4**, 15877–15885.

88. Zhang J., Sheng W., Guo C., Li W. Acetylene hydrochlorination over bimetallic Ru-based catalysts. RSC Adv., 2013, **3**, 21062–21068.

89. Shang S., Zhao W., Wang Y., Li X., Zhang J., Han Y., Li W., Highly efficient Ru at IL/AC to substitute mercuric catalyst for acetylene hydrochlorination. ACS Catal., 2017, **7**, 3510–3520.

90. Xu J., Zhao J., Zhang T., Di X., Gu S., Ni J., Li X., Ultra-low Ru-promoted $CuCl_2$ as highly active catalyst for the hydrochlorination of acetylene. RSC Adv., 2015, **5**, 38159–38163.

91. Xu N., Zhu M., Zhang J., Zhan, H., Dai B. Nitrogen functional groups on an activated carbon surface to effect the ruthenium catalysts in acetylene hydrochlorination. RSC Adv., 2015, **5**, 86172–86178.

92. Zhang H., Li W., Li X., Zhao W., Gu J., Qi X., Dong Y., Dai B., Zhang J., Non-mercury catalytic acetylene hydrochlorination over bimetallic Au-Ba(II)/AC catalysts. Catal. Sci. Technol., 2015, **5**, 1870–1877.

93. Hou L., Zhang J., Pu Y., Li, W. Effects of nitrogen-dopants on Ru-supported catalysts for acetylene hydrochlorination. RSC Adv., 2016, **6**, 18026–18032.

94. Jin Y., Li G., Zhang J., Pu Y., Li, W. Effects of potassium additive on the activity of Ru catalyst for acetylene hydrochlorination. RSC Adv., 2015, **5**, 37774–37779.

95. Man B., Zhang H., Zhang J., Li X., Xu N., Dai H., Zhu M., Dai B., Oxidation modification of Ru-based catalyst for acetylene hydrochlorination. RSC Adv., 2017, **7**, 23742–23750.

96. Wang Y., Nian Y., Zhang J., Li W., Han Y., MOMTPPC improved Cu-based heterogeneous catalyst with high efficiency for acetylene hydrochlorination. Mol. Catal., 2019, **479**, 1–12

97. Hu Y., Wang Y., Li W., Zhang J., Han Y., High performance of supported Cu-based catalysts modulated via phosphamide coordination in acetylene hydrochlorination. Appl. Catal. A Gen., 2020, **591**, 117408–117418.

98. Tian X., Hong G., Liu Y., Jiang B., Yang, Y,. Catalytic performance of Au(III) supported on SiO_2 modified activated carbon. RSC Adv., 2014, **4**, 36316–36324.

99. Dai B., Li X., Zhang J., Yu F., Zhu M., Application of mesoporous carbon nitride as a support for an Au catalyst for acetylene hydrochlorination. Chem. Eng. Sci., 2014, **135**, 472–478.

100. Li G., Li W., Zhang H., Pu Y., Sun M., Zhang J., Non-mercury catalytic acetylene hydrochlorination over Ru catalysts enhanced by carbon nanotubes. RSC Adv., 2015, **5**, 9002–9008.

101. Wang L., Wang F., Wang J., Enhanced stability of hydrochlorination of acetylene using polyaniline-modified Pd/HY catalysts. Catal. Commun., 2016, **74**, 55–59.

102. Dawson S., Pattisson S., Malta G., Dummer N. F., Smith L. R., Lazaridou A., Allen C. S., Davies T. E., Freakley S. J., Kondrat S. A., Kiely C. J., Johnston P., Hutchings G. J., Sulfur promotion in Au/C catalyzed acetylene hydrochlorination. Small, 2021, **17**, 1-10.

103. Smith, D. M., Walsh, P. M. & Slager, T. L., Studies of silica-supported metal chloride catalysts for the vapor-phase hydrochlorination of acetylene. J. Catal., 1968, **11**, 113–130.

104. Chen Z., Chen Y., Chao S. L., Dong X., Chen W., Luo J., Liu C.,Wang, D., Chen C., Li W., Li J., Li Y., Single-atom AuI-N_3 site for acetylene hydrochlorination reaction. ACS Catal., 2020, **10**, 1865–1870.

105. Shen Z., Liu Y., Han Y., Qin Y., Li J., Xing P., Jiang B., Nitrogen-doped porous carbon from biomass with superior catalytic performance for acetylene hydrochlorination. RSC Adv., 2020, **10**, 14556–14569

106. Hutchings G. J., Grady D. T., Hydrochlorination of acetylene: The effect of mercuric chloride concentration on catalyst life, Applied Catal., 1985, **17**, 155-160

107. Wang J., Zhao F., Zhan, C., Kan, L., Zhu M., A novel S, N dual doped carbon catalyst for acetylene hydrochlorination. Appl. Catal. A Gen., 2018, **549**, 68–75

108. Wu L., Xin J., Xia D., Sun J., Liang J., Enhanced production of hydrocarbons from the catalytic pyrolysis of maize straw over hierarchical ZSM-11 zeolites. Appl. Catal. B Environ., 2022, **317**, 121775–1217789

109. Wang J., Gong W., Zhu M., Dai B., Effect of carbon defects on the nitrogen-doped carbon catalytic performance for acetylene hydrochlorination. Appl. Catal. A Gen., 2018, **564**, 72–78.

110. Kaiser S. K., Song K. S., Mitchell S., Coskun A., Pérez-Ramírez, J., Nitrogen-doped carbons with hierarchical porosity via chemical blowing towards long-lived metal-free catalysts for acetylene hydrochlorination. ChemCatChem., 2020, **12**, 1922–1925.

111. Li X., Wang Y., Kang L., Zhu M., Dai B., A novel, non-metallic graphitic carbon nitride catalyst for acetylene hydrochlorination. J. Catal., 2014, **311**, 288–294.

112. Shen Z, Liu Y, Han Y, Qin Y, Li J, Xing P, Jiang B., Nitrogen-doped porous carbon from biomass with superior catalytic performance for acetylene hydrochlorination. RSC Adv., 2020, **25**, 14556-14569.

113. Li X., Zhang J., Li W., MOF-derived nitrogen-doped porous carbon as metal-free catalysts for acetylene hydrochlorination. J. Ind. Eng. Chem., 2016, **44**, 146–154.

114. Yang Y., Lan G., Wang X., Li Y., Direct synthesis of nitrogen-doped mesoporous carbons for acetylene hydrochlorination. Chin. J. Catal., 2016, **37**, 1242–1248.

115. Qiao X., Zhou Z., Liu X., Zhao C., Guan Q., Li W., Constructing a fragmentary g-C_3N_4 framework with rich nitrogen defects as a highly efficient metal-free catalyst for acetylene hydrochlorination. Catal. Sci. Technol., 2019, **9**, 3753–3762

116. Zhao C., Qiao X., Yi Z., Guan, Q., Li, W., Active centre and reactivity descriptor of a green single component imidazole catalyst for acetylene hydrochlorination. Phys. Chem. Chem. Phys., 2020, **22**, 2849–2857

117. Wang X., Dai B., Wang Y., Yu, F., Nitrogen-doped pitch-based spherical active carbon as a nonmetal catalyst for acetylene hydrochlorination. ChemCatChem., 2014, **6**, 2339–2344

118. Lu Y., Lu F., Zhu M., Nitrogen-modified metal-free carbon materials for acetylene hydrochlorination. J. Taiwan Inst. Chem. Eng., 2020, **113**, 198–203.

119. Liu X., Qiao X., Zhou Z., Zhao C., Guan Q., Li W., Mechanism exploring of acetylene hydrochlorination using hexamethylenetetramine as a single active site metal-free catalyst. Catal. Commun., 2020, **147**, 106147–106152.

120. Qi X., Chen W., Zhang J., Sulphur-doped activated carbon as a metal-free catalyst for acetylene hydrochlorination. RSC Adv., 2020, **10**, 34612–34620.

121. Liu Y., Zhang H., Li X., Wang L., Dong Y., Li W., Zhang J., Solvent-assisted synthesis of N-doped activated carbon-based catalysts for acetylene hydrochlorination. Appl. Catal. A Gen., 2021, **611**, 117902–117913.

122. Lu F., Xu D., Lu Y., Dai B., Zhu M., High nitrogen carbon material with rich defects as a highly efficient metal-free catalyst for excellent catalytic performance of acetylene hydrochlorination. Chin. J. Chem. Eng., 2021, **29**, 196–203.

123. Qiao X., Zhao C., Zhou Z., Guan Q., Li W., Constructing pyridinic N-rich aromatic ladder structure catalysts from industrially available polyacrylonitrile resin for acetylene hydrochlorination. ACS Sustain. Chem. Eng., 2019, **7**, 17979–17989

124. Mei S., Gu J., Ma T., Li X., Hu Y., Li W., Zhang J., Han Y., N-doped activated carbon from used dyeing wastewater adsorbent as a metal-free catalyst for acetylene hydrochlorination. Chem. Eng. J., 2019, **371**, 118–129.

125. Liu X., Conte M., Elias D., Lu L., Morgan D. J., Freakley S. J., Johnston P., Kiely C. J., Hutchings G. J., Investigation of the active species in the carbon-supported gold catalyst for acetylene in hydrochlorination. Catal. Sci. Technol., 2016, **6**, 5144–5153.

Chapter 4

Investigation of different activated carbon supports for the acetylene hydrochlorination reaction.

4.1 Introduction

In this chapter, the role of the support in the preparation of active Au catalysts *via* a simple wet impregnation method will be investigated. The attention will be drawn specifically on activated carbons as supports. The physical and chemical properties of the support materials will be discussed, with the aim of identifying and understanding the set of parameters that facilitate the generation of highly active catalysts.

4.2 Overview

The nature of the support in heterogeneous catalysis plays a vital role in the activity. Activated Carbon (AC) has been extensively used either as catalyst support or as a catalyst on its own.[1] AC is a general name describing amorphous, high surface area, well-structured and porous carbonaceous materials. This class of materials are imperative in a wide array of applications, varying from energy conversion and storage to carbon dioxide capture and heterogeneous catalysis.[2-4] When used as a catalyst, AC is used for the manufacture of phosgene,[5] the production of S halides,[6] the catalytic removal of SO_2/NO_x from flue gases,[7] while it has also found practical use in numerous industrial and fine chemical roles.[8] In addition, Acs have extensively been used as supports for the preparation of metal based catalysts and are nowadays predominantly used in stabilising metal sites from nanoparticles to single metal atoms.[9]

A diverse sources of parent resources can be used in AC production such as coal, petroleum and biomass.[10] AC can be retrieved from precious metal catalysts *via* combustion, making it a favourable host for catalytic reactions operated on an industrial scale. In addition, the advanced physical and chemical properties of AC materials such as the high porosity, high surface area, chemical stability, enhanced acetylene adsorption capacity, have set Acs attractive supports for the preparation of catalysts for acetylene hydrochlorination.[11] In literature, the majority of catalytic systems used in the acetylene hydrochlorination report AC derived from coal, pitch, coconut, and wheat, as well as other

types of chemically produced AC.[12] The wide scope of Acs employed in the acetylene hydrochlorination is related to intrinsic characteristics of carbon, such as the surface area, metal mobility, acetylene adsorption capacity, and O functionalities.[13-15] Other supports such as silica,[16] alumina,[17] zeolites,[18,19] have also been investigated, yet they result in active catalytic systems. Specifically, the high chemical inertness of AC and its affinity to organic materials provides this matrix with a distinctive capability of maintaining high acetylene adsorption even during exposure to HCl, in contrast to other types of supports such as ceria.[20,21]

The method of catalyst preparation is crucial for its catalytic activity.[13,22,23] Aqua regia, a mixture of HCl and HNO_3 in 3:1 ratio, has been widely used in research for catalyst preparation. Carbon characteristically can reduce Au during the catalyst preparation, as observed during deposition-precipitation for Au supported on carbon catalysts. However, the oxidising nature of aqua regia prevents the reduction of Au on the highly reducing carbon support surface ensuring the stabilisation of the Au^{n+} species.[24] Comparison of aqua regia to its composite acids, HNO_3 and HCl, confirms that aqua regia generates highly active catalysts for the acetylene hydrochlorination reaction as an effect of the oxidising HNO_3, which stabilises the Au(III) and Au(I) centres, while the nucleation capacity of HCl favours the generation of anchoring sites for the Au on the carbon.[25] The dominance of aqua regia in the catalyst preparation was associated with the above factors, as highly dispersed oxidised Au atoms on the carbon support can be generated.

From an industrial point of view, aqua regia is a non-desirable solvent to use. The corrosive, hazardous, environmentally unfriendly profile of this solvent raises many concerns regarding its practice. In addition, Au/AC aqua regia generated catalysts suffer from rapid deactivation due to polymerisation of acetylene on the acid sites introduced as a result of the solvent during catalyst preparation.[26] Au/AC prepared using a water solvent resulted in inactive catalysts due to the formation metallic Au nanoparticles. Alternatives of aqua regia have been investigated. It is reported that solvents such as the organic aqua regia (OAR) which is a mixture of thionyl chloride ($SOCl_2$) and organic solvents such as pyridine, N,N-dimethylformamide, and imidazole can also be employed.[27] It has been previously reported that organic aqua regia can enable the selective dispersion of metal precursors, a practice that is beneficial for selective retrieval of metals from bimetallic catalysts or for microelectronic applications.[28] In addition, OAR has been used for the preparation of Au on carbon catalysts for the acetylene hydrochlorination reaction, resulting in catalysts with improved in comparison to those prepared using aqua regia.[29] Nevertheless, both traditional and organic aqua regia are still highly oxidising, toxic solvents, not considered to be

environmentally friendly nor suitable for commercial application. Therefore, the use of alternative simple, non-oxidising non acidic solvents has been investigated as alternatives. It has been reported that low polarity, low boiling point solvents can also produce atomically dispersed Au cationic species. Using acetone as a solvent produces Au catalysts with comparable performance to those prepared with aqua regia, while ensuring high dispersion of Au cationic species on the surface of the catalyst.[23] In addition, acetone prepared catalysts have a greatly reduced induction period compared to the aqua regia prepared catalysts. The employment of acetone as a solvent medium ensures the study of the support as it does not alter the physical and chemical properties of the matrix, due to its mild nature.[23] The substitution of aqua regia solvent with acetone has removed the requirement of handling highly acidic waste upon catalyst preparation, whilst opening the possibility to generating highly dispersed Au catalysts with high metal loadings, skipping the requirement of using solely water-soluble metal salts.[26] The dominance of aqua regia as a solvent over the past years limited the scope of the supports, a crucial aspect in catalyst preparation. The selection of the support material is vital as it must endure the harsh operational conditions, inherent in the reaction. In addition, it must stabilise high dispersion of the active species on its surface while precluding the reduction and the agglomeration of Au cationic moieties. Finally, the support must be financially viable as it should be suitable for scale-up operations and industrial applications. The role of the support will be investigated in this chapter. In this chapter, the catalytic profile of commercially available Acs produced from different suppliers that were prepared using various activation methods will be discussed. The Acs have been used as supports for the preparation of active Au catalysts *via* a simple wet impregnation method. The physical and chemical characteristics were analysed including surface area, pore size, surface graphitization, and surface oxygenated acid site distribution. The relationships between catalytic activity and structural aspects of Acs has been investigated to obtain a guide for further exploration of efficient catalysts for VCM production. The aim of this work is to examine the role of the support to obtain a better understanding of:

- The interactions between Au metal centres and supports.
- The role of functionalities on the support and how they influence the chemistry of reaction.
- Determine the differences among supports that affect the activity of Au supported catalysts.

4.3 Experimental

4.3.1 Catalyst preparation

All carbon-supported Au catalysts were prepared *via* a previously reported wet impregnation method.[23]

The Au precursor, $HauCl_4 \cdot 3H_2O$ (Alfa Aesar, 20 mg, assay 49%) was dissolved in dry acetone (2.7 ml, assay 99.8%) and allowed to stir for 10 mins. Accordingly, the solution was added dropwise, with stirring, to the support (0.99 g). In this chapter, different sources of support materials are investigated (table 4.1). The solution was left to stir for 1 h and finally dried under N_2 at 45 °C for 16 h. Unless specified otherwise, all catalysts were prepared with a 1 wt. % Au loading. Novel prepared catalysts are denoted as 1 wt.% Au/AC. All supports were used without any additional treatment.

4.3.2 Reaction Conditions

Unless otherwise stated, reactions were performed using the following conditions:

Condition A: 45 mg of sample and 45 mg of SiC, 24.00 mL min^{-1} C_2H_2 (5% acetylene in Argon), 30.00 mL min^{-1} HCl (5% hydrogen chloride in Argon) and 4.10 mL min^{-1} Ar, 200 ^oC.

Condition B: 300 mg of sample and 150 mg of SiC, 24.00 mL min^{-1} C_2H_2 (5% acetylene in Argon), 30.00 mL min^{-1} HCl (5% hydrogen chloride in Argon) and 4.10 mL min^{-1} Ar, 200 ^oC.

Two distinctly different reaction conditions were employed in order to study the behaviour of the materials. Condition A relates to kinetic studies with catalysts studied at conversion levels <30%,[30] while condition B related to mass transfer limitation studies in order to further investigate the stability of catalysts. The deactivation rate of the catalyst is calculated as shown in equation 4.1.

$$Deactivation\ rate\ (\%\ h^{-1}) = \frac{X_{residual}(\%) - X_{max}(\%)}{\Delta t(h)}\ eq.4.1$$

4.4 Selection of carbon supports

Support choice is of a paramount importance for single atom catalyst preparation.[31] The catalytic activity depends on the surface area, structural properties and defects of support as they lead in different interactions with the metal atoms.[32] At the atomic scale, the surface free energy of the metal atoms is enhanced, promoting particle formation *via* metal agglomeration of small atoms and clusters.[33] The main pathway for single atom aggregation occurs *via* Ostwald ripening, particle agglomeration and coalescence.[34] Therefore, the

selection of an appropriate support to prevent or minimise the particle migration is highly important, and typically one that has high surface area and is suitable in robust applications, while ensuring anchoring of the metal center.[35] AC is traditionally employed as a support due its low cost, high surface area, and high stability under acidic, high temperature conditions.

Two main routes are followed when producing Acs. In the first method, known as chemical activation, the precursor material and dehydrating chemical agent are combined and mixed before undergoing thermal degradation. Accordingly, the activation and the carbonization are performed in a one-step method. The second process, known as physical activation, includes the carbonisation of the source material in absence of air.[36] Both types of activation are widely used however, the method of preparation depends on the final desired properties of the generated materials. Overall, the chemical activation offers wider scope of benefits over physical activation such as the requirement of lower activation temperatures, the generation of materials with higher surface areas and improved porous properties, the applicability of controlled process, and minor mineral impurities.[37]

Five types of commercially available Acs produced by different companies and sources were included in this study. In this work, the Acs investigated are the coconut-based AC (noted as NORIT ROX 0.8, by Cabot Corporation), wood-based (noted as DARCO KB-B, by Cabot Corporation), peat-based (marked as NORIT GSX, by Cabot Corporation), and pine wood-based (CECAL4S and CECAL2S, by Calgon Carbon Corporation). All the Acs are produced *via* physical activation, apart from the DARCO KB-B which is produced *via* chemical activation, in which phosphoric acid treatment was employed. All Acs have neutral pH, apart from the DARCO KB-B which has acidic character. The physical and chemical features of the resulting Acs differ based on the type of precursor material, on the activation method and the modification chosen.[38] For acid Acs, the quantity and nature of O-containing surface groups can be influenced by the identity of the treatment with different acids, thus enhancing the acidic behaviour and the resulting surface chemistry.[39]

Unfortunately, it has not been possible to receive any additional information regarding the activation temperatures of the steam prepared Acs. The supplier, source of origin, activation method and pH of the different Acs materials are summarised in Table 4.1. All the Acs were used as received, without any additional treatment.[38] Therefore, the physical and chemical properties of the AC supports are fundamentally different as it will be shown later.

Supplier	Product name AC	Source of origin	Method of Activation	pH
CABOT	NORIT ROX 0.8	Coconut	Steam	Neutral
CABOT	DARCO KB-B	Wood	H_3PO_4	Acid
CABOT	NORIT GSX	Peat	Steam	Neutral
Calgon Carbon	CECAL4S	Pine wood	Steam	Neutral
Calgon Carbon	CECAL2S	Pine wood	Steam	Neutral

Table 4.1: List of various Acs used as supports for the preparation of 1wt.% Au/Acs catalysts.

The question that is raised is how the physical and chemical properties of the host can define the activity of the catalysts for the acetylene hydrochlorination reaction. To answer this question, different analytical techniques have been employed to study the properties of the AC supports.

4.5 Surface characterization of different supports

X-ray photoelectron spectroscopy (XPS) has been employed for the study of AC supports. XPS is a useful analytical technique that offers quantitative information of functional groups on the surface of the AC materials after spectra deconvolution.[40] Analysis of the AC samples was performed by referencing the Carbon 1s electron binding at 284.6 eV. XPS spectra deconvolution of a Carbon 1s can be indicative of different components. XPS fittings was made utilizing fittings relative the nature of the carbon material, be it more graphitic or aliphatic. The components of a typical C 1s XPS spectrum (Figure 4.1) corresponding to graphitic carbon (C sp^2), carbon species in alcohol, ether groups and/or C-O-P linkage (C sp^3), carbon in carbonyl groups (-C=O), carboxyl and/or ester groups (-COOH), and shake-up satellite due to π-π^* transitions.[41] Figure 4.1 represents the C_{1s} fitting of NORIT ROX 0.8 as an example of the AC hosts.

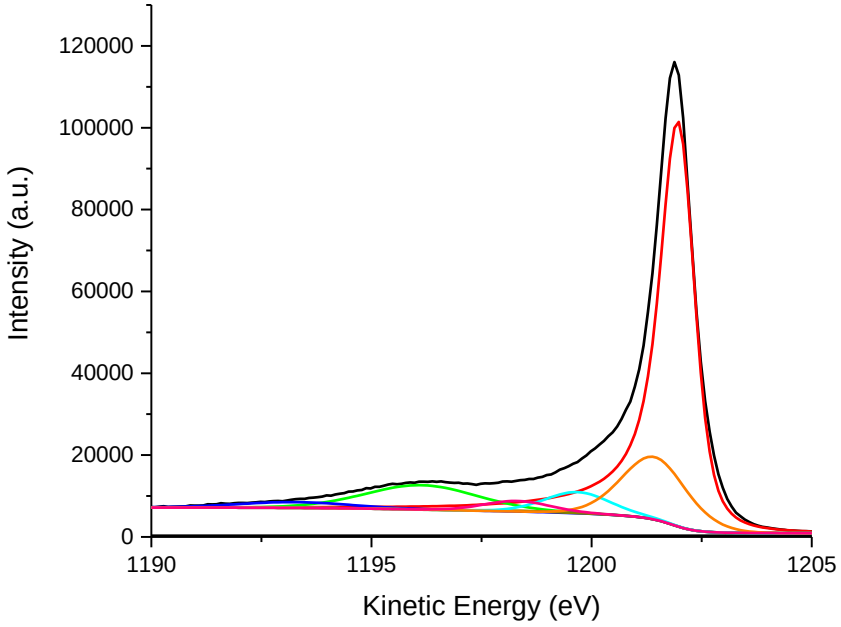

Figure 4.1: Deconvolution of the different groups on a typical C 1s XPS spectrum of carbon samples.

The relative amount of different functional groups of the Acs are presented in Table 4.2. The different commercial Acs present significant differences in the relative content of functional groups. NORIT ROX 0.8 presents relatively high graphitic character (60.9 at.%), only lower than the CECAL4S (71.9 at.%), while DARCO KB-B exhibits the lowest graphitic content (44.6 at.%). The DARCO KB-B appears to lack C=O functionality despite presenting the highest carboxylic (3.4 at.%) and alcohol/ether (6.9 at.%) content among the samples. Interestingly, despite the CECAL2S and CECAL4S originating from the same source material and undergo a similar steam activation method, the two samples present intrinsic differences in functionality. The level of graphitic character and amount of the alcohol/ether, carboxyl and carbonyl groups can all be seen to vary between the two materials. Those differences imply that the activation method and conditions of the CECAL2S and CECAL4S have significantly impacted on the chemical surface functionalities of the two materials.

Acs	XPS fitting of Carbon at.%					
	C sp^2	C sp^3	C=O	C-O	O-C=O	pi-pi*
NORIT ROX 0.8	60.9	20.4	1.9	4.3	2.1	10.4
DARCO KB-B	44.6	37.9	-	6.9	3.4	7.2
NORIT GSX	49.7	30.4	1.1	5.2	2.9	10.7

CECAL2S	53.7	27.8	1.6	6.1	1.1	9.7
CECAL4S	71.9	12.8	0.6	2.7	2.1	9.9

Table 4.2: Deconvolution results of XPS spectra of carbons.

The catalytic activity depends on the chemisorbing ability of the reactants and desorption of the products. Chemical functional groups such as O,[42] and N significantly contribute in this context.[43,44] XPS surface analysis of Acs reveals that the N content in all the samples is relatively low (less than 0.3 at.%) indicating that the effect of N content, for the novel catalysts prepared using the Acs of choice, should have a neglegible effect on the activity of the catalysts. On the other hand, the total O content of the materials differs significantly among the samples (Table 4.3). DARCO KB-B (8.9 at.%) has the highest amount of O, followed by NORIT ROX 0.8 (4.6 at.%) and NORIT GSX (4.1 at.%). Conversely, the CECAL2S (2.9 at.%) and CECAL4S (3.0 at.%) present the lowest O content.

	XPS elemental analysis at. %				
	C 1s	Cl 2p	N 1s	O 1s	S 2p
NORIT ROX 0.8	94.7	0.1	0.2	4.6	0.4
DARCO KB-B	90.8	<0.1	0.2	8.9	<0.1
NORIT GSX	95.3	<0.1	0.3	4.1	0.2
CECAL2S	96.9	<0.1	0.1	2.9	<0.1
CECAL4S	96.9	<0.1	<0.1	3.0	<0.1

Table 4.3: Detailed content of different elements of various catalysts obtained from the XPS analysis.

The textural properties of the Acs such as the surface area, micropore volume, average pore size diameter and the microporosity of Acs samples were analysed *via* N_2 adsorption desorption isotherm measurements at 77 K. Acs are classified as microporous solids with high surface areas and relatively small external surfaces.[45] The N_2 uptake (Figure 4.2) at relative low pressures P/Po of less than 0.1 is high for all the samples, indicating that all Acs possess high surface areas. DARCO KB-B (1574 m^2/g) and NORIT ROX 0.8 (1532 m^2/g) exhibit the highest surface areas, followed by CECAL4S (1047 m^2/g), CECAL2S (949 m^2/g) and NORIT GSX (929 m^2/g) (Table 4.4). Interestingly, the micropore area follows a different trend with the NORIT ROX 0.8 (1420 m^2/g) having the highest value followed by DARCO KB-B (955 m^2/g), NORIT GSX (716 m^2/g), CECAL4S (611 m^2/g) and finally CECAL2S (564 m^2/g).

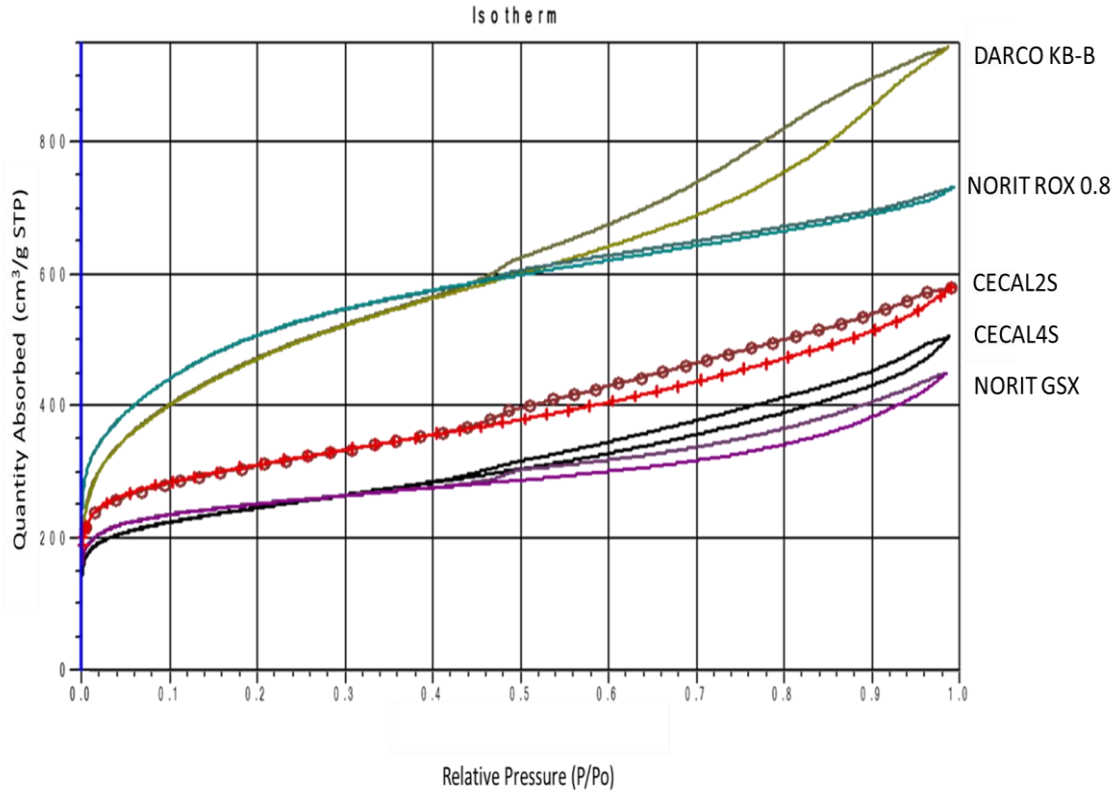

Figure 4.2: N_2 adsorption-desorption isotherms of Acs.

There are many studies that suggest that microporosity is a desirable feature for AC supports for the acetylene hydrochlorination reaction.[46,47] The pore classification is related to the pore size according to which macroporous materials have average pore sizes of 50 nm or greater, mesoporous materials of 2.0–50 nm, and microporous materials have average pore sizes of less than 2.0 nm.[48] According to this classification method, NORIT ROX 0.8 (1.3 nm) and NORIT GSX (1.5 nm) are predominantly microporous materials, while CECAL2S (2.3 nm), CECAL4S (2.5 nm) and DARCO KB-B (3.6 nm) are mesoporous materials. Table 4.4 summarizes the surface characterization properties of the Acs.

Acs	Surface Characterisation					
	BET Surface Area (m^2/g)	Micropore Area (m^2/g)	External Surface (m^2/g)	Total Pore Volume	Micropore Volume (cm^3/g)	Average Pore Size (nm)
NORIT ROX 0.8	1532	1420	112	0.74	0.60	1.3
DARCO KB-B	1574	955	618	1.23	0.53	3.6
NORIT GSX	929	716	213	0.56	0.31	1.5

CECAL2S	949	564	384	0.67	0.26	2.3
CECAL4S	1047	611	436	0.75	0.28	2.5

Table 4.4: N_2 physisorption analysis of Acs. Surface and pore characteristics of carbon materials.

Overall, it can be concluded that all the Acs of this study are high surface area materials with relatively small external surface areas and small average pore size diameters. The remarkable examples in this study are the NORIT ROX 0.8, as it is the AC with the smallest pore size and the highest micropore volume, and the DARCO KB-B which is the material with wider pores. It is suggested that steam Acs lead to materials with the lower micropore volumes,[49] a fact that comes with agreement for the NORIT ROX 0.8, NORIT GSX, CECAL2S and CECAL4S, while the acid Acs are expected to exhibit larger pore structures,[38] as confirmed in this study for the case DARCO KB-B.

Further investigations of the physical properties of carbonaceous materials were conducted to explain the differences among the AC supports. Raman spectroscopy is a vital tool for the structural determination of Acs as it provides information related to the degree of defects and graphitization on the surface.[50] A typical Raman spectrum consists of two sharp peaks at approximately 1600 cm^{-1} and about 1350 cm^{-1}, referred to as the band G (graphite) and band D (disorder), respectively (Figure 4.3). The peak intensity of the D band is related to the sp^2 bonds which are associated with sites arranged in either aromatic rings or olefinic chains, while the peak intensity of the G band describes sp^3 defect sites.[51] The positions, widths and intensity ratio of D and G bands (I_D/I_G) represent the sp^2/sp^3 carbon ratio providing information related to the structure of the carbon materials and the degree of graphitization. Table 4.5 gives the ID/IG ratio values of the Acs samples. The I_D/I_G ratio changes in the following order: NORIT ROX 0.8 < NORIT GSX < CECAL2S < CECAL4S < DARCO KB-B. The greater the value of I_D/I_G, the more defects are present in the surface of the AC materials.[52] The defective sites are a highly valuable feature for Acs supports, with multiple studies associating a smaller surface graphitization degree with higher number of active sites for the acetylene hydrochlorination, as the surface defects of Acs are considered as possible active centres.[53-55]

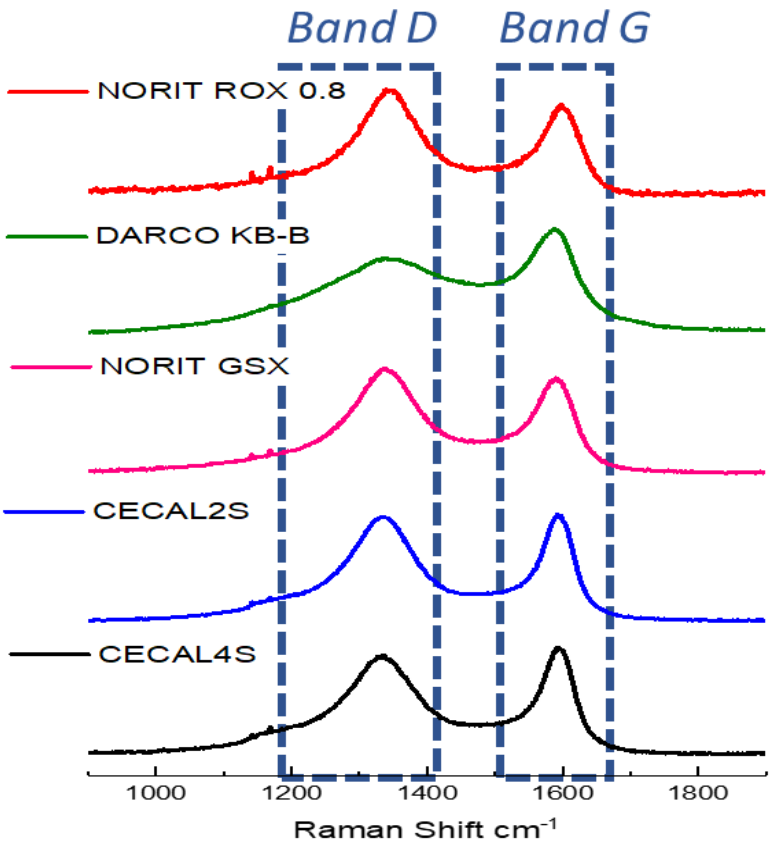

Figure 4.3: Raman spectra of Acs.

Acs	Raman Characterisation				
	Band D	Band G	Band D Intensity	Band G Intensity	I_D/I_G
NORIT ROX 0.8	1339	1597	8645	7471	1.16
DARCO KB-B	1337	1587	30672	42622	0.72
NORIT GSX	1338	1590	22196	20182	1.10
CECAL2S	1333	1592	28282	28845	0.98
CECAL4S	1337	1591	19957	21555	0.93

Table 4.5: Raman analysis of Acs.

Additionally, Boehm titration was employed to establish the amount of the acidic O surface functionalities on the Acs. Boehm titration is a widely used analytical technique, in which different bases are responsible for neutralising specific functional groups. For instance, sodium bicarbonate, as a weak base, is utilised for the quenching of carboxylic groups. Sodium carbonate, as an intermediate strength base, can neutralise carboxylic and lactonic

groups. Sodium hydroxide, as a strong base, can be used for the neutralisation of carboxylic, lactonic and phenolic groups. It should be noted that the absolute value of each base uptake cannot be used for quantitative analysis but can provide a qualitative insight into the overall acidic O surface functional groups of the AC samples.[56]

Overall, as seen from table 4.6, DARCO KB-B is the AC that has the highest uptake of each base, suggesting that this carbon has the highest quantity of acidic O surface functionalities. This observation can be attributed to the formation of acid groups upon the preparation of the material as it is the only AC of our study that has been made *via* an acid activation. NORIT GSX has the second largest value of each base uptake, implying the coexistence of the different acidic oxygenated groups in significant quantities. As seen from table 4.6, NORIT ROX O.8, CECAL2S AND CECAL4S present a similar base consumption in total, suggesting that these materials have approximately the same amount of acidic O surface functionalities, and lower than DARCO KB-B and NORIT GSX. Each base uptake is associated with a specific functional group, however, there is a need to further investigate the identity and the quantity of those groups, therefore additional analytical techniques have been employed.

Acs	Boehm Titration			
	NaOH (ml)	$NaHCO_3$ (ml)	Na_2CO_3 (ml)	Overall base uptake (ml)
NORIT ROX 0.8	8.1	9.0	7.5	24.6
DARCO KB-B	12.7	10.2	13.1	36.0
NORIT GSX	10.4	9.7	11.4	31.5
CECAL2S	9.9	9	7.5	26.4
CECAL4S	9.2	9.1	9.8	28.1

Table 4.6: Boehm titration base uptake.

Acs are complex materials that bear a wide range of different functional groups.[57-61] The identification of which is not trivial. Among the techniques that are used for the detection of the surface functionalities is temperature programmed desorption (TPD). When undergoing thermal treatments, the oxygenated functional groups on the surface of the Acs decompose. This decomposition leads to emission of carbon monoxide and carbon dioxide.[62] At different temperatures, different functionalities will decompose leading to the equivalent discharge of CO and CO_2. AC materials include a variety of O functional groups that, upon

decomposition, generate CO and CO_2 (Figure 4.4). The presence of N in the structure of the carbon support is associated with the origin of the precursor, whilst the presence of O functionalities is related to the preparation method of the AC material. The type and quantity of oxygenated surface functional groups is related mainly to the thermal and oxidative treatment that the precursor undergoes upon the preparation of the AC support. The temperatures at which the main functionalities decompose to form CO_2 and CO can be seen in Figure 4.5 a, and b respectively.

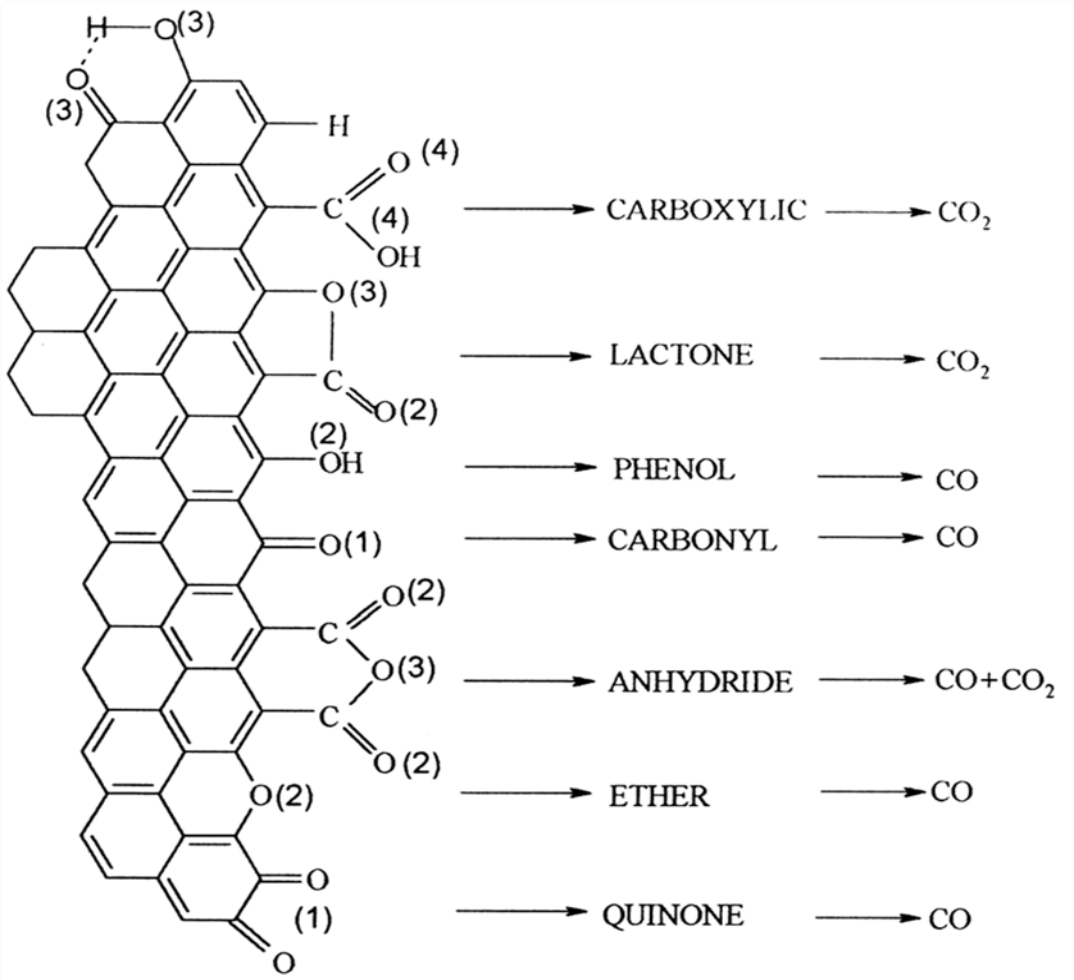

Figure 4.4: O containing surface groups on carbon.[63]

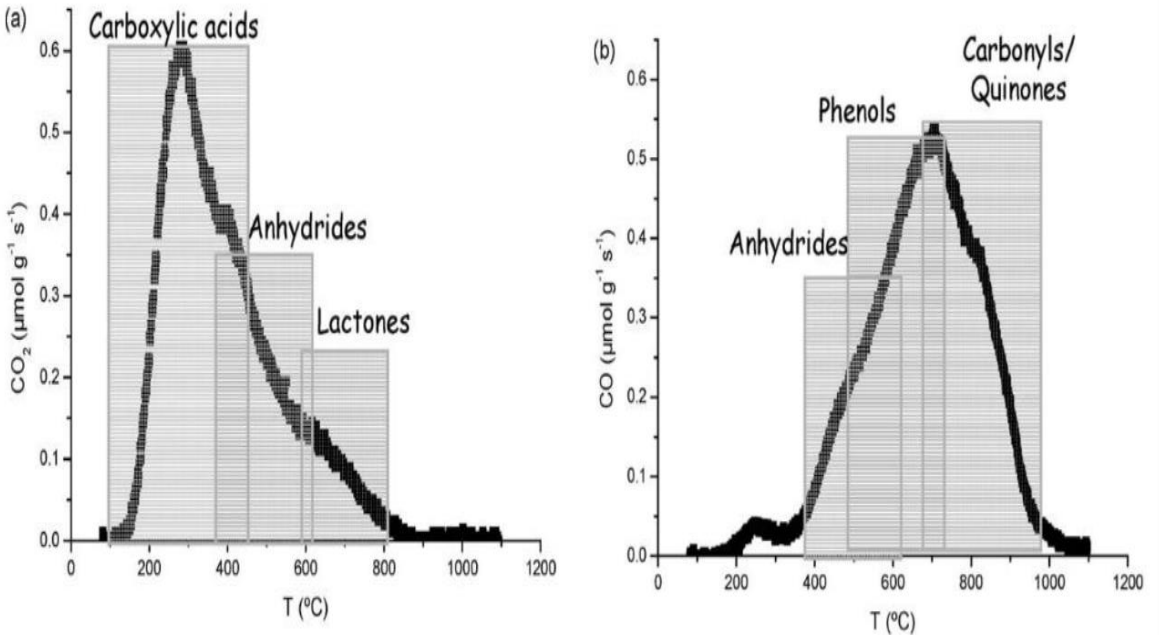

Figure 4.5: Temperature ranges corresponding to the evolution of (a) CO_2 and (b) CO upon decomposition of the various types of O functional groups.[64]

Figure 4.6 displays results TPD in conjugation with FT-IR for different Acs. Through these studies, carbon supports were heated under a N_2 flow, under a constant heating rate, while the FT-IR was employed to monitor the concentration of the emitted gases. Depending on the temperature and type of functionality, CO and CO_2 was generated. Unfortunately, due to equipment limitations, the analysis could be performed only up to 600 ^oC. The gas emissions are recorded in a temperature range that covers the following surface oxygenated functionalities, as seen from the table 4.7.

Functional Group	Desorbed Species	Decomposition Temperature (^oC)
Carboxylic acid	CO_2	100-350
Anhydride	CO_2	350-600
Lactone	CO_2	550-800
Anhydride	CO	350-600
Phenol	CO	450-750
Carbonyl/Quinone	CO	700-1000

Table 4.7: Temperature ranges for decomposition of various types of O functional groups on carbon to the evolution of CO and CO_2.[64]

As shown in figure 4.6 DARCO KB-B demonstrates the highest emission of CO_2 at temperatures lower than 300 ^oC, suggesting that this AC support has a high content of

carboxylic acid groups. In addition, further gradual heating of the DARCO KB-B generates high emissions of CO_2, a fact that implies the presence of high amount of surface O acidic functionalities. In contrast, NORIT GSX records lower CO_2 emission at temperatures below 300 ^oC, in comparison to DARCO KB-B, while upon continuous heating of the carbon support it exceeds in CO_2 emissions the DARCO KB-B. These trends imply that both DARCO KB-B and GSX have a high volume of acidic surface functional groups..

NORIT ROX 0.8 has a low CO_2 emission at lower temperatures, and it exhibits a sudden decrease in CO_2 emission at 315 ^oC. This trend can be attributed to the complete decomposition of carboxylic acid groups that are present on the surface. Upon heating of the NORIT ROX 0.8 to higher temperatures, it can be observed that the CO_2 gradually increases and eventually stabilises. For the CECAL2S and CECAL4S, the CO_2 emission profile is very similar. At a wide range of temperatures both materials are emitting relatively low amounts of CO_2. Overall, NORIT ROX 0.8, CECAL2S and CECAL4S supports that have the lowest acidic surface functional groups.

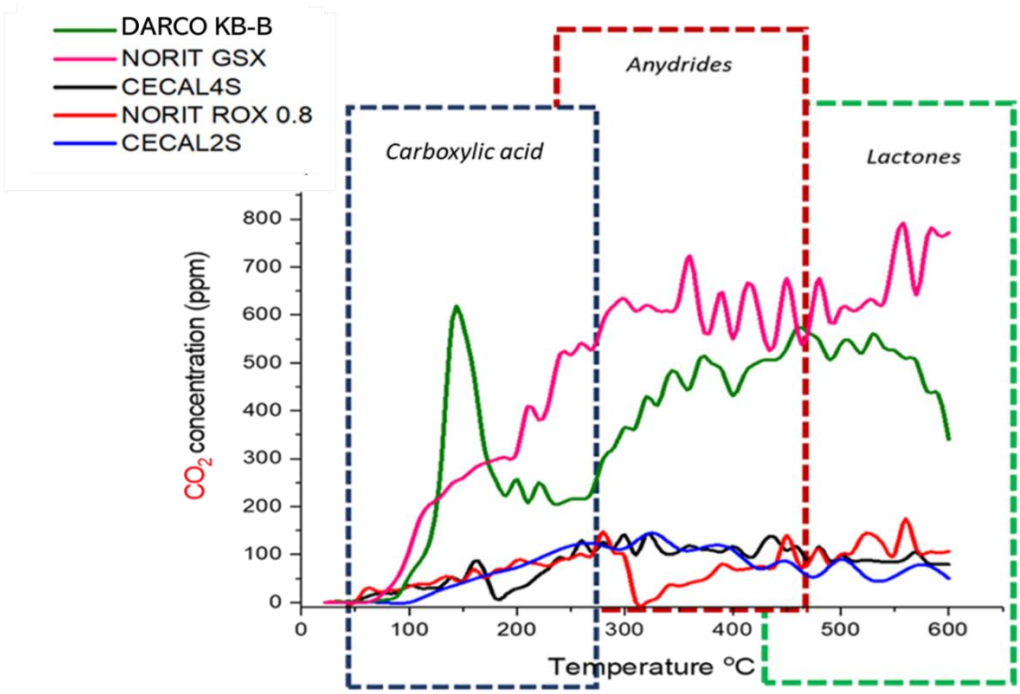

Figure 4.6: Temperature ranges of decomposition of various types of O functional groups on carbon supports to the evolution of CO_2.

Additionally, figure 4.7 illustrates the temperature ranges of decomposition of the various types for O functional groups on carbon supports to the evolution of CO. The emission of CO is only observed at temperatures higher than 350 ^oC, which is associated with the desorption of the anhydride groups from the surface of the support.[64] Gradual heating of the

support leads to higher CO evolution, with the DARCO KB-B emitting the highest content, followed by the NORIT GSX. The CECAL2S, CECAL4S and NORIT ROX 0.8 again demonstrate a lower content of acidic O surface functionalities on these materials.

Due to limitations related to the instrumentation, it is not feasible to expose the samples to temperatures higher than 600 °C, therefore, a qualitative representation of the overall O content of the samples will not provide a representative value. In addition, applying this methodology it is not feasible to determine the content of each functional group, but rather get an understanding of the qualitative characteristics that samples exhibit.

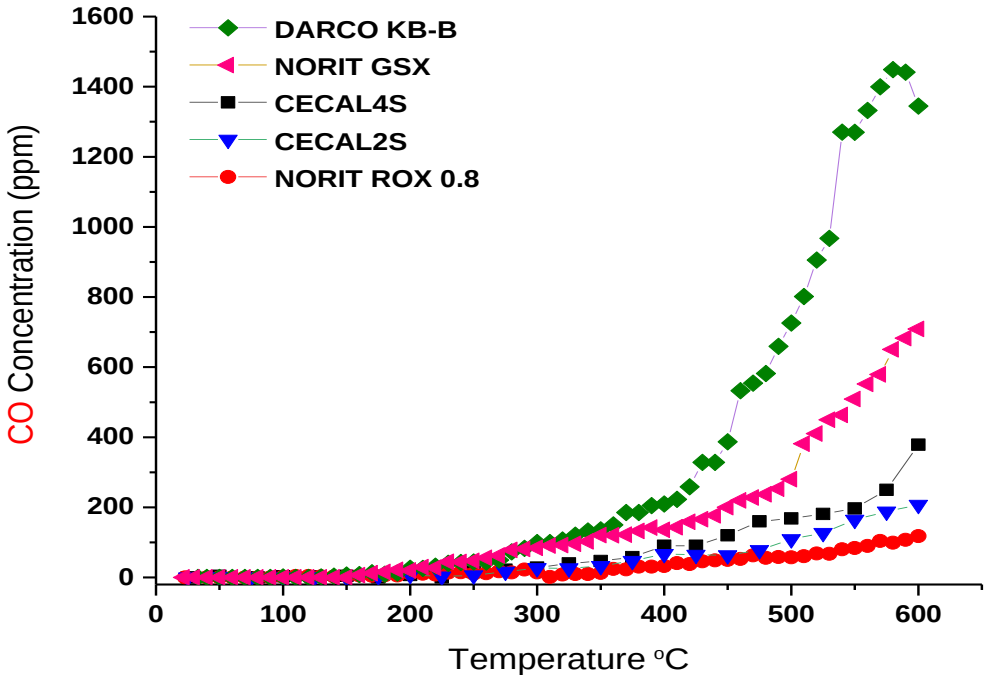

Figure 4.7: Temperature ranges of decomposition of various types of O functional groups on carbon supports to the evolution of CO.

4.6 Comparison of activity profile of AC-supported Au catalysts

In the previous sections of this chapter, the physical and chemical properties of the AC supports have been investigated. The question that is inevitably being raised is how the physical and chemical properties of the ACs are affecting the activity profile of the catalysts. Answering this question is not easy, as different parameters should be taken into consideration. For this reason, a set of two experiments, conducted at different conditions were performed. The 1 wt.% Au supported on AC support has been tested at the following experimental conditions:

- 45 mg of sample and 45 mg of SiC, 24.00 mL min^{-1} C_2H_2 (5% acetylene in Argon), 30.00 mL min^{-1} HCl (5% hydrogen chloride in Argon) and 4.10 mL min^{-1} Ar (Kinetic regime conditions), 200 ^oC.
- 300 mg of sample and 150 mg of SiC, 24.00 mL min^{-1} C_2H_2 (5% acetylene in Argon), 30.00 mL min^{-1} HCl (5% hydrogen chloride in Argon) and 4.10 mL min^{-1} Ar. (Diffused conditions)), 200 ^oC.

Catalytic activity is associated with the nature, concentration and accessibility of its active sites which is proportional to the physical properties of the materials such as the surface area. However, relying solely on the physical properties of the materials implies that deactivation and/or diffusion phenomena must not be present. The crucial role of surface chemistry on the catalytic properties of carbon materials has long been recognized.[64] Many studies suggest that N and O functional groups play a vital role in the activity. Therefore, the catalytic activity should take into regard the role of the surface chemistry equally to the physical properties of the carbon supports.

The catalytic activity of the 1 wt.% Au/ACs has been investigated in the kinetic regime to avoid diffusive and mass transfer effects (Figure 4.8). For data to be acquired under kinetic control, it is essential to work at low conversions hence when doubling the catalyst mass, reaction rate will be doubling as well. Due to high pressure issues associated with the fineness of the carbonaceous materials, the amount of the sample has been reduced to 45 mg of catalyst. Each catalyst was tested under the same experimental conditions. The highest catalytic activity was attributed to 1 wt.% Au on CECAL2S (17.5%), followed by 1 wt.% Au on CECAL4S (16%), 1 wt.% Au on NORIT GSX (14.6%),1 wt.% Au on NORIT ROX 0.8 (10%) and lastly by 1 wt.% Au on DARCO KB-B (8.2%).

When testing the catalysts under the kinetic regime, it can be noted that at the steady state conditions the catalytic activity profiles of the Au supported on the CECAL2S, CECAL4S and NORIT GSX are similar, with high activity and stability. Au on NORIT ROX 0.8 also demonstrates good stability albeit at a lower overall activity. Au on DARCO KB-B follows a different pattern starting from a conversion of 14.5%, and deactivates rapidly over the duration of the test, reaching a less than 9% conversion, presenting a deactivation rate of 1.5 % h^{-1}, as calculated based on equation 4.1.

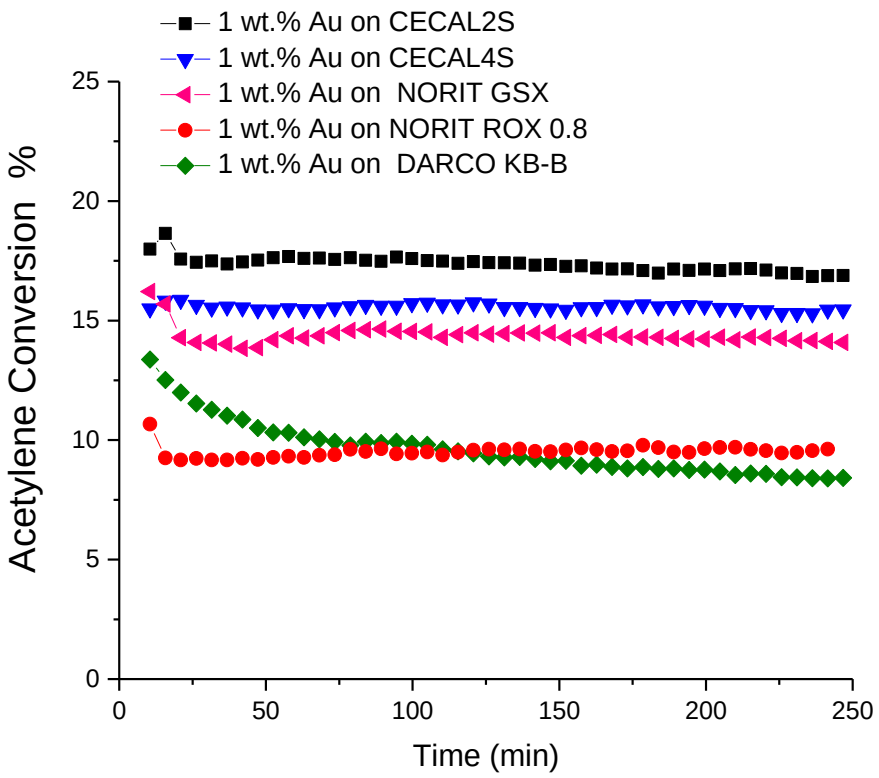

Figure 4.8: Catalysts time-on-line data test of 45 mg of sample and 45 mg of SiC, at 24.00 mL min-1 C_2H_2 (5% acetylene in Argon), 30.00 mL min-1 HCl (5% hydrogen chloride in Argon) and 4.10 mL min-1 Ar, 200 ^oC.

The catalytic activity of the materials has also been studied at deactivation conditions, where 300 mg of catalyst have been tested in each case. It must be noted that the reactor configuration has been amended to comply with these experimental requirements. For this set of tests, a reactor tube of larger diameter (0.5 cm) is employed, preventing the pressure build-up, thus allowing to study higher volumes of catalysts. As seen in figure 4.9 the order of the reaction remains the same with the highest catalytic activity credited to 1 wt.% Au on CECAL2S (41.5%), followed by 1 wt.% Au on CECAL4S (40%), 1 wt.% Au on NORIT GSX (39.1%),1 wt.% Au on NORIT ROX 0.8 (37.5%) and lastly by 1 wt.% Au on DARCO KB-B (25%).

Testing the catalysts under diffusion limited conditions demonstrates that the activity trend for the best-in-class catalysts does not change significantly, however the relative difference between the activities is reduced. Au supported on the CECAL2S, CECAL4S and NORIT GSX again exhibit a stable profile, while presenting the highest activity. Once again, Au on NORIT ROX 0.8 and Au on DARCO KB-B illustrate some differences in their activity profiles. For Au on NORIT ROX 0.8, after undergoing a small period induction, which is not observed in the previous kinetic studies, it is eventually increasing in activity, closing the gap with the

best-in-class. Whereas, for the Au on DARCO KB-B, it is observed that the catalyst starts with a higher activity (37%) and within the time-online study the conversion has dropped to 26%, therefore, the deactivation rate of the catalyst is increased to 2.5 % h^{-1}. The increased deactivation for the Au on DARCO KB-B from 1.5% to 2.5% relates to the reaction conditions. The diffusion limited studies performed allowed the investigation of the stability of the catalysts, as a result of increased contact time due to the larger volume of catalyst being exposed to lower reactant flows.

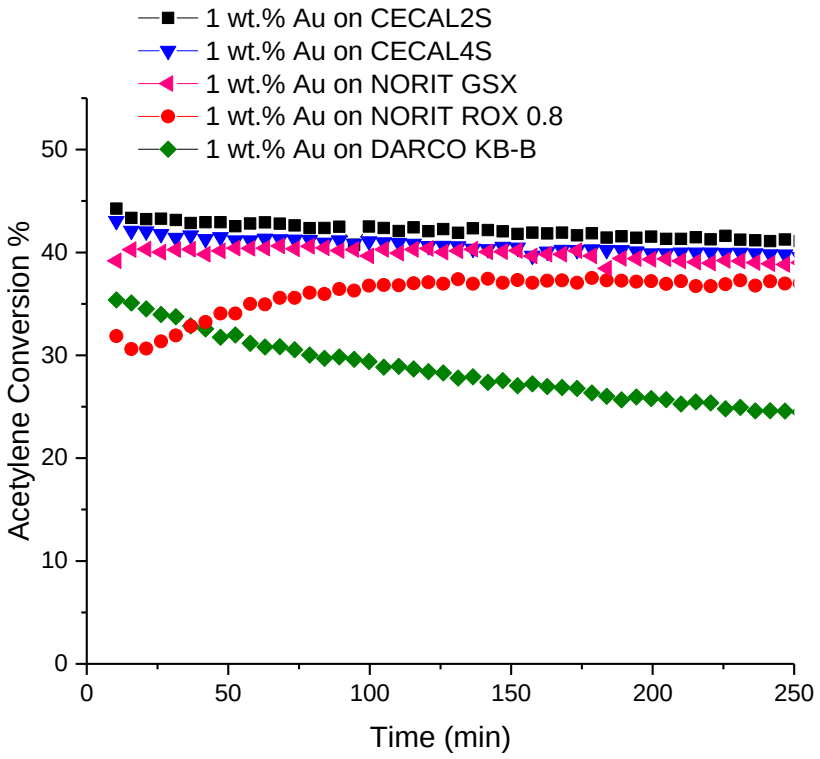

Figure 4.9: Catalysts time-on-line data test of 300 mg of sample and 150 mg of SiC, at 24.00 mL min^{-1} C_2H_2 (5% acetylene in Argon), 30.00 mL min^{-1} HCl (5% hydrogen chloride in Argon) and 4.10 mL min^{-1} Ar, 200 ^{o}C.

4.7 Correlation of catalytic activity with textual and chemical properties

How can the activity of the catalysts be associated with the physical and chemical properties of the materials? Why do the activity profiles of Au on DARCO KB-B and Au on NORIT ROX 0.8 significantly differentiate from the rest of the catalysts?

In the case of the Au on DARCO KB-B, the physical and chemical properties of the matrix material can offer an adequate explanation of the activity behaviour. It is well established in literature that acid sites on the matrix support can lead to catalysts with low activity,[53] as well as poor stability.[26,53] For DARCO KB-B, as it has been confirmed by XPS, TPD studies

and Boehm titration analysis, the amount of acid sites is the highest in comparison to any other carbon material. Therefore, the deactivation that the acid sites promote are intense for this particular catalyst. The correlation between the activity of all the catalysts and the overall base uptake, which is a representative indicator for acid sites (Figure 4.10). As illustrated, DARCO KB-B has the highest overall base uptake and exhibits the lowest activity, while the decrease in the base uptake leads to catalysts with higher activity. This trend does not include the Au on NORIT ROX 0.8 catalyst, which seems to fall from the general trend.

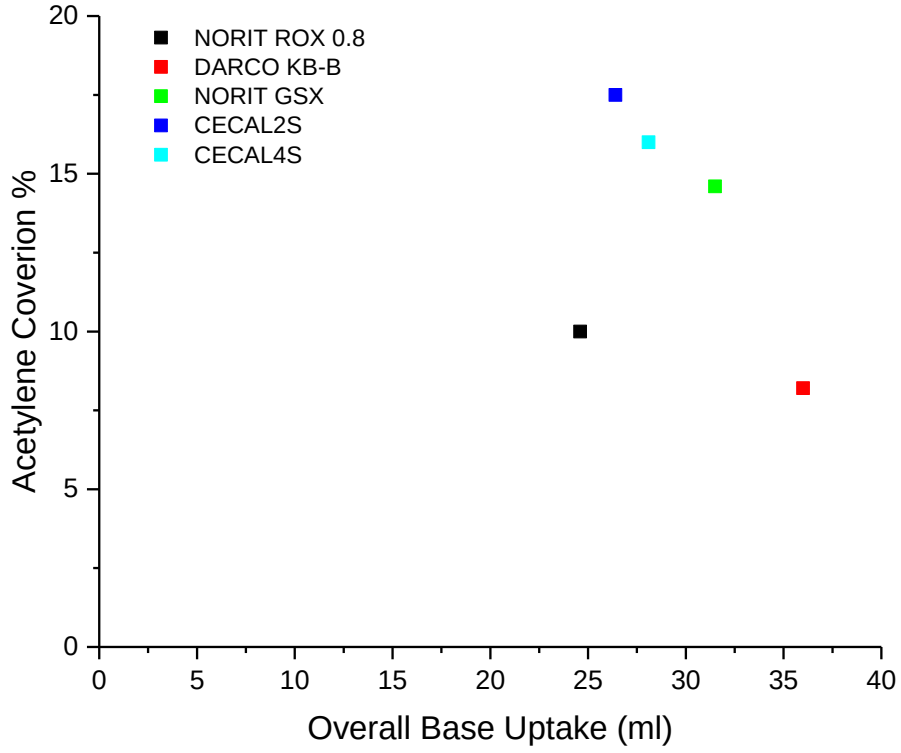

Figure 4.10: Relationship between catalytic activity and overall base uptake quantity.

In addition, a correlation between catalyst's activity and at.% O concentration can be observed. The role of the O on the surface support has been investigated by Pattisson *et al.*[42] who modified the surface of the support using a Hummers chemical oxidation method before depositing Au. It was reported that highly oxidized carbon supported catalysts exhibited an advanced activity when compared to standard Au/C material, with an optimum level of 18 O at %, as further oxidation leads to surface area and microporosity decrease leading to less active materials. Despite the high activity, the catalysts suffered from rapid deactivation. O functionalities, in the form of phenol, carboxylate, and ether, are considered to the descriptors of low temperature activity with the relative concentration of O directly correlating with light-off temperatures. In addition, Pérez-Ramírez *et al.*[46] reported that

oxygenated surface functional groups influence the catalyst's stability. Study on a range of carbons with variable O amounts illustrated that high level of acidic functionalities on the carbon host leads greater amount of coking in Pt and Ru catalysts, significantly increasing the deactivation rate. Similarly, Au catalysts exhibited a higher activity, yet poor stability on supports that bore higher amounts of O. In this study it is confirmed that excessive levels of surface oxygenated functional groups (SOFG) can affect the activity (Figure 4.11), as the lower the amount of SOFG leads to catalysts with a better activity.

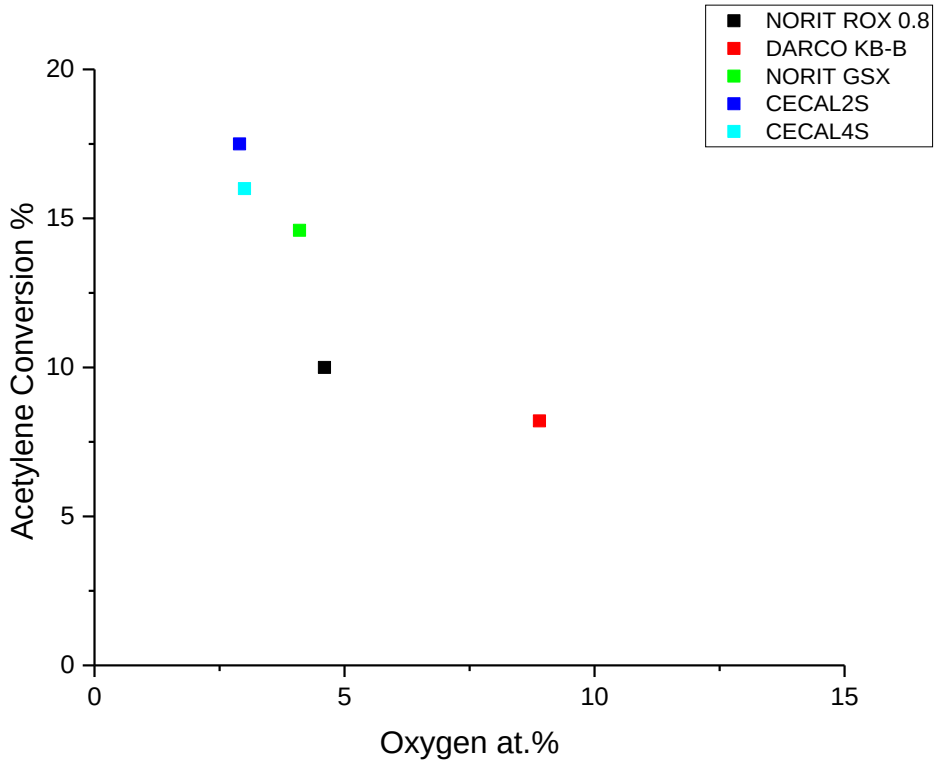

Figure 4.11: Relationship between catalytic activity and O at.%.

There is a volcano type correlation between the catalyst's activity and pore volume (Figure 4.12). Higher pore volumes lead to catalysts with higher activities in acetylene hydrochlorination. Ramirez *et al*.[46] reported that carbon supports with high surface areas and accessible pores are beneficial hosts for the preparation of Au-based catalysts for the acetylene hydrochlorination reaction. In addition, Zhang *et al*.[53] also have described that hierarchical pore structures that contain micro- and meso-pores are among the desired characteristics that AC supports should bear. In this study, it can be observed that the material with the highest pore volume, DARCO KB-B, exhibits the lowest activity. As discussed, earlier Au on DARCO KB-B presents the highest volume of acidic sites which are postulated to lead to the catalyst's deactivation. The deactivation pathway of the Au on DARCO KB-B catalyst will be thoroughly investigated in section 4.7. However, in addition it

can be postulated that excessively large pore volumes can have a detrimental factor, leading to poor catalysts, as larger pores are susceptible to coke blockages, promoting deactivation.[65] In the case of the Au on NORIT ROX 0.8, the physical and textural properties of the material determine its catalytic behaviour. When it comes to this host, as seen from the physisorption studies, it has been confirmed that it is the host that exhibits the highest micropore volume while it has the smallest average size pore diameter, therefore it is possible that this material has a large number of sites that are not accessible by the reactants, prohibiting the adsorption of reactants and/or preventing the desorption of the product. For the rest of the materials, it is observed that the optimum pore volume is detected for the Au on CECAL2S.

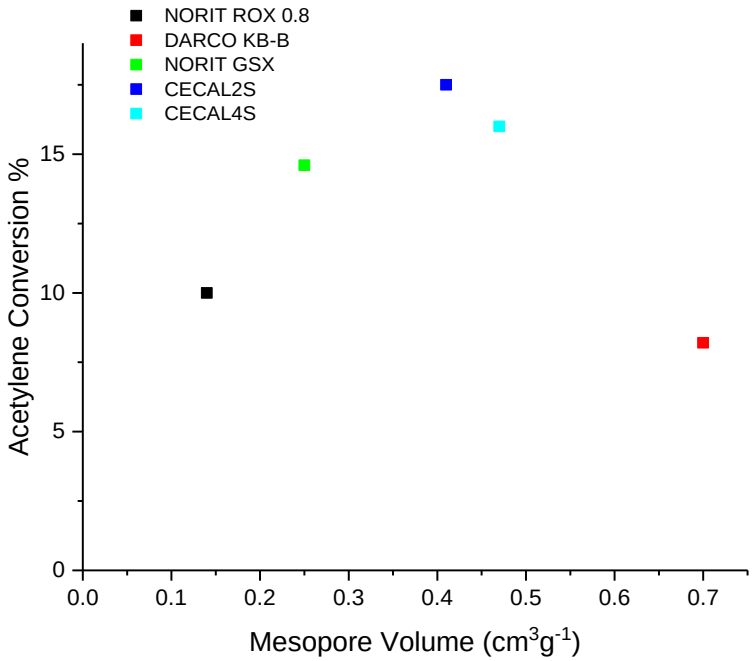

T

Figure 4.12: Relationship between catalytic activity and mesopore volume.

The relationship between catalytic activity and graphitization degree has also been studied (Figure 4.13). It is widely suggested that samples bearing more defective sites can provide more sites for metals to be stabilised or in the case of metal free catalysts these sites are considered to be the active sites.[66,67] In particular the larger the value of I_D/I_G, the more defects exist in the surface, therefore catalysts are having higher activities.[68] In this study, it can be observed that Au on DARCO KB-B has the lowest I_D/I_G and it exhibits the lowest activity, as expected. For Au on NORIT ROX 0.8, despite having the highest I_D/I_G value, it illustrates the second lowest activity, a fact that is associated with the nature and the potential accessibility of the active sites. As discussed earlier in this chapter, NORIT ROX

0.8 is the material that has the highest micropore volume while having the smallest pores, suggesting that the accessibility of those sites is in question. Overall, there seems to be a r volcano type trend between the activity and the I_D/I_G parameters, with the optimum value being observed for the Au on CECAL2S. There are studies that suggest that the direct correlation between the sp^2 and sp^3 structure, and the interface between the two-dimensional planar structure and the three-dimensional spatial structures in the carbon which deliver active sites for the catalysis of acetylene hydrochlorination is not linearly associated with the activity.[53,66,67] Therefore, the graphitisation degree can provide information about structural-activity correlations.

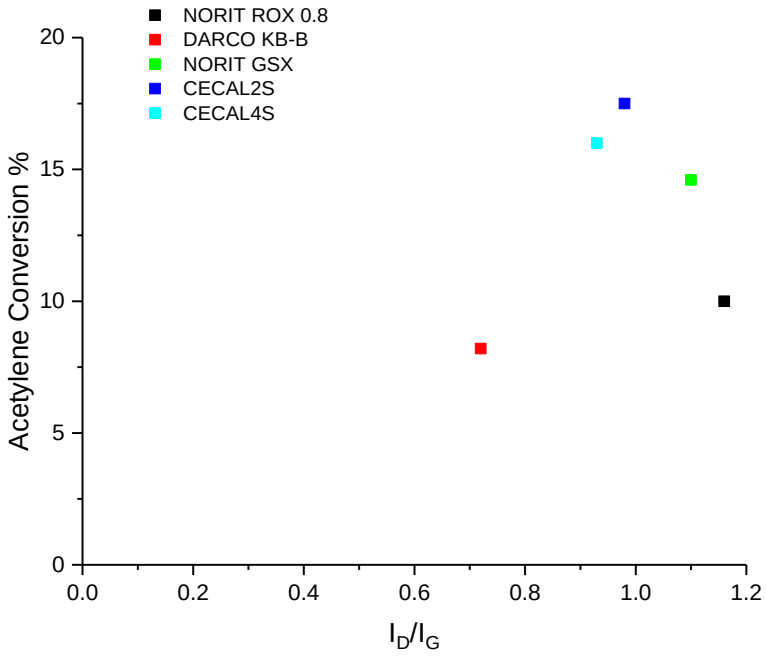

Figure 4.13: Relationship between catalytic activity and graphitization degree.

In summary, figure 4.14 shows the connection between activity of Au catalysts supported on ACs and key subjective parameters of ACs. Five types of dimensionless properties of AC samples were evaluated and assessed applying a multi-objective optimization analysis method. The lowest activity is observed for the Au on DARCO KB-B, which corresponds to the highest area the region of red-line pentagon, while it scores the lowest in the graphitisation degree. On the other hand, the best-in-class catalysts, Au on CECAL2S (blue line) and Au on CECAL4S (cyan line), cover the smallest areas on the pentagon graph, while they present relatively high graphitisation degrees. This graph can be used for a rapid classification of other materials, provided that the 5 parameters that have been selected in this study are evaluated.

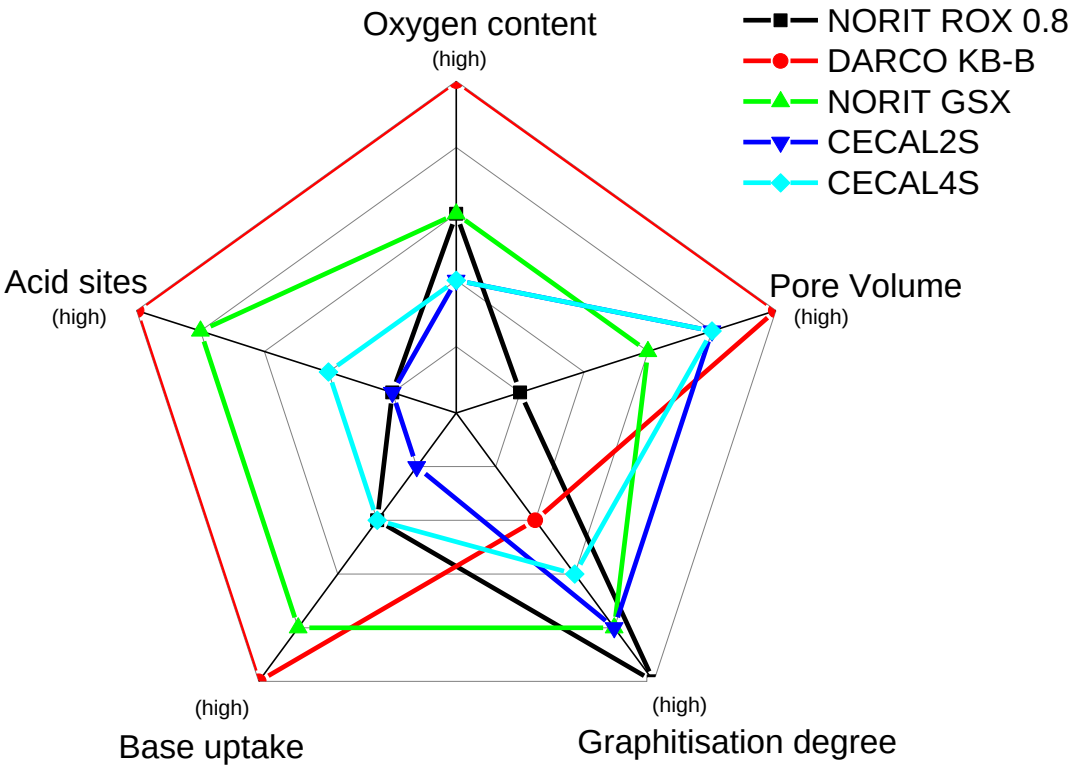

Figure 4.14: Relationship between dimensionless chemical and structural properties and the subsequent activity.

4.8 Investigation of Au on DARCO KB-B

The catalytic activity of DARCO KB-B has been further investigated, as it is the only catalyst that deactivates rapidly. In order to study the performance of 1 wt.% Au on DARCO KB-B the catalyst has been tested at a range of temperatures varying from 160 to 200 ^{o}C. As seen in figure 4.15, the temperature is detrimental to the catalytic performance. Increasing the temperature leads to lower activities. In particular the residual activity after 4 hours on-line for the catalyst tested at 160 ^{o}C is at 13.2% and decreases to 8.6%. DARCO KB-B is the only AC in the current study that has been prepared using an acid preparation method. Therefore, it is the only support that has high acid oxygenated surface functional groups, and it suffers from rapid deactivation. The deactivation of the catalyst can be attributed to the formation of Au (0) nanoparticles that is relative to the temperature of the reaction. It should be noted that it is possible that the advance activity observed at lower temperatures might be related to the increased adsorption of reactants. The adsorption capacity of reactant gases increases with decreasing reaction temperatures.[68] However, this trend can also be attributed to the mobility of the Au centres on the surface of the catalyst.

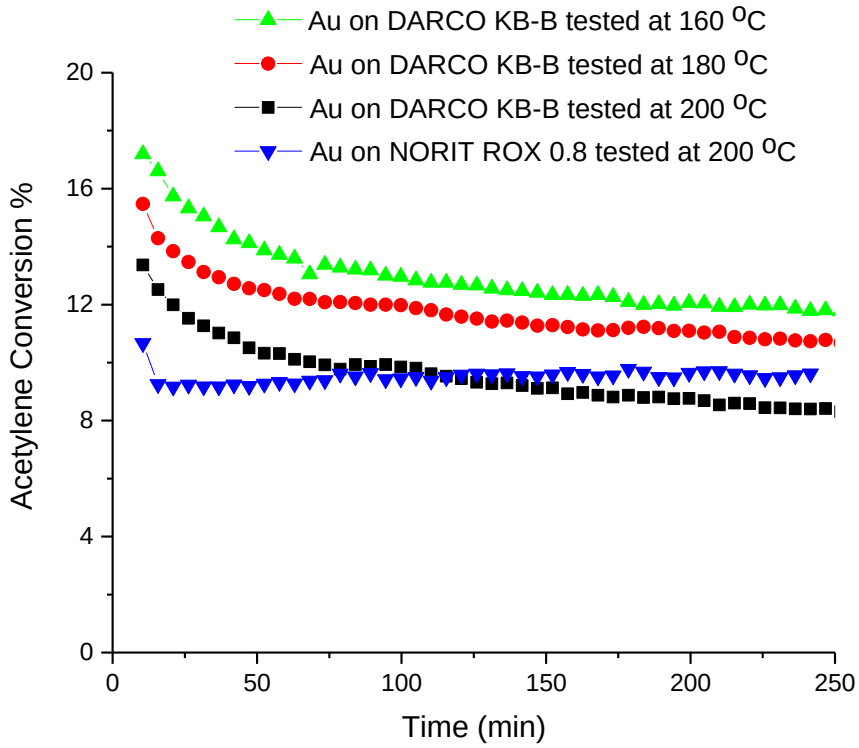

Figure 4.15: Catalysts time-on-line data test of Au on DARCO KB-B at a range of temperatures. 45 mg of sample and 45 mg of SiC, at 24.00 mL min-1 C_2H_2 (5% acetylene in Argon), 30.00 mL min-1 HCl (5% hydrogen chloride in Argon) and 4.10 mL min^{-1} Ar.

XRD analysis was performed to determine if any Au (0) nanoparticles were present on heated and used catalysts, as it has been suggested in current literature Au nanoparticles are inactive species for the acetylene hydrochlorination reaction.[9,25] The XRD profile (Figure 4.16), of fresh catalyst illustrates that there are no metallic Au reflections present on the 1wt.% Au on DARCO KB-B. In contrast, the XRD profile (Figure 4.17), of the heated catalyst show that Au nanoparticles are present on the 1wt.% Au on DARCO KB-B. The agglomeration of Au and the formation Au nanoparticles on heated samples explains the poor catalytic activity of the materials. Used samples, (Figure 4.18) display a higher volume of Au nanoparticles, suggesting that the deactivation of the catalysts is associated with the mobility of cationic Au species that agglomerate and form Au particles as the reaction proceeds. In particular, Au on DARCO KB-B shows Au nanoparticles of an average size of 19 nm when heated to 160 °C, 26 nm when heated at 180 °C and 39 nm when heated at 200°C. Used Au on DARCO KB-B reveals the presence of Au reflections of approximate size of 32 nm when tested at 160°C, 44 nm when tested at 180 °C and 56 nm when tested at 200 °C. As seen from this behaviour, heating up and testing the catalyst to higher temperatures, leads to higher amounts of Au clusters.

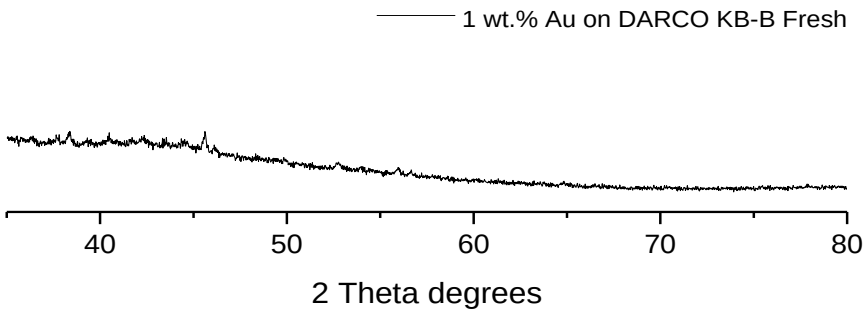

Figure 4.16: XRD profile of fresh at range of temperatures of Au on DARCO KB-B.

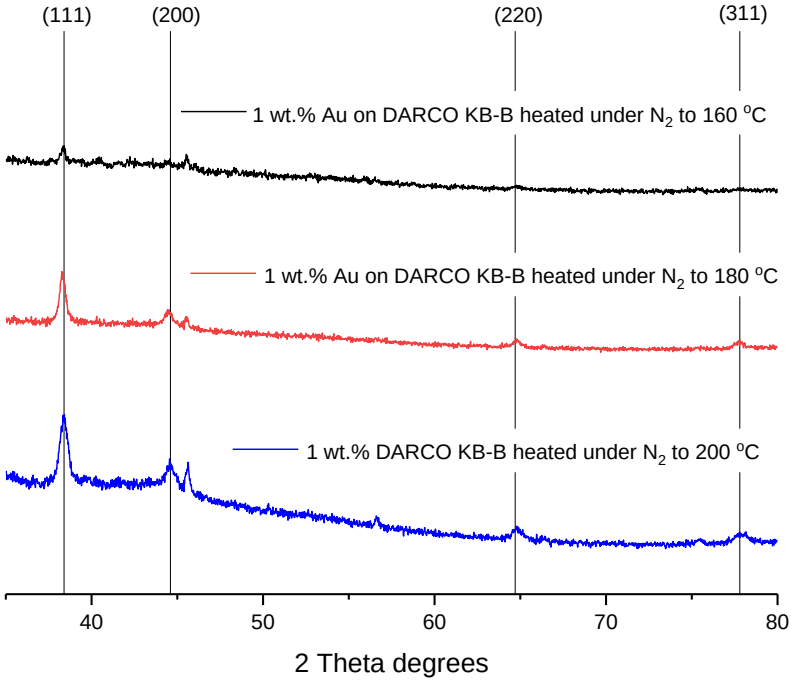

Figure 4.17: XRD profile of Au on DARCO KB-B heated under N_2 at range of temperatures. Reflections at 38, 44, 65 and 78, 2 theta degrees correspond to FCC metallic Au crystallite sites.

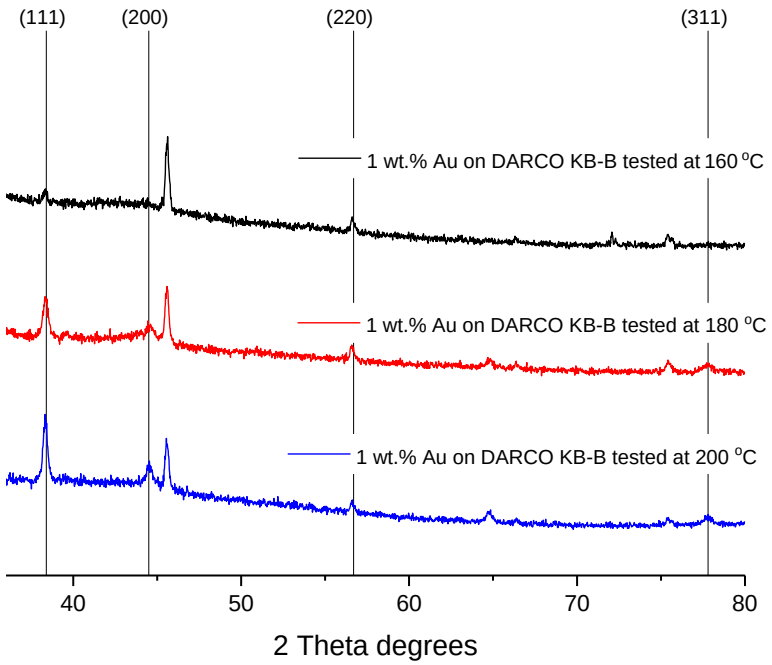

Figure 4.18: XRD profile of tested at range of temperatures of Au on DARCO KB-B. Reflections at 38, 44, 65 and 78, 2 theta degrees correspond to FCC metallic Au crystallite sites.

4.9 XAFS Identification of active sites

According to earlier studies conducted by Hutchings and co-workers,[27] VCM productivity is related to the ratio of Au(I) : Au(III) active speciation. Study of the Au oxidation state of the catalysts was conducted on both fresh catalysts and samples heated to reaction temperature prior the introduction of reactant gases. The 1 wt.% Au on AC catalysts have been compared to three Au standard materials, namely the potassium gold (III) chloride [Au(III)], gold(I) chloride [Au(I)] and gold foil [Au(0)]. Au L_3-edge XANES was employed to identify the nature of the Au species on the catalysts. For fresh and heated to reaction temperature catalysts, the Au L_3-edge XANES is presented in the Appendix (Figure S4.1-S4.6). For the fresh 1wt.% Au on DARCO KB-B fresh catalyst (Figure 4.19), the Au is entirely in cationic state. As it can be noticed the Au is mainly dispersed as Au(I), while heating up the catalysts to reaction temperature seems to have a little to no effect to the Au(I) : Au(III) ratio, for the majority of the catalysts, with the exception of the Au on DARCO KB-B (Figure 4.20). Emphasis in the differences among the fresh and heated Au on DARCO KB-B is given on figure 4.21, where the differences in the normalised absorption profile between the 2 samples can be observed. For the 1 wt.% Au on DARCO KB-B it is observed that the heating up the catalyst leads to Au nanoparticle formation on the expense of Au (III). The mobility of the Au cationic species and the formation of Au nanoparticles, verify

the poor activity and instability that is observed for this catalyst during the activity studies as described in section 4.5.

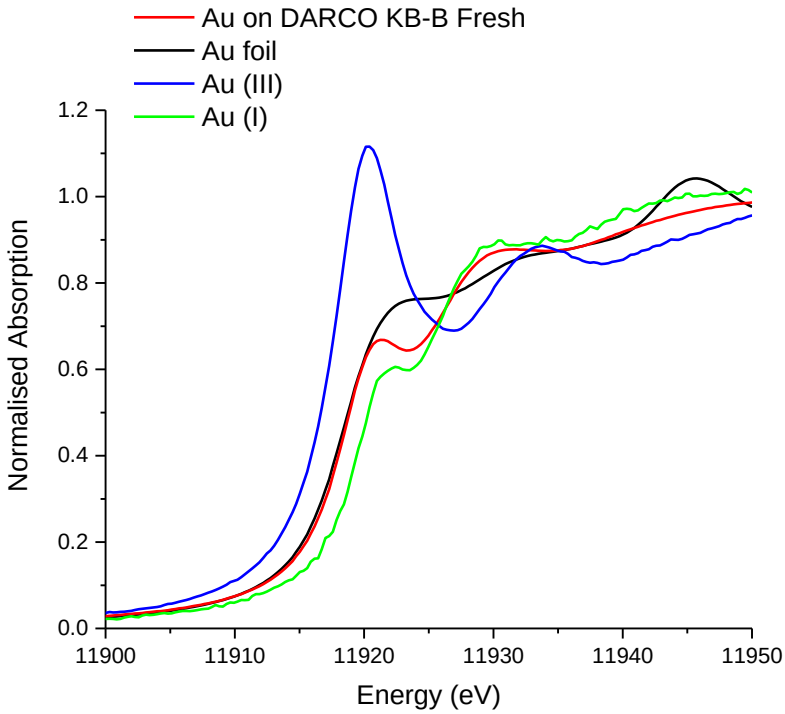

Figure 4.19: Au L_3-edge XANES of fresh Au on DARCO KB-B catalyst, $KAuCl_4$/$[AuCl_4]^-$ (Au(III)), $[AuCl_2]^-$ (Au(I) and Au foil (Au(0)).

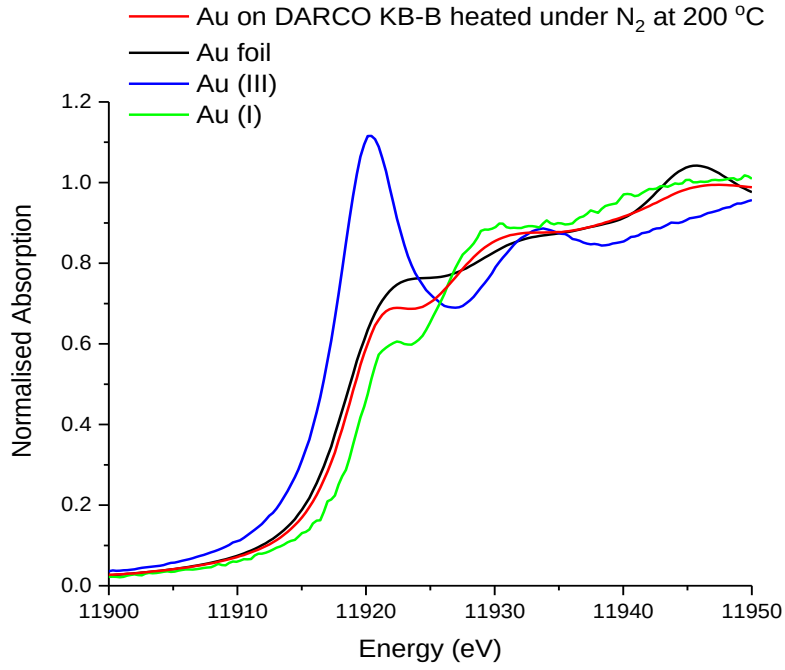

Figure 4.20: Au L_3-edge XANES of heated Au on DARCO KB-B catalyst, $KAuCl_4$/$[AuCl_4]^-$ (Au(III)), $[AuCl_2]^-$ (Au(I) and Au foil (Au(0)).

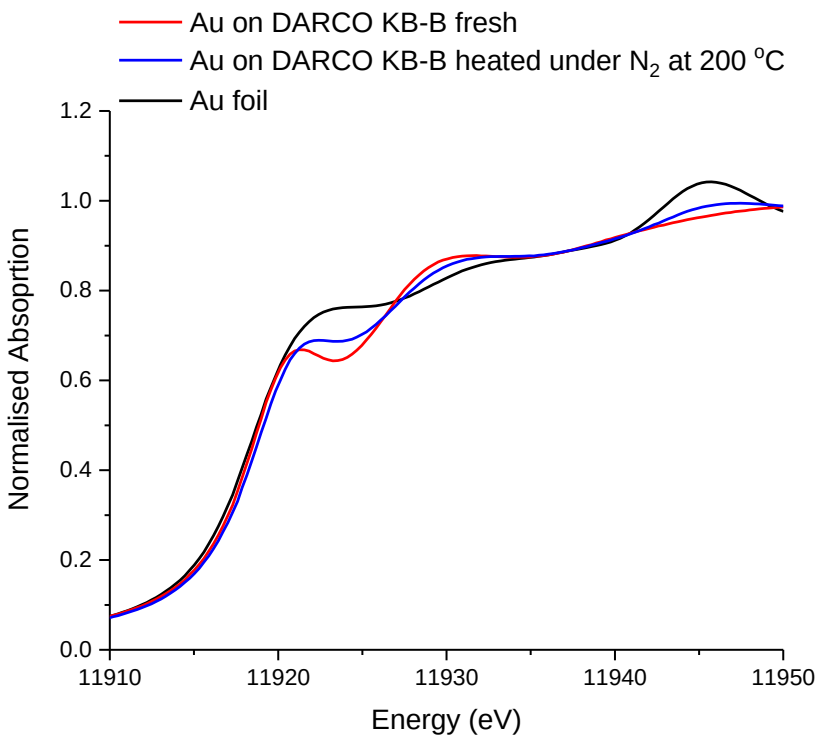

Figure 4.21: Au L_3-edge XANES of fresh, heated Au on DARCO KB-B and Au foil (Au(0)).

A linear combination fitting (LCF) of the XANES data was made with reference to the standards. Fresh and heated catalysts are comprised of predominantly Au(I) species accompanied by Au (III) centres (Figure 4.22). Additionally, the XANES data fitting of the LCF for fresh and heated samples are presented in the figures S.4.7-S.4.14 in the Appendix Section. Heating up the catalyst does not lead to re-equilibration of the Au species as they are stabilised on the surface support, with the exception of DARCO KB-B. The formation of Au nanoparticles only on the DARCO KB-B indicates that the Au has sintered due to the instability of the mobile Au^+ species on the carbon support. The similar values of the cationic Au species among the catalyst imply that the nature of the support is predominantly responsible for the catalytic activity as the speciation of Au centres is similar among the samples.

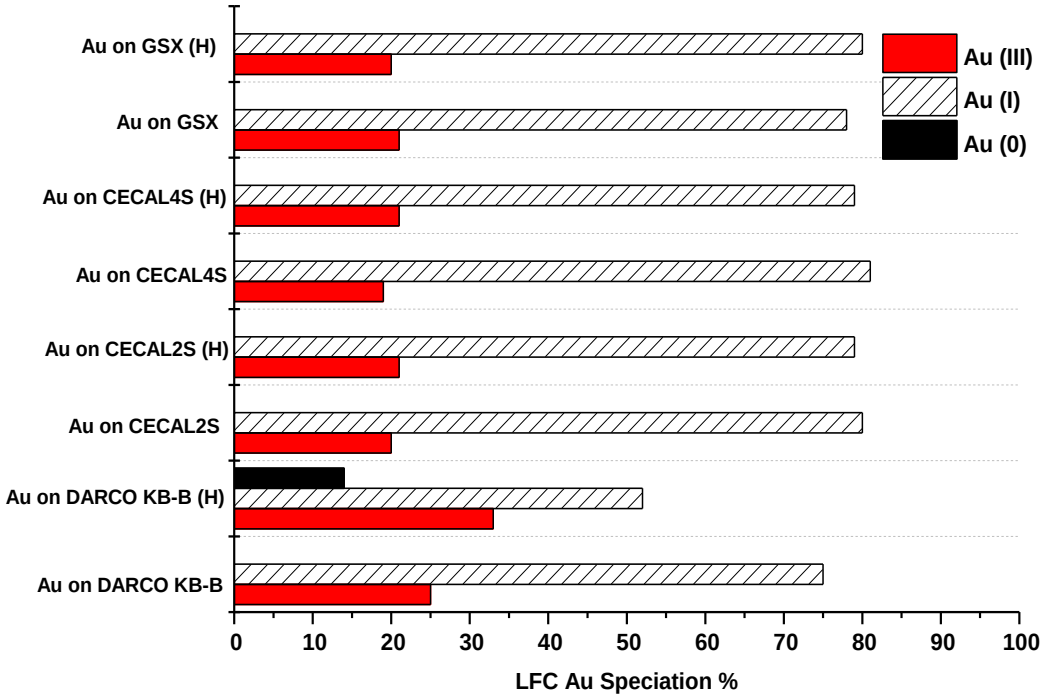

Figure 4.22: Linear combination fitting XANES for the fresh and heated (H) to reaction temperature catalysts.

The EXAFS analysis of fresh and heated to reaction temperature Au supported on AC catalysts were performed, to verify the short-range order of the catalysts (Figure 4.23). Fresh and heated catalysts exhibit a sharp peak at 1.8 Å, which corresponds to Au-Cl interaction. The exception in this general trend is noted only for the heated Au on DARCO KB-B, which displays a decrease in the peak size at 1.8 Å, whilst it shows an intense double peak at 2.5 and 3.0 Å, which is associated to metallic Au interactions, confirming the metallic nature of the material. Au foil is used as a refence, evidently showing the position of the double peak, revealing the differences and similarities among the catalysts. Additionally, the k^3-weighted EXAFS data for fresh and heated samples has been compared with that of Au(III) and Au(0) standards as presented in figures S.4.15-S.4.22 in the Appendix Section. The k^3-weighted data of the fresh and heated samples present similar phasing and amplitude of the $[AuCl_4]^-$ standard. The data generated are in good agreement with the findings from the XANES analysis.

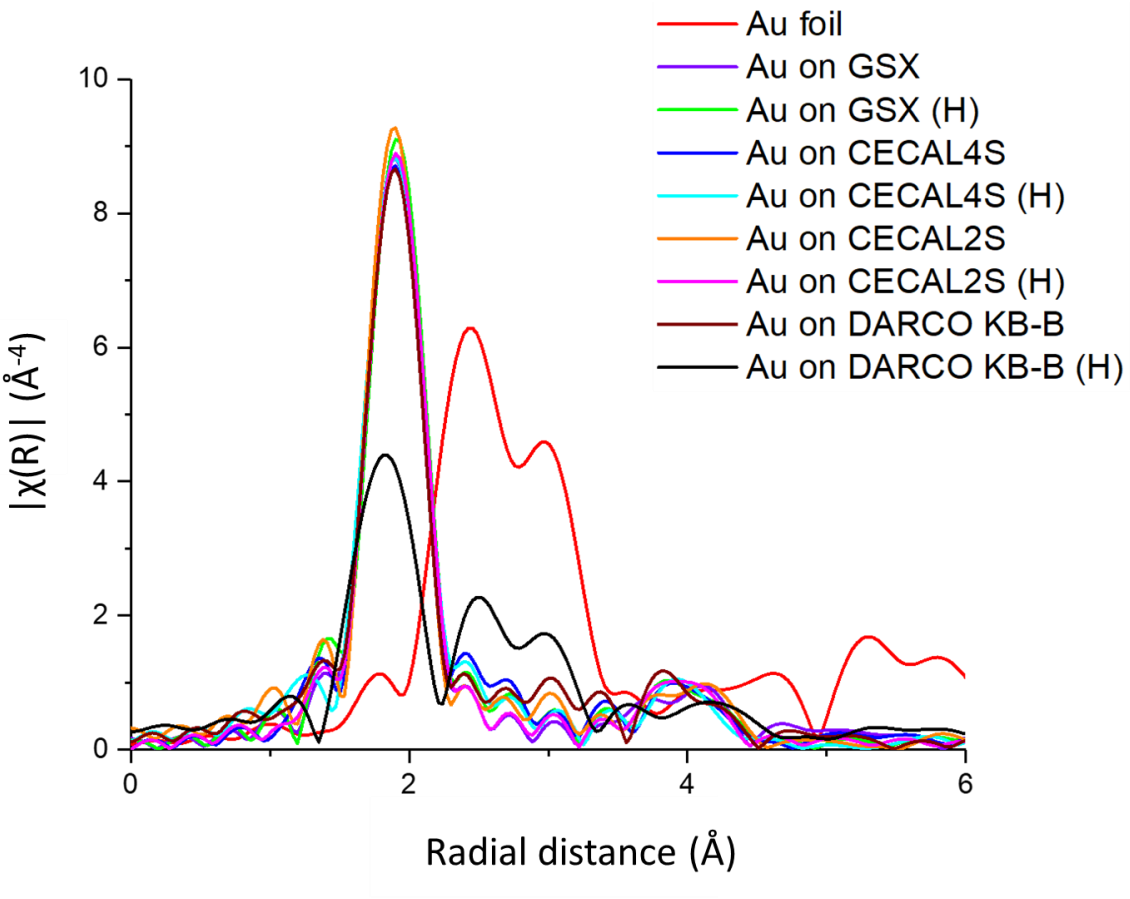

Figure 4.23: Fourier transform of the k^3-weighted χ EXAFS data of fresh and heated Au supported on ACs catalysts and Au foil as reference.

4.10 Conclusions

In this work a range of commercially available ACs have been investigated as supports for the preparation of novel Au-based catalysts for the acetylene hydrochlorination reaction. The ACs of the study originated from different sources and were activated under different physical or chemical conditions. All Au catalysts were prepared using a simple wet impregnation method using an acetone solvent, while the activity measurements were conducted in a set of two different experiments to unveil the structure-activity relationship among the catalysts. A wide range of different characterization techniques were conducted on the ACs, including textural studies, porosity analysis, surface graphitization, surface functional groups identification, and oxygenated surface acidic sites distribution.

In this study, it was found that association of catalytic activity distinctively with physical properties such as surface area and porosity of the carbon material offers a limited understanding of a catalyst's behaviour. Catalytic activity relates to the nature, concentration and accessibility of its active sites which is proportional to the physical

properties of the materials such as the surface area. However, merely considering the physical properties of the materials entails that deactivation and/or diffusion phenomena are absent. In this study we confirmed that surface chemistry of materials plays a conclusive role on the catalytic properties of carbon materials. Therefore, this study suggests surface chemistry functionalities are equally important to the physical properties of the carbon supports when identifying the crucial parameters that define a catalyst's activity profile.
X-ray absorption spectroscopy studies of fresh and heated catalysts eased the identification of active sites for this reaction. As it has been previously reported in literature the active sites for the Au based catalysts are the cationic A(I) and Au (III) species.24 Characterisation of the fresh Au on AC catalysts using Au L_3-edge XANES validated cationic nature of Au which was dispersed as Au(I) and Au(III) on all the carbon supports. The same trend and profile were also identified for all the heated to reaction temperature catalysts as well, with the exception of Au supported on DARCO KB-B, which when heated illustrated a high content of metallic Au being present. The instability that Au on DARCO KB-B exhibited during the reaction is attributed to the formation of inactive metallic Au clusters on the surface of the catalyst upon heating, which continue growing during the reaction, as demonstrated X-ray diffraction studies.

In the case of Au on DARCO KB-B, reaction temperature regulates the activity behaviour of the catalyst, as it was shown that lower reaction temperatures minimise Au agglomeration, hence optimising the catalytic activity of the catalyst. X-Ray diffraction profiles of heated and used Au DARCO KB-B, to a range of different temperatures reveals that exposure of the catalyst to lower temperatures is associated with smaller Au nanoparticle reflections, explaining the higher activity of the catalyst at lower temperatures. The instability of the catalyst is associated with the high content of acidic oxygenated functionalities that promote Au agglomeration. The high content of carboxylic groups and their decomposition at low temperatures leads to accumulation of Au particles as the surface chemistry of the catalyst is altering upon heating to reaction temperatures.

Future work should focus on identifying the role of functional surface groups on the activity and stability of the catalysts. Selective thermal degradation of the O functional groups can ensure only certain oxygenated species remain on the surface of the supports. Here, heating up the host materials under inert atmosphere at a range of different temperatures, as reported in literature, will produce a wide range of hosts that will bear only specific functionalities. Using the thermally treated supports, stripped of their functional groups for the preparation of 1 wt.% Au catalysts can ensure a direct correlation between the activity and the existent functional groups. For this reason, thermogravimetric analysis (TGA) in inert gas coupled to mass spectrometry (MS) should be employed. This technique will also

provide a quantitative method for identification of specific functionality, to complement the TPD experiments described in this chapter. In addition, the porosity of the ACs materials should be further investigated. Unlike N_2 that is diffusion restricted into very small micropores, CO_2 can access smaller pores, allowing the analysis to be completed in a couple of hours, instead of the usual 40 hours analysis when utilizing N_2. CO_2 adsorption is considered complementary to N_2 adsorption for smaller pores.[69] Finally, reactant adsorption studies, for HCl and Acetylene, should be performed on the carbon materials to provide a clearer understanding of the absorption capacity and differences between the materials.

4.11 References

1. Twigg M. V., Catalyst Handbook, Johnson Matthey, 2nd edn., 1989.

2. Zhai Y., Dou Y., Zhao D., Fulvio P. F., Mayes R. T., Dai S., Carbon Materials for Chemical Capacitive Energy Storage. Adv. Mater., 2011, **23**, 4828–4850.

3. Yan Y., Miao J., Yang Z., Xiao F., Yang H., Liu B., Yang Y., Carbon nanotube catalysts: Recent advances in synthesis, characterization and applications. Chem. Soc. Rev., 2015, **44**, 3295–3346.

4. Singh G., Lee J., Karakoti A., Bahadur R., Yi J., Zhao D., AlBahily K., Vinu A., Emerging trends in porous materials for CO_2 capture and conversion. Chem. Soc. Rev., 2020, **49**, 4360–4404.

5. Schneider W., Diller W., Ullmann's Encyclopedia of Industrial Chemistry. Wiley-VCH, 7th edn., 2011.

6. Ott J., Gronemann V., Pontzen F., Fiedler E., Grossman G., Burkhard K., Weiss G., Witte C., Methanol: Ullmann's Encyclopedia of Industrial Chemistry. Wiley-VCH, 1st edn., 2012.

7. Jüntgen H., Richter E., Knoblauch K., Hoang-Phu T., Catalytic NO_x reduction by ammonia on carbon catalysts. Chem. Eng. Sci., 1988, **43**, 419-428.

8. Rodríguez-Reinoso F.,The role of carbon materials in heterogeneous catalysis. Carbon, 1998, **36**, 159-175.

9. Kaiser S. K., Fako E., Surin I., Krumeich F., Kondratenko V. A., Kondratenko E. V., Clark A. H., López N., Pérez-Ramírez J., Performance descriptors of nanostructured metal catalysts for acetylene hydrochlorination. Nat. Nanotechn., 2022, **1**7, 606–612.

10. Heidarinejad Z., Dehghani M. H., Heidari M., Javedan G., Ali I., Sillanpää M., Methods for preparation and activation of activated carbon: A review. Environ. Chem. Lett., 2020, **18**, 393–415.

11. Zhu M., Wang Q., Chen K., Wang Y., Huang C., Dai H., Yu F., Kang L., Dai B., Development of a heterogeneous non-mercury catalyst for acetylene hydrochlorination. ACS Catal., 2015, **5**, 5306–5316.

12. Zhong J., Xu Y., Liu Z., Heterogeneous non-mercury catalysts for acetylene hydrochlorination: progress, challenges, and opportunities. Green Chem., 2018, **20**, 2412-2427.

13. Conte M., Davies C. J., Morgan D. J., Davies T. E., Elias D. J., Carley A. F., Johnston P., Hutchings G. J., Aqua regia activated Au/C catalysts for the hydrochlorination of acetylene. J. Catal., 2013, **297**, 128–136.

14. Zhao J., Xu J., Xu J., Zhang T., Di X., Ni J., Li X., Enhancement of Au/AC acetylene hydrochlorination catalyst activity and stability via nitrogen-modified activated carbon support. Chem. Eng. J., 2015, **262**, 1152–1160.

15. Chao S., Guan Q., Li W., Study of the active site for acetylene hydrochlorination in $AuCl_3$/C catalysts. J. Catal., 2015, **330**, 273–279.

16. Smith D. M., Walsh P. M., Slager T. L., Studies of silica-supported metal chloride catalysts for the vapor-phase hydrochlorination of acetylene. J. Catal., 1968, **11**, 113–130.

17. Zhao J., Zeng J., Cheng X., Wang L., Yang H., Shen B., A Au–Cu bimetal catalyst for acetylene hydrochlorination with renewable γ-Al_2O_3 as the support. RSC Adv., 2015, **5**, 16727-16734.

18. Song Z., Liu G., He D., Pang X., Tong Y., Wu Y., Yuan D., Liu Z., Xu Y., Acetylene hydrochlorination over 13X zeolite catalysts at high temperature. Green Chem., 2016, **18**, 5994-5998.

19. Wang L., Wang F., Wang J., Tang X., Zhao Y., Yang D., Jia F., Hao T., Hydrochlorination of acetylene to vinyl chloride over Pd supported on zeolite Y. React. Kinet. Mech. Catal., 2013, **110**, 187–194.

20. O'Connell K. C., Monnier J. R., Regalbuto, J. R., The curious relationship of sintering to activity in supported gold catalysts for the hydrochlorination of acetylene. Appl. Catal. B Environ., 2018, **225**, 264–272.

21. Ye L., Duan X., Wu S., Wu T. S., Zhao Y., Robertson A. W., Chou H. L., Zheng J., Ayvalı T., Day S., Tang C., Soo Y. L, Yuan Y., Tsang S. C. E., Self- regeneration of Au/CeO_2 based catalysts with enhanced activity and ultra-stability for acetylene hydrochlorination. Nat Commun., 2019, **10**, 914-924.

22. Malta G., Kondrat S. A., Freakley S. J., Morgan D. J., Gibson E. K., Wells P. P., Aramini M., Gianolio D., Thompson P. B. J., Johnston P., Hutchings G. J., In situ K-edge X-ray absorption spectroscopy of the ligand environment of single-site Au/C catalysts during acetylene hydrochlorination. Chem. Sci., 2020, **11**, 7040-7052.

23. Sun X., Dawson S. R., Parmentier T. E., Malta G., Davies T. E., He Q., Li L., Morgan M. D., Carthey N., Johnston P., Kondrat A. S., Freakley J. S., Kiely C. J., Hutchings G. J., Facile synthesis of precious-metal single-site catalysts using organic solvents. Nat Chem., 2020, **12**, 560–567.

24. Malta G., Freakley S. J., Kondrat S. A., Hutchings G. J., Acetylene hydrochlorination using Au/carbon: A journey towards single site catalysis. Chem. Comm., 2017, **53**, 11733–11746.

25. Malta G., Kondrat S. A., Freakley S. J., Davies C. J., Lu L., Dawson R. S., Thetford A., Gibson K. E., Morgan D. J., Jones W., Wells P. P., Johnston P., Catlow R. A., Christopher J., Kiely C. J., Hutchings G. J., Identification of single-site gold catalysis in acetylene hydrochlorination. Science, 2017, **355**, 1399–1403.

26. Johnston P., Carthey N., Hutchings G. J., Discovery, development, and commercialization of gold catalysts for acetylene hydrochlorination. J. Am. Chem. Soc., 2015, **137**, 14548–14557.

27. He H., Zhao J., Wang B., Yue Y., Sheng G., Wang Q., Yu L., Hu Z. T., Li X., Highly active AuCu-based catalysts for acetylene hydrochlorination prepared using organic aqua regia. Materials, 2019, **12**, 1310-1315.

28. Lin W., Recovery of high purity Pt from Pt-Au bimetallic nanoparticles using organic aqua regia. Rare Met., 2012, **31**, 92–95.

29. Zhao J., Wang B., Xu X., Yu Y., Di S., Xu H., Zhai Y., He H., Guo L., Pan Z., Li X., Alternative solvent to aqua regia to activate Au/AC catalysts for the hydrochlorination of acetylene. J. Catal., 2017, **350**, 149–158.

30. Lazaridou A, Smith L. R., Pattisson S., Dummer N .F., Smit J. J., Johnston P., Hutchings G. J., Recognizing the best catalyst for a reaction. Nat. Rev. Chem., 2023, **7**, 287–295.

31. Chen, G., Zhong, H., Feng, X., Active site engineering of single-atom carbonaceous electrocatalysts for the oxygen reduction reaction. Chem. Sci., 2021, **12**, 15802–15820.

32. Liu, J., Catalysis by Supported Single Metal Atoms. ACS Catal., 2017, **7**, 34–59.

33. Yang X., Wang A., Qiao B., Liu J., Zhang T., Single-atom catalysts: A new frontier in heterogeneous catalysis. Acc. Chem. Res., 2013, **46**, 1740–1748.

34. Hansen T. W., Delariva A. T., Challa S. R., Datye A. K., Sintering of catalytic nanoparticles: Particle migration or ostwald ripening? Acc. Chem. Res., 2013 **46,** 1720–1730.

35. Qiao B., Liang J. X. Wang A., Xu C. K., Li J., Zhang T., Liu J., Ultrastable single-atom gold catalysts with strong covalent metalsupport interaction (CMSI). Nano Res., 2015, **8**, 2913–2924.

36. Hadi P., To M. H., Hui C. W., Lin C. S. K., McKay G., Aqueous mercury adsorption by activated carbons. Water Res., 2015, **73**, 37–55.

37. Demiral İ., Samdan C., Demiral H., Enrichment of the surface functional groups of activated carbon by modification method. Surfaces and Interfaces, 2021, **22**, 1–14.

38. Iwanow M., Gärtner T., Sieber V., König B., Activated carbon as catalyst support:Precursors, preparation, modification and characterization. Beilstein J. Org. Chem., 2020, **16**, 1188–1202.

39. Budinova T., Ekinci E., Yardim F., Grimm A., Björnbom E., Minkova V., Goranova M., Characterization and application of activated carbon produced by H_3PO_4 and water vapor activation. Fuel Process. Technol., 2006, **87**, 899–905.

40. Burke G. M., Wurster D. E., Berg M. J., Veng-Pedersen P., Schottelius D. D., Surface characterization of activated charcoal by X-ray photoelectron spectroscopy (XPS): Correlation with phenobarbital adsorption data. Pharm Res., 1992, **9**, 126–130.

41. Lennon D., Lundie D. T., Jackson S. D., Kelly, G. J.. Parker, S. F., Characterization of activated carbon using X-ray photoelectron spectroscopy and inelastic neutron scattering spectroscopy. Langmuir, 2002, **18**, 4667–4673.

42. Pattisson S., Malta G., Dawson S., Dummer N. F., Smith L. R., Lazaridou A., Morgan D. J., Freakley S. J., Kondrat S. A., Smit J. J., Johnston P., Hutchings G. J., Lowering the operating temperature of gold acetylene hydrochlorination catalysts using oxidized carbon supports. ACS Catal., 2022, **22**, 14086–14095.

43. Shen Z., Liu Y., Han Y., Qin Y., Li J., Xing P., Jiang B., Nitrogen-doPed porous carbon from biomass with superior catalytic performance for acetylene hydrochlorination. RSC Adv., 2020 **10**, 14556–14569.

44. Lu Y., Lu F., Zhu M., Microporous nitrogen-doped carbon from polyaniline as a highly efficient and stable catalyst for acetylene hydrochlorination. J. Taiwan Inst. Chem. Eng., 2021, **126**, 80–87.

45. Naji S. Z., Tye C. T., A review of the synthesis of activated carbon for biodiesel production: Precursor, preparation, and modification. Energy Convers. Manag. X., 2022, **13**, 1–15.

46. Kaiser S. K., Surin I., Amorós-Pérez A., Büchele S., Krumeich F., Clark A. H., Román-Martínez M. C., Lillo-Ródenas M. A., Pérez-Ramírez J., Design of carbon supports for metal-catalyzed acetylene. Nat. Commun., 2021, **12**, 4016–4024.

47. Zhao H, Chen S, Guo M, Zhou D, Shen Z, Wang W, Feng B, Jiang B., Catalytic dehydrochlorination of 1,2-dichloroethane into vinylchloride over nitrogen-doped activated carbon. ACS Omega, 2019, **4**, 2081–2089.

48. McGlashan M. L., Manual of symbols and terminology for physicochemical quantities and units. Pure Appl. Chem., 1970, **21**, 1–44.

49. Román S., González J. F., González-García C. M., Zamora F., Control of pore development during CO_2 and steam activation of olive stones. Fuel Process. Technol., 2008, **89**, 715–720.

50. Shimodaira N., Masui A., Raman spectroscopic investigations of activated carbon materials. J. Appl. Phys., 2002, **92**, 902–909.

51. Itoh T., Sujith A., Ozaki, Y., Surface-enhanced Raman scattering spectroscopy: electromagnetic mechanism and biomedical applications. Front. Mol. Spectrosc., 2009, **10**, 289–319.

52. Lazzarini A., Piovano A., Pellegrini R., Agostini G., Rudić S., Lamberti C., Groppo E., Graphitization of activated carbons: A molecular-level investigation by INS, DRIFT, XRD and Raman techniques. Phys. Procedia, 2016, **85**, 20–26.

53. Liu Y., Zhang H., Dong Y., Li W., Zhao S., Zhang J., Characteristics of activated carbons modulate the catalytic performance for acetylene hydrochlorination. Mol. Catal., 2020, **483**, 110707–110716.

54. Lan G., Qiu Y., Fan J., Wang X., Tang H., Han F., Liu H., Song S., Li Y., Defective graphene on diamond hybrid nanocarbon material as an effective and stable metal-

free catalyst for acetylene hydrochlorination. Chem. Commun., 2019, **55**, 1430–1433.

55. Zhao F., Kang L., The neglected significant role for graphene-based acetylene hydrochlorination catalysts intrinsic graphene defects. Chem. Select, 2017, **2**, 6016–6022.

56. Oickle A. M., Goertzen,S. L., Hopper K. R., Abdalla Y. O., Andreas, H. A., Standardization of the Boehm titration: Part II. Method of agitation, effect of filtering and dilute titrant. Carbon N. Y., 2010, **48**, 3313–3322.

57. Biniak S., Szymański G., Siedlewski J., Światkoski A., The characterization of activated carbons with oxygen and nitrogen surface groups. Carbon N. Y., 1997, **35**, 1799–1810.

58. Pels J. R., Kapteijn F., Moulijn,J. A., Zhu Q., Thomas K. M., Evolution of nitrogen functionalities in carbonaceous materials during pyrolysis. Carbon N. Y., 1995, **33**, 1641–1653.

59. Boehm H. P., Some aspects of the surface chemistry of carbon blacks and other carbons. Carbon N. Y., 1994, **32**, 759–769.

60. Fuente E., Menendez J. A., Suarez D., Montes-Mora M. A., Basic surface oxides on carbon materials : A global view. Langmuir, 2003, **19**, 3505-3511.

61. Snoeyink V. L., Weber W. J., The surface chemistry of active carbon; A discussion of structure and surface functional groups. Environ. Sci. Technol., 1967, **1**, 228–234.

62. Dandekar A., Baker R. T. K., Vannice M. A., Characterization of activated carbon, graphitized carbon fibers and synthetic diamond powder using TPD and DRIFTS. Carbon N. Y., 1998, **36**, 1821–1831.

63. Figueiredo J. L., Pereir M. F. R., Freitas M. M. A., Órfão J. J. M., Modification of the surface chemistry of activated carbons. Carbon N. Y., 1999, **37**, 1379–1389.

64. Figueiredo, J. L., Pereira, M. F. R.. The role of surface chemistry in catalysis with carbons. Catal. Today, 2010, **150**, 2–7.

65. Lu F., Lu Y., Zhu M., Dai B., Macroporous carbon material with high nitrogen content for excellent catalytic performance of acetylene hydrochlorination. Chem. Select, 2020, **5**, 878–885.

66. Qiu Y., Fan D., Lan G., We S., Hu X., Li Y., Generalized reactivity descriptor of defective carbon catalysts foracetylene hydrochlorination: The ratio of sp^2:sp^3 hybridization. Chem. Commun., 2020, **56**, 14877–14880.

67. Lu F., Wei C., Yin X., Kang L., Zhu M., Dai B., The effect of sp^2 content in carbon on its catalytic activity for acetylene hydrochlorination. Nanomat., 2022, **12**, 2619-2630.

68. Chen S., Jin L., Chen X., The effect and prediction of temperature on adsorption capability of coal/CH_4. Procedia Eng., 2011, **26**, 126–131.

69. Cychosz K. A., Thommes M., Progress in the physisorption characterization of nanoporous gas storage materials. Eng., 2018, **4**, 559–566.

Chapter 5

Investigation of Single Site Au-Organic Compound based catalysts for acetylene hydrochlorination.

5.1 Introduction

In this chapter, the implementation of different organic compounds in the preparation of novel single site Au catalysts for the acetylene hydrochlorination reaction will be discussed. Au-N-methyl-pyrrolidone (Au-NMP) supported on activated carbon has been identified as the best-in-class catalyst for this reaction out of a range of organic compounds. The role that this particular compound plays in stabilising and improving the activity of Au centres is investigated. The characterisation of Au-NMP interactions both before and after the catalyst preparation, as well as the characterisation of fresh and tested Au-NMP catalyst will be discussed thoroughly in this chapter using a range of different techniques.

5.2 Overview.

It has recently been established that the single site cationic Au is the active species for acetylene hydrochlorination.[1,2] The catalytic systems that will be described in the following chapter are also composed of highly dispersed single site Au catalysts as it will be described below. Hutchings *et al*. using *in situ* XAFS studies on Au/AC catalysts illustrated that the activity of the catalysts is related to the Au(I)/Au(III) ratio,[1] and there is a close association of the redox potential of the Au(I)/Au(III) and the high activity of Au catalysts.[3] The ratio of the Au(I)/Au(III) can be regulated by the nature of the solvent.[4,5] The choice of the solvent is therefore of high importance that must be taken under consideration during the preparation of the catalysts.[5]

Despite their high activity, monoatomic Au catalysts suffer from rapid deactivation that can be attributed to agglomeration and the reduction of Au^{n+} to Au^{0} species.[6] There are examples in the literature which aim to improve the activity and stability of Au catalysts using different approaches such as including additional metals,[7-10] introducing heteroatoms through doping or ligands,[11-13] and employing ionic liquid modification techniques.[14-16] The introduction of heteroatoms through doping or ligand coordination can improve the activity and stability of the catalytic systems, as the heteroatoms can:

a) Act as anchoring sites for the active Au centres, stabilising the active and mobile Au species. The activity and stability of the heteroatom doped Au catalysts are improved as the reduction and agglomeration of the active centres is inhibited.[17]
b) Generate highly dispersed metal centre catalysts.[18]
c) Increase the electron density of the active sites through electron transfer from the additives to the active species therefore, enhancing the chemisorption capacity of HCl over the electron-rich catalyst. The adsorbed HCl can stabilise the metal species to preserve their oxidative state while inhibit their reduction by C_2H_2.[19]
d) Prevent coke deposition.[20]

As discussed in Chapter 3, the identification of the exact catalytic role in doped materials is a subject of dispute. In N-doped materials, the coexistence of different N species (e.g., pyrrolic N, pyridinic N, quaternary N) makes it difficult to assess the respective catalytic roles, therefore, there is no consensus regarding the active site for N-heteroatom-doped carbon materials. The presence of heteroatoms through doping or ligand coordination has raised controversy about the precise role of the mechanism of the novel doped catalysts. Luo *et al*. suggest that the introduction of N-containing ligands changes the reaction pathways and the adsorption energy of the reactants.[21] Ramirez *et al.* concludes that the presence of N does not influence the catalytic activity, but it affects the deactivation mechanism of the Au based catalysts with pore blockage being observed for Au on N-doped supports whilst particle agglomeration is reported for Au on activated carbon supports.[22]

Previous studies described highly active and stable Au catalyst, due to the coordination of a Au precursor to ligands. The ligands can modify electronic properties of catalytic metal centres acting as structural and electronic modulators stabilising the active Au^{n+} species. It has been demonstrated that Au complexes containing S containing ligands display a greater stability and activity. Johnston *et al*. reported a 0.1% Au loading prepared that was prepared by immobilization of $Na_3Au(S_2O_3)_2$ from aqueous solution on carbon extrudates with high activity.[2] Other S-containing ligands involved glutathione (GSH),[23] thiourea,[24] thiocyanate,[25] and trichloroisocyanuric acid (TCCA).[26] In addition, N-containing ligands have also been investigated. For example, Au(III)/Schiff-based catalyst $[AuCl_2(phen)]Cl$ reported to exhibit enhanced catalytic activity and stability,[27] while a triphenylphosphine (TPP)-ligated Au-based catalyst ($AuPPh_3Cl$/AC) was also reported to aid HCl adsorption while weakening the C_2H_2 and VCM adsorption, resulting in improved catalytic activity and long-term stability.[28]

In this study, a variety of different organic compounds that bear a wide range of functional groups are investigated with the aim of:

- Coordinating Au centres with different organic functionalities.
- Functionalising support material with Au-organic complex
- Investigating the relationship between functional groups with the catalytic activity.

5.3 Experimental

5.3.1 Catalyst Preparation.

All carbon-supported Au catalysts were prepared via a wet impregnation method. Activated carbon was initially ground to obtain a powder (150 mesh). The various organic compounds (OCs) and the Au precursor, $HAuCl_4 \cdot 3H_2O$ (Alfa Aesar, assay 49%) were dissolved in dry acetone (3 mL). The Au-OC (Molar ratio 1:X, where X is 1.2, 2 or 4) complex solution was left to be stirred overnight. Subsequently, the solution was added dropwise, with stirring to the activated carbon in order to obtain a catalyst with a final metal loading of 1 wt.%. The resulting powder was dried at 45 °C for 16 h under a flow of N_2.

The Au catalysts prepared using different OCs are denoted as Au-OCs. The novel catalysts will be compared to a standard Au catalyst denoted as Au/AC which refers to 1wt.% Au supported on Activated Carbon. The Au/AC catalyst was prepared via wet impregnation method where the Au precursor, $HAuCl_4 \cdot 3H_2O$ (Alfa Aesar, assay 49%) was dissolved in dry acetone and allowed to stir for 10 mins. Subsequently, the solution was added dropwise, with stirring, to the ground, activated, dry carbon. The solution was left to stir for 1 h and finally dried under nitrogen at 45 °C for 16 h.

5.3.2 Reaction Conditions

All reactions were performed using the following conditions unless stated otherwise: 90 mg of sample, 24.00 mL min^{-1} C_2H_2 (5% acetylene in Argon), 30.00 mL min^{-1} HCl (5% hydrogen chloride in Argon) and 4.10 mL min^{-1}, Ar 180 °C, ambient pressure.

5.4 Exploring the Scope of Organic Compounds

The Au-OCs catalysts display an interesting activity profile. For better understanding of the activity, we will divide the OCs into 3 distinctive groups; phenanthroline analogues, mercaptan-derivatives and a later group that will include the tetra-methyl-thiourea, benzyl isothiocyanate and pyrrolidone compounds. All the reagents were used without further purification.

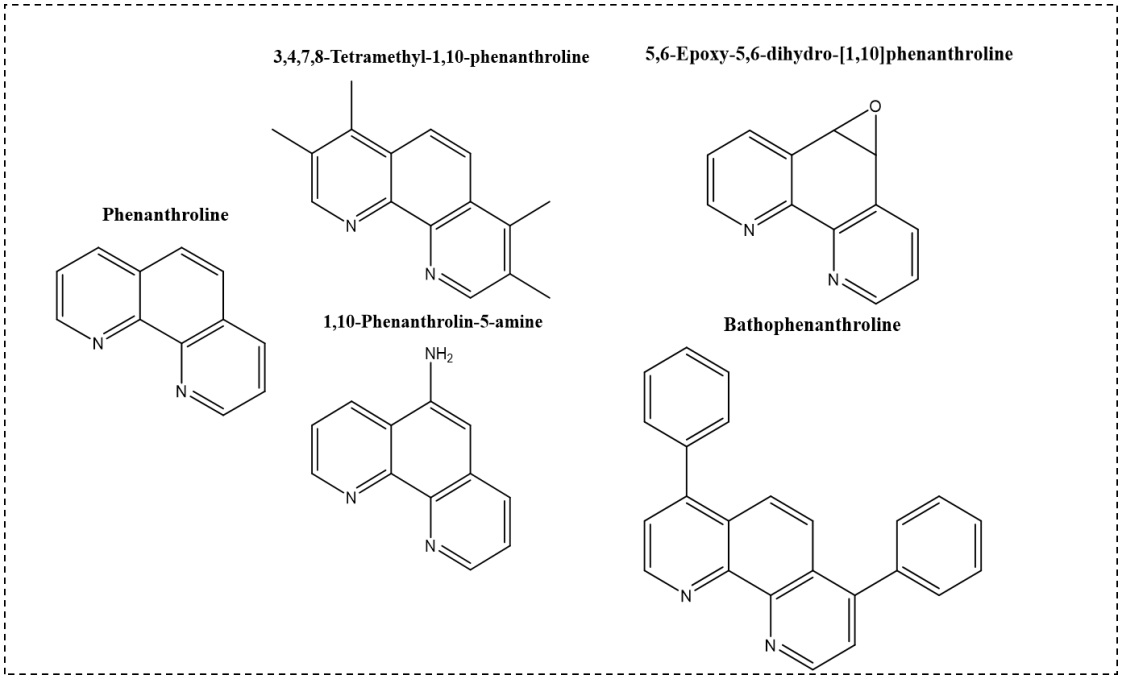

Figure 5.1: Molecular structure of five phenanthroline based analogues used in this study.

Dai *et al*. illustrated that the $[AuCl_2(phen)]Cl$ Au /Schiff-based complex catalyst exhibited great activity and stability, which was attributed to the prevention of Au^{n+} reduction.[29] The Au/Schiff-based catalysts have a higher redox potential than the $AuCl_3$ compounds, thus the presence of N ligand increases the activity and the stability of the catalyst. A range of different phenanthroline based compounds (Figure 5.1) have been investigated. In the current work, (Figure 5.2), the Au-Phenanthroline catalysts started with a better initial activity than the standard Au/AC catalyst, followed by a small induction period and thereafter deactivated rapidly. The Au-5,6-epoxy-5,6-dihydro-[1,10]phenanthroline and Au-1,10-phenanthrolin-5-amine catalysts started with a maximum conversion and rapidly deactivated throughout the reaction time. The Au-3,4,7,8-tetramethyl-1,10-phenanthroline and the Au-bathophenanthroline catalysts exhibited a lower activity profile than the Au/AC catalyst. Interestingly, the presence of the electron withdrawing group on the phenanthroline moiety, such as the O on the Au-5,6-epoxy-5,6-dihydro-[1,10]phenanthroline compound generated a catalyst with high initial activity that deactivated rapidly. The presence of the electron donating amine on the Au-1,10-phenanthrolin-5-amine did not present any significant impact on the activity of the catalyst as this catalyst presented the same activity profile with the Au-phenanthroline. Furthermore, the presence of bulkier phenanthroline compounds such as 3,4,7,8-Tetramethyl-1,10-phenanthroline and bathophenanthroline led to catalysts with a lower activity due to potential steric hinderance of the OCs that prohibited the accessibility of the reactants to the active Au centres.

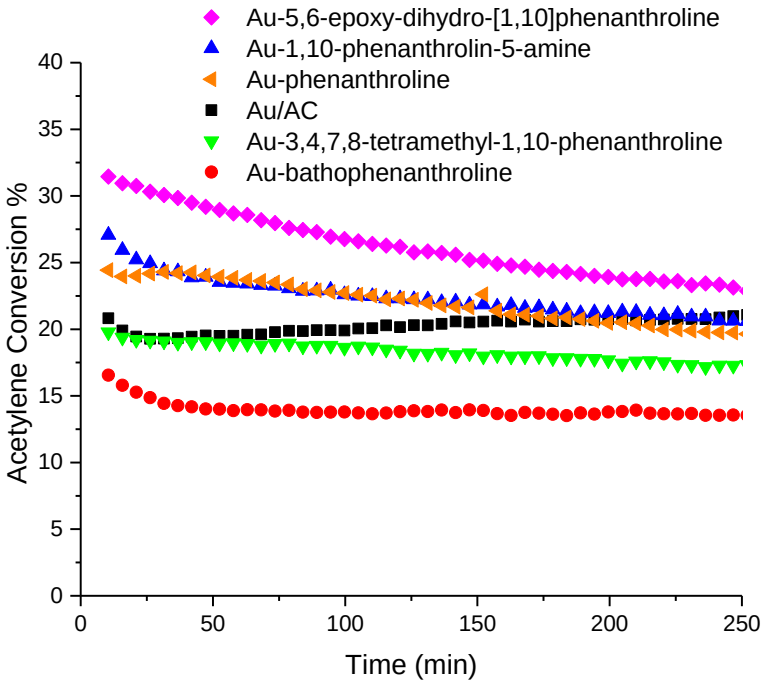

Figure 5.2: Comparison of acetylene conversions for Au-Phenanthroline based compounds.

The X-Ray Diffraction (XRD) profile, (Figure 5.3), of fresh Au-phenanthroline based catalysts does not reveal any Au nanoparticle associated diffractions. However the XRD of the tested catalysts (Figure 5.4) suggests that the deactivation of the Au-5,6-epoxy-5,6-dihydro-[1,10]phenanthroline catalyst is attributed the agglomeration of Au species and the formation of Au nanoparticles which is a known deactivation pathway for Au on activated carbons catalysts.[6] On the contrary, for the rest of Au-phenanthroline derivatives, the XRD of the tested catalysts does not suggest the presence of Au nanoparticles. This may suggest the absence of Au nanoparticles, or just none which exceed the resolution of the technique. Nanoparticles of a size less than 5 nm cannot be detected via the XRD.[30] Alternatively, it has been proposed that a reason of deactivation of Au catalysts might be the coke deposition on the surface and thereby decreasing the VCM selectivity and catalyst lifetime.

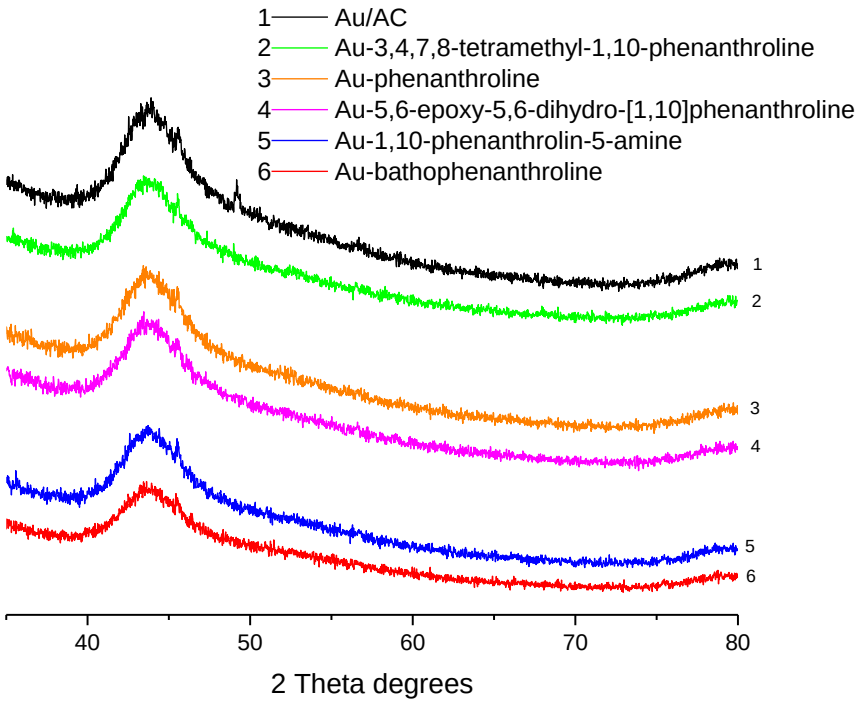

Figure 5.3: XRD of fresh catalysts for Au-Phenanthroline based compounds.

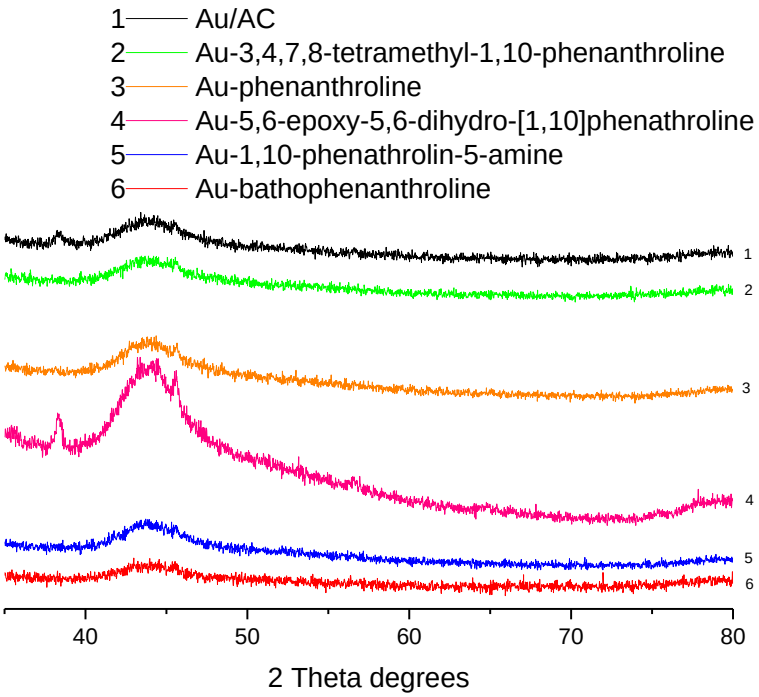

Figure 5.4: XRD profile of tested catalysts for Au-Phenanthroline based compounds. Reflections at 38, 44, 65 and 78 / 2Θ correspond to FCC metallic Au crystallites.

Much attention has been paid to sulphur in stabilising the Au active sites either as non-metallic promoters on S-doped supports,[31,32] or as stabilising ligands.[2,33,34] The commercially available catalyst developed within Johnson Matthey employs a Au centre coordinated to a thiosulfate ligand.[2] The Au-sulphur complexes are found to be highly active and stable, as the presence of the sulphur helps to immobilize the Au species thus preventing the reduction and sintering of the Au. Aiming to develop a Au complex that will employ a sulphur containing complex, 2-mercaptobezimidazole and 2-mercaptobenzoxazole (Figure 5.5) were used.

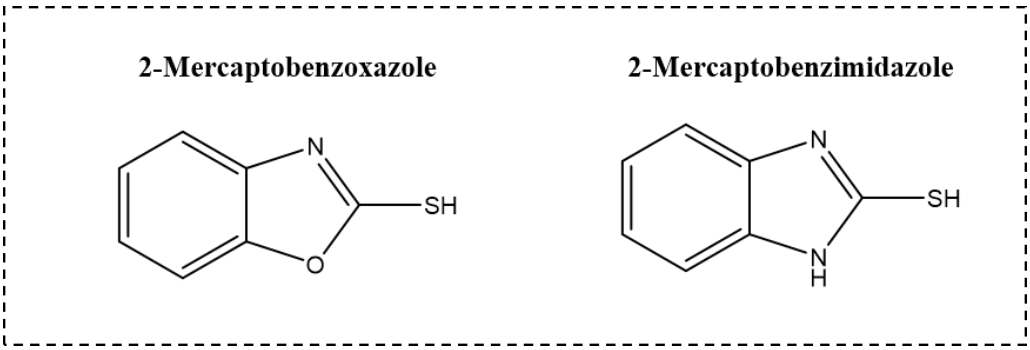

Figure 5.5: Molecular structure of Mercapto-based compounds of 2-Mercaptobenzoxazole and 2-Mercaptobenzimidazole

Despite the difference in structure of just one heteroatom, there is a difference in the induction period of the two catalysts (Figure 5.6). The Au-2-mercaptobenzoxazole catalyst seems to start with a high initial conversion, and rapidly deactivates. Conversely, the Au-2-mercaptobenzimidazole reaches its maximum activity after 45 minutes on-line after which its activity rapidly declines. Both Au-mercapto-based catalysts present a significantly lower activity in contrast to the Au/AC catalyst. This observation comes in agreement with the current literature, as it is postulated that low valence type molecules of -SH destabilize the cationic Au centres whilst, high valency S species of $-SO_3H$ and $-SO_2H$ preserve the cationic nature of Au species.[34] S species act as a double-edged sword for the Au catalysts; depending on the sulphur species valency Au sites can be either stabilised or destabilised.

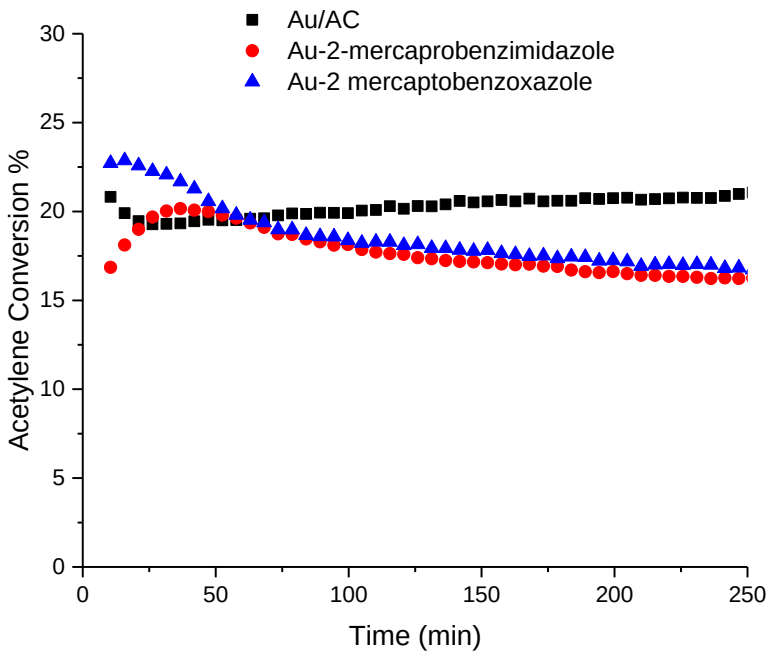

Figure 5.6: Comparison of acetylene conversions for Au-2-Mercapto based compounds.

The XRD profile of the fresh and tested Au-2-mercapto based catalysts (Figure 5.7) suggests a possible difference in the deactivation mechanism of the two catalysts. Fresh catalysts do not present any Au reflections, while in contrast the tested Au-2-Mercaptobenzoxazole shows the reflection of Au nanoparticles, indicating that the agglomeration of Au species and the formation of metallic Au is the main reason of deactivation. However, no Au reflections are observed in the tested Au-2-mercaptobenzimidazole catalyst, suggesting either that the Au particles are below the achievable resolution of XRD or that another mechanism is responsible for the deactivation of this material.

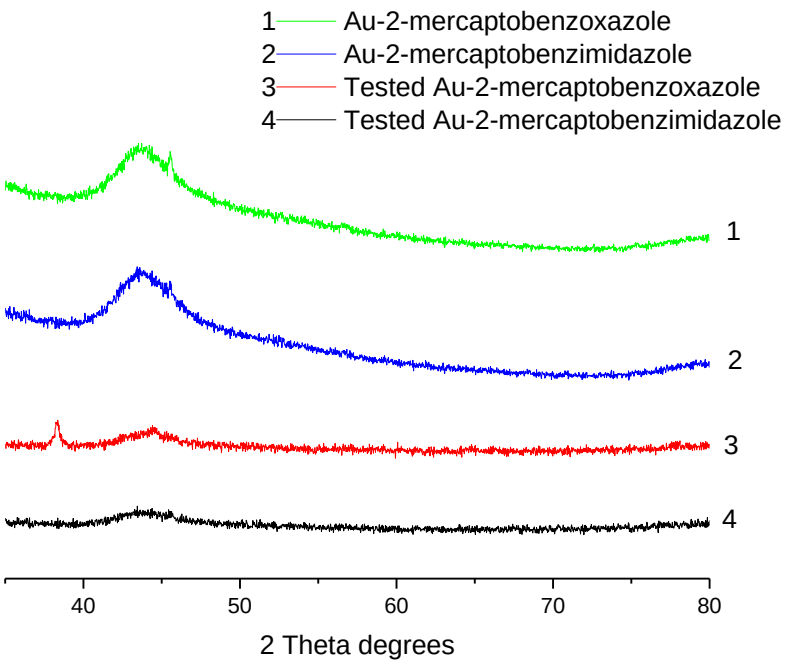

Figure 5.7: XRD profile of fresh and tested catalysts for Au-2-Mercapto based compounds. Reflections at 38, 44, 65 and 78 / 2Θ correspond to FCC metallic Au crystallites.

Additionally, other sulphur containing complexes such as tetramethylthiourea (TMTU) and benzyl isothiocyanate were also tested. Moreover, N-methyl-pyrrolidone (NMP) has also been employed and investigated in this study due to high impact of the pyrrolidone analogue catalysts that have been reported for other catalytic systems (Figure 5.8).[35,36] Zhao et al. reported a Cu-N-methyl-pyrrolidone supported on spherical activated carbon (Cu-NMP/SAC) catalyst that exhibited improved activity and stability in comparison to Cu/ SAC catalyst. It is postulated that the addition of NMP ligand enables the high dispersion of Cu species, while stabilising the active Cu^{+} and Cu^{2+}, and restrain the coke deposition.[35] DFT studies propose that high reactivity is attributed to the favourable catalyst–ligand interactions which reduce the adsorption of C_2H_2 and VCM, while enhance the adsorption of HCl, and prevent the carbon deposition caused by acetylene agglomeration.[36]

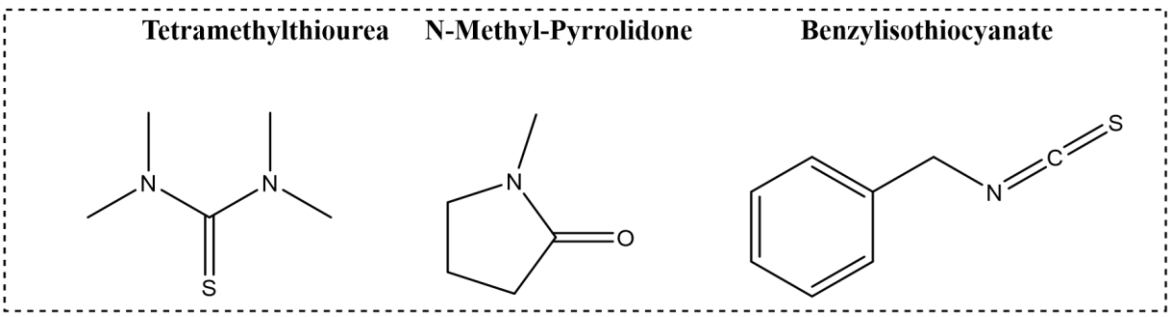

Figure 5.8: Molecular structure of tetramethylthiourea, N-methyl-pyrrolidone and benzyl isothiocyanate.

As seen in Figure 5.9 it seems that the Au-N-methyl-pyrrolidone appears to be the most promising candidate. The coexistence of N and O improves the activity of the catalyst coming into accordance with the reported literature, as it is reported that the N containing ligands facilitate the dispersion of the Au^{n+} species while the O containing ligands increase the activity of the Au-based catalysts by reducing the adsorption of acetylene whistle enhancing the adsorption and activation of HCl.[11,35,37] The Au-TMTU catalyst seems to be rapidly deactivating, while the Au-benzyl isothiocyanate is a low activity catalyst that gradually gets better while on-line. The XRD profile of the used catalysts suggest the formation of Au nanoparticles being the main reason of deactivation (Figure 5.10).

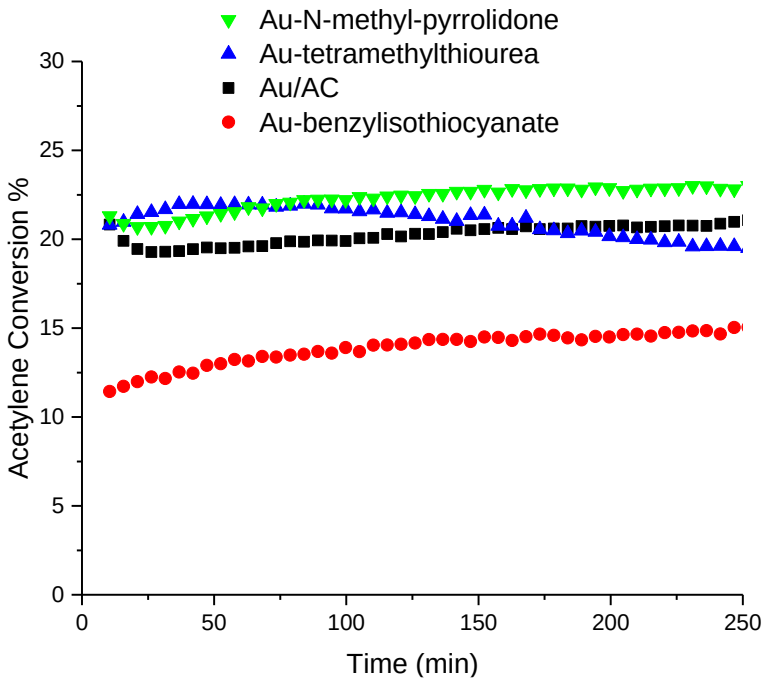

Figure 5.9: Comparison of acetylene conversions for other Au-OCs based compounds.

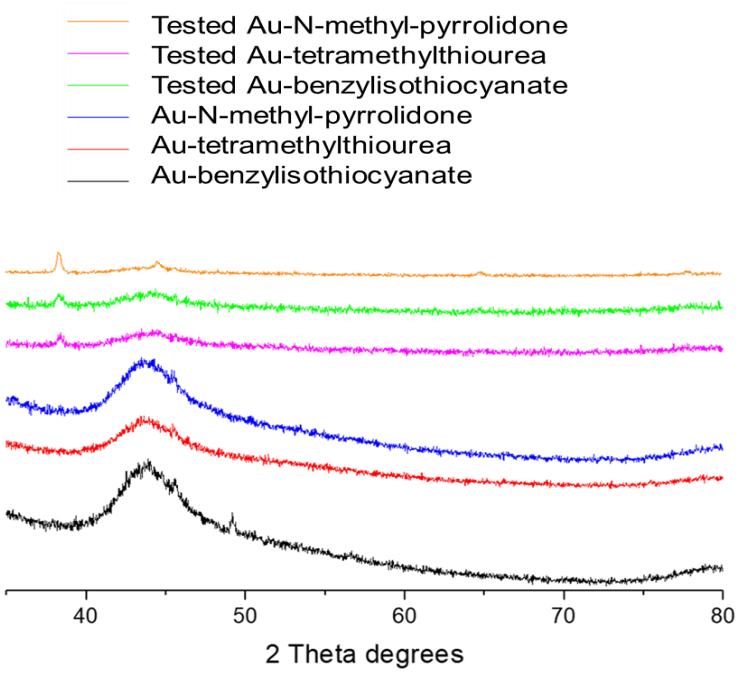

Figure 5.10: XRD profile of fresh and tested catalysts for Au-OCs based compounds. Reflections at 38, 44, 65 and 78 / 2Θ correspond to FCC metallic Au crystallites.

Thermogravimetric analysis (TGA) was performed on the fresh (Figure 5.11), and tested catalysts (Figure 5.12). An initial mass loss between 30 – 100 °C is observed in fresh and used catalysts, due to evaporation of adsorbed water. The comparison of the data above 100 °C shows only minor differences between any of the catalysts. Both fresh and tested catalysts have similar mass loss weight profiles between 100 – 200 °C, indicating good functional group stability at the reaction temperatures used in this work. Also, the stable and similar profile of weight loss between fresh and tested catalysts shows that any observed deactivation is related to Au agglomeration and not coke deposition.[38] According to literature the mass losses above 100 °C were due to carboxylic groups between 150 – 350 °C, hydroxyl groups between 350 – 500 °C and thermal oxidation of the remaining carbon above 500 °C.[39]

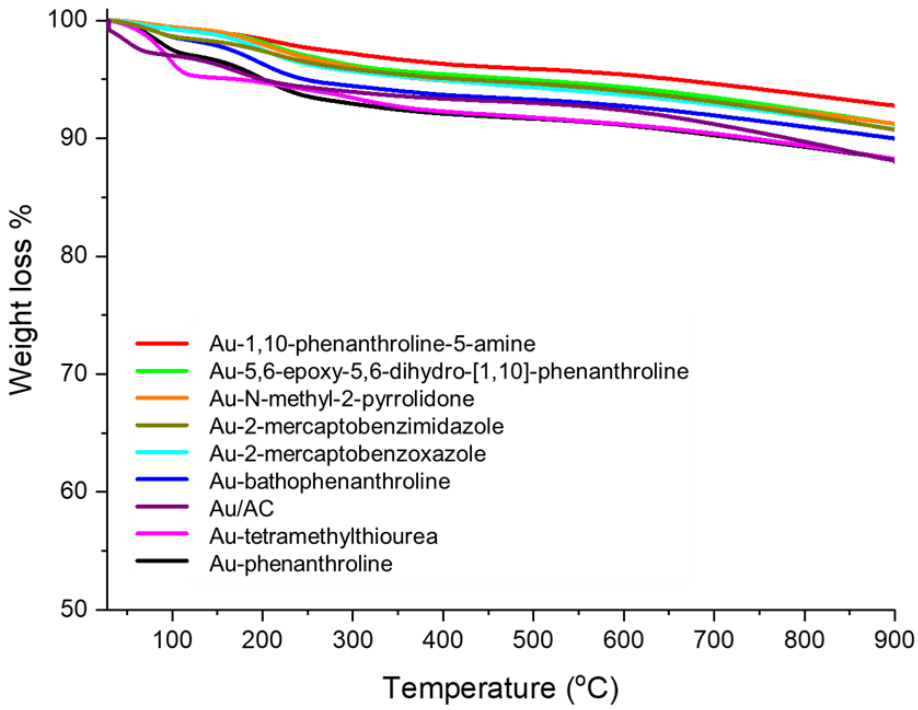

Figure 5.11: TGA profile of fresh AU-OCs catalysts. TGA under N_2: 1) Hold for 2.0 min at 30.00°C 2) Heat from 30.00°C to 900.00°C at 10.00°C/min, 3) Hold for 2.0 min at 900.00°C.

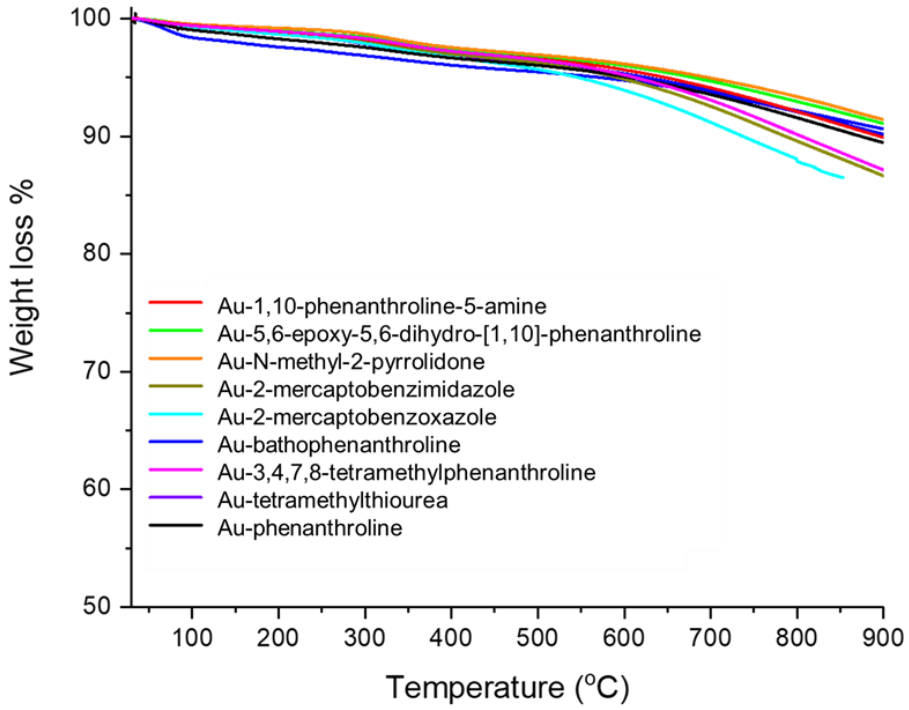

Figure 5.12: TGA profile of tested AU-OCs catalysts. TGA under N_2: 1) Hold for 2.0 min at 30.00°C 2) Heat from 30.00°C to 900.00°C at 10.00°C/min, 3) Hold for 2.0 min at 900.00°C.

5.4 Identification of N-methyl-pyrrolidone (NMP) as a novel candidate.

In the above section, NMP was identified as the most promising additive among a range of organic compounds. The current section will describe the effect of the NMP in the catalyst's behaviour. The time-on-line data for Au-NMP (Figure 5.13) shows that there is an increase in the acetylene conversion when increasing the molar ratio of Au to NMP from 1.2 to 4. As seen from Figure 5.13, when at steady state the acetylene conversion increases from 22.8% to 25.3% as the molar ratio of NMP also increases from 1.2 to 4 in respect to Au. In order to demonstrate that the excess NMP is not beneficial, NMP was used as a solvent during catalyst preparation. In this case the NMP was used as a solvent instead of dry acetone and the catalyst was prepared accordingly:

1. $HAuCl_4$ precursor was dissolved in 3 ml of NMP.
2. The solution was left stirring overnight.
3. 0.99 g of activated carbon NORIT ROX 0.8 was added to the solution.
4. Mixture sealed and stirred for 1 h at room temperature.
5. Catalyst loaded in a drying boat and dried at 212 ˚C for 16 h under N_2 flow.

The catalyst prepared with the above method, using NMP as a solvent is denoted as "Solvent preparation" (Figure 5.13). The catalyst that was prepared with this method exhibited the lowest activity, while the XRD profile (Figure 5.14) revealed the presence of metallic Au in fresh catalyst. Since the activity for this reaction is related to the Au cationic species and it has been established that metallic Au is not an active site, the low activity of the solvent prepared catalyst is explained. In addition, it has been also reported that NMP as a solvent can lead to the synthesis of small AuNPs.[40]

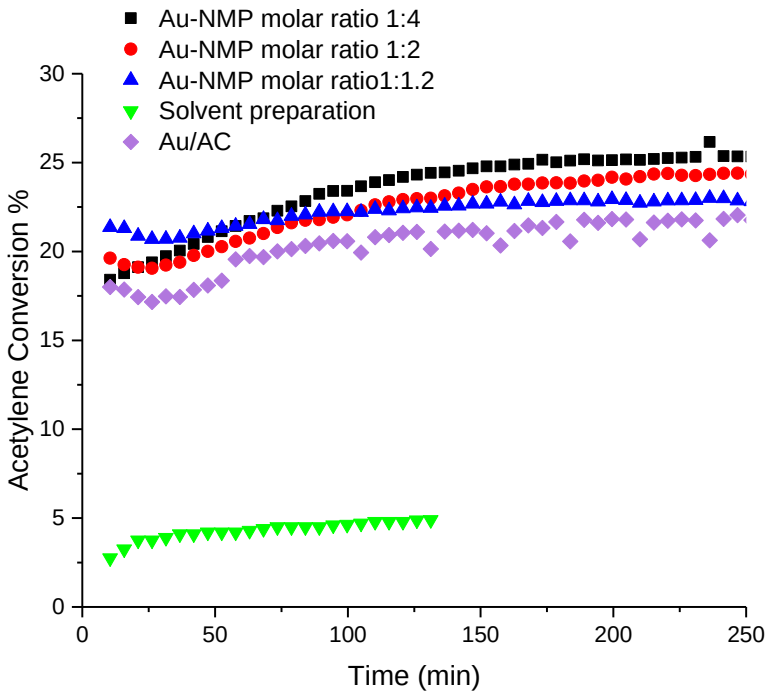

Figure 5.13: Activity profile of Au-NMP catalysts with different molar ratios of NMP.

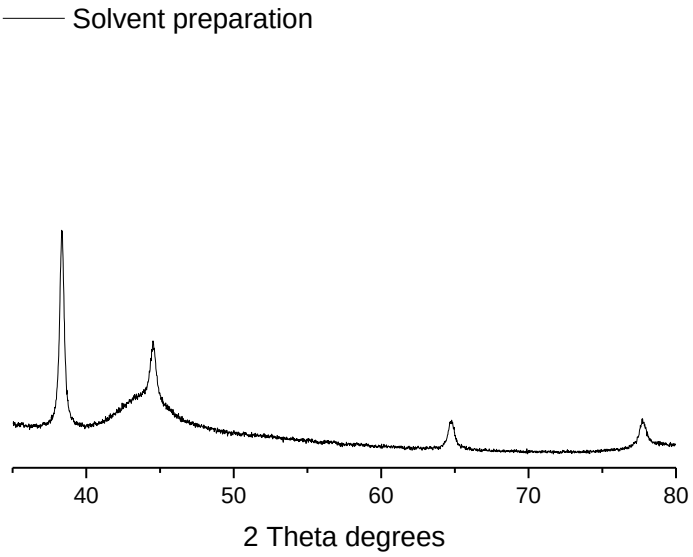

Figure 5.14: XRD profile of fresh catalysts for solvent prepared Au-NMP catalyst. Reflections at 38, 44, 65 and 78 / 2Θ correspond to FCC metallic Au crystallites.

Analysis of the fresh and used catalysts via X-ray photoelectron spectroscopy (XPS) is challenging and does not provide accurate quantification of the Au cationic species, due to the photoreduction caused by the XPS beam.[41] XPS incident photon energies (1.25–2.98 keV) can produce a major signal of metallic Au (Figure 5.15) because of the photoreduction of cationic metal species. During analysis time it has been reported that $AuCl_4^-$ salts

experience photo-reduction to metallic Au.[42] In addition, it must be noted that XPS is a surface analysis technique, thus the total Au content can vary among sample of same metal loading. Despite its limitations, XPS can provide some insight into the change in of carbon and other atoms on the surface of the catalysts. As seen in table 5.1, a comparison between fresh and tested samples shows that the at. % of N and O before and after reaction do not change, indicating the stability of the NMP under the reaction conditions.

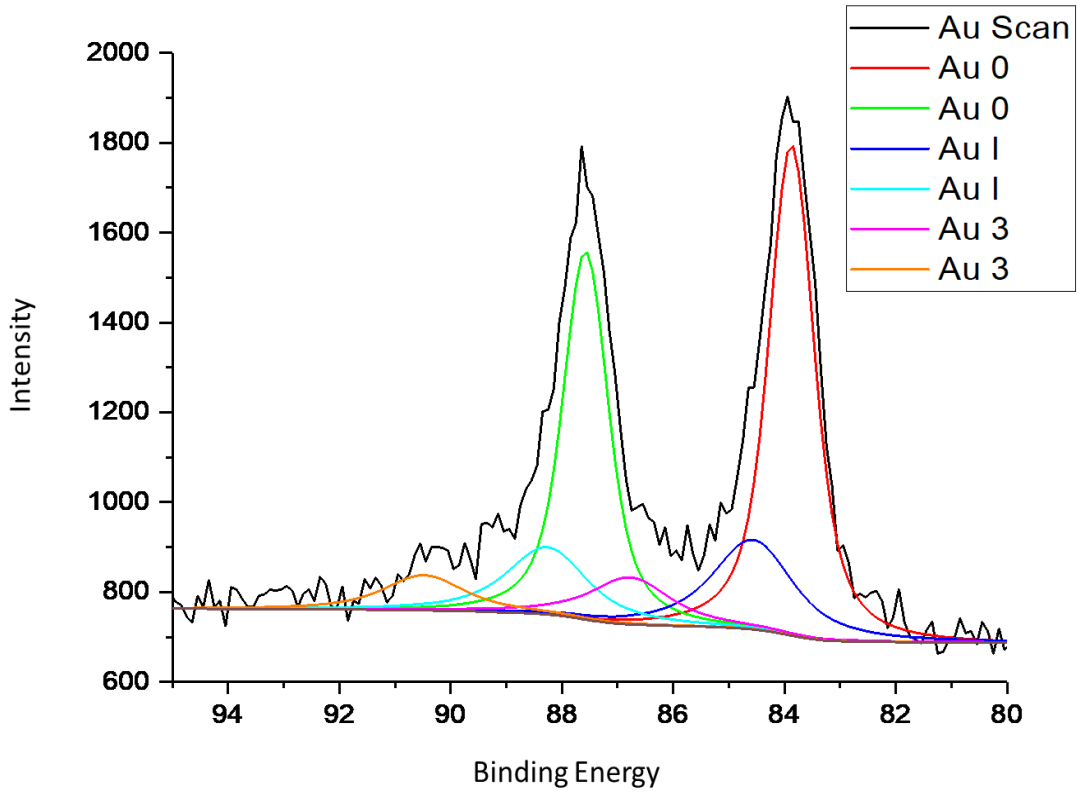

Figure 5.15: XPS Au(4f) spectrum of Au/AC showing Au0 at 84.0 (red) and 87.5 eV (green).

Element At %	AC	Au/AC	Au NMP 1:1.2	Au NMP 1:1.2 Tested	Au NMP 1:2	Au NMP 1:1.2 Tested	Au NMP 1:4	Au NMP 1:4 Tested
Au	0.0	0.1	0.1	0.1	0.1	0.1	0.1	0.1
C	94.5	94.3	94.5	94.1	94.2	94.5	94.1	94.3
Cl	0.2	0.3	0.4	0.6	0.4	0.4	0.3	0.5
N	0.2	0.2	0.3	0.4	0.6	0.5	0.6	0.7
O	4.9	4.8	4.5	4.5	4.7	4.3	4.7	4.2
S	0.2	0.3	0.2	0.3	0.2	0.2	0.2	0.2

Table 5.1. Atomic % of Au, Cl, N, O and S in support, Au/AC and Au-NMP catalyst, determined via XPS.

5.5 An alternative catalyst preparation using the Au-NMP as a precursor material.

Peter Johnston from Johnson Matthey kindly prepared and supplied an isolated Au-NMP precursor material. The preparation of the Au-NMP complex included the addition of $HAuCl_4$ (40.02% Au) in 15 ml of acetone until the complete solubilisation of the Au precursor in the solution. Accordingly, NMP (2.01 g) was added in the solution and the mixture was allowed to stir for 30 min. Subsequently, the solution was evaporated under vacuum producing an oily residue, which afterwards was washed with aliquots of cyclohexane, generating eventually a solid product. The solid product was recrystallised in 1-propanol - cyclohexane yielding a crop of bright yellow needles (Figure 5.16).

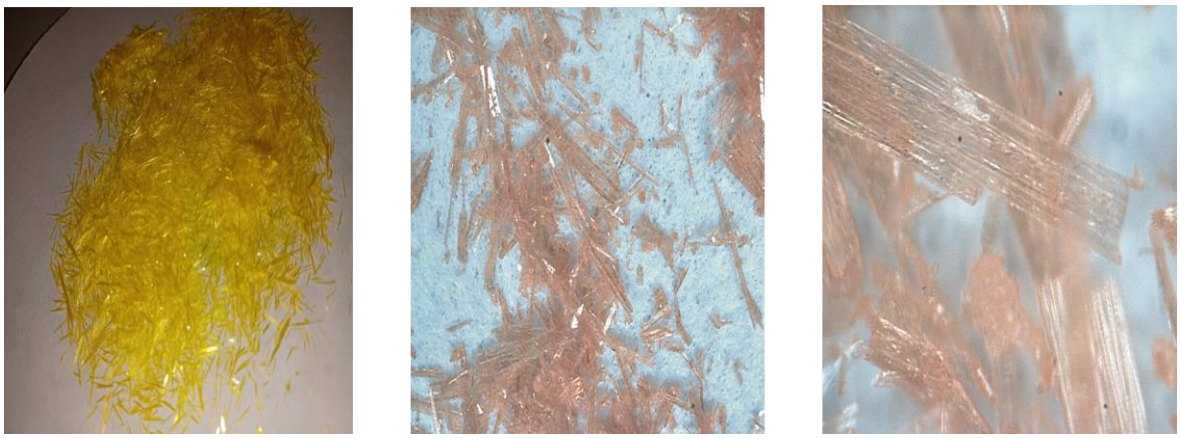

Figure 5.16: Images of the isolated Au-NMP crystals as prepared at Johnson Matthey.

The isolated Au-NMP crystals were used for the production of a catalyst using acetone as a solvent. The preparation of the novel catalyst involves thaccording to which:

1. Au-NMP crystal precursor was dissolved in 3 ml of acetone.
2. 0.99 g of activated carbon NORIT ROX 0.8 was added to the solution.
3. Mixture sealed and stirred for 1 h at room temperature.
4. Catalyst loaded in a drying boat and dried at 45 ˚C for 16 h under N_2 flow.
   The novel catalyst is noted as Au-NMP JM catalyst.

The similar activity of the Au-NMP and the Au-NMP JM catalysts (Figure 5.17) indicates that both preparation methods lead to active catalysts that have the similar activity profiles.

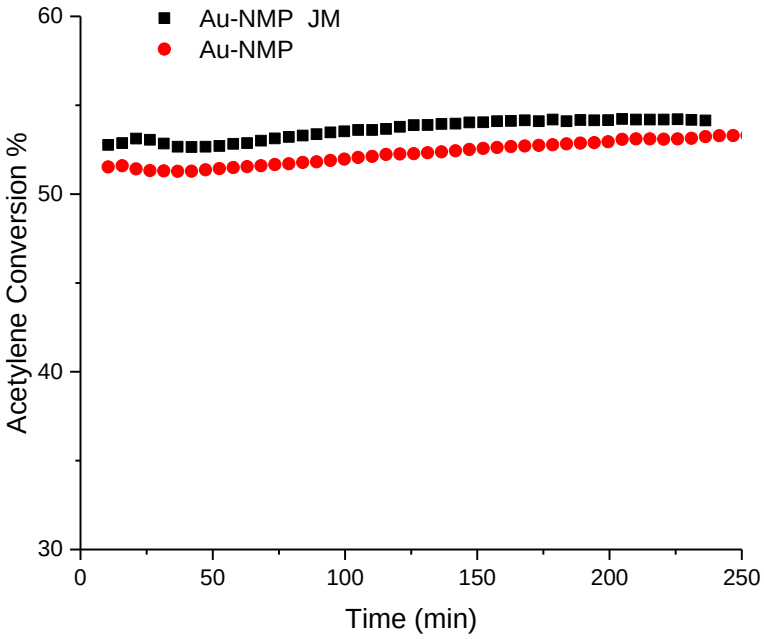

Figure 5.17. Activity profile of Au-NMP catalysts prepared via different methods. Test Conditions: 300 mg of sample and 150mg SiC, total flow 12.5 mL min^{-1}, HCl/C_2H_2 = 1.02 at 180 °C.

Furthermore, as shown in figure 5.18, the XRD of fresh and tested catalysts confirms that the fresh catalyst does not have any metallic Au character, since no peaks related to FCC metallic Au crystallites are observed. On contrary, both tested catalysts display metallic Au reflections, with the average size of crystals, as calculated using the Scherrer equation, of approximately 20 nm.

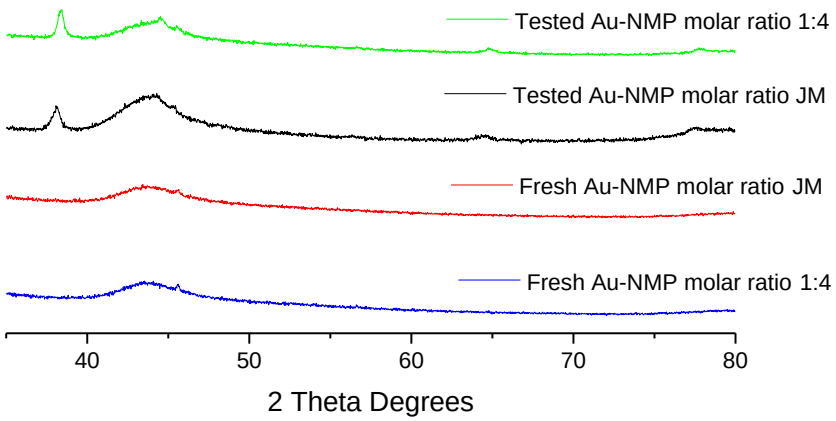

5.18: XRD profile of fresh and tested catalysts for Au-NMP based compounds. Reflections at 38, 44, 65 and 78 / 2Θ correspond to FCC metallic Au crystallites.

Furthermore, the role of NMP on support has been also investigated. In this part, two different catalysts that incorporated the NMP at different stages of the catalyst preparation were investigated. The catalyst denoted as STD+NMP refers to a standard Au catalyst that has been further treated with NMP and then dried. The catalyst presented as NMP/AC+Au refers to the pre-treatment of the Activated carbon with NMP and its use afterwards as a support for Au deposition. As shown in the figure 5.19, the Au-NMP catalyst exhibits a higher activity than the pre-treated with NMP catalyst, suggesting that the Au speciation and active sites are different among these two catalysts. In addition, the preparation of a standard catalyst and further addition of the NMP gives a catalyst with lower activity. The XRD of fresh samples (Figure 5.20) did not show any reflections of metallic Au character. This suggests that the way in which NMP is introduced to the final catalyst is crucial to the observed activity enhancement.

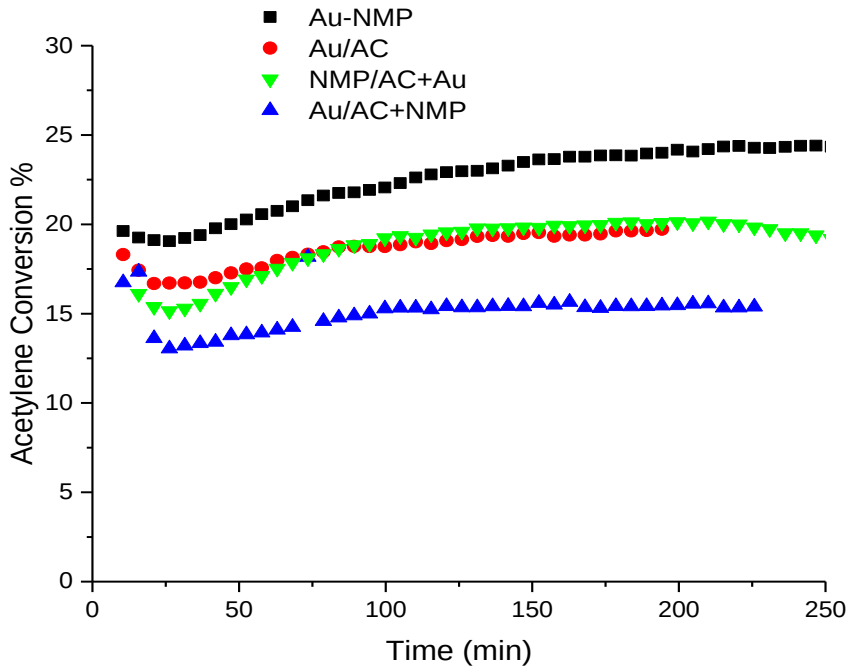

Figure 5.19: Comparison of acetylene conversions for Au-NMP and alternations in the preparation method.

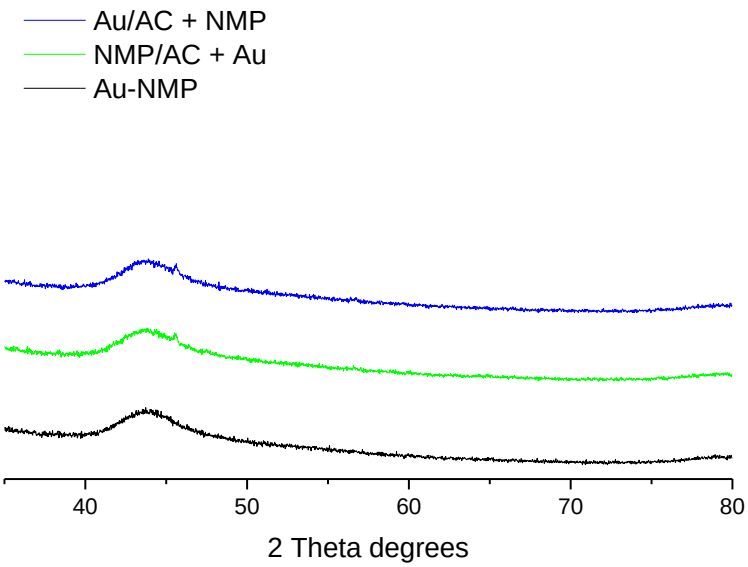

Figure: 5.20: XRD profile of fresh catalysts for Au-NMP based compounds

In addition, the activity of the Au-NMP was compared to the commercially validated Au-Thiosulfate catalyst (Figure 5.21). The Au-thiosulfate catalyst was provided by Johnson Matthey, the synthesis of which is based on the in-situ formation of an Au–thiosulfate complex using aqueous metal-precursor solutions before immobilisation onto carbon support. The active form of the catalyst has been shown to consist of atomically dispersed cationic Au species under reaction conditions.[2] The Au-NMP catalyst was also prepared in accordance to section 5.3.1. Both catalysts had a metal loading of 1 wt.% Au and, for this study, 300 mg of catalyst sample and 150 mg Silicon carbide were tested under a total gas flow of 12.5 ml/min at 180 °C with C_2H_2/HCl=0.98. At steady state, the activity of the Au-NMP catalysts of 51.2% is higher than the Au-thiosulfate 46%. The Au-thiosulfate catalyst has been industrially validated for the acetylene hydrochlorination reaction as a replacement for the current toxic mercuric chloride catalyst. It has been reported that the use of soft donor ligands such as thiosulphate can produce a class of active and stable catalysts due to the increased stability constants of the Au–S species.[3]

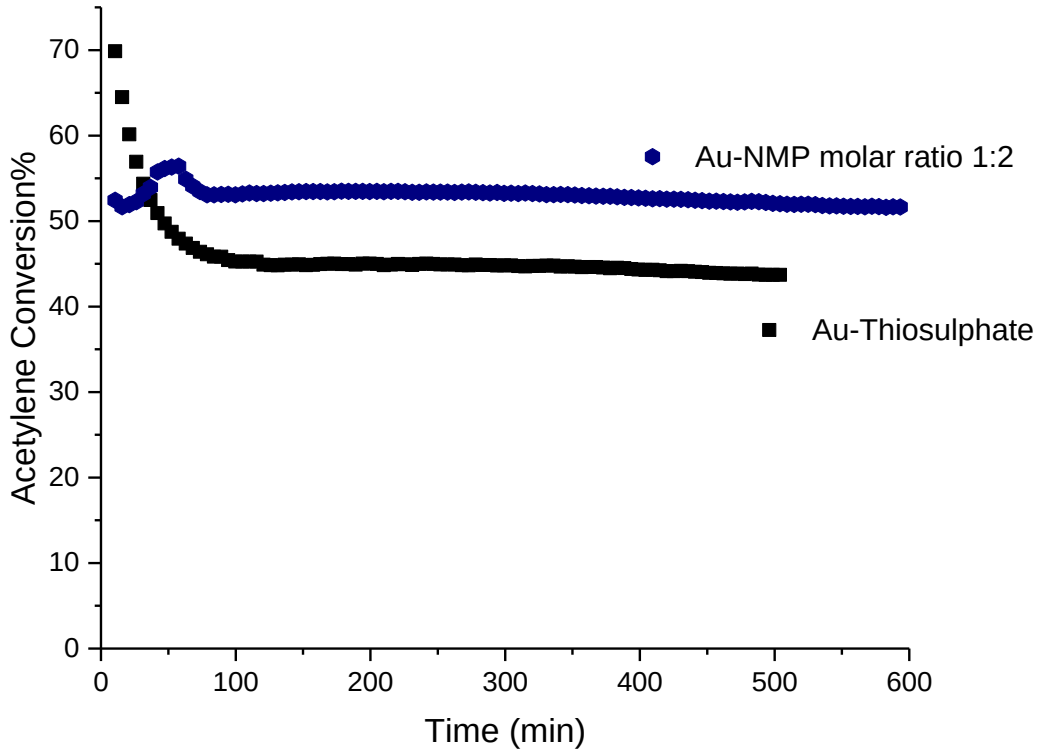

Figure 5.21: Activity profile of Au-NMP and commercially validated Au-Thiosulfate. Test Conditions: 300 mg of sample and 150mg SiC, total flow 12.5 mL min^{-1}, HCl/C_2H_2 = 1.02 at 180 °C.

Recent work by Hutchings and co-workers revealed that an optimised Au (I) :Au (III) ratio is needed to achieve a consistent conversion during the reaction.(270) In order to determine the relative changes in Au oxidation states, the catalysts were compared to three Au standard materials; $KAuCl_4$/$[AuCl_4]^-$ (Au(III)), $[AuCl_2]^-$ (Au (I) and gold foil (Au (0)). The Au foil reference is used in all XAFS experiments, whilst the Au(III) was obtained from previous work within the group on $KAuCl_4$.[43] The Au(I) standard was obtained from calculated difference spectra obtained from previously reported work on $[AuCl_2]^-$.[44] As described in Chapter 2, the transition at the Au L_3-edge from Au $2p_{3/2} \rightarrow 5d$ gives rise to an appreciable peak in the XANES region, known as the white line. The prominence of this white line is dependent on the oxidation state of the Au with Au (III) giving rise to a normalised white line height of 1.1, Au (I) giving rise to a normalised white line height 0.6 and Au (0) showing the usual Au absorption edge shape with no peak (Figure 5.22).

In situ K-edge X-ray absorption spectroscopy of the single-site Au/C catalysts during acetylene hydrochlorination shows that the Au–Cl species are dynamic during heating and under reaction conditions. The mobile nature of the Cl species leads to changes in the Au–Cl bond hybridisation and length. Furthermore, it has been proven that C–Cl is found to be

titrated from the carbon surface during reaction suggesting the potential importance of these surface groups in influencing the Au–Cl speciation.[45] The presence of Cl species in the structure of the Au catalysts is of a paramount importance as it is a species that is native to the reaction itself, as one of the reactants is the HCl gas. So, overall, the presence of Cl species in the structure of the catalyst is essential.

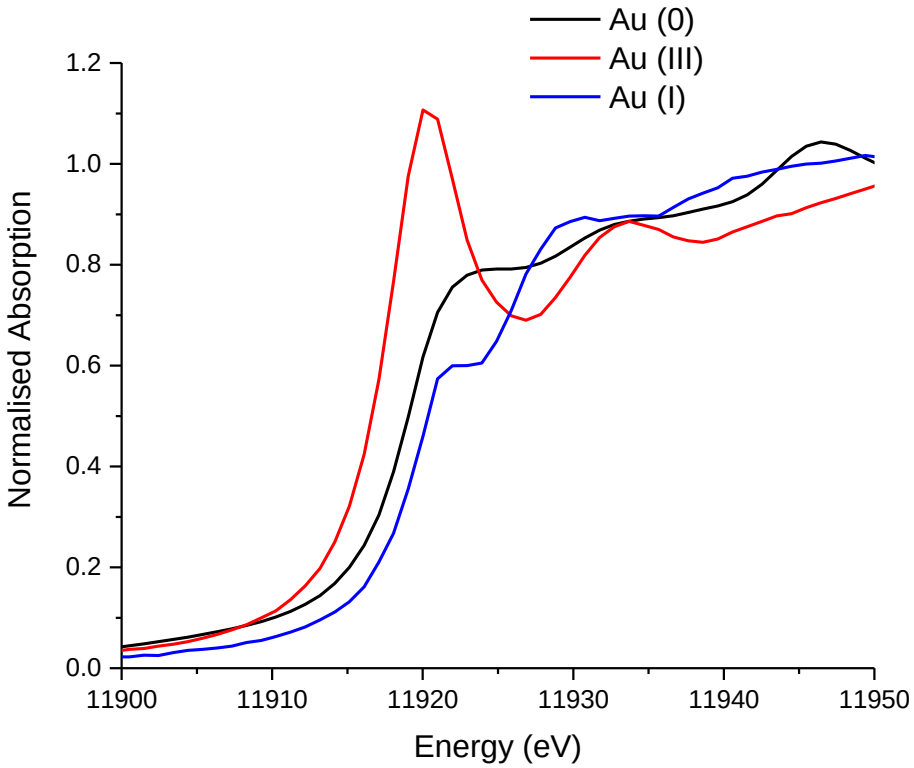

Figure 5.22: Au L_3-edge XANES of $KAuCl_4$/$[AuCl_4]^-$ (Au(III)), $[AuCl_2]^-$ (Au(I) and Au foil (Au(0)).

Au-L_3-edge XANES was used to investigate the Au oxidation state of the Au-NMP catalyst. A fresh Au-NMP catalyst and used Au-NMP, which had been tested for 8 h, were analysed to determine the effect of reaction conditions. The cationic state of the Au species is consistent between fresh and used samples (Figure 5.23), which agrees with the experimental testing data. The Au is predominantly Au(I) in both fresh and tested catalysts have a white line height of ~0.7. The Au foil reference has no white line height, as it is composed of only Au (0). Interestingly the white line intensity of the fresh catalyst is slightly higher than the tested one, implying the higher degree of resemblance of the sample with the standard Au (III) moieties, and suggesting that the sample consist of more Au (III) in comparison to the tested material. EXAFS analysis of the samples, (Figure 5.24), demonstrates an increased intensity at distances equivalent to those of the Au foil in the tested catalyst, in addition to a reduction in the Au–Cl bond length to 2.0(1). This is

consistent with the formation of small amounts of Au (0). These Au (0) species are inactive in acetylene hydrochlorination.

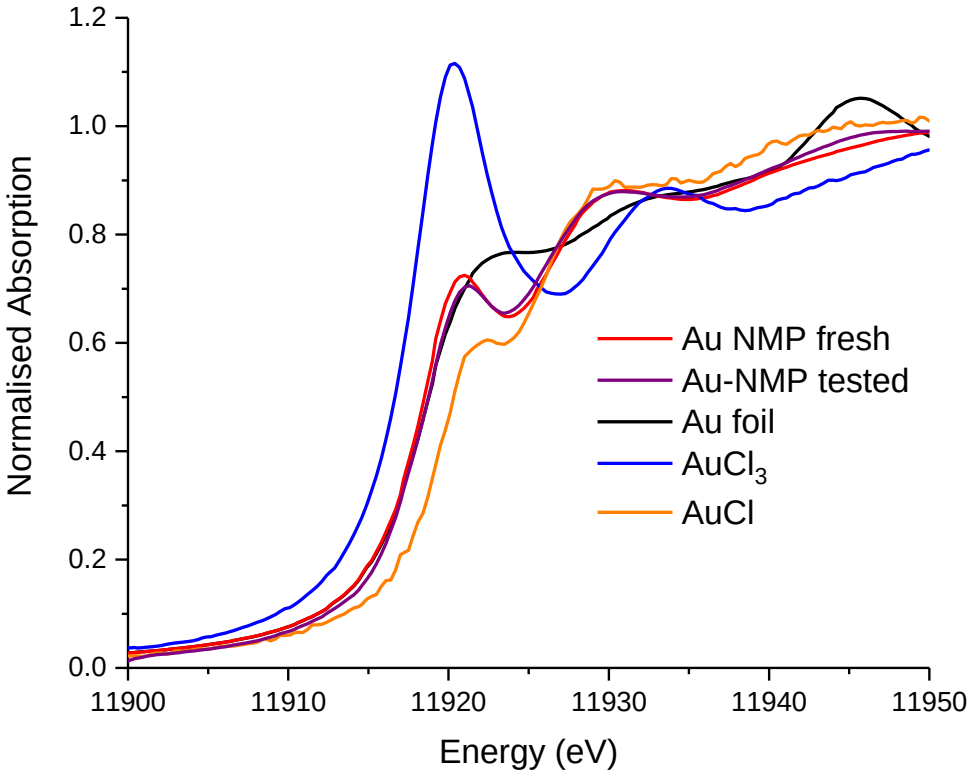

Figure 5.23. Au L_3-edge XANES of fresh, used and at steady state catalysts.

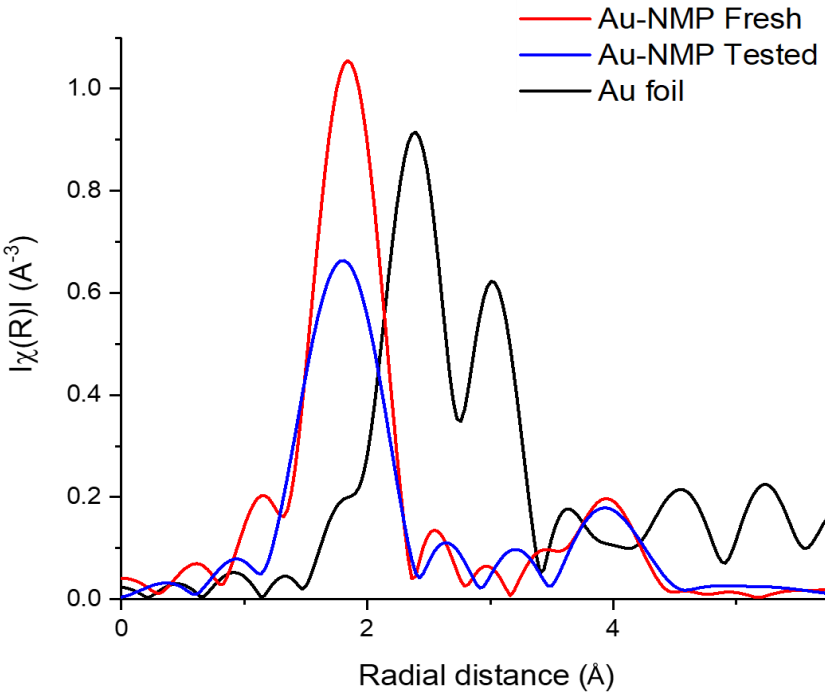

Figure 5.24: Fourier transform of the k^3-weighted χ-EXAFS data for the Au NMP catalysts fresh and tested.

A linear combination fitting (LCF) of the XANES data was performed with reference to the standards (Figure 5.25). Additionally, the XANES data fitting of the LCF for fresh and tested samples are presented in the figures S.5.4-S.5.7 in the Appendix Section. These results confirmed that the fresh Au-NMP catalyst consists primarily of 67% Au(I) and the remainder 32% Au (III) while the standard fresh Au/AC comprises of 72% Au (I) and 27% Au (III). For the tested catalysts, the Au-NMP contains a significantly higher level of Au (I) species which are estimated to 66%, whilst for the standard Au/AC catalyst the Au (I) species amount to 46%. In addition, the amount of metallic Au between the Au/AC and Au-NMP catalyst are similar while there is a considerable difference among the Au (III) species of 47% and 25% respectively. The higher ratio of Au (I): Au (III) on the Au-NMP catalyst in comparison to the Au/AC rationalises the differences in the activity among the two samples, as higher ratios are beneficial for the activity, due to the correlation between VCM productivity and Au (I) speciation. The k^3-weighted EXAFS data for fresh and tested samples are presented in figures S.5.8-S.5.11 in the Appendix Section. The k^3-weighted data of the freshly prepared materials when compared to Au (III) and Au foil standard materials, show a similar phasing and amplitude with the Au(III) standard.

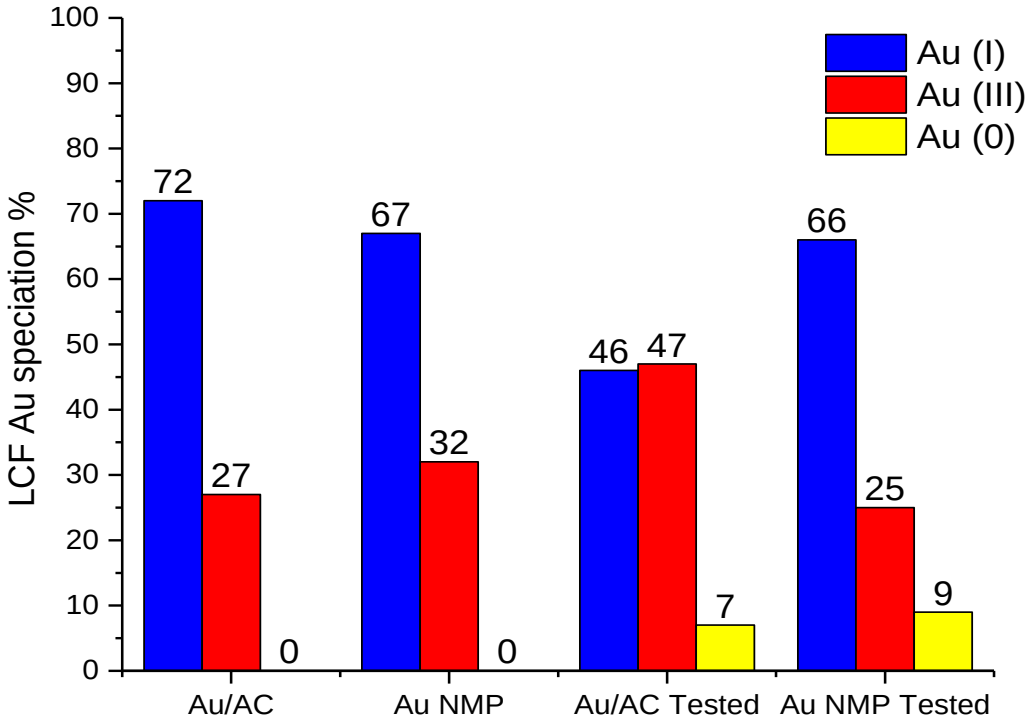

Figure 5.25: Linear combination fitting of the Au L_3-edge XANES for Au/AC and Au-NMP catalysts both fresh and tested.

Nuclear Magnetic Resonance (NMR) spectra between the uncoordinated NMP and the Au-NMP complex helped to gain an understanding of the interaction between NMP and Au

centre. As seen from the NMR spectrum (Figure 5.26) there is a significant difference in the chemical shift between the coordinated and un-coordinated NMP. These chemical trends can be explained satisfactorily as the shift to lower fields (lower δ) for the protons of NMP evidence a significant increase in magnetic deshielding of these nuclei upon coordination to positively charged Au species. For the coordinated Au-NMP in deuterated chloroform ($CDCl_3$) ^{1}H-NMR (500 MHz) shows multiplet peaks of chemical shifts δ: 1.95 ppm (**A**-CH_2), 2.35 ppm (**B**-CH_2), 3.35 ppm, (**D**-CH_2) and a singlet at 2.77 ppm (**C**-CH_3). In comparison, the ^{1}H-NMR (500 MHz) of the uncoordinated NMP shows multiplet peaks at δ: 2.25 ppm (**A**-CH_2), 2,9 ppm (**B**-CH_2) and 3.60 ppm (**D**-CH_2), as well as a singlet at 3.13 ppm (**C**-CH_3). The NMP compound has been extensively studied in literature and the spectrum of the uncoordinated specimen is in accordance with the bibliography.[46] In addition, comparative TLC of the free NMP and the Au-NMP at different ratios confirmed the coordination of the NMP to the Au centre. Commercially available NMP was used in a 5% Methanol/Chloroform solvent system. R_f value of NMP was recorded at 0.54, whist for the Au-NMP complexed compounds the R_f values were similar among them and recorded at 0.32. The Cerium Molybdate stain was employed to confirm the presence of the NMP since it is not a UV active molecule and cannot be spotted under UV exposure. The stain is highly sensitive to multifunctional groups and to be appeared it is required to thermally expose the TLC plate heat.[47] The TLC plate itself is also tainted as a light blue upon treatment while the colour of the commercial NMP is dark blue whistle the colour of the Au-NMP appears as brownish spots.

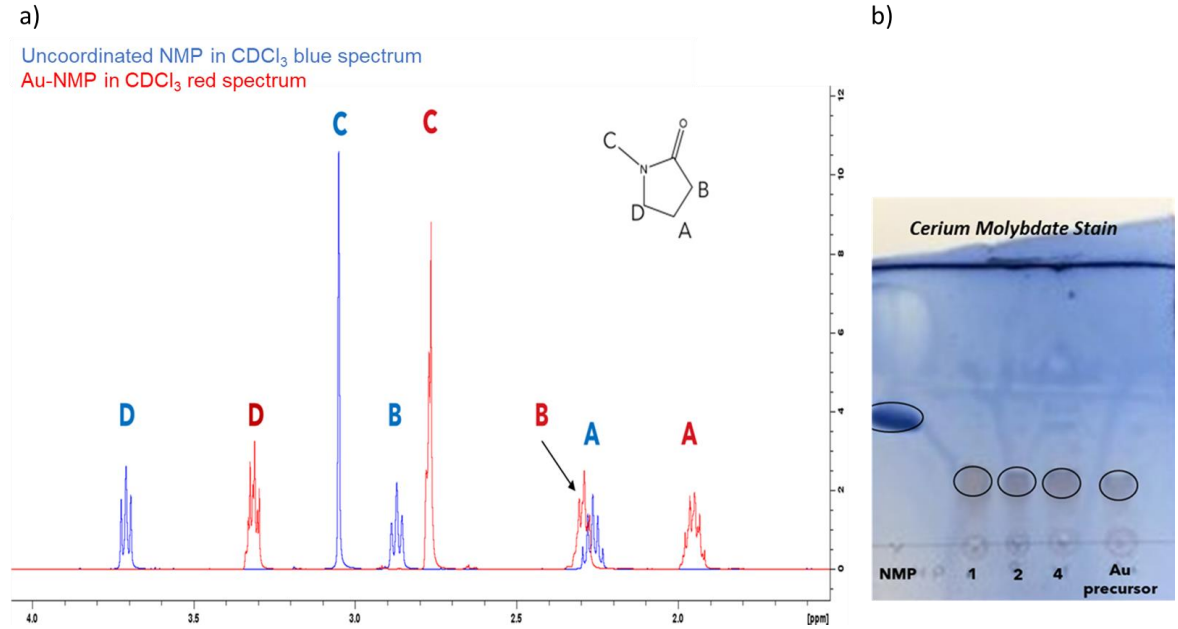

Figure 5.26. a) Stacked NMR spectra of N-methyl-pyrrolidone (blue) and coordinated Au-N-methyl-pyrrolidone b) TLC of the free NMP and the Au-NMP at ratios 1:1, 1:2, 1:4 and $HAuCl_4$

Fourier Transform Infrared Spectroscopy (FT-IR) was used to determine the characteristic functional groups for the pure isolated Au-NMP compound and the commercially available NMP. The spectra of those samples exhibit some clear differences. As seen from the stacked spectra of the NMP (Figure 5.27), the peak at 1673 cm^{-1} is attributed to the C=O stretching vibrations of NMP. The C=O stretching vibration of Au-NMP was observed at 1633 cm^{-1}, indicating that the C=O stretching vibrations of Au-NMP shifted by 40 cm^{-1} compared to that of the free NMP. In addition, the IR spectrum of the isolated Au-NMP (Figure 5.27, black line) shows a medium intensity stretch at 3100–3500 cm^{-1} which corresponds to OH or NH groups, whereas the NMP IR spectrum (Figure 5.27, red line) shows only a weak feature at around 3500 cm^{-1}, most likely for absorbed moisture.[48] The distinctive differences in the 2 spectra indicate the existence of an Au–NMP complex, that is not the same to the free uncoordinated NMP. In addition, the Raman spectrum of the Au-NMP was compared to the uncoordinated NMP (Figure 5.28). Comparing the two spectra, differences among the samples can be observed. The intensity of Au-Cl stretches that occur in the range 320-350 cm^{-1} differ among the Au-NMP and the Au precursor indicating a difference in the chemical environment of the two species.

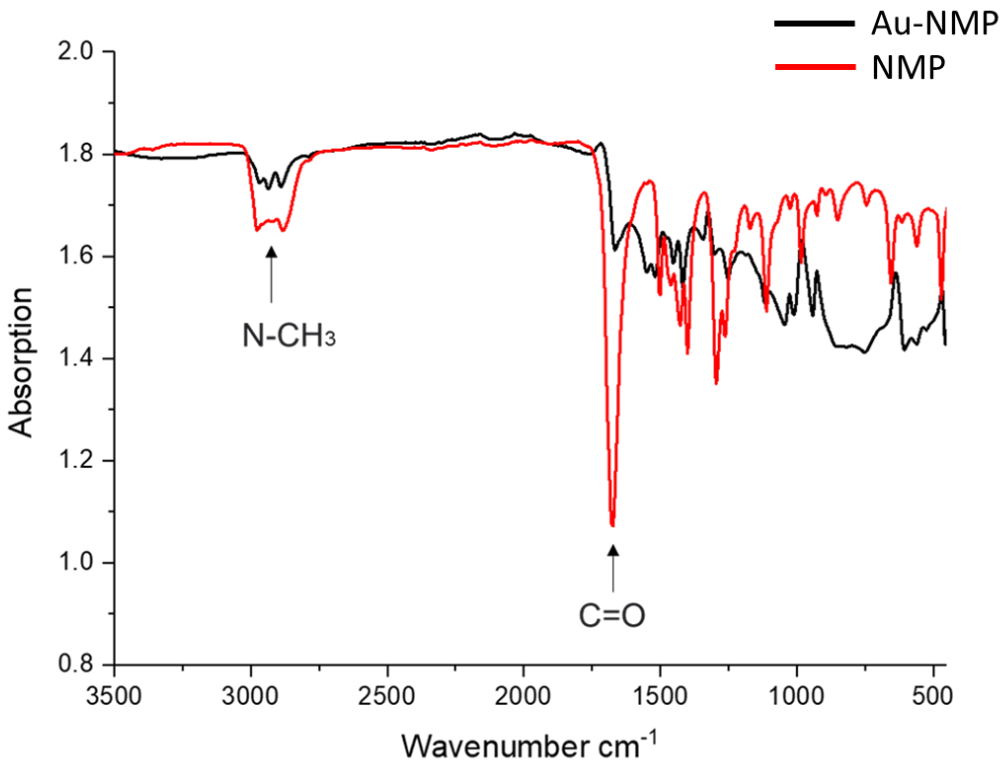

Figure 5.27: Stacked IR spectra of free NMP (black) and Au-NMP (red).

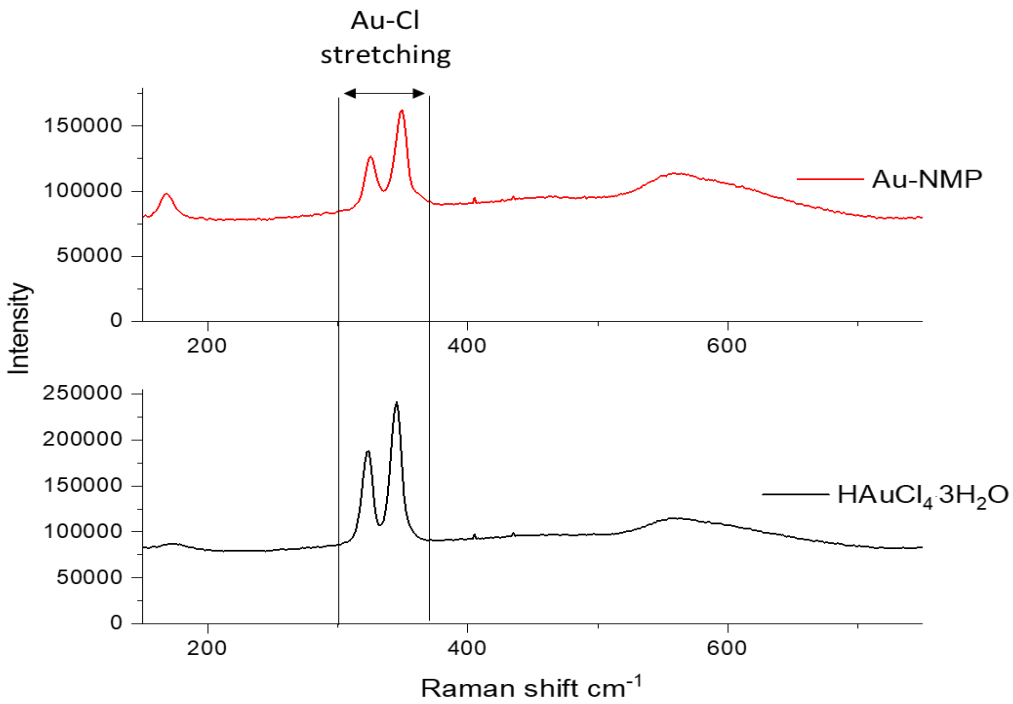

Figure 5.28: Raman spectra of free Au precursor (black) and Au-NMP (red).

Furthermore, mass of the pure isolated crystal of the Au-N-methyl-pyrrolidone also confirmed the presence of a novel compound that has a mass of 538 and corresponds to a Au tetrachloride and two N-methyl-pyrrolidone units. In addition, with the elemental analysis of C, N, Cl, and H table 5.2, it is confirmed that the new compound includes the presence Au and the NMP. All the above results indicate that the novel Au-NMP compound consists of a Au centre coordinated to 2 NMP units.

Expected elemental		CHN ANALYSIS	
Elemental analysis	Units %wt./wt. for $AuC_{10}Cl_4H_{19}N_2O_2$	Units %wt./wt.	Units %wt./wt.
Carbon	22.32	22.30	22.28
Hydrogen	3.56	3.52	3.50
Nitrogen	5.21	5.19	5.18
Chlorine	26.35	26.38	26.42
Oxygen	5.95		
Gold	36.61		
❖ Mass Spectroscopy m/z= 538.9			

Table 5.2: CHN analysis of $AuC_{10}Cl_4H_{19}N_2O_2$

Single crystal X-ray diffraction was implemented to elucidate the solid-state structure of the Au-NMP complex. Crystals suitable for single crystal XRD were provided by Dr Pete Johnston from Johnson Matthey. Crystals were prepared using $HAuCl_4$ and NMP according to the method mentioned earlier in Section 5.5. Analysis of the sample was conducted by Dr Benson Kariuki who is a Senior Experimental Officer in X-Ray Crystallography according to the following method: Single-crystal X-Ray Diffraction data were recorded at ambient temperature on an Agilent SuperNova Dual Atlas diffractometer, using Cu and Mo mirror monochromators of wavelengths λ = 1.5418 and λ = 0.7107 Å respectively. Crystal structure solution was conducted by SHELXT1 and refined with a SHELXL2. Non-hydrogen atoms were refined with anisotropic displacement parameters.

Analysis of the Au-NMP crystal structure shows that the complex has two distinctive units that interact with each other (Figure 5. 29). As seen from the structure there is a $AuCl_4$ centre that is coordinated to two NMP units. Specifically for the crystal structure the space group is $P2_{1/n}$ with cell dimensions of a = 14.2719(8) Å, α= 90°.b = 7.6086(5) Å, β = 98.485(7) ° and c = 16.5447(15) Å, γ =90°. With four formula units per unit cell and a cell volume of 1776.9(2) $Å^3$, the calculated density is 2.01 mg/m^3 and a crystal size of 0.380 x 0.140 x 0.090 mm^3. Additional structure refinement and crystal data are listed in the Table S.5.1-S.5.4 in the Appendix Section. As seen from the structure (Figure 5.22), the new complex is a $AuCl_4$ coordinated to two NMP molecules at distances of 3.726 Å and 3.929 Å. The distances of Au centre NMP units are different, due to the existence of two distinctive NMP species. One in two NMP molecules is protonated allowing the development of hydrogen bonds among O-H···O of different NMP units (Figure 5.30). The Au – N distance to the NMP unit that is forming hydrogen bonds with nearby NMP+ unit is 3.726 Å while The Au – N distance to the NMP unit that doesn't form hydrogen bonds with nearby molecules is at 3.929 Å.

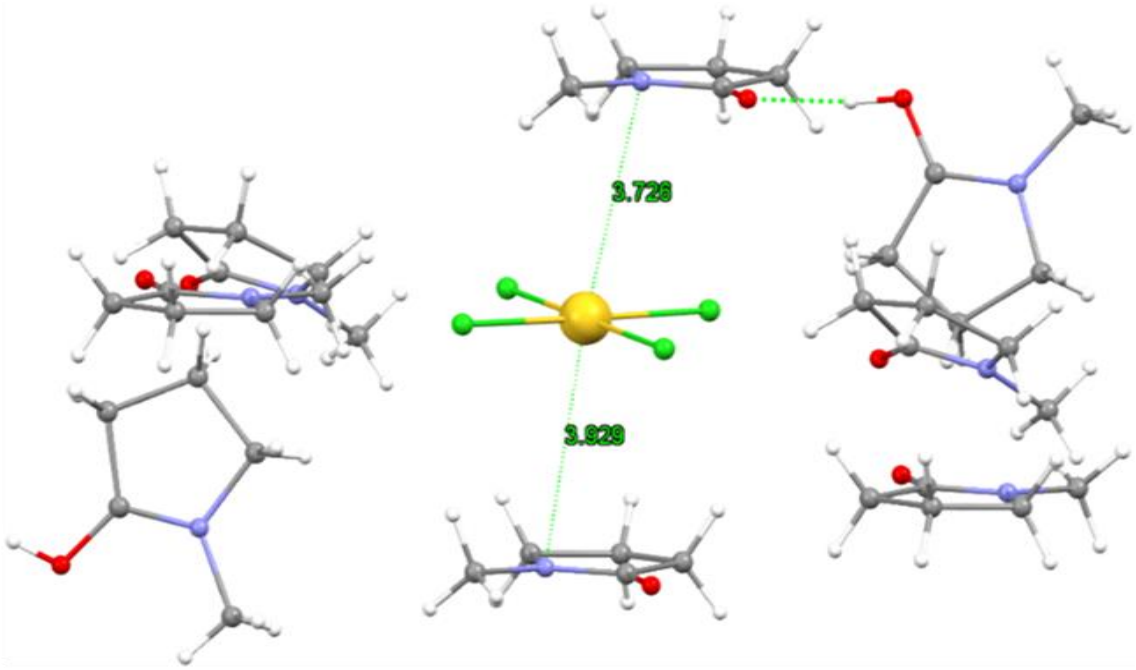

Figure 5.29. Three-dimensional structure of $AuCl_4NMP_2$.

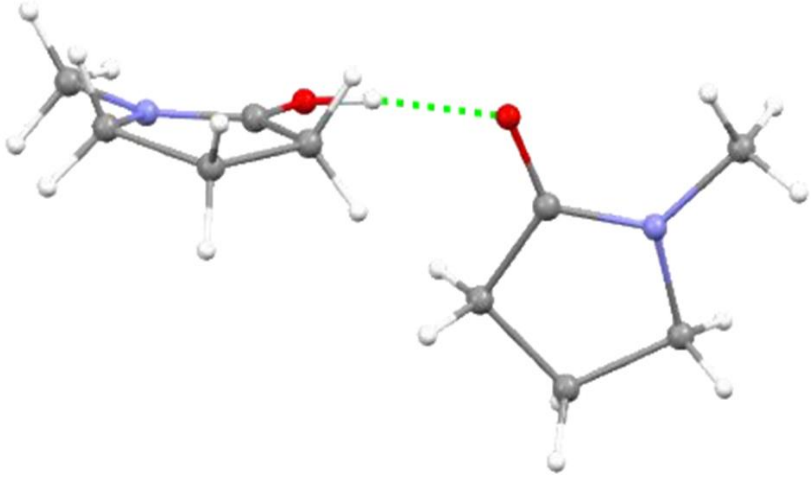

Figure 5.30: Hydrogen bonds among two different NMP units.

Furthermore, as seen from the structure of the crystal the Au-NMP complex is a salt of ratio 1: 2 (Figure 5.30). The $AuCl_4$ centre is surrounded by the 2 NMP units, without forming bonds with the N atoms of the NMP, but is rather coordinated, with the closest Au···NMP contact being face-to-face. The $AuCl_4$ centre has a square-planar conformation geometry, and the average Au-Cl bond is 2.2637 Å in contrast to the average Au-Cl bond length is 2.276 Å of the $AuCl_4$ anion crystal structure. Overall, the average bond length of Au-Cl in the Au-NMP is 0.5% shorter than in the $AuCl_4$ ion as seen in the table 5.3. Differences in the bond length of Au-Cl between the $AuCl_4$ that is surrounded by NMP units and the free

$AuCl_4^-$ can be attributed to the presence of coinage-metal bonds (CMB).[49] CMB refers to non-covalent interactions that are developed between B···MX where B is a Lewis base, M is a coinage-metal and X is a halogen atom. In this study the NMP acts as a Lewis base, Au is the coinage metal and Cl atoms are the halogen groups. These interactions decrease the negative charge on the $AuCl_4^-$ anion to the point that the soft Au atom of the $AuCl_4^-$ forms two short contacts with two different electron-rich sites, such as the hard N atom of the NMP. Eventually this leads to decrease in the negative charge of the anion enough to enable the Au centre in $AuCl_4$ to increase its electrophilic character. Moreover, Au is less electronegative than Cl and it can be expected that Cl-Au bonds in $AuCl_4^-$ are polarized, and the net negative charge of the polyatomic anion is partitioned mostly on the Cl atoms. The soft character of Au also favours this partitioning.[50] Overall, the above interactions are leading to the increase of the electrophilic character of Au.

Au-Cl (X)	Bond lengths (Å) $AuCl_4NMP_2$	Bond lengths (Å) $AuCl_4$.[51]	Au-S (X)	Bond lengths (Å) $Na_3Au(S_2O_3)_2$.[52]
Au-Cl (1)	2.2579	2.281	Au-S (1)	2.281
Au-Cl (2)	2.2614	2.278	Au-S (2)	2.272
Au-Cl (3)	2.2675	2.266		
Au-Cl (4)	2.2680	2.279		
Average Au-Cl	2.2637	2.276	Average Au-S	2.2765

Table 5.3: Bond lengths of $AuCl_4NMP_2$, $AuCl_4$ and $Na_3Au(S_2O_3)_2$.

Finally, the $AuCl_4NMP_2$ crystals were analysed via X-Ray Absorption Spectroscopy (XAS) The Au-L_3-edge XANES shows that the normalised absorption for the $AuCl_4NMP_2$ is identical to the standard $KAuCl_4/[AuCl_4]^-$ (Au (III)), while it has no resemblance to the (Au (III)), $[AuCl_2]^-$ (Au (I) and gold foil (Au (0)) standards. The normalised absorption peak for the standard Au (III) and the $AuCl_4NMP_2$ are overlapping in the XANES area, while they differentiate in EXAFS area (Figure 5.31). The XANES data fitting of the LCF crystal and the experimental k^3-weighted EXAFS data for the Au-NMP crystal are shown in the figure S.5.12 and S.5.13 in the Appendix Section. This observation can be attributed to the presence of NMP in close distance to the Au centre. The LCF of the XANES data was

performed with reference to the standards, (Figure 5.32). These results confirmed that the $AuCl_4NMP_2$ crystal does not consist of Au(I) (0 %) and is entirely Au (III) (100 %).

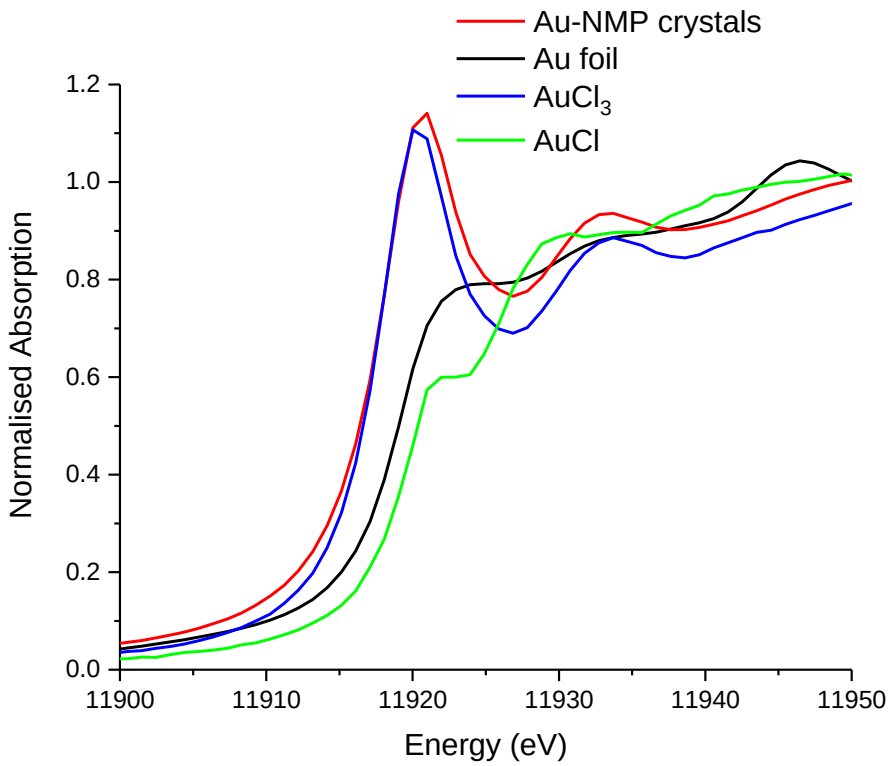

Figure 5.31: L_3-edge XANES spectra of the $AuCl_4NMP_2$ crystals and various Au standard materials (Au foil, $K[AuCl_4]$/$[AuCl_4]^-$and $[AuCl_2]^-$)

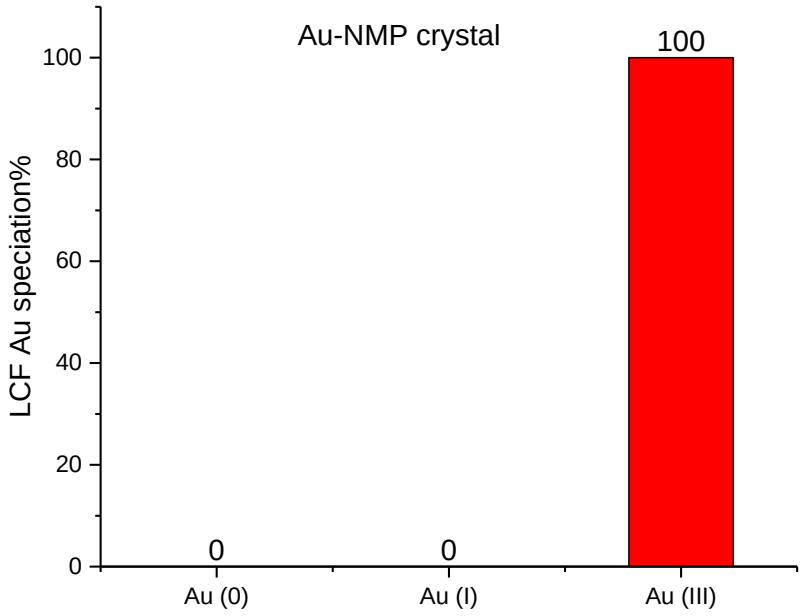

Figure 5.32: LCF of the Au speciation from the Au L_3-edge XANES data of the $AuCl_4NMP_2$ crystals and Au standard materials (Au foil, $K[AuCl_4]$/$[AuCl_4]^-$and $[AuCl_2]^-$).

5.7 Investigation of functional groups in the N-methyl-pyrrolidone and their effect

Aiming to establish the role of the N and O atoms in the NMP unit, various compounds that presented structural similarities to the NMP, were investigated. It has been reported that ligands containing N atoms can improve the activity of the catalysts,[25,26] while metal-O interactions can also lead to improvement of catalysts for this reaction.[35] The NMP analogues were used to distinguish the role of the functional groups in stabilising the Au centres (Figure 5.33). The molar ratio of Au to the NMP analogues were 1 to 2 as well as 1 to 4. The catalysts were prepared via wet incipient method as described earlier in this chapter (section 5.3.1).

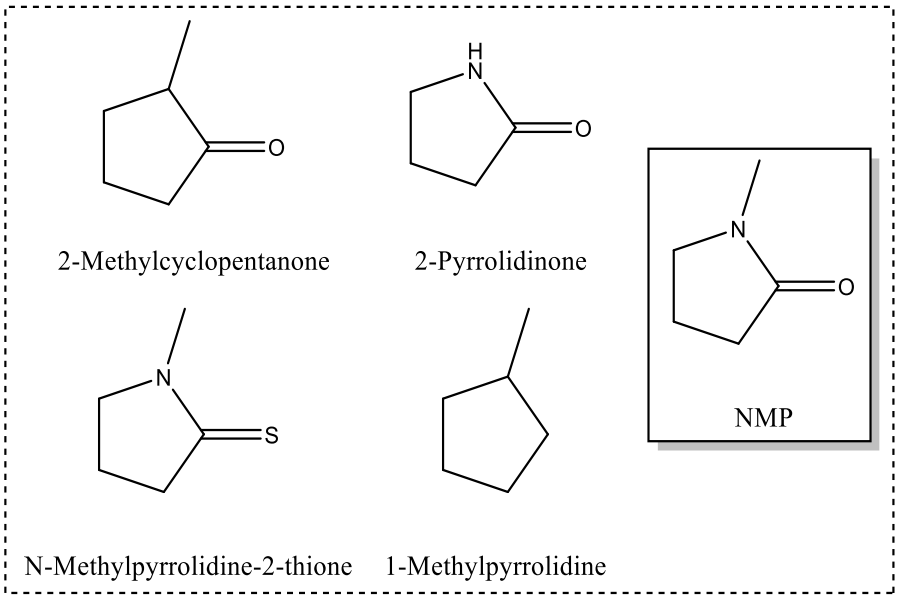

Figure 5.33. Structure of NMP analogues used for this study.

Catalysts synthesised using compounds with structures similar to N-Methyl pyrrolidone did not improve the activity or stability of the catalysts during the 4-hour reaction. Au-OC catalysts of molar ratio 1:2 displayed the following order of activities: Au-N-methyl pyrrolidone > Au/AC > Au-N-methylpyrolidine >Au-2-pyrrolidone > Au-N-methylpyrrolidine-2-thione > Au-methylcyclo-pentanone (Figure 5.34). Au-OC catalysts of molar ratio 1:4 displayed the following order of activities: Au-N-methyl-pyrrolidone > Au/AC >Au-2-pyrrolidone > Au-N-methylpyrrolidine-2-thione > Au-methyl cyclopentanone> Au-N-methylpyrolidine (Figure 5.35). These results confirmed that the optimum structure for

improved catalysis is the NMP and highlights the importance of the coexistence of the N and O moieties. Furthermore, comparing catalysts that were prepared at ratios 1:2 and 1:4 also shows the same order of activity, except for the Au-N-Methyl-pyrrolidine catalyst.

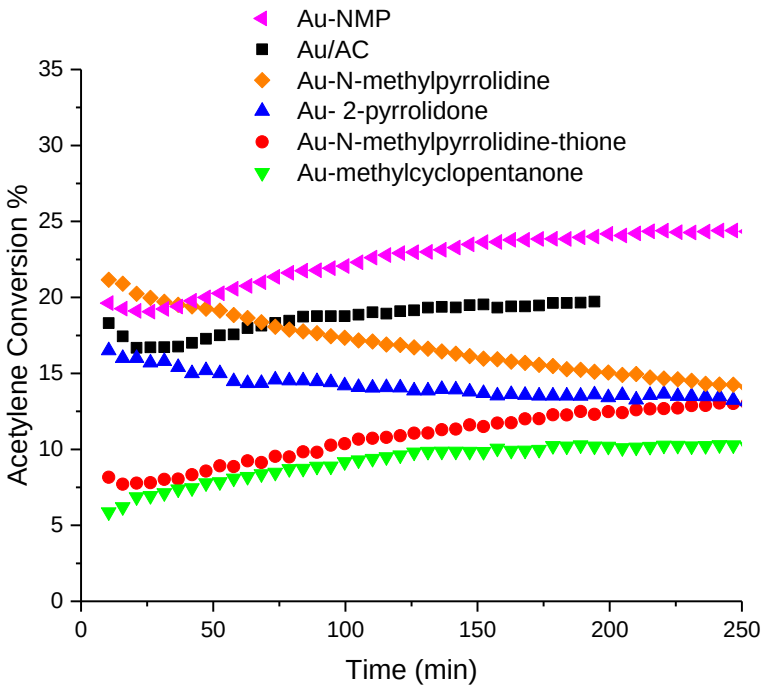

Figure 5.34. Comparison of acetylene conversions for Au and NMP analogue based compounds molar ratio 1 to 2.

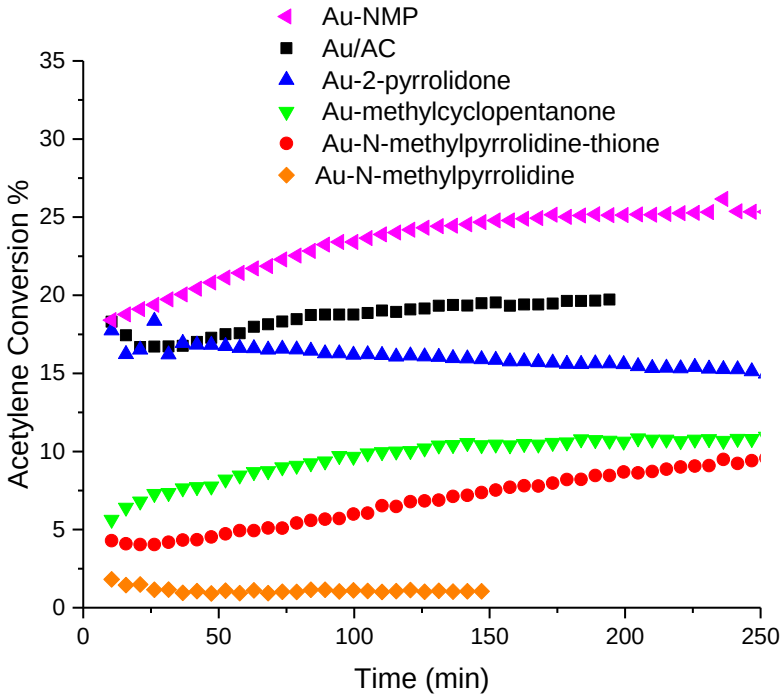

Figure 5.35: Comparison of acetylene conversions for Au and NMP analogue based compounds molar ratio 1 to 4.

Interestingly, increasing the ratio of the N-Methyl-pyrrolidine leads to inactive catalysts. During the preparation procedure, formation of metallic Au was apparent (Figure S.5.1 and S.5.2 Appendix). This phenomenon has been reported in the literature and is associated to the reductive nature of the amines. Amines that have a reduction potential between that of the oxidation of Au^0 to Au^{1+} and the reduction of $HAuCl_4$ to Au (0) are feasible to act as reducing agents. Those with oxidation potentials outside this range will not react with the $HAuCl_4^-$ precursor to form AuNPs.[53] It should be stated that for all the above reactions selectivity of the catalysts is 100%, with only VCM being detected.

5.8 Pilot plant test of 0.1 wt.% Au-NMP catalyst

Peter Johnson from Johnson Matthey kindly prepared and tested a 0.1 wt.% Au-NMP and a 0.1 wt.% Au-Thiosulfate catalyst. The catalysts have been prepared based on the following method:

1. 0.1 % Au-NMP

A solution of $HAuCl_4$ (%Au = 41.76%, Johnson Matthey) containing 0.100g Au was solubilised in 96 ml of acetone. To this solution was added 4 molar equivalents of N-Methyl-Pyrrolidone (0.202g). The Au-based solution was then added to 100g of commercially available activated carbon extrudate pellets, via the wet impregnation technique. The impregnated catalyst was left to stand for 30 minutes at ambient temperature and accordingly the catalyst was dried overnight under flowing N_2 at room temperature. The material was finally dried at 105°C to give an Au/C catalyst containing 0.1 % Au. This catalyst is denoted as 0.1 wt.% Au-NMP.

2. 0.1 % Au-Thiosulfate

A solution of $HAuCl_4$ containing 0.100g Au (%Au = 41.76%, Johnson Matthey) was solubilised in 31 ml of demineralised water. Separately 0.380g ammonium thiosulphate and 0.070g $CaCl_2$ were dissolved in 31 ml demineralised water. The Au-based solution was then added to the ammonium thiosulphate while stirring, to produce a $(NH_4)_3Au(S_2O_3)_2$ solution. The resultant Au-Thiosulfate solution was then added to 100g commercially available activated carbon pellets, via the wet impregnation technique. The impregnated catalyst was

left to stand for 30 minutes at ambient temperature. The material was then dried at 105°C overnight to give an Au/C catalyst containing 0.1 % Au. This catalyst is denoted as 0.1 wt.% Au-Thiosulfate.

Comparison of 0.1 wt.% Au-NMP and 0.1 wt.% Au-Thiosulfate (Figure 5.36) illustrates that the activity profile of the materials is similar. This is an interesting finding as in the past a direct comparison of a $HAuCl_4$ aqua regia prepared catalyst to the commercially validated catalyst Au-Thiosulfate showed that the Au prepared in aqua regia rapidly deactivated. The deactivation of the $HAuCl_4$ aqua regia catalyst was attributed in the past to the agglomeration of a carbon polymer on the surface of the catalyst, as a result of polymerization of the acetylene on acid sites of the catalyst.[2] The of 0.1 wt.% Au-NMP and 0.1 wt.% Au-Thiosulfate were tested for 50 hours as following: 5g of 0.1 wt.% Au catalyst, was loaded into a 2 cm diameter stainless steel tube, and the bed formed was supported at either end on silica wool packing. The tube was then placed in a tube furnace. A mixture of HCl and C_2H_2 of a molar ratio 1.2:1 was passed over the catalyst at a total flow rate of 240 ml/min, at a temperature of 130 ^oC. The conversion of C_2H_2 and HCl to VCM was measured by FTIR spectroscopy by passing the gas flow from the reactor exit into an *in-situ* IR gas cell.

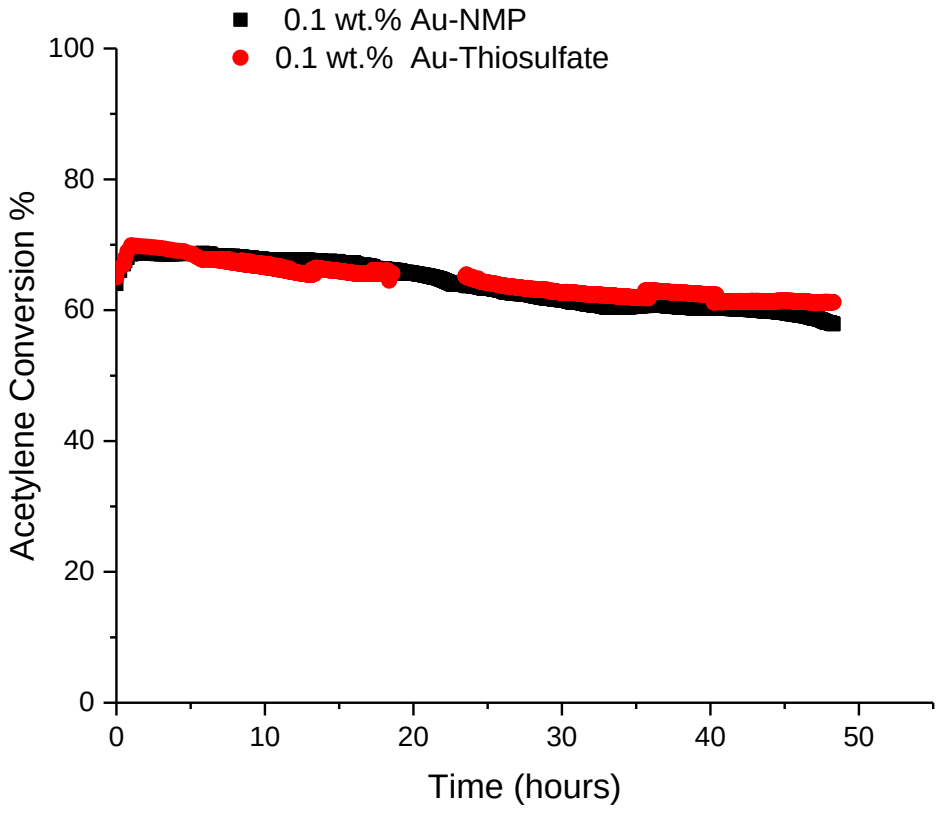

Figure 5.36: Activity profile of 0.1 wt.% Au-NMP and commercially validated 0.1 wt.% Au-Thiosulfate.

5.9 Conclusions

In summary, a series of activated carbon supported Au-OCs catalysts was prepared via a simple incipient wetness impregnation method using dry acetone as a solvent and then studied for the acetylene hydrochlorination. The catalytic assessment suggested that N-methyl-pyrrolidone (NMP) can significantly improve the activity and stability of Au catalysts. Notably a direct comparison of the Au-NMP catalyst with the commercially validated Au-Thiosulfate illustrated that the activity of the novel pyrrolidone Au catalyst was remarkably higher. Further characterisation of the fresh and tested Au-NMP catalyst via Au L_3-edge XANES confirmed the Au appeared as cationic Au(I)/Au(III) on the carbon support. The high activity of the Au-NMP catalyst over the Au/AC catalyst is associated with the higher level of Au(I) content.

In addition, the thorough characterization of the isolated Au-NMP crystal confirmed that the NMP is coordinating to the Au centre via the N interactions. In particular NMR, IR, Raman and Single crystal X-ray diffraction studies suggested the presence of a Au-NMP complex. The Au-NMP was confirmed to be a Au and NMP salt unit rather than a Au and NMP ligand moiety with a ratio of 1:2 respectively. Unfortunately, it has not been feasible to identify via the XAFs studies the nature of the Au-NMP unit upon the deposition on the carbon support.

Finally, a sequence of Au-NMP derivatives have also been studied. The role of the O and N functionalities of the NMP unit, was identified to be crucial for the activity of the Au-NMP catalyst. The coexistence of the O and N on the structure of the molecule seem to be displaying a crucial effect on stabilising and improving the activity of the Au centre. This study suggests that NMP can be a great candidate for efficient and effective, well stabilised Au-based catalysts.

Future work should focus on underpinning the role of the NMP. DFT studies are required to confirm the plausibility of the NMP on stabilizing the active Au centres. In situ-XAFs studies should be performed with the aim of monitoring the change of the speciation species of the Au centres during the reaction time. As it was shown the formation of the Au nanoparticles is apparent, yet the determination of the conditions that lead to their formation is vital. Furthermore, the scope of NMP derivatives should also be expanded, with more compounds to be investigated. It would be interesting to study compounds that have

additional similarities to the NMP. Finally, it would be interesting to expand the scope of the M-NMP candidates, where M is Pt, Cu, Ir, Rh to investigate whether the similar effects are observed across other metals.

5.10 References

1. Malta G., Kondrat S. A., Freakley S. J., Davies C. J., Lu L., Dawson R. S., Thetford A., Gibson K. E., Morgan D. J., Jones W., Wells P. P., Johnston P., Catlow R. A., Christopher J., Kiely C. J., Hutchings G. J., Identification of single-site gold catalysis in acetylene hydrochlorination. Science, 2017, **355**, 1399–1403.

2. Johnston P., Carthey N., Hutchings G. J., Discovery, development, and commercialization of gold catalysts for acetylene hydrochlorination. J. Am. Chem. Soc., 2015, **137**, 14548–14557.

3. Hutchings G. J., Vapor phase hydrochlorination of acetylene: Correlation of catalytic activity of supported metal chloride catalysts. J. Catal., 1985, **96**, 292–295.

4. Zhao J., Wang B., Xu X., Yu Y., Di S., Xu H., Zhai Y., He H., Guo L., Pan Z., Li X., Alternative solvent to aqua regia to activate Au/AC catalysts for the hydrochlorination of acetylene. J. Catal., 2017, **350**, 149–158.

5. Sun X., Dawson S. R., Parmentier T. E., Malta G., Davies T. E., He Q., Li L., Morgan M. D., Carthey N., Johnston P., Kondrat A. S., Freakley J. S., Kiely C. J., Hutchings G. J., Facile synthesis of precious-metal single-site catalysts using organic solvents. Nat Chem., 2020, **12**, 560–567.

6. Malta G., Kondrat S. A., Freakley S. J., Davies C. J., Dawson S., Liu X., Lu L., Dymkowski K., Fernandez-Alonso F., Mukhopadhyay S., Gibson E. K., Wells P. P., Parker S. F., Kiely C. J., Hutchings G. J., Deactivation of a single-site gold-on-carbon acetylene hydrochlorination catalyst: An X-ray absorption and inelastic neutron scattering study. ACS Catal., 2018, **8**, 8493–8505.

7. Conte M., Carley A. F., Attard G., Herzing A. A., Kiely C. J., Hutchings G. J., Hydrochlorination of acetylene using supported bimetallic Au-based catalysts. J Catal., 2008, **257**, 190–198.

8. Dong Y., Zhang H., Li W., Sun M., Guo C., Zhang J., Bimetallic Au–Sn/AC catalysts for acetylene hydrochlorination. J. Ind.Eng. Chem., 2016, **35**, 177–184.

9. Zhang J., Sheng W., Guo C., Li W., Acetylene hydrochlorination over bimetallic Ru-based catalysts. RSC Adv., 2013, **3**, 21062–21068.

10. Zhao J., Xu J., Xu J., Ni J., Zhang T., Xu X., Li X., Activated-carbon-supported gold-cesium(I) as highly effective catalysts for hydrochlorination of acetylene to vinyl chloride. ChemPlusChem., 2015, **80**, 196–201.

11. Li Y., Zhang C., Zhang H., Li L., Zhang J., Oh R., Yao L., Cai M., Li J., Zhang M., Li F., Effects of N-, P-, or O-containing ligands on gold-based complex catalysts for acetylene hydrochlorination. Appl. Catal. A Gen., 2021, **612**, 1–10 .

12. Zhang S., Shang R., Nakamoto M., Yamamoto Y., Adachi Y., Ohshita J., Luminescent di- and tetranuclear gold complexes of bis(diphenylphosphinyl)-functionalized dipyrido-annulated N-heterocyclic carbene. Inorg. Chem., 2019, **58**, 6328–6335.

13. Zhang C., Zhang H., Li Y., Xu L., Li J., Li L., Ming C., Zhang J.,Hydrochlorination of acetylene over the activated carbon supported Au catalysts modified by N-P-O-containing ligand. ChemCatChem., 2019, **11**, 3441–3450.

14. Zhao J., Yue Y., Sheng G., Wang B., Lai H., Di S., Zhai Y., Guo L., Li X., Supported ionic liquid-palladium catalyst for the highly effective hydrochlorination of acetylene. Chem. Eng. J., 2019, **360**, 38–46.

15. Zhao J., Yu Y., Xu X., Di S., Wang B., Xu H., Ni J., Guo L., Pan Z., Li X., Stabilizing Au(III) in supported-ionic-liquid-phase (SILP) catalyst using $CuCl_2$ via a redox mechanism. Appl. Catal. B Environ., 2017, **206**, 175–183.

16. Shang S., Zhao W., Wang Y., Li X., Zhang J., Han Y., Li W., Highly efficient Ru at IL/AC to substitute mercuric catalyst for acetylene hydrochlorination. ACS Catal., 2017, **7**, 3510–3520.

17. Wang L., Wang F., Wang J., Non-mercury catalytic acetylene hydrochlorination over a NH_4F-urea-modified Pd/HY catalyst for vinyl chloride monomer production. New J. Chem., 2016, **40**, 3019–3023.

18. Li G., Li W., Zhang J., Strontium promoted activated carbon-supported gold catalysts for non-mercury catalytic acetylene hydrochlorination. Catal. Sci. Technol., 2016, **6**, 3230–3237.

19. Hou L., Zhang J., Pu Y., Li W. Effects of nitrogen-dopants on Ru-supported catalysts for acetylene hydrochlorination. RSC Adv., 2016, **6**, 18026–18032.

20. Hou R., Tian F., Li D., Zhao Z., Duan D., Zhang H., Sha X., Liu B., Cui T., Ab initio study of germanium-hydride compounds under high pressure. RSC Adv., 2015, **5**, 19432-19438.

21. Xu H., Meng S., Luo G., Ionic liquids-coordinated Au catalysts for acetylene hydrochlorination: DFT approach towards reaction mechanism and adsorption energy. Catal. Sci. Technol., 2018, **8**, 1176–1182.

22. Kaiser S. K., Lin R., Mitchell S., Fako E., Surin I., Krumeich F., Hauert R., Safonova O. V., Kondratenko V. A., Kondratenko E. V., Collins S. M., Midgley M., López N., Pérez-Ramírez J., Controlling the speciation and reactivity of carbon supported gold nanostructures for catalysed acetylene hydrochlorination. Chem. Sci., 2019, **10**, 359-369.

23. Qi X., Li W., Gu J., Gu C., Zhang J., Gold-glutathione complex catalysts with carbon support for non-mercury catalytic acetylene hydrochlorination. RSC Adv., 2016, **6**, 105110–105118.

24. Yin X., Huang C., Kang L., Zhu M., Dai B., Novel $AuCl_3$-thiourea catalyst with a low Au content and an excellent catalytic performance for acetylene hydrochlorination. Catal. Sci. Technol., 2016, **6**, 4254–4259.

25. Zhou K., Jia J., Li C., Xu H., Zhou J., Luo G., Wei F., A low content Au-based catalyst for hydrochlorination of C_2H_2 and its industrial scale-up for future PVC processes. Green Chem., 2015, **17**, 356–364.

26. Xu H., Zhou K., Si J., Li C., Luo G., A ligand coordination approach for high reaction stability of an Au-Cu bimetallic carbon-based catalyst in the acetylene hydrochlorination process. Catal. Sci. Technol., 2016, **6**, 1357–1366.

27. Huang C., Zhu M., Kang L., Dai, B., A novel high-stability Au(III)/Schiff-based catalyst for acetylene hydrochlorination reaction. Catal. Commun., 2014, **54**, 61–65.

28. Dong Y., Li W., Yan Z., Zhang J., Hydrochlorination of acetylene catalyzed by an activated carbon supported chlorotriphenylphosphine gold complex. Catal. Sci. Technol., 2016, **6**, 7946–7955.

29. Zhong J., Xu Y., Liu Z., Heterogeneous non-mercury catalysts for acetylene hydrochlorination: progress, challenges, and opportunities. Green Chem., 2018, **20**, 2412-2427.

30. Malta G., In situ Study of Au/C Catalysts for the Hydrochlorination of Acetylene. Doctoral dissertation, Cardiff University, Cardiff, 2018.

31. Wang J., Zhao F., Zhang C., Kang L., Zhu M., A novel S, N dual doped carbon catalyst for acetylene hydrochlorination. Appl. Catal. A Gen., 2018, **549**, 68–75.

32. Di X., Zhao J., Yu Y., Xu X., Gu S., He H., Zhang T., Li X., One-pot synthesis of nitrogen and sulfur co-doped activated carbon supported $AuCl_3$ as efficient catalysts for acetylene hydrochlorination. Chin. Chem. Lett., 2016, **27**, 1567–1571.

33. Dawson S. R., Pattisson S., Malta G., Dummer N. F., Smith L. R., Lazaridou A., Allen C. S., Davies T. E., Freakley S. J., Kondrat S. A., Kiely C. J., Johnston P., Hutchings G. J., Sulfur promotion in Au/C catalyzed acetylene hydrochlorination. Small, 2021, **17**, 1-10.

34. Duan X., Ning L., Yin Y., Huang Y., Gao J., Lin H., Tan K., Fang H., Ye L., Lu X., Yuan Y., Sulfur moiety as a double-edged sword for realizing ultrafine supported metal nanoclusters with a cationic nature. ACS Appl. Mater. Interf., 2019, **11**, 11317-11326.

35. Zhao C., Zhang X., He Z., Guan Q., Li W., Demystifying the mechanism of NMP ligands in promoting Cu-catalyzed acetylene hydrochlorination: Insights from a density functional theory study. Inorg. Chem. Front., 2020, **7**, 3204–3216.

36. Han Y., Wang Y., Wang Y., Hu Y., Nian Y., Li W., Zhang J., Pyrrolidone ligand improved Cu-based catalysts with high performance for acetylene hydrochlorination. Appl. Organomet. Chem., 2021, **35**, 1–13.

37. Pattisson S., Malta G., Dawson S. R., Dummer N. F., Smith L. R., Lazaridou A., Morgan D. J., Freakley S. J., Kondrat S. A., Smit J. J., Johnston P., Hutchings G. J., Lowering the operating temperature of gold acetylene hydrochlorination catalysts using oxidized carbon supports. ACS Catal., 2022, **22**, 14086–14095.

38. Li B., Gonzalez R. D., The measurement of small amounts of coke by a sensitive TGA/FTIR technique. Catal. Letters, 1998, **54**, 5–8.

39. Velasco-Santos C., Martinez-Hernandez A. L., Castano V. M.,. Carbon Nanotubes-Polymer Nanocomposites. IntechOpen, 1st edn., 2011.

40. Esfahani M. M., Goerlitzer E. S. A., Kunz U., Vogel N., Engstler J., Brunsen A. A., N-methyl-2-pyrrolidone as a reaction medium for gold(III)-ion reduction and star-like gold nanostructure formation. ACS Omega, 2022, **7**, 9484–9495.

41. Dai B., Wan Q., Yu F., Zhu M., Effect of Au nano-particle aggregation on the deactivation of the $AuCl_3$/AC catalyst for acetylene hydrochlorination. Sci. Rep., 2015, **5**, 2–11.

42. Fong Y. Y., Visser B. R., Gascooke J. R., Cowie B. C. C., Thomsen L,. Metha G. F., Buntine M. A., Harris H. H., Photoreduction kinetics of sodium tetrachloroaurate under synchrotron soft X-ray exposure. Langmuir, 2011, **27**, 8099–8104.

43. Dawson, S. R. Acetylene Hydrochlorination using Gold Catalysts. Doctoral dissertation, Cardiff University, Cardiff, 2019.

44. Chang S. Y., Uehara A., Booth S. .G., Ignatyev K., Mosselmans J. F. W., Dryfe R. A. W., Schroeder S. L. M., Structure and bonding in Au(I) chloride species: A critical

examination of X-ray absorption spectroscopy (XAS) data. RSC Adv., 2015, **5**, 6912-6918.

45. Malta G., Kondrat S. A., Freakley S. J., Morgan D. J., Gibson E. K., Wells P. P., Aramini M., Gianolio D., Thompson P. B. J., Johnston P., Hutchings G. J., In situ K-edge X-ray absorption spectroscopy of the ligand environment of single-site Au/C catalysts during acetylene hydrochlorination. Chem. Sci., 2020,**11**, 7040-7052.

46. Radhika G., Venkatesan R., Kathiroli S., N-methylpyrrolidone: Isolation and characterization of the compound from the marine sponge Clathria frondifera (class:Demospongiae). Indian J. Mar. Sci., 2007, **36**, 235–238.

47. Gayathri T., Types of Stains to develop TLC Plates. J. Adv. Res. Eng. Technol., 2014, **5**, 79–83.

48. Yau H. C., Bayazit M. K., Steinke J. H. G., Shaffer M. S. P., Sonochemical degradation of N-methylpyrrolidone and its influence on single walled carbon nanotube dispersion. Chem. Commun., 2015, **51**, 16621–16624.

49. Legon A. C., Walker, N. R. What's in a name? 'Coinage-metal' non-covalent bonds and their definition. Phys. Chem. Chem. Phys., 2018, **20**, 19332–19338.

50. Daolio A. Pizzi A., Terraneo G., Ursini M., Frontera A., Resnati G., Anion···anion coinage bonds: The case of tetrachloridoaurate. Angew. Chemie - Int. Ed., 2021, **60**, 14385–14389.

51. Hargittai M., Schulz A., Réffy B., Kolonits M., Molecular structure, bonding, and Jahn−Teller effect in gold chlorides: Quantum chemical study of $AuCl_3$, Au_2Cl_6, $AuCl_4^-$, AuCl, and Au_2Cl_2 and electron diffraction study of Au_2Cl_6. J. Am. Chem. Soc., 2001, **123**, 1449–1458.

52. Ruben H., Zalkin A., Faltens M. O., Templeton, D. H., Crystal structure of sodium gold(I) thiosulfate dihydrate, $Na_3Au(S_2O_3)_2{\cdot}2H_2O$. Inorg. Chem., 1974, **13**, 1836–1839.

53. Newman J. D. S., Blanchard G. J., Formation of gold nanoparticles using amine reducing agents. Langmuir, 2006, **22**, 5882–5887.

Chapter 6

Conclusions and Future work

6.1 Systematic review and data comparison of best-in-class catalysts for the acetylene hydrochlorination.

A general approach for the comparison of different catalytic systems with fundamentally different properties that has been examined at a range of experimental reaction conditions, has been introduced. Sourcing information from the available literature for the acetylene hydrochlorination reaction, a direct comparison of the catalysts reported has been achieved. The normalized productivity of the different catalytic systems, as calculated, proved that the best-in-class catalysts consist of Au as the active metal centre. It was validated by this study that the majority of literature reported Au-based catalysts not only exhibited a higher activity in comparison to the other metal systems, but in addition, they presented a lower deactivation rate. The study confirmed, once again, the initial prediction by Hutchings that Au is the best candidate for this reaction. Plotting the catalytic activity of the best catalyst of each metal versus the standard electrode potential verified that there is a linear correlation between these values, as previously reported by other studies and researchers.

Future work should focus on comparing the catalysts that are being reported to validate that the suggested generalized methodology facilitates the identification of the best catalysts. Ideally, this study will set the frame for research groups to provide experimental details that will allow the calculation of the important parameters that are required for a meaningful comparison of catalysts. In addition, this study should be used for the adaptation of the up-to-date standard materials for more useful conclusions. For instance, Au- aqua regia prepared catalysts are often presented as the “standard material” to compare the activity of novel catalysts. However, the usage of aqua regia in the catalyst preparation is unattractive and cannot find practical application due to poor activity and stability. If the use of standardized reaction conditions is not feasible, a suitable catalytic standard would greatly facilitate useful comparisons to be made.

6.2 Investigation of different activated carbon supports for the acetylene hydrochlorination reaction.

In this work, a range of commercially available activated carbons have been investigated as supports for the preparation of novel Au-based catalysts for the acetylene

hydrochlorination reaction. The activated carbons used originated from different sources and were activated under different chemical and physical conditions. A wide range of different characterizations were conducted on the activated carbons, including textural studies, porosity analysis, surface graphitization, surface functional group identification, and oxygenated surface acidic sites distribution. In this study, it was validated that association of catalytic activity distinctively with physical properties such as surface area and porosity of the carbon material offers a limited understanding of a catalyst's behaviour. Catalytic activity correlates with the nature, concentration and accessibility of its active sites which is proportional to the physical properties of the materials such as the surface area. In this study we confirmed that the surface chemistry of materials is equally important to the physical properties of the carbon supports. In the study, it was also shown that the instability of the catalysts is associated with the high content of acidic oxygenated functionalities that promote Au agglomeration.

Future work should focus on identifying the role of functional surface groups in the activity and stability of the catalysts. Thermal degradation of the O functional groups can ensure specific oxygenated species on the surface of the supports. Heating up the host materials under inert atmosphere at a range of temperatures, as reported in literature, can enable production of a wide range of hosts bearing only specific functionalities. Using the thermally treated supports, stripped of their functional groups, for the preparation of 1 wt.% Au catalysts would elucidate whether there is a direct correlation between the activity and the existent functional groups. For this reason, thermogravimetric analysis (TGA) in inert gas coupled to mass spectrometry (MS) should be employed for confirmation of evolved gases and remaining functionality. Furthermore, future work should be aimed at establishing the functionalities responsible for the changes in acetylene conversion. STEM analysis should be performed to monitor the distribution of Au and O of fresh and tested catalysts. Also, the microporosity of the materials should be further investigated using CO_2 physisorption. Unlike N_2, that is diffusion restricted into very small micropores, CO_2 can access smaller pores, allowing the analysis to be completed in a couple of hours, instead of the usual 40 hours analysis when utilizing N_2 and CO_2 adsorption is considered complementary to N_2 adsorption for smaller pores. Finally, reactant adsorption studies, for HCl and Acetylene, should be performed on the carbon materials to provide a clearer understanding of the adsorption capacity and differences between the materials.

6.3 Investigation of Single Site Au-Organic Compounds based catalysts for acetylene hydrochlorination reaction.

In this work, a series of Au-Organic compound supported on activated carbon catalysts was prepared via a simple incipient wetness impregnation method, using dry acetone as a solvent, and then studied for the acetylene hydrochlorination. The catalytic assessment suggested that N-methyl-pyrrolidone (NMP) can significantly improve the activity and stability of Au catalysts. Notably, a direct comparison of the Au-NMP catalyst with the commercially validated Au-Thiosulfate illustrated that the activity of the novel Au-NMP catalyst was remarkably higher. Further characterization of the fresh and tested Au-NMP catalyst via Au L_3-edge XANES confirmed that the Au appeared as cationic Au(I)/Au(III) on the carbon support. The high activity of the Au-NMP catalyst compared to the Au/AC catalyst is associated with the higher level of Au(I) content. In addition, the thorough characterization of the isolated Au-NMP crystal confirmed that the NMP is coordinating to the Au center via the N interactions. In particular, NMR, IR, Raman and Single crystal diffraction studies suggested the presence of a Au-NMP complex. The Au-NMP was confirmed to be a Au and NMP salt unit rather than a Au and NMP ligand moiety with a structure ratio of 1:2 respectively. Unfortunately, it has not been feasible to identify via XAFs studies the nature of the Au-NMP unit upon the deposition on the carbon support. Finally, a sequence of Au-NMP derivatives has also been studied. The presence of both O and N functionalities of the NMP unit was identified to be crucial for the activity of the Au-NMP catalyst. The coexistence of O and N on the structure of the molecule seems to be displaying a crucial effect in stabilising and improving the activity of the Au center. This study suggests that NMP can be a great candidate for efficient and effective, well stabilized Au-based catalysts.

Future work should focus on confirming the role of the NMP. DFT studies are required to confirm the plausibility of the NMP on stabilizing the active Au centres under working conditions. In situ-XAFS studies should be performed with the aim of monitoring the change of the speciation species of the Au centres during the reaction. In this study, the formation of the Au nanoparticles was apparent, yet the determination of the conditions that lead to their formation is vital. Furthermore, the scope of NMP derivatives should also be expanded, with more compounds to be investigated. It would be interesting to study compounds that have additional similarities to the NMP. Finally, it would be interesting to expand the scope of the M-NMP candidates, where M is Pt, Cu, Ir, Rh to investigate whether similar effects are observed across other metals.

Appendix

Chapter 4

Investigation of different activated carbon supports for the acetylene hydrochlorination reaction.

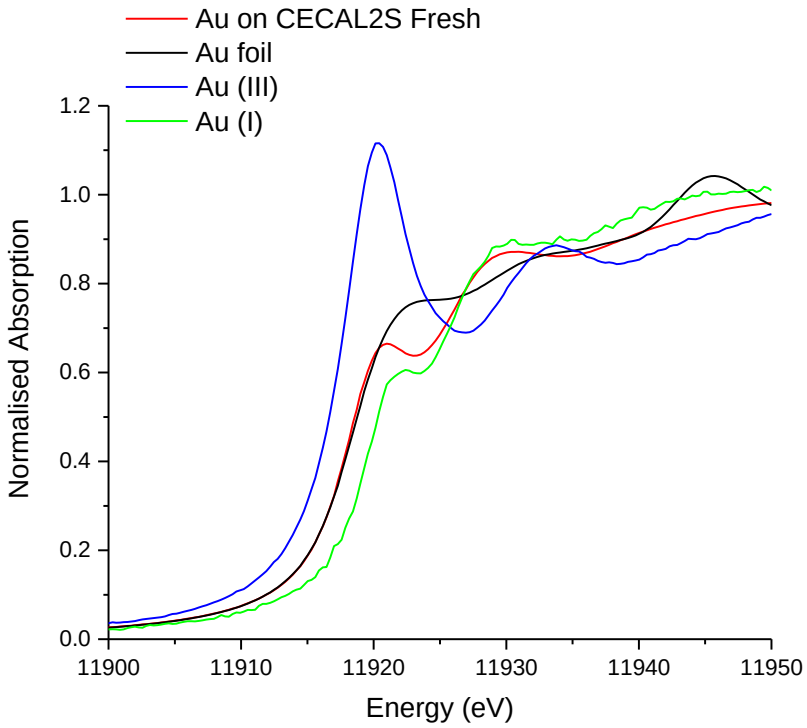

Figure S.4.1: Au L_3-edge XANES of fresh Au on CECAL2S catalyst, $KAuCl_4$/$[AuCl_4]^-$ (Au(III)), $[AuCl_2]^-$ (Au(I) and Au foil (Au(0)).

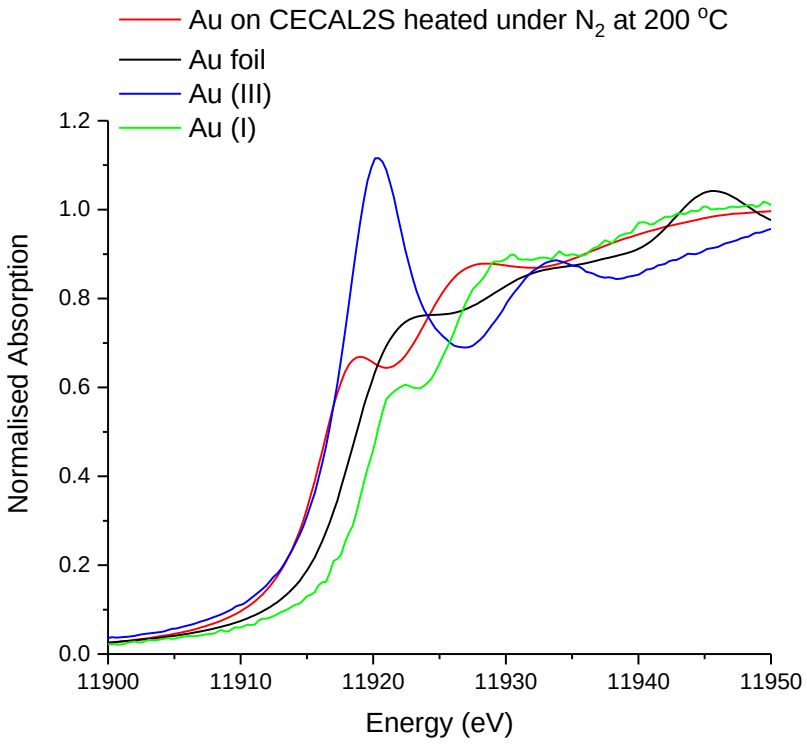

Figure S.4.2: Au L_3-edge XANES of fresh Au on CECAL2S heated under N_2 at 200 °C catalyst, $KAuCl_4$/$[AuCl_4]^-$ (Au(III)), $[AuCl_2]^-$ (Au(I) and Au foil (Au(0)).

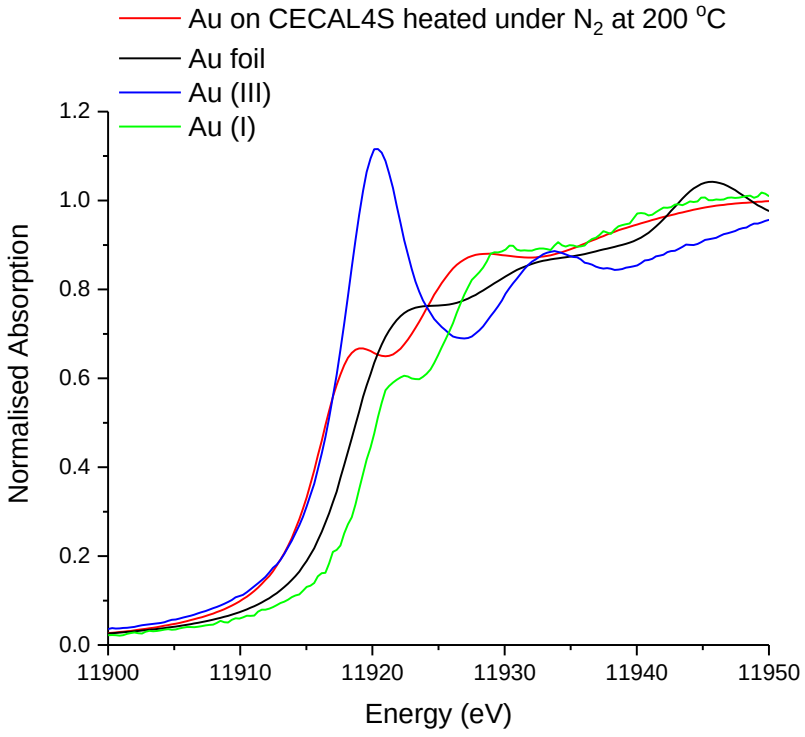

Figure S.4.3: Au L_3-edge XANES of fresh Au on CECAL4S fresh catalyst, $KAuCl_4$/$[AuCl_4]^-$ (Au(III)), $[AuCl_2]^-$ (Au(I) and Au foil (Au(0)).

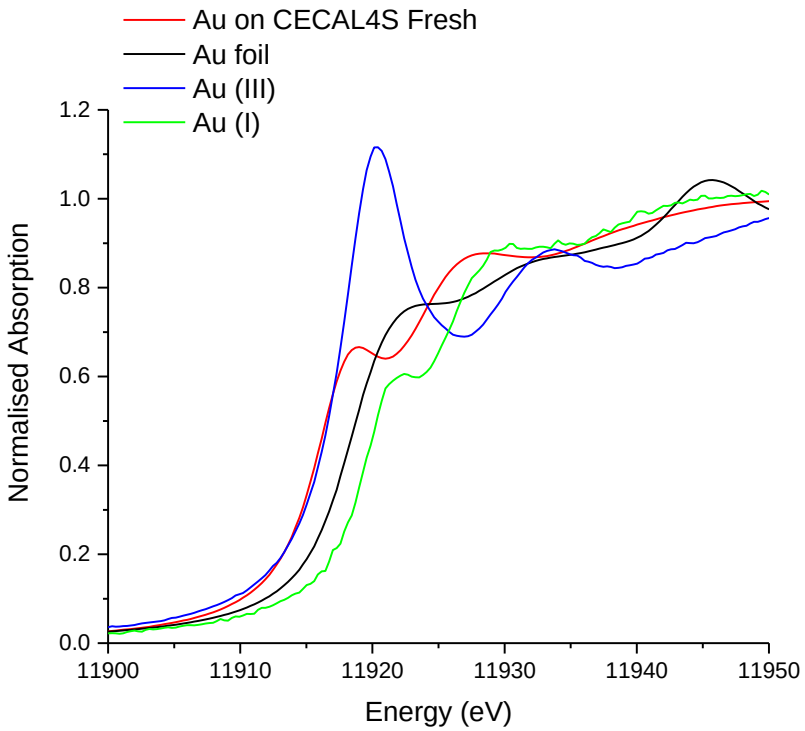

Figure S.4.4: Au L_3-edge XANES of fresh Au on CECAL4S heated under N_2 at 200 ^oC catalyst, $KAuCl_4$/$[AuCl_4]^-$ (Au(III)), $[AuCl_2]^-$ (Au(I) and Au foil (Au(0)).

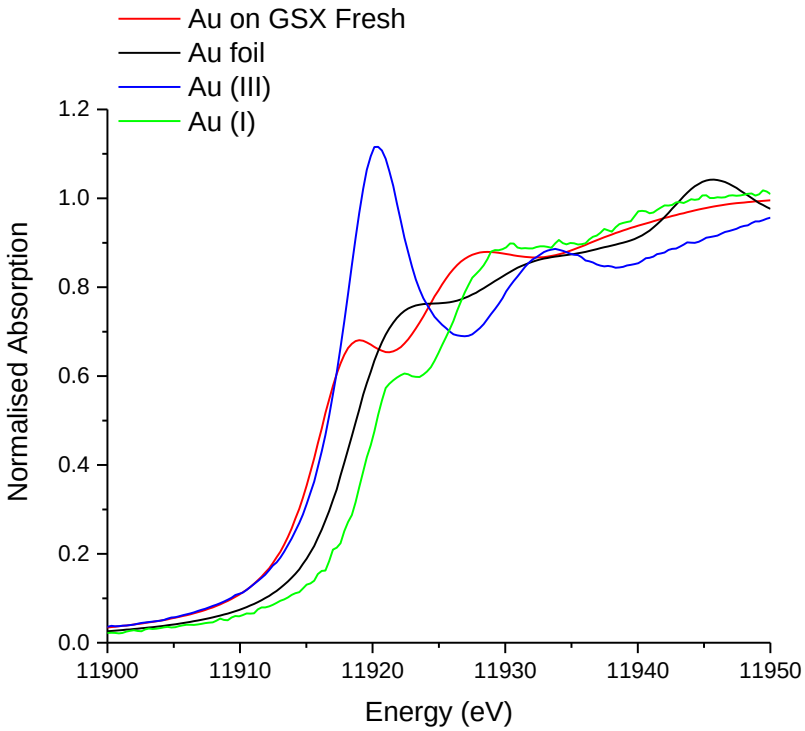

Figure S.4.5: Au L_3-edge XANES of fresh Au on GSX catalyst, $KAuCl_4$/$[AuCl_4]^-$ (Au(III)), $[AuCl_2]^-$ (Au(I) and Au foil (Au(0)).

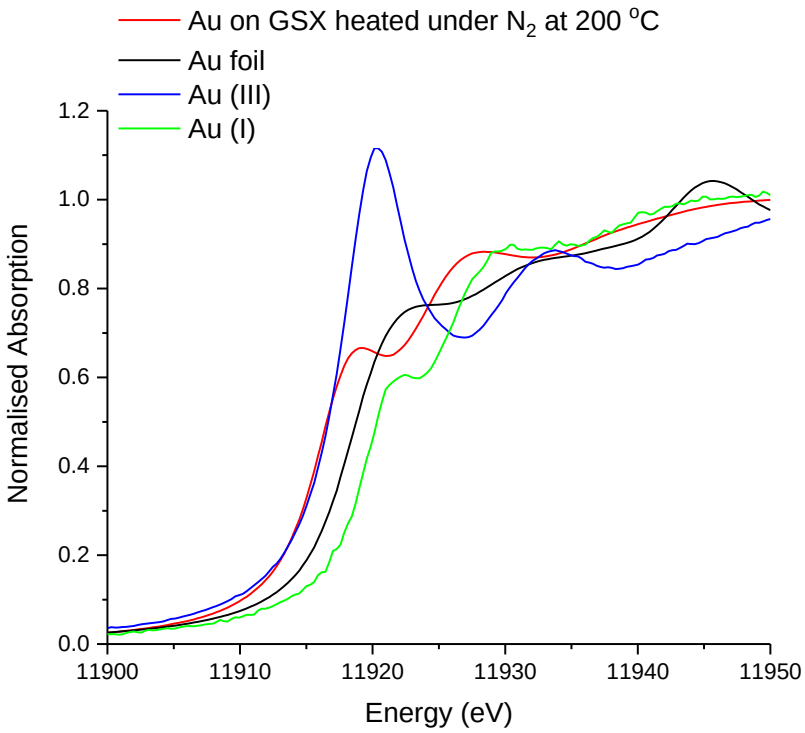

Figure S.4.6: Au L_3-edge XANES of fresh Au on GSX heated under N_2 at 200 °C catalyst, $KAuCl_4$/$[AuCl_4]^-$ (Au(III)), $[AuCl_2]^-$ (Au(I) and Au foil (Au(0)).

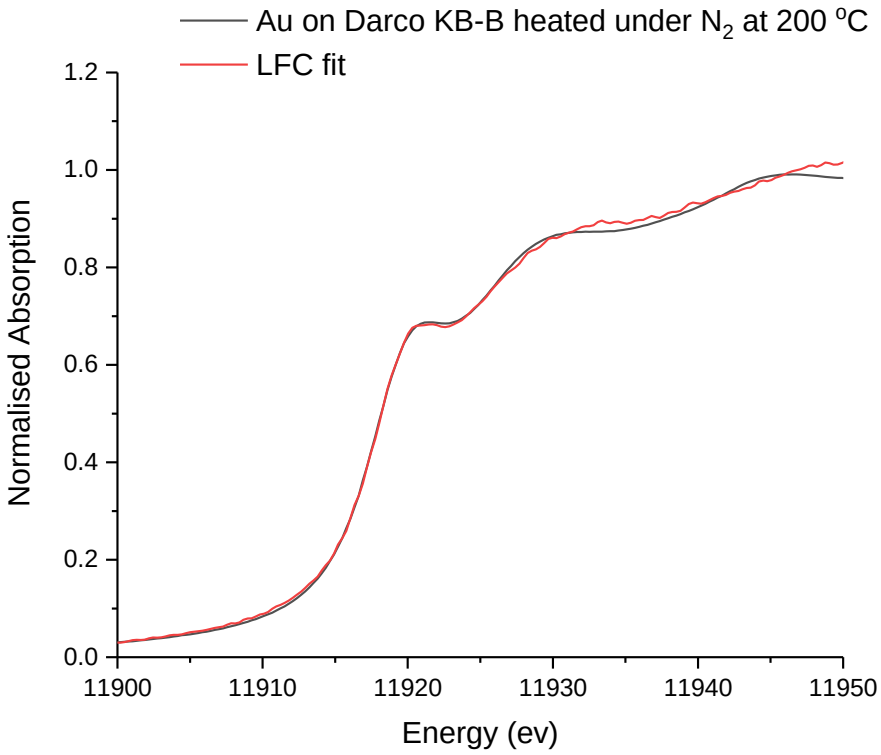

Figure S.4.7: XANES data fitting for Au on Darco KB-B heated under N_2 at 200 °C.

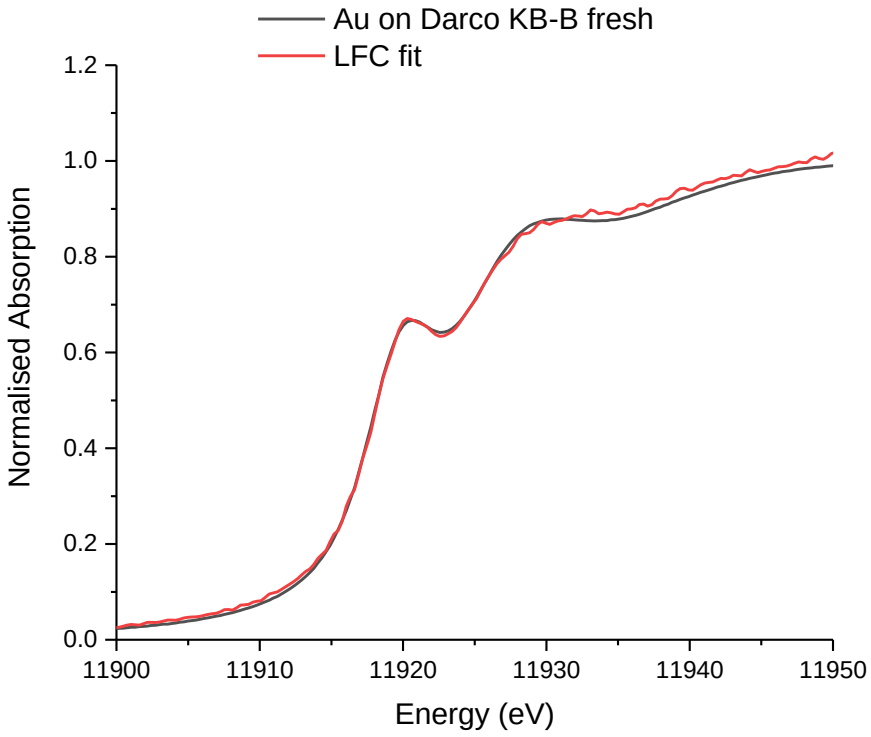

Figure S.4.8: XANES data fitting for Au on Darco KB-B fresh.

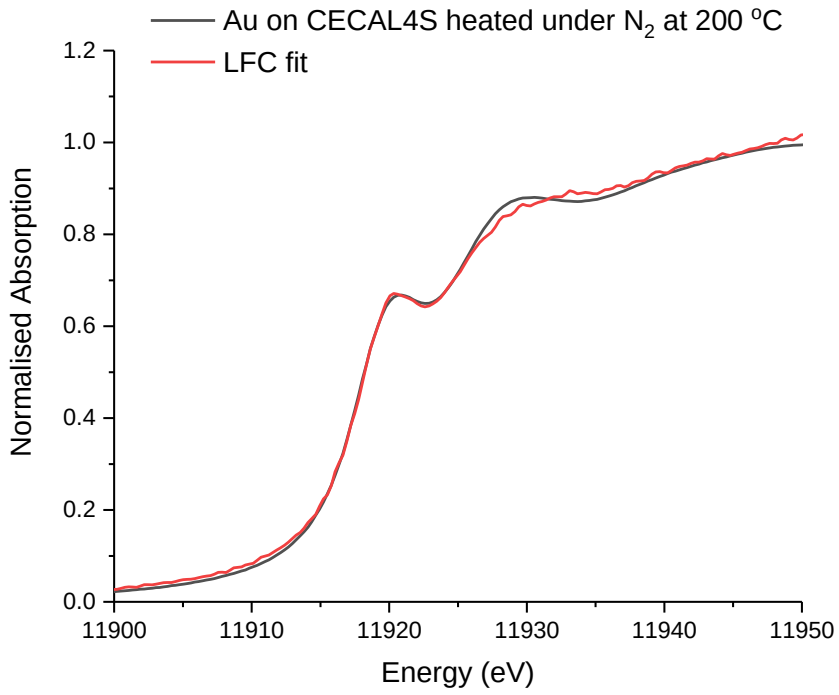

Figure S.4.9: XANES data fitting for Au on CECAL4S heated under N_2 at 200 °C.

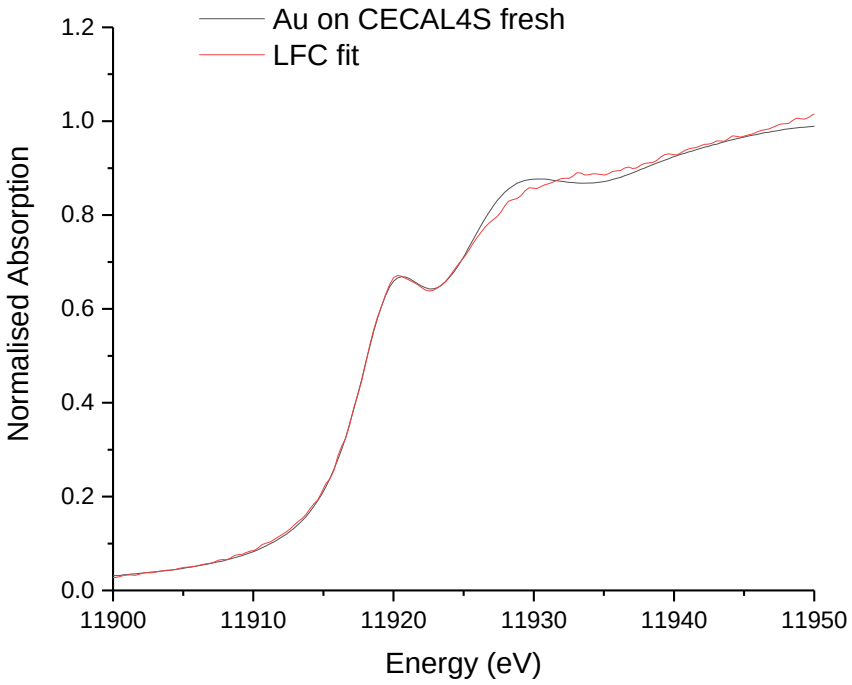

Figure S.4.10: XANES data fitting for Au on CECAL4S fresh.

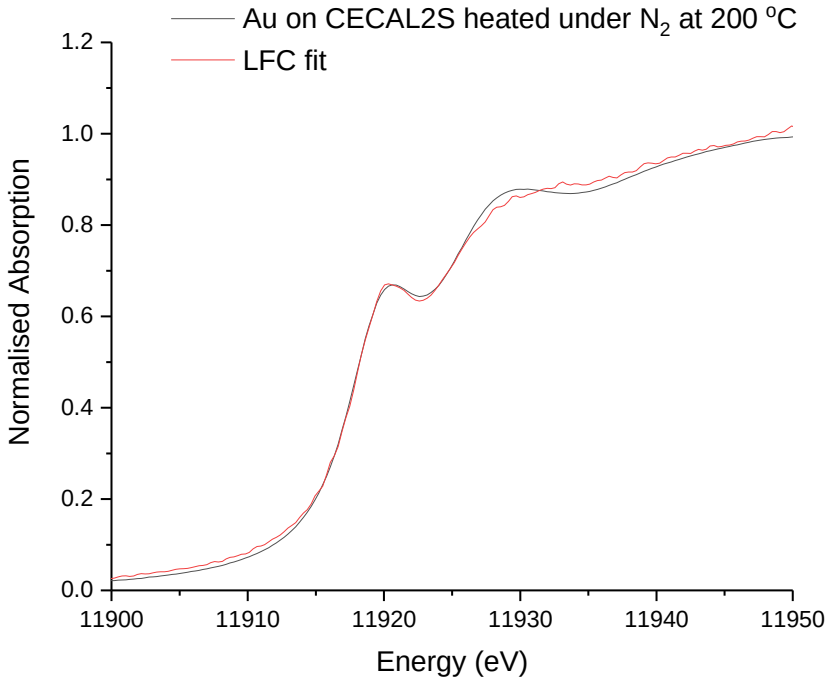

Figure S.4.11: XANES data fitting for Au on CECAL2S heated under N_2 at 200 ^oC.

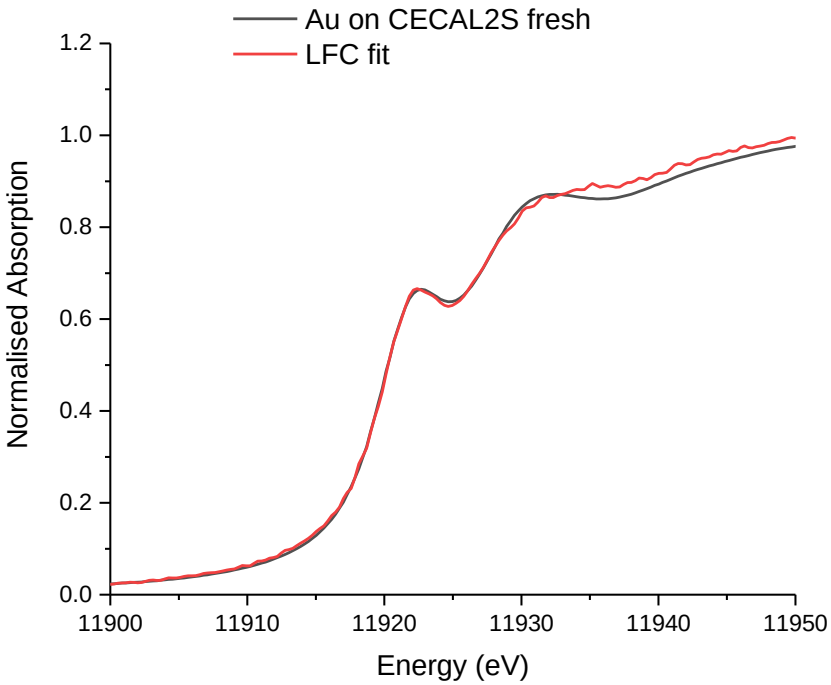

Figure S.4.12: XANES data fitting for Au on CECAL2S fresh.

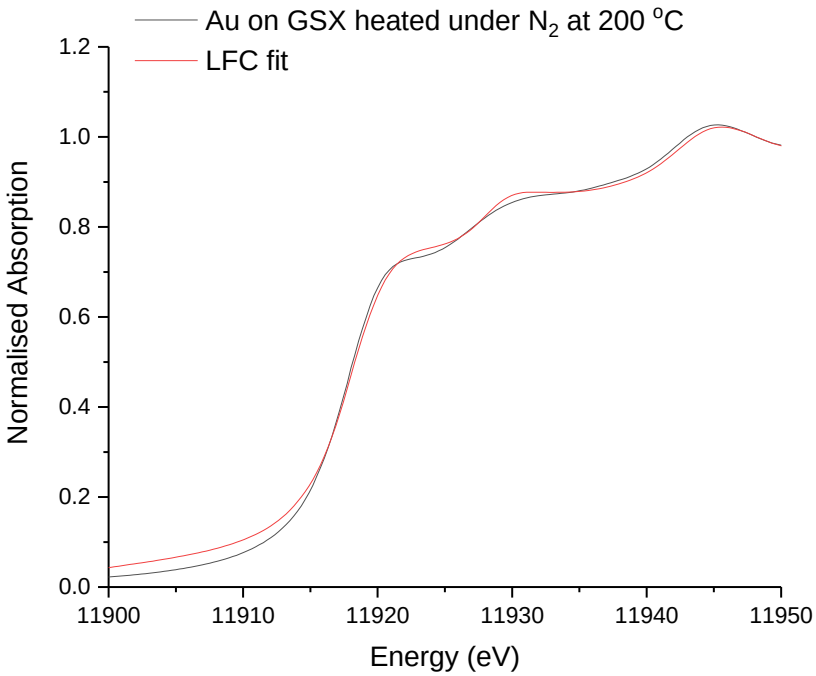

Figure S.4.13: XANES data fitting for Au on GSX heated under N_2 at 200 °C.

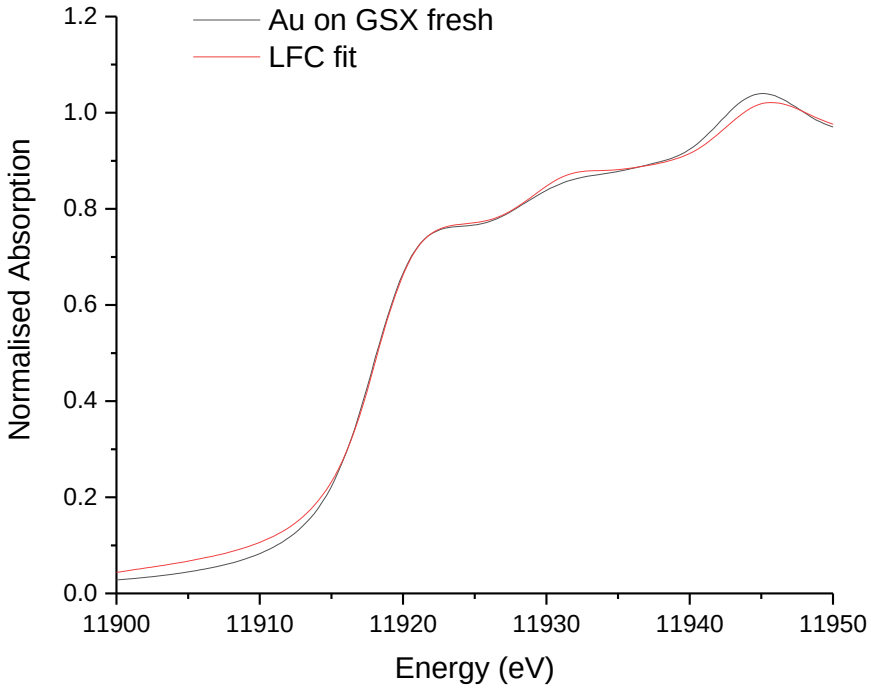

Figure S.4.14: XANES data fitting for Au on GSX fresh.

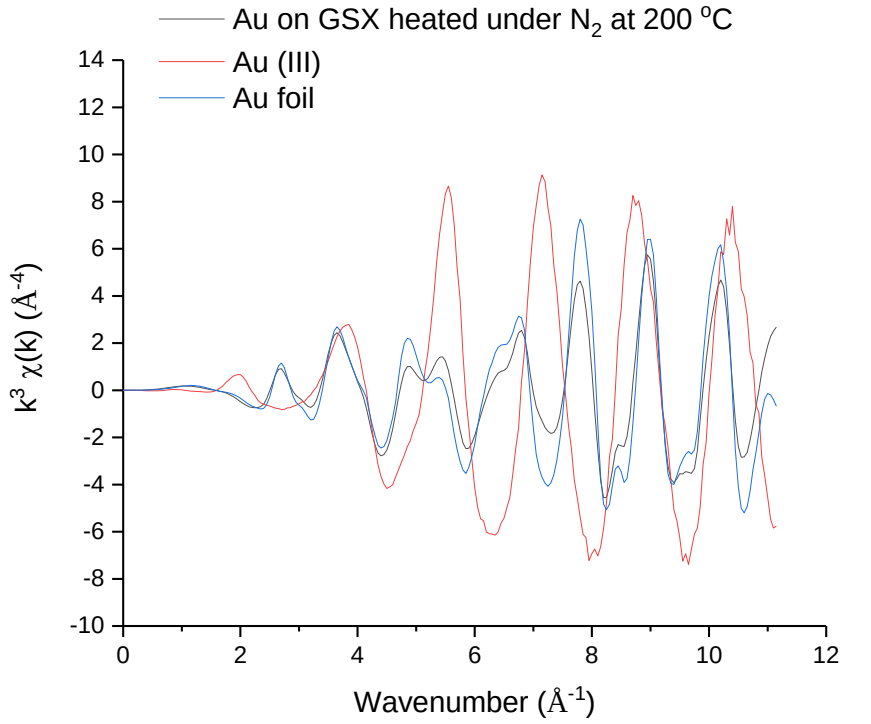

Figure S.4.15: Experimental k^3-weighted EXAFS data for the Au on GSX heated under N_2 at 200 °C.

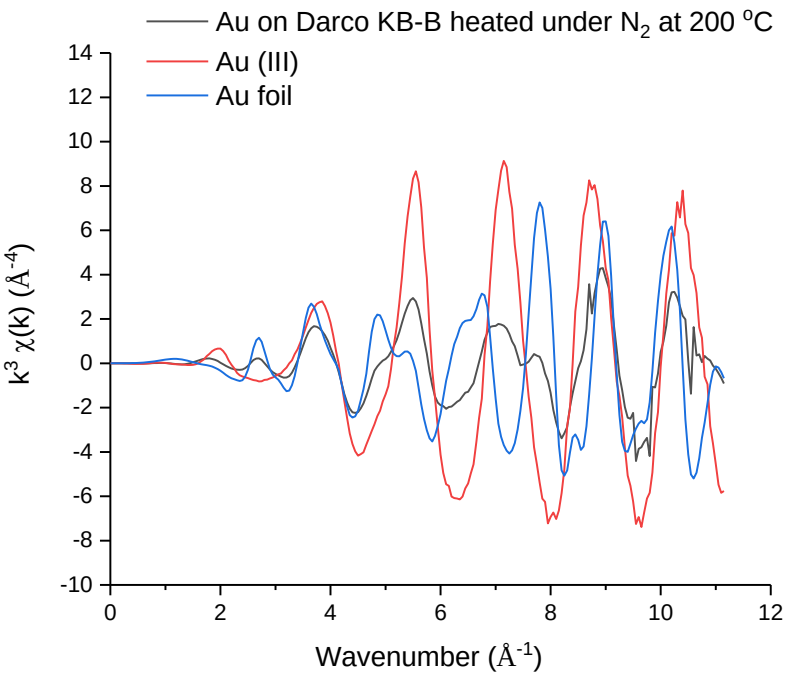

Figure S.4.16: Experimental k^3-weighted EXAFS data for the Au on Darco KB-B heated under N_2 at 200 °C.

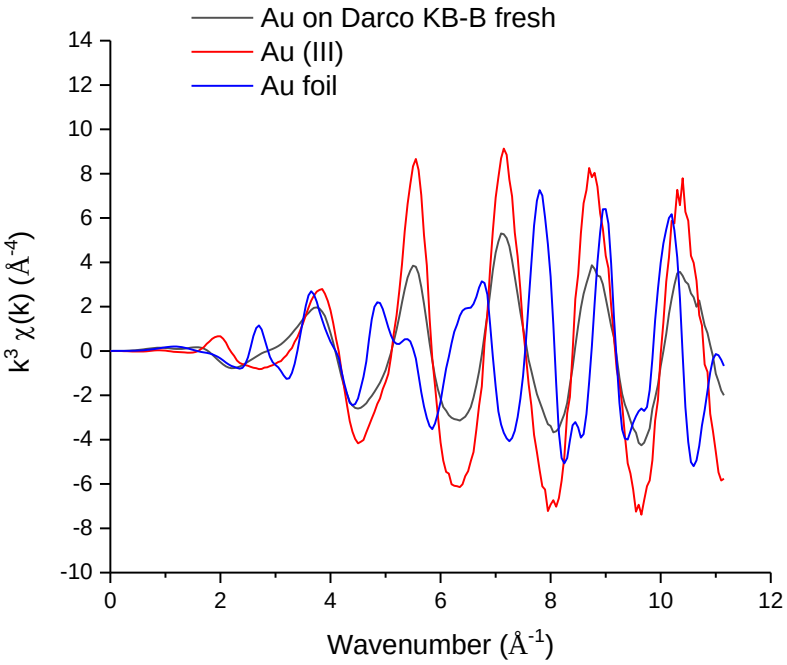

Figure S.4.17: Experimental k^3-weighted EXAFS data for the Au on Darco KB-B fresh.

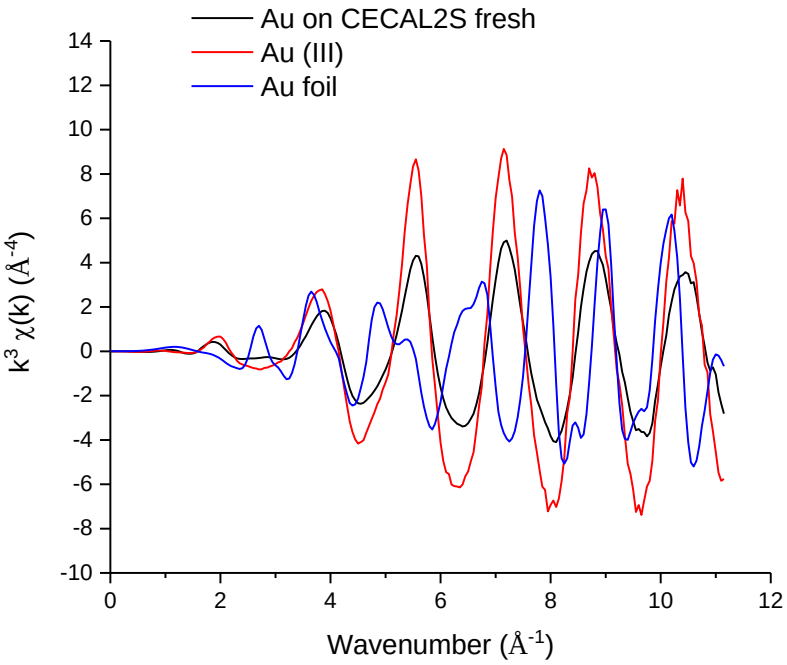

Figure S.4.18: Experimental k^3-weighted EXAFS data for the Au on CECAL2S fresh.

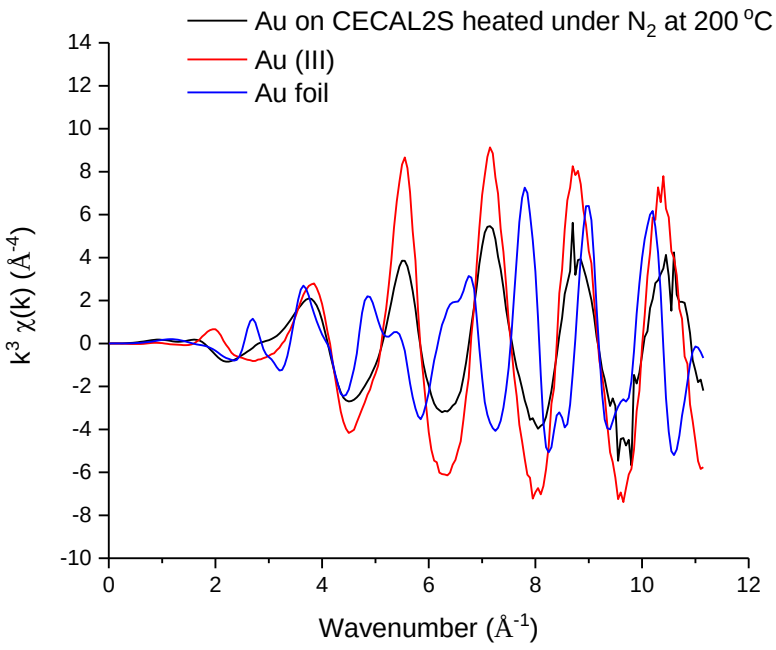

Figure S.4.19: Experimental k^3-weighted EXAFS data for the Au on CECAL2S heated under N_2 at 200 °C.

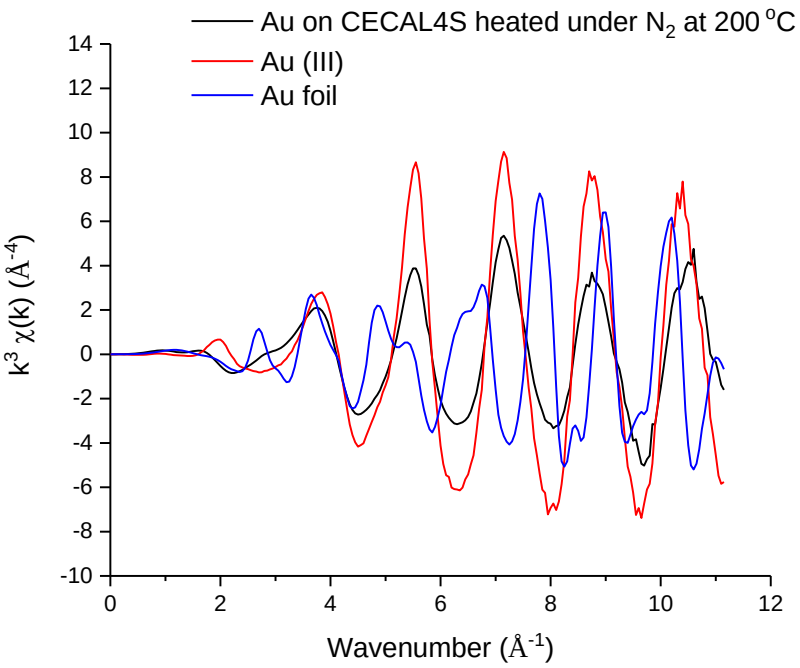

Figure S.4.20: Experimental k^3-weighted EXAFS data for the Au on CECAL4S heated under N_2 at 200 °C.

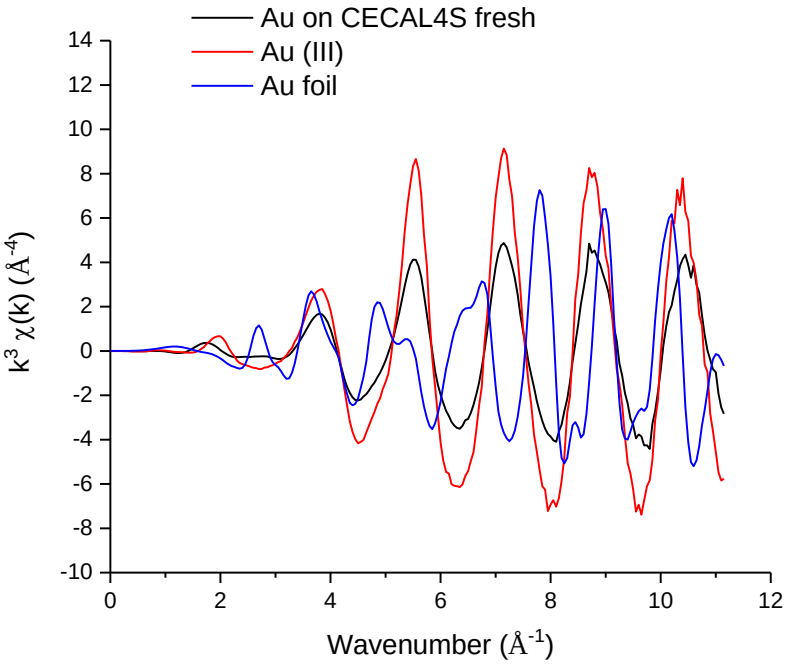

Figure S.4.21: Experimental k^3-weighted EXAFS data for the Au on CECAL4S fresh.

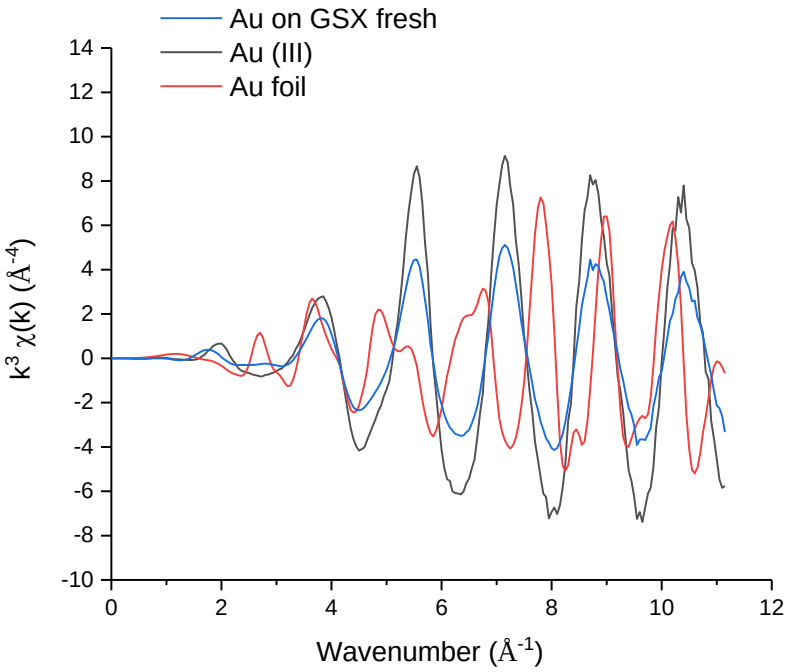

Figure S.4.22: Experimental k^3-weighted EXAFS data for the Au on GSX fresh.

Chapter 5

Investigation of Single Site Au-Organic Compound based catalysts for acetylene hydrochlorination.

Table S.5.1.

Crystal data and structure refinement for gjh2201.

Empirical formula	$C_{10}H_{19}AuCl_4N_2O_2$	
Formula weight	538.04	
Temperature	296(2) K	
Wavelength	0.71073 Å	
Crystal system	Monoclinic	
Space group	P 2_1/n	
Unit cell dimensions	a = 14.2719(8) Å	a= 90°.
	b = 7.6086(5) Å	b= 98.485(7)°.
	c = 16.5447(15) Å	g = 90°.
Volume	1776.9(2) $Å^3$	
Z	4	
Density (calculated)	2.011 Mg/m^3	
Absorption coefficient	8.879 mm^{-1}	
F(000)	1024	
Crystal size	0.380 x 0.140 x 0.090 mm^3	
Theta range for data collection	3.366 to 29.715°.	
Index ranges	-19<=h<=18, -10<=k<=10, -22<=l<=13	
Reflections collected	16208	
Independent reflections	4384 [R(int) = 0.0307]	
Completeness to theta = 25.242°	99.8 %	
Refinement method	Full-matrix least-squares on F^2	
Data / restraints / parameters	4384 / 0 / 175	
Goodness-of-fit on F^2	1.026	
Final R indices [I>2sigma(I)]	R1 = 0.0304, wR2 = 0.0527	
R indices (all data)	R1 = 0.0512, wR2 = 0.0598	
Largest diff. peak and hole	0.708 and -0.940 e.$Å^{-3}$	

Table S.5.2. Atomic coordinates (x 10^4) and equivalent isotropic displacement parameters ($Å^2$x 10^3)
for gjh2201. U(eq) is defined as one third of the trace of the orthogonalized U^{ij} tensor.

	x	y	z	U(eq)
C(1)	7937(3)	8331(5)	4676(3)	58(1)
C(2)	8911(3)	8903(7)	5012(4)	76(1)
C(3)	8921(5)	8941(8)	5922(4)	105(2)
C(4)	7918(5)	8521(7)	6067(4)	99(2)
C(5)	6416(3)	7679(7)	5113(4)	93(2)
C(6)	9072(3)	7310(6)	2700(3)	60(1)
C(7)	8796(3)	5484(7)	2827(3)	82(2)
C(8)	9448(4)	4436(7)	2376(4)	99(2)
C(9)	9912(4)	5736(7)	1862(4)	87(2)
C(10)	10059(4)	9048(8)	1905(4)	97(2)
N(1)	7415(3)	8152(5)	5259(3)	67(1)
N(2)	9687(2)	7421(5)	2198(2)	65(1)
O(1)	7624(2)	8072(4)	3939(2)	74(1)
O(2)	8770(3)	8679(4)	3024(2)	82(1)
Au(1)	2477(1)	6713(1)	4490(1)	56(1)
Cl(1)	944(1)	5932(2)	4497(1)	95(1)
Cl(2)	2619(1)	7191(2)	5852(1)	100(1)
Cl(3)	4017(1)	7456(2)	4502(1)	98(1)
Cl(4)	2329(1)	6246(3)	3129(1)	119(1)

Table S.5.3. Bond lengths [Å] and angles [°] for gjh2201.

C(1)-O(1)	1.251(6)
C(1)-N(1)	1.310(6)
C(1)-C(2)	1.484(6)
C(2)-C(3)	1.505(8)
C(2)-H(2A)	0.9700
C(2)-H(2B)	0.9700
C(3)-C(4)	1.520(8)

C(3)-H(3A)	0.9700
C(3)-H(3B)	0.9700
C(4)-N(1)	1.449(7)
C(4)-H(4A)	0.9700
C(4)-H(4B)	0.9700
C(5)-N(1)	1.455(6)
C(5)-H(5A)	0.9600
C(5)-H(5B)	0.9600
C(5)-H(5C)	0.9600
C(6)-O(2)	1.275(5)
C(6)-N(2)	1.298(5)
C(6)-C(7)	1.467(7)
C(7)-C(8)	1.504(7)
C(7)-H(7A)	0.9700
C(7)-H(7B)	0.9700
C(8)-C(9)	1.520(8)
C(8)-H(8A)	0.9700
C(8)-H(8B)	0.9700
C(9)-N(2)	1.452(6)
C(9)-H(9A)	0.9700
C(9)-H(9B)	0.9700
C(10)-N(2)	1.456(6)
C(10)-H(10A)	0.9600
C(10)-H(10B)	0.9600
C(10)-H(10C)	0.9600
O(2)-H(2)	0.8200
Au(1)-Cl(4)	2.2579(18)
Au(1)-Cl(2)	2.2614(17)
Au(1)-Cl(3)	2.2675(12)
Au(1)-Cl(1)	2.2680(11)

O(1)-C(1)-N(1)	122.8(4)
O(1)-C(1)-C(2)	126.2(4)
N(1)-C(1)-C(2)	111.0(5)
C(1)-C(2)-C(3)	104.5(4)
C(1)-C(2)-H(2A)	110.9
C(3)-C(2)-H(2A)	110.9
C(1)-C(2)-H(2B)	110.9

C(3)-C(2)-H(2B)	110.9
H(2A)-C(2)-H(2B)	108.9
C(2)-C(3)-C(4)	106.5(5)
C(2)-C(3)-H(3A)	110.4
C(4)-C(3)-H(3A)	110.4
C(2)-C(3)-H(3B)	110.4
C(4)-C(3)-H(3B)	110.4
H(3A)-C(3)-H(3B)	108.6
N(1)-C(4)-C(3)	104.2(5)
N(1)-C(4)-H(4A)	110.9
C(3)-C(4)-H(4A)	110.9
N(1)-C(4)-H(4B)	110.9
C(3)-C(4)-H(4B)	110.9
H(4A)-C(4)-H(4B)	108.9
N(1)-C(5)-H(5A)	109.5
N(1)-C(5)-H(5B)	109.5
H(5A)-C(5)-H(5B)	109.5
N(1)-C(5)-H(5C)	109.5
H(5A)-C(5)-H(5C)	109.5
H(5B)-C(5)-H(5C)	109.5
O(2)-C(6)-N(2)	121.2(4)
O(2)-C(6)-C(7)	126.8(4)
N(2)-C(6)-C(7)	112.0(4)
C(6)-C(7)-C(8)	103.4(4)
C(6)-C(7)-H(7A)	111.1
C(8)-C(7)-H(7A)	111.1
C(6)-C(7)-H(7B)	111.1
C(8)-C(7)-H(7B)	111.1
H(7A)-C(7)-H(7B)	109.0
C(7)-C(8)-C(9)	106.6(4)
C(7)-C(8)-H(8A)	110.4
C(9)-C(8)-H(8A)	110.4
C(7)-C(8)-H(8B)	110.4
C(9)-C(8)-H(8B)	110.4
H(8A)-C(8)-H(8B)	108.6
N(2)-C(9)-C(8)	102.8(4)
N(2)-C(9)-H(9A)	111.2
C(8)-C(9)-H(9A)	111.2

N(2)-C(9)-H(9B)	111.2
C(8)-C(9)-H(9B)	111.2
H(9A)-C(9)-H(9B)	109.1
N(2)-C(10)-H(10A)	109.5
N(2)-C(10)-H(10B)	109.5
H(10A)-C(10)-H(10B)	109.5
N(2)-C(10)-H(10C)	109.5
H(10A)-C(10)-H(10C)	109.5
H(10B)-C(10)-H(10C)	109.5
C(1)-N(1)-C(4)	113.6(5)
C(1)-N(1)-C(5)	123.6(5)
C(4)-N(1)-C(5)	122.7(5)
C(6)-N(2)-C(9)	113.4(4)
C(6)-N(2)-C(10)	125.5(4)
C(9)-N(2)-C(10)	120.8(4)
C(6)-O(2)-H(2)	109.5
Cl(4)-Au(1)-Cl(2)	179.74(6)
Cl(4)-Au(1)-Cl(3)	89.74(7)
Cl(2)-Au(1)-Cl(3)	90.39(6)
Cl(4)-Au(1)-Cl(1)	90.91(7)
Cl(2)-Au(1)-Cl(1)	88.96(6)
Cl(3)-Au(1)-Cl(1)	178.91(6)

Table S.4.4 Anisotropic displacement parameters ($Å^2 x\ 10^3$) for gjh2201. The anisotropic displacement factor exponent takes the form: $-2p^2[\ h^2a^{*2}U^{11} + ... + 2\ h\ k\ a^*\ b^*\ U^{12}\ ]$

	U^{11}	U^{22}	U^{33}	U^{23}	U^{13}	U^{12}
C(1)	53(2)	61(3)	63(3)	2(2)	17(2)	7(2)
C(2)	58(2)	80(3)	89(5)	-8(3)	4(3)	2(2)
C(3)	122(5)	91(4)	91(6)	-1(4)	-25(4)	11(4)
C(4)	167(6)	71(3)	62(4)	4(3)	32(4)	16(3)
C(5)	80(3)	87(3)	124(6)	14(4)	59(3)	8(3)
C(6)	62(2)	74(3)	46(3)	-2(2)	8(2)	1(2)
C(7)	90(3)	84(4)	70(4)	9(3)	5(3)	-15(3)
C(8)	126(5)	79(4)	86(5)	-6(3)	-10(4)	16(3)
C(9)	84(3)	97(4)	77(4)	-16(3)	5(3)	18(3)
C(10)	115(4)	105(4)	79(5)	-5(4)	41(4)	-23(4)
N(1)	74(2)	69(2)	63(3)	3(2)	28(2)	9(2)

N(2)	65(2)	81(3)	48(3)	-8(2)	10(2)	0(2)
O(1)	62(2)	101(3)	61(3)	-8(2)	13(2)	-3(2)
O(2)	99(3)	89(2)	67(3)	-2(2)	41(2)	-1(2)
Au(1)	51(1)	51(1)	65(1)	2(1)	8(1)	4(1)
Cl(1)	53(1)	95(1)	137(2)	-17(1)	13(1)	-7(1)
Cl(2)	105(1)	127(1)	68(1)	-9(1)	10(1)	-13(1)
Cl(3)	62(1)	102(1)	135(2)	7(1)	28(1)	-12(1)
Cl(4)	137(1)	156(2)	64(1)	-7(1)	11(1)	16(1)

Table S.5.5 Hydrogen coordinates (x 10^4) and isotropic displacement parameters ($Å^2$x 10^3) for gjh2201.

	x	y	z	U(eq)
H(2A)	9044	10060	4809	91
H(2B)	9377	8080	4866	91
H(3A)	9110	10092	6140	126
H(3B)	9361	8074	6187	126
H(4A)	7910	7508	6422	118
H(4B)	7638	9514	6312	118
H(5A)	6039	8706	5163	139
H(5B)	6290	6818	5507	139
H(5C)	6262	7201	4573	139
H(7A)	8138	5283	2601	98
H(7B)	8889	5188	3403	98
H(8A)	9093	3562	2030	119
H(8B)	9923	3840	2759	119
H(9A)	10592	5554	1921	104
H(9B)	9648	5645	1288	104
H(10A)	9802	10031	2163	145
H(10B)	9882	9130	1324	145
H(10C)	10737	9055	2037	145
H(2)	8341	8405	3279	123

❖ *1 wt.% Au-N-Methylpyrrolidine**(acetone)***
molar ration of Au to OL is 1:2, ***time 0***

❖ *1 wt.% Au-N-Methylpyrrolidine**(acetone)***
molar ration of Au to OL is 1:2, ***time 16h***

Figure S.5.1: Solution of Au-N-methylpyrrolidine molar ratio 1 to 2 in dry acetone a) at time = 0h and b) 16h later.

❖ *1 wt.% Au-N-Methylpyrrolidine**(acetone)***
molar ration of Au to OL is 1:4, ***time 0***

❖ *1 wt.% Au-N-Methylpyrrolidine**(acetone)***
molar ration of Au to OL is 1:4, ***time 16h***

Figure S.5.2: Solution of Au-N-methylpyrrolidine molar ratio 1 to 4 in acetone a) at time = 0h and b) 16h later.

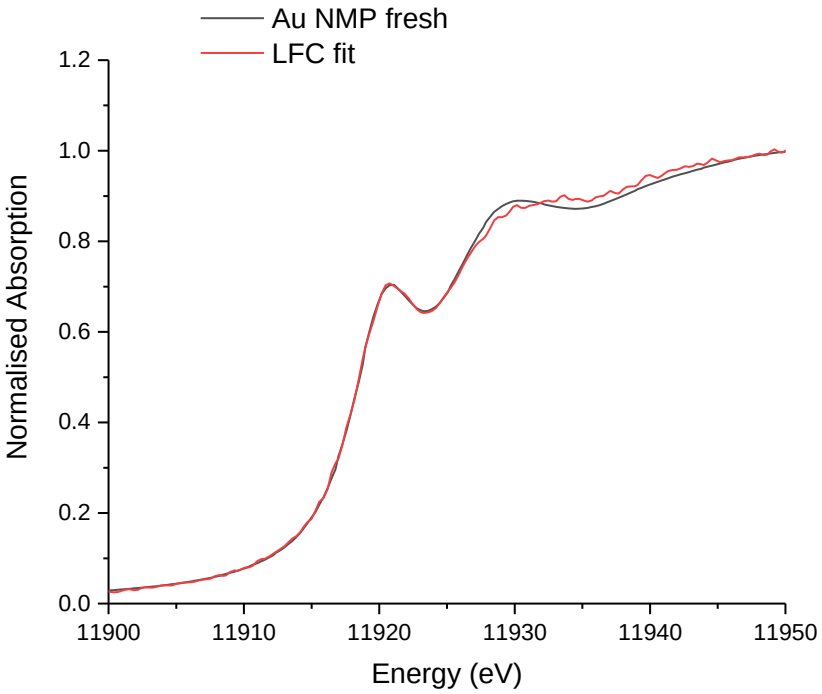

Figure S.5.3: XANES data fitting for Au-NMP fresh.

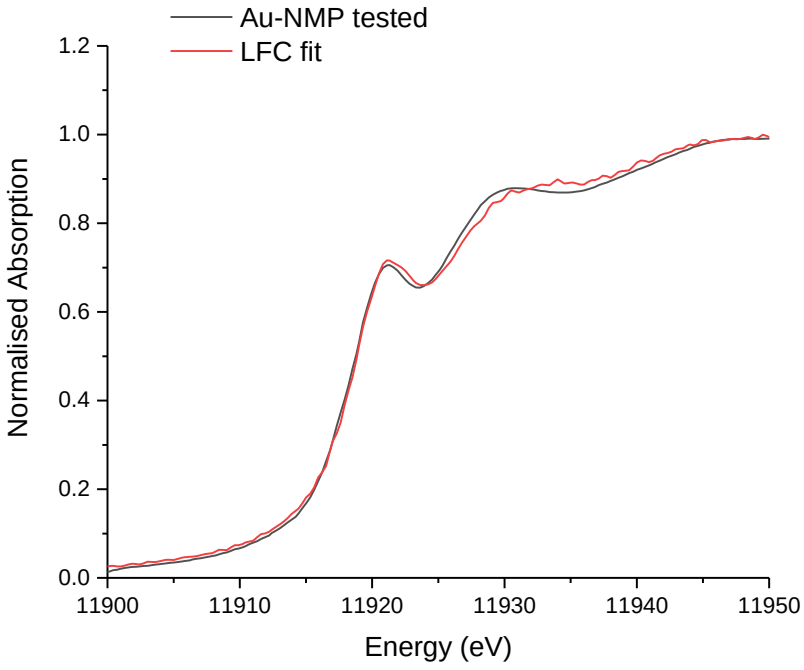

Figure S.5.4: XANES data fitting for Au-NMP tested.

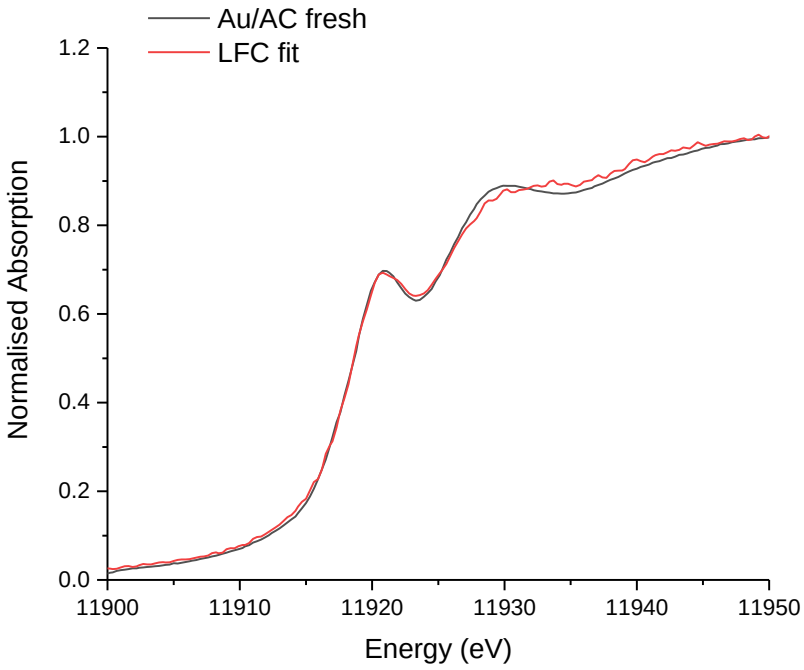

Figure S.5.6: XANES data fitting for Au/AC fresh.

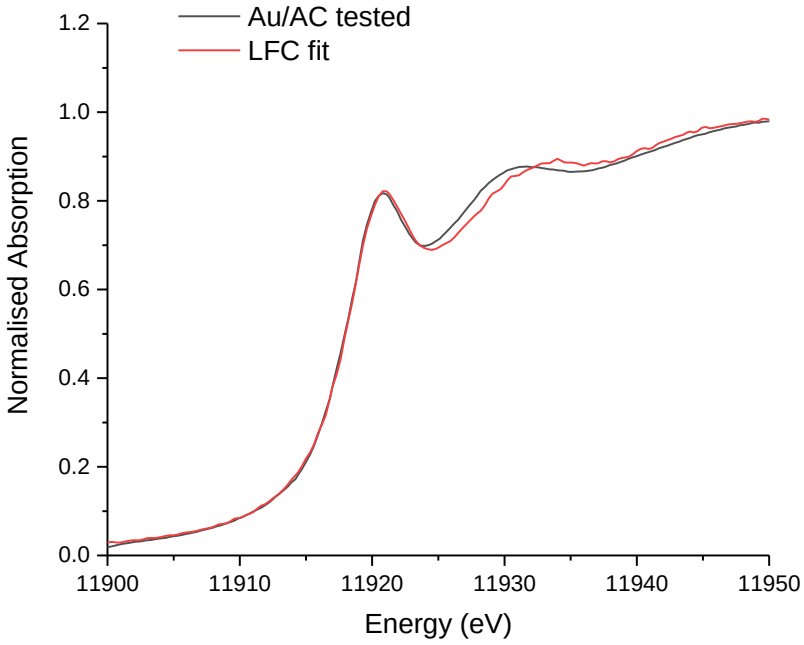

Figure S.5.7: XANES data fitting for Au/AC tested.

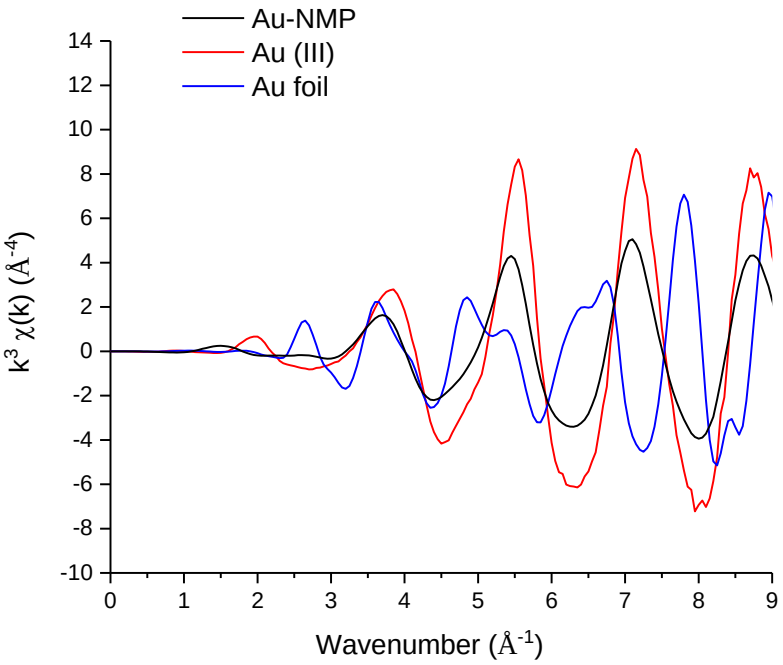

Figure S.5.8: Experimental k^3-weighted EXAFS data for the Au-NMP.

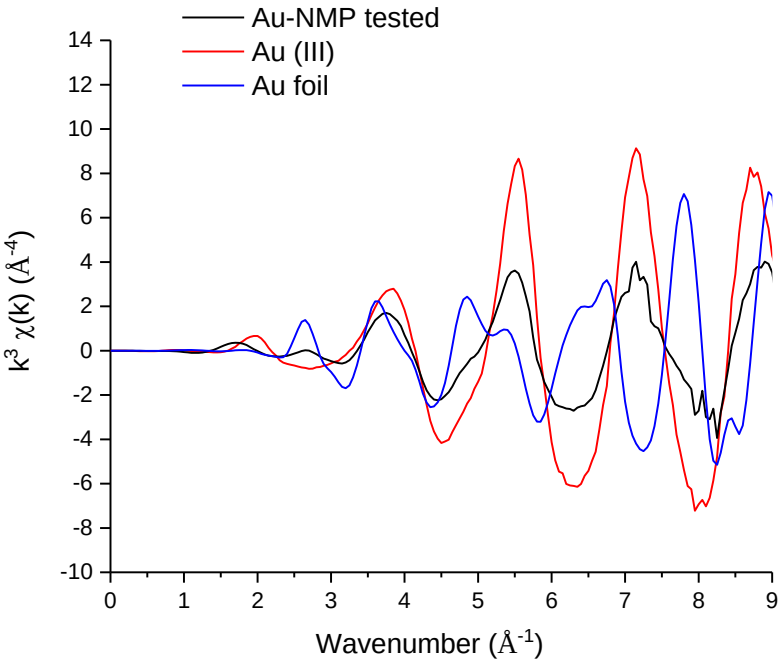

Figure S.5.9: Experimental k^3-weighted EXAFS data for the Au-NMP tested.

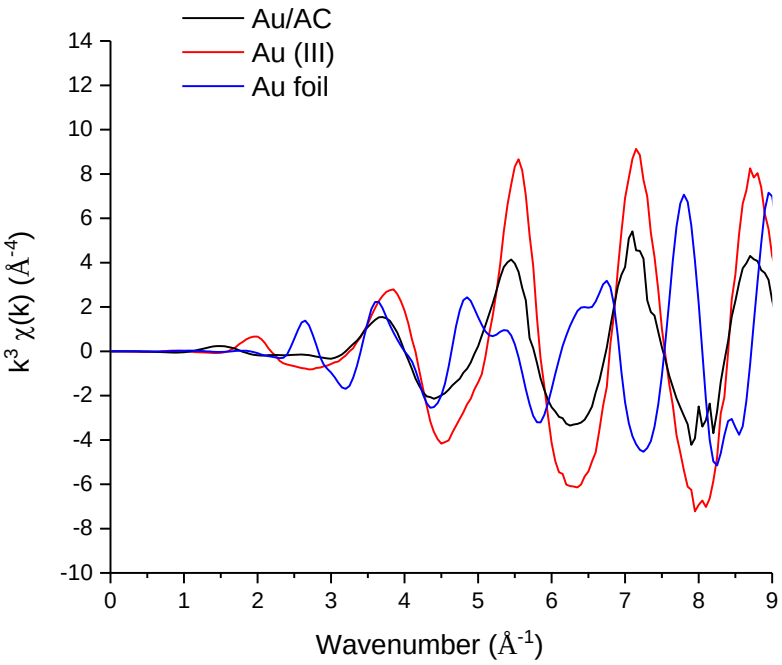

Figure S.5.10: Experimental k^3-weighted EXAFS data for the Au/AC.

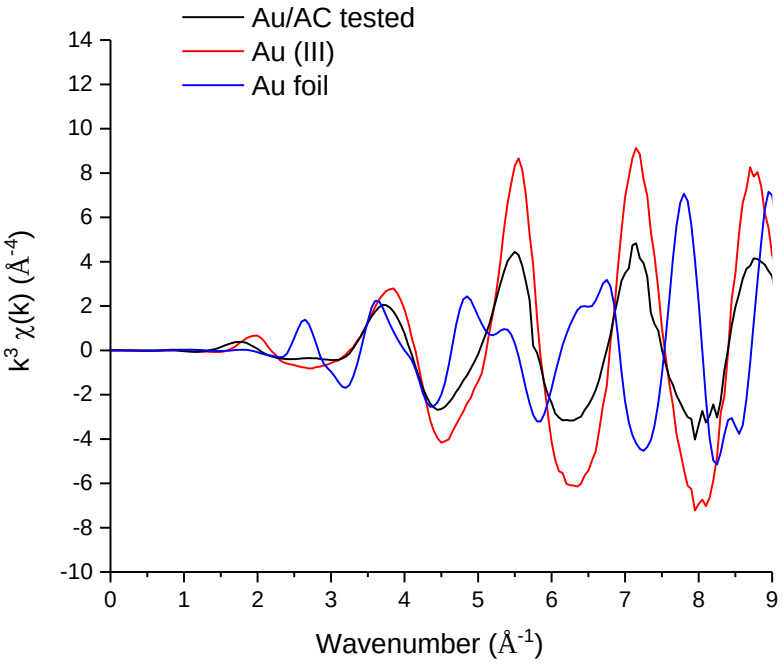

Figure S.5.11: Experimental k^3-weighted EXAFS data for the Au/AC tested.

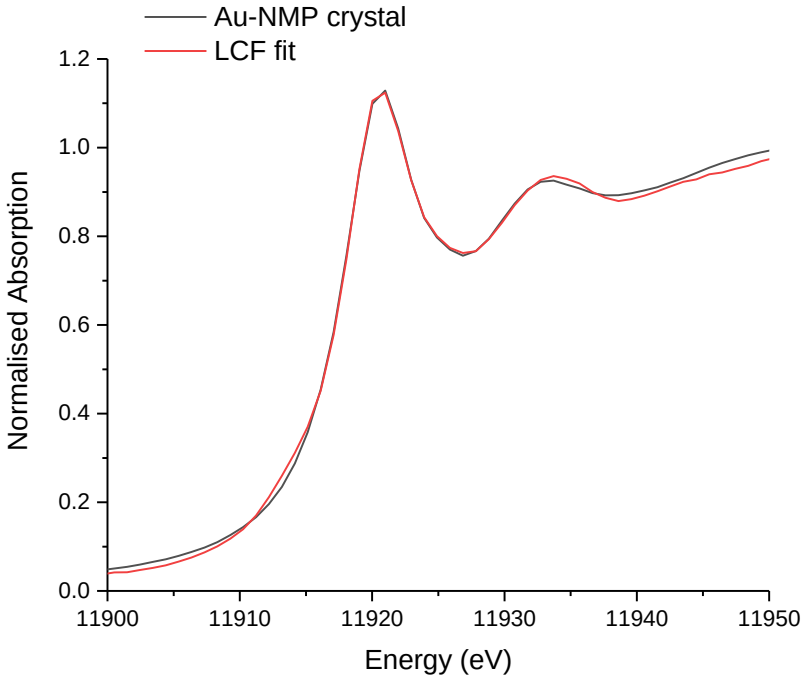

Figure S.5.12: XANES data fitting for Au-NMP crystal.

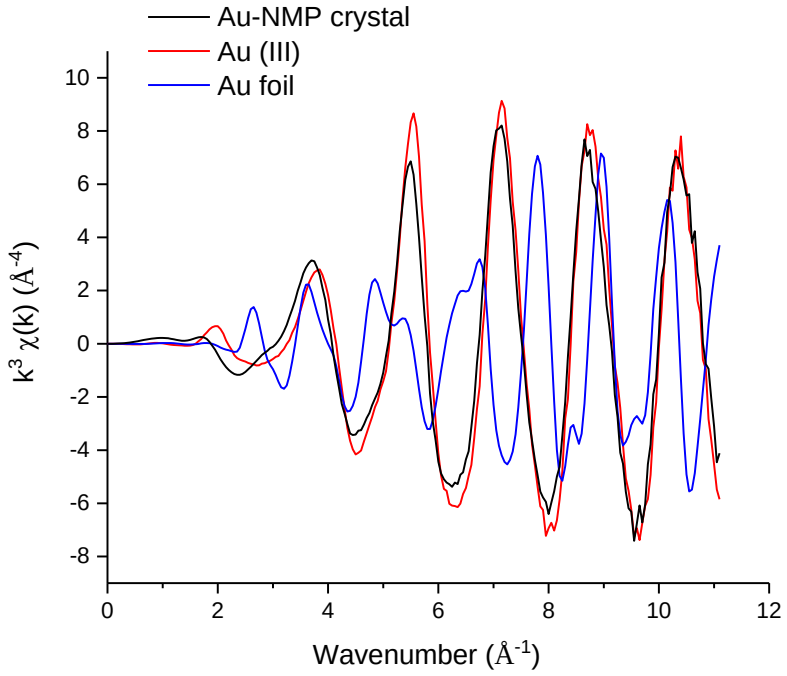

Figure S.5.13: Experimental k^3-weighted EXAFS data for Au-NMP crystal.